

Understanding the chemotherapy-induced bystander effect; an evaluation of the role of cytokine storm in an *in vitro* model of the human bone marrow

Harshini Shanika Hewagama Asurappulige

This thesis is submitted in partial fulfilment of the requirements of the University of the West of England for the degree of Doctor of Philosophy in Biomedical Science

Faculty of Health and Applied Sciences, University of the West of England, Bristol

June 2024

Abstract

The phenomenon of donor cell leukaemia (DCL) occurs following haematopoietic stem cell transplantation (HSCT), but its aetiology is currently unknown. Previous work within the research group identified a chemotherapy-induced bystander effect (CIBE) in an *in vitro* bone marrow (BM) model, which has been suggested to play a role in DCL. As DCL predominantly occurs as myeloid lineages, this research study investigated the role of cytokines in CIBE. Utilising the same *in vitro* model, the induction of cytokine ‘storm’ was measured in the human bone marrow mesenchymal stem cell line HS-5. Five candidate cytokines (TNF- α , IL-6, β - β 1, G-CSF and GM-CSF) were selected and tested, either alone or in combination, for their ability to directly induce genotoxicity in the form of micronuclei in TK6 cells. IL-6 was focussed on for mechanisms of action; IL-6 production was knocked down in HS-5 cells, and IL-6 signalling pathways were inhibited in TK6 cells to ascertain the role of IL-6 in genotoxicity.

The chemotherapeutic agents chlorambucil and mitoxantrone, induced an overall increase in cytokine secretion, with all 80 cytokines detected in either treated or untreated cells. This heightened cytokine response, resembled a cytokine storm, and for the first time, provided a profiling of cytokine secretion in the HS-5 cell line. ELISA results confirmed storm levels of expression of the five selected cytokines, by HS-5 cells *in vitro*. Additionally, the study revealed the direct genotoxic effects at their healthy (TNF- α and TGF- β 1) and storm levels (all five cytokines) on the TK6 cell line, with combination treatments exacerbating genotoxicity.

IL-6 emerged as a central candidate, with significant baseline expression and sustained elevated secretion post-chemotherapy, as well as a notable contribution to genotoxicity induction in bystander cells. The central role of IL-6 in CIBE was shown for the first-time using IL-6 gene knockdown in HS-5 cells, resulting in reduction of micronuclei in bystander TK6 cells to levels similar to untreated cells; this proved significant for chlorambucil ($p < 0.05$). This novel finding underscores IL-6 as a central contributor to the induction of genotoxic effects in studies using bystander models.

Efforts to mitigate IL-6-induced genotoxicity using JAK/STAT and RAS/MAPK pathway inhibitors to TK6 yielded unexpected results, in that micronuclei increased significantly ($p < 0.05$) in the presence of the pathway inhibitors FLLL-32 and BAY-293 with IL-6

treatment, compared to the samples without IL-6. These data suggest that alternative pathways, perhaps more relevant to genotoxicity, may be promoted when using these inhibitors in the presence of IL-6, highlighting the complexity of IL-6 signalling pathways.

In conclusion, this study illuminates the intricate dynamics of cytokines in the context of CIBE and their possible contribution to DCL, offering valuable insights for further investigations and potential therapeutic interventions. The complexities unveiled underscore the need for continued exploration into the multifaceted mechanisms governing HSCT outcomes and associated complications.

Acknowledgements

I extend my deepest gratitude to my parents, Mr. & Mrs. Hemasiri, for their unwavering support and belief in me. Your presence through my ups and downs has been my pillar of strength. Your encouragement during my failures has fuelled my determination, and I am committed to making you proud.

To my beloved siblings, Hashini, Hiruni, Harshi, and Hashan, your understanding of my frustrations and tolerance of my shortcomings have been invaluable. I appreciate your love, moral, emotional, financial, and social support. A special thanks to my little sister, Harshi, for standing by me throughout my PhD journey.

My heartfelt thanks go to my amazing husband, Deepal Dewapura Dewage. Completing this PhD would not have been possible without your unwavering support. Your sacrifices of time and resources, spanning five years, reflect your belief in my success. My gratitude extends to our son, Diyon, who brought joy and strength into my life. You, were my first PhD, teaching me that love can heal wounds that science cannot. I am proud to have conquered my fears while being a devoted mother to you.

A special acknowledgment goes to Dr. Ruth Morse, my Director of Studies and mentor. Your guidance, patience, and encouragement shaped me into the professional researcher I am today. Your words of support were my fuel during challenging times. I am forever grateful for your mentorship. I also want to express my appreciation to Dr. Adam Thomas, my second supervisor, for his contributions to data analysis and proofreading. For Prof. Michael Lodomery for supporting with knockdown technique and risk assessment. Your remarkable efforts enhanced the quality of my research, and I sincerely thank you.

I acknowledge the contributions of my professional colleagues, the academic support team, and the technical team at the Centre for Biosciences (CRIB) laboratory, especially David Corry and Alison Halliday. Your support, knowledge transfer, and expertise were invaluable.

To my dear friends, senior team members (Kelechi, Sultan, Alex, and Arinze), and lab colleagues, your contributions were instrumental in the success of this research. Finally, to my office mates (Hy, Stephi, Dami, Sunday, Praise, and Liz), I apologize for the missed hangouts due to tight schedules. The journey is over; let's celebrate together. Thank you all for being part of this significant chapter in my academic journey.

Table of Contents

Abstract.....	ii
Acknowledgements.....	iv
Table of Contents.....	v
List of Figures.....	xi
List of Tables.....	xiii
Abbreviations.....	xiv

CHAPTER 1

INTRODUCTION.....	1
1.1 Leukaemia.....	1
1.1.1 Classification and clinical manifestation.....	1
1.1.2 Epidemiology.....	3
1.1.3 Aetiology and risk factors.....	7
1.1.4 Diagnosis.....	8
1.1.5 Therapeutic regimens.....	9
1.2 Chemotherapeutic agents and mechanisms of action.....	10
1.2.1 Mechanism of action of alkylating agents.....	13
1.2.1.1 Chlorambucil.....	16
1.2.2 Mechanism of action of topoisomerase inhibitors.....	18
1.2.2.1 Mitoxantrone.....	21
1.3 Haematopoietic stem cell transplantation.....	23
1.4 Post transplant complications.....	26
1.5 Donor cell leukaemia.....	29
1.5.1 Clinical manifestation and epidemiology.....	29
1.5.2 Hypothesis of the aetiology of DCL.....	31
1.5.2.1 Intrinsic donor factors.....	32
1.5.2.2 Host Extrinsic factors.....	33
1.5.3 Diagnosis and treatments of DCL.....	35
1.6 Bone marrow microenvironment.....	36
1.6.1 Haematopoiesis and supportive factors.....	36
1.6.2 Aberrant bone marrow and cytokines.....	40
1.6.2.1 Cytokine storm.....	41

1.6.3 Bystander effect.....	44
1.6.3.1 Radiation-induced bystander effects.....	45
1.6.3.2 Chemotherapy-induced bystander effects.....	46
1.6.3.3 Cytokines and bystander effect.....	47
1.7 Hypothesis.....	50
1.8 Aims.....	51

CHAPTER 2

MATERIALS AND METHODS.....	52
2.1 Materials.....	52
2.1.1 Cell lines.....	52
2.1.1.1 Mesenchymal stromal cell line; HS-5.....	52
2.1.1.2 Lymphoblastoid cell line; TK6.....	52
2.1.2 Chemotherapeutic agents.....	53
2.1.3 Recombinant cytokines.....	55
2.1.4 Mitomycin C.....	55
2.2 Methods.....	56
2.2.1 Cell culture.....	56
2.2.1.1 Standard culture conditions.....	56
2.2.1.2 Thawing of cryopreserved cell lines.....	57
2.2.1.3 Cryopreservation of cells.....	57
2.2.1.4 Detachment of HS-5 adherent cells by trypsinization.....	58
2.2.1.5 Manual cell counting; trypan blue exclusion assay.....	58
2.2.1.6 Automated cell counting; fluorescent image-based automated cell counter.....	58
2.2.1.7 Bystander co-culture model.....	59
2.2.2 Cytokine array analysis of drug treated HS-5 cells.....	60
2.2.2.1 Establishing the HS-5 culture for drug treatment.....	60
2.2.2.2 Abcam cytokine microarray protocol.....	61
2.2.2.3 Cytokine microarray results analysis.....	62
2.2.3 Enzyme-linked immunosorbent assay (ELISA).....	64
2.2.3.1 In-house ELISA assay for TNF- α , IL-6, GM-CSF.....	64
2.2.3.2 ELISA commercial kits.....	66
2.2.4 <i>In vitro</i> micronucleus assay.....	68

2.2.4.1 Cytotoxicity detection.....	69
2.2.4.2 Genotoxicity detection.....	69
2.2.5 Cytokine signalling pathway inhibition.....	72
2.2.5.1 FLLL-32.....	72
2.2.5.2 BAY-293.....	72
2.2.6 Cytokine expression inhibition in co-culture models.....	73
2.2.6.1 IL-6 siRNA knockdown.....	73
2.2.6.2 IL-6 chemical inhibition by resatorvid.....	74
2.2.7 Statistical analysis.....	75

CHAPTER 3

METHOD DEVELOPMENT.....	76
3.1 Introduction.....	76
3.2 Methods.....	81
3.2.1 Cell culture medium optimisation.....	81
3.2.1.1 Media selection assay for HS-5.....	81
3.2.1.2 Media selection assay for TK6.....	81
3.2.1.3 TK6 growth curve development.....	81
3.2.2 ELISA development.....	82
3.2.2.1 Capture and detection antibodies optimisation.....	82
3.2.2.2 Standard curve optimisation.....	85
3.2.2.3 Sensitivity optimisation.....	88
3.2.2.4 Intra- and Inter-assay reproducibility.....	88
3.3 Results.....	90
3.3.1 Evaluation of optimum culture conditions for cell lines.....	90
3.3.1.1 Mesenchymal stem cell line; HS-5.....	90
3.3.1.2 Lymphoblast cell line; TK6.....	94
3.3.1.3 TK6 growth curve.....	96
3.3.2 ELISA assay development.....	97
3.3.2.1 Development of optimum signal-to-background ratio.....	97
3.3.2.2 Development of standard curve.....	99
3.3.2.3 Sensitivity optimisation.....	100
3.3.2.4 Intra- and inter-assay reproducibility.....	109

3.4 Discussion.....	111
3.5 Conclusion	116

CHAPTER 4

ARRAY ANALYSIS OF CYTOKINE SECRETION FROM HS-5 EXPOSED TO

CHEMOTHERAPY..... 118

4.1 Introduction	118
4.2 Methods	120
4.2.1 Cytokine array	120
4.2.2 Array validation ELISA	121
4.3 Results	123
4.3.1 Cytokine Array.....	123
4.3.1.1 Profile of cytokine secretion from HS-5 cells.....	123
4.3.1.2 Absolute change of cytokine expression following drug exposure	125
4.3.1.3 Fold change of cytokine expression following drug exposure	127
4.3.1.4 Cytokine secretion due to drug treatment; switching on gene expression.....	130
4.3.1.5 Functional assessment of cytokine profile	131
4.3.2 Array validation ELISA	135
4.3.2.1 TNF- α expression by TK6 and HS-5	136
4.3.2.2 TGF- β 1 expression by TK6 and HS-5	137
4.3.2.3 IL-6 expression by TK6 and HS-5.....	138
4.3.2.4 GM-CSF expression by TK6 and HS-5	140
4.3.2.5 G-CSF expression by TK6 and HS-5.....	141
4.4 Discussion.....	142
4.5 Conclusion.....	155

CHAPTER 5

EVALUATION OF CYTOTOXICITY AND GENOTOXICITY IN AN *IN VITRO*

CULTURE MODEL..... 156

5.1 Introduction	156
5.2 Methods	164
5.2.1 Cytotoxicity assessment	164
5.2.2 Micronucleus assay	164

5.2.3 IL-6 pathway inhibition <i>in vitro</i> MN assay	164
5.2.3.1 Optimisation of inhibitor dose	164
5.2.3.2 Cytotoxicity and genotoxicity following chemical inhibition	165
5.3 Results	167
5.3.1 Cytotoxicity	167
5.3.2 Genotoxicity evaluation	169
5.3.2.1 TNF- α recombinant treatments	169
5.3.2.2 TGF- β 1 recombinant treatments	171
5.3.2.3 IL-6 recombinant treatments	173
5.3.2.4 GM-CSF recombinant treatments	175
5.3.2.5 G-CSF recombinant treatments	177
5.3.3 Inhibition of IL-6 signalling pathways	179
5.3.3.1 Assessment of optimal inhibitor dosing	179
5.3.3.2 Cytotoxicity assessment	181
5.3.3.3 Micronucleus assay	181
5.4 Discussion	183
5.5 Conclusion	196

CHAPTER 6

KNOCKDOWN AND INHIBITION IN BYSTANDER MODELS	198
6.1 Introduction	198
6.2 Methods	214
6.2.1 IL-6 siRNA oligo	214
6.2.1.1 IL-6 siRNA concentration and longevity optimisation	214
6.2.1.2 IL-6 siRNA longevity assay with drug	215
6.2.1.3 IL-6 knockdown HS-5 co-cultured with TK6	215
6.2.2 Resatorvid	216
6.2.2.1 Resatorvid dose response assay	216
6.2.2.2 Resatorvid inhibition and longevity with drugs	217
6.2.2.3 Resatorvid inhibition of HS-5 co-cultured with TK6	217
6.3 Results	219
6.3.1 siRNA Oligo optimisation	219
6.3.1.1 Knockdown concentration and longevity optimisation	219

6.3.1.2 Knockdown longevity assay with drug treatments	223
6.3.1.3 TK6 co-cultured with IL-6 knockdown HS-5.....	225
6.3.1.4 MN analysis in TK6 co-cultured with IL-6 knockdown HS-5	227
6.3.2 Resatorvid.....	228
6.3.2.1 Resatorvid cell viability and IL-6 inhibition longevity assay.....	228
6.3.2.2 Resatorvid longevity assay with chemotherapies	231
6.3.2.3 Resatorvid treated HS-5 co-cultured with TK6 in the bystander assay	233
6.3.2.4 MN analysis in bystander TK6 co-cultured with IL-6 resatorvid inhibited HS-5	234
6.4 Discussion.....	235
6.5 Conclusion	246

CHAPTER 7

FINAL DISCUSSION	249
7.1 Summary of findings	249
7.2 Limitations of the study.....	254
7.3 Future considerations.....	255
7.4 Final conclusion.....	258

CHAPTER 8

REFERENCES	260
------------------	-----

Appendices

Appendix I: Cytokine names according to the membrane spot.....	290
Appendix II: Cytokine concentrations reference to literature	291
Appendix III: Micronuclei addition or potentiation.	292

List of Figures

Figure 1. 1. Classical symptoms of leukaemia	1
Figure 1. 2. Five most prevalent cancers by age.....	6
Figure 1. 3. Classical mechanisms of action of the alkylating agents.....	15
Figure 1. 4. DNA adducts caused by alkylating agents	16
Figure 1. 5. DNA interstrand cross-link formation by chlorambucil.....	18
Figure 1. 6. Mechanism of action of topoisomerase inhibitors	20
Figure 1. 7. Possible DNA lesions induced by mitoxantrone	22
Figure 1. 8. Proposed aetiological factors influencing the development of DCL.....	32
Figure 1. 9. Cytokine regulation in bone marrow haematopoiesis and plasticity.....	39
Figure 1. 10. A model for propagating cancer therapy-induced genomic imbalance.....	49
Figure 2. 1. Co-culture model to determine the bystander effect.....	59
Figure 2. 2. HS-5 cells confluence assay	60
Figure 2. 3. Incubation of array membranes with conditioned medium.....	62
Figure 2. 4. Cytokine membranes after chemiluminescence detection	64
Figure 2. 5. Visual presentation of micronuclei following cytokine treatments.....	71
Figure 3. 1. Different types of ELISA	79
Figure 3. 2. ELISA plates for GM-CSF antibody titration	84
Figure 3. 3. ELISA standard curve development.....	87
Figure 3. 4. Morphology of HS-5 in different culture media.....	91
Figure 3. 5. HS-5 live cells count (A) and viability (B) in different media.....	93
Figure 3. 6. TK6 live cells (A), viability (B) and size (C) in different media	95
Figure 3. 7. TK6 growth curve development.....	96
Figure 3. 8. Signal to background ratio development for GM-CSF antibody titration.....	98
Figure 3. 9. Standard curve development using horseradish peroxidase.....	99
Figure 3. 10. Sensitivity development for GM-CSF ELISA	103
Figure 3. 11. Sensitivity development for IL-6 ELISA	104
Figure 3. 12. Sensitivity development for G-CSF ELISA	106
Figure 3. 13. Sensitivity development for TGF- β 1 ELISA.	108
Figure 3. 14. Intra- and inter-assay reproducibility for GM-CSF.....	110
Figure 4. 1. Profile of cytokine secretion by untreated HS-5 cells.....	124

Figure 4. 2. Cytokine expression from HS-5 following chemotherapies	126
Figure 4. 3. Fold change of cytokine expression following chemotherapies.....	129
Figure 4. 4. Detection of cytokines secreted only in response chemotherapies	130
Figure 4. 5. ELISA analysis of TNF- α from TK6 and HS-5 cells.....	137
Figure 4. 6. ELISA analysis of TGF- β 1 from TK6 and HS-5 cells	138
Figure 4. 7. ELISA analysis of IL-6 from TK6 and HS-5 cells.....	139
Figure 4. 8. ELISA analysis of GM-CSF from TK6 and HS-5 cells.....	140
Figure 4. 9. ELISA analysis of G-CSF from TK6 and HS-5 cells.....	141
Figure 5. 1. Micronucleus formation during mitotic cell division.....	157
Figure 5. 2. IL-6 signalling pathways.	161
Figure 5. 3. TK6 cell viability following recombinant cytokines treatments	168
Figure 5. 4. The induction of micronuclei due to treatment with recombinant TNF- α	170
Figure 5. 5. The induction of micronuclei due to treatment with recombinant TGF- β 1.	172
Figure 5. 6. The induction of micronuclei due to treatment with recombinant IL-6.	174
Figure 5. 7. The induction of micronuclei due to treatment with recombinant GM-CSF.	176
Figure 5. 8. The induction of micronuclei due to treatment with recombinant G-CSF.....	178
Figure 5. 9. TK6 cell counts following IL-6 pathway inhibitor treatment.	180
Figure 5. 10. Micronuclei in TK6 treated IL-6 signalling pathway inhibitors	182
Figure 6. 1. The mechanism of RNA interference.....	206
Figure 6. 2. TLR4 signalling pathway and resatorvid inhibition.....	209
Figure 6. 3. Morphology (A) and IL-6 expression (B) from HS-5 transfected with IL-6 siRNA over five days.....	221
Figure 6. 4. IL-6 expression from HS-5 cells transfected with IL-6 siRNA with and without chemotherapies	224
Figure 6. 5. IL-6 expression from IL-6 knockdown HS-5 alone vs co-culture with TK6.....	226
Figure 6. 6. Micronuclei in TK6 cells co-cultured with IL-6 knockdown HS-5	227
Figure 6. 7. Live cell count (A) and IL-6 expression (B) by HS-5 exposure to resatorvid. ..	229
Figure 6. 8. IL-6 expression from HS-5 exposed to resatorvid and chemotherapies.....	232
Figure 6. 9. IL-6 expression from resatorvid treated HS-5 alone vs HS-5 co-cultured with TK6 in a bystander assay	233
Figure 6. 10. The induction of micronuclei in TK6 cells co-cultured with resatorvid treated HS-5	234

List of Tables

Table 1. 1. Classes of chemotherapeutic agents	12
Table 2. 1. Plasma concentrations of chemotherapeutic agents.....	54
Table 2. 2. Cytokine concentrations used to treat TK6 cells.	55
Table 2. 3. Capture and detection antibody concentrations	65
Table 4. 1. Cytokine functionality table with respect to expression pattern in the cytokine array	131

Abbreviations

µg	Microgram
µl	Microlitre
µM	Micromolar
°C	Degree Celsius
AIF	Apoptosis-inducing factor
ALL	Acute lymphoblastic leukaemia
AML	Acute myeloid leukaemia
BE	Bystander effect
BM	Bone marrow
CAP	Capture
CIBE	Chemotherapy-induced bystander effect
CLL	Chronic lymphocytic leukaemia
CML	Chronic myeloid leukaemia
CNS	Central nervous system
CNTF	Ciliary neurotrophic factor
COSHH	Control of substances hazardous to health
CSF	Colony-stimulating factors
DAMPs	Damage-associated molecular patterns
DCL	Donor cell leukaemia
DSB	Double strand breaks
dsRNA	Double-stranded RNA
EDTA	Ethylenediaminetetracetic acid
ELISA	Enzyme-linked immunosorbent assay
EPO	Erythropoietin
ERK	Extracellular signalregulated kinase 1/2
FISH	Fluorescent <i>in situ</i> hybridisation
G-CSF	Granulocyte colony-stimulating factor
GEF	Guanine nucleotide exchange factor
GM-CSF	Granulocyte-macrophage colony-stimulating factor
GPCRs	G-protein-coupled receptors
GvL	Graft versus leukaemia

HIV	Human immunodeficiency virus
HMGB1	High-mobility group box 1
HQ	High quality
HRP	Horseradish peroxidase
HSC	Haematopoietic stem cells
HSCT	Haematopoietic stem cell transplantation
IL	Interleukin
IL-6	Interleukin-6
LIF	Leukaemia inhibitory factor
LPS	Lipopolysaccharide
LQ	Low quality
mAb	Monoclonal antibody
MAPK	Mitogen-activated protein kinase
MDS	Myelodysplastic syndrome
miRNA	microRNA
MN	Micronucleus
MRI	Magnetic resonance imaging
NER	Nucleotide excision repair
NHEJ	Non-homologous end joining
OECD	Organisation for Economic Co-operation and Development
OSM	Oncostatin M
PAMPs	Pathogen-associated molecular patterns
PB	Peripheral blood
PCR	Polymerase chain reaction
PET	Polyethylene terephthalate
PTLD	Post-transplant lympho-proliferative disorder
qPCR	Quantitative real-time PCR
RIA	Radio immune assay
RIBE	Radiotherapy induced bystander effect
RISC	RNA-induced silencing complex
SD	Standard deviation
shRNAs	Short hairpin RNAs
SIDPs	Short inversion or deletion polymorphisms

siRNAs	Small interfering RNAs
SNPs	Single nucleotide polymorphisms
SOS	Son of Sevenless
SSB	Single strand breaks
STR	Short tandem repeat
TGF- β 1	Transforming growth factor beta 1
TLR4	Toll-like receptor 4
TNF- α	Tumour necrosis factor-alpha
TPO	Thrombopoietin
TRL	Therapy-related leukaemia
UCB	Umbilical cord blood
VNTRs	Variable number tandem repeats

CHAPTER 1

INTRODUCTION

1.1 Leukaemia

1.1.1 Classification and clinical manifestation

Leukaemia is a malignancy of the bone marrow, resulting in accumulation of abnormal white blood cells due to uncontrolled proliferation, lack of differentiation and apoptosis in the bone marrow (BM) through haematopoietic mis-regulation and immune-suppression (Medinger *et al.*, 2016). The leukaemic cells can spread into other parts of the body, including the central nervous system (CNS) through the blood or lymphatic system (Hoffbrand *et al.*, 2011). Signs of leukaemia are usually related to leukocyte infiltration of lymphatic nodes and organs. The resulting lymphadenopathy, hepatomegaly, or splenomegaly can cause symptoms owing to organ bulk (Grigoropoulos *et al.*, 2013). In many cases, symptoms typical to BM failure are present, such as frequent and spontaneous bruises due to a decreased number of platelets, bleeding, anaemia, and recurrent infections due to neutropenia. Infrequent involvement of the CNS, as well as meningeal and cutaneous infiltration may result in headache, gum swelling, and

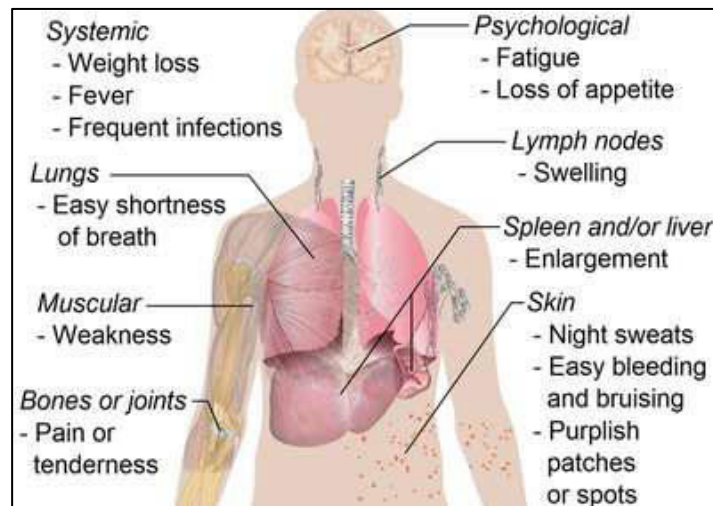


Figure 1. 1. Classical symptoms of leukaemia. This highlights the classical symptoms in leukaemia patients. However, it will also depend on the disease condition: acute or chronic, and the type of blood cells it affects. But certain symptoms overlap and are common in all forms of leukaemia. Taken from Pokharel (2012) under the free creative common license.

cranial and peripheral nerve defects (Grigoropoulos *et al.*, 2013). However, classic symptoms include fever, night sweats, weight loss, fatigue and bone/joint pains (Fig. 1.1).

Factors to be considered for staging or prognosis of leukaemia include: age, white cell and platelet counts, history of a previous blood disorder, bone damage or enlarged liver/spleen, and chromosomal abnormality. According to Cancer Treatment Centres of America (CTCA, 2020), leukaemia can be classified as acute (immature cell types -blasts) or chronic (mature cell type -cytes); and based on the cellular lineage into lymphoid (T and B lymphocytes/ natural killer cells) or myeloid (monocytes, basophils, eosinophils and neutrophils) giving four main categories including acute lymphoblastic leukaemia (ALL), acute myeloid leukaemia (AML), chronic lymphocytic leukaemia (CLL) and chronic myeloid leukaemia (CML) (Pokharel, 2012; Grigoropoulos *et al.*, 2013; Jin *et al.*, 2016). In chronic leukaemia, the mature cancerous cells retain their normal functions, which lead to a slow progression of the disease, whereas in acute leukaemia, abnormal immature blood cells cannot perform proper functions, which increase the disease progression quickly (Jin *et al.*, 2016). Other types of leukaemia include hairy cell leukaemia (rare subtype of CLL), acute promyelocytic leukaemia, large granular lymphocytic leukaemia, lymphoma (Hodgkin lymphoma and non-Hodgkin lymphoma), myeloma, myelodysplastic syndromes (MDS) and myeloproliferative neoplasms (Swerdlow *et al.*, 2016).

ALL stands as the predominant form of leukaemia in children, with approximately three-quarters of cases occurring in individuals under 6 years of age. Among paediatric ALL cases, approximately 75% exhibit an enlarged liver or spleen, while nearly 60% present lymphadenopathy (Davis *et al.*, 2014). Despite its frequency, paediatric ALL demonstrates a favourable response to chemotherapy, with an 85% long-term survival rate (Swerdlow *et al.*, 2016). In addition to vincristine, asparaginase, and mitoxantrone, chemotherapy regimens for ALL commonly include drugs such as prednisone, daunorubicin, cyclophosphamide, cytarabine, methotrexate, and 6-mercaptopurine in combination to maximize efficacy (table 1.1). Conversely, AML emerges as the most prevalent form of leukaemia in adults and the 2nd most common type of leukaemia in children. Adult AML is characterized by infrequent occurrences of hepatosplenomegaly and lymphadenopathy, however these manifestations are observed in approximately 50% of adult ALL cases (Davis *et al.*, 2014). The treatment of AML is fraught with significant challenges, with approximately 2,700 AML-related deaths occurring annually in the UK. This staggering figure translates to over 7 lives lost every day, underscoring the urgent need for advancements in AML research and therapeutic interventions (Cancer

Research, UK, 2017). The subtype of AML is M0 to M7 and is classified based on the French-American-British (FAB) classification using number of healthy blood cells, size and number of leukaemia cells, chromosome changes in leukaemia cells and other genetic abnormalities (CTCA, 2020). According to table 1.1, AML can be treated with the "3+7" regimen, which typically consists of cytarabine (Ara-C) given continuously for 7 days and daunorubicin given for 3 days. AML may include various other chemotherapy agents depending on factors such as patient age, cytogenetics, and overall health status. Some additional agents commonly used in AML treatment regimens include etoposide, fludarabine and cladribine. Chronic leukaemia predominantly manifests in adults compared to children and is frequently diagnosed for an unrelated reason (Grigoropoulos *et al.*, 2013). CLL is the most prevalent form of chronic leukaemia in adults. Common manifestations include hepatosplenomegaly and lymphadenopathy, particularly in the cervical, axillary, and inguinal regions. In contrast, CML is relatively rare, and is characterized by common splenomegaly that may extend beyond the umbilicus (Davis *et al.*, 2014). Notably, the t(9;22) translocation, recognized as the Philadelphia chromosome, serves as the genetic hallmark of CML (Swerdlow *et al.*, 2016). CLL uses both Rai (based on blood cell counts) and Binet systems (evaluates the areas of the affected lymphoid tissue) to classify where CML is staged (depending on the number of diseased cells) into chronic (mild symptoms), accelerated (more aggressive or noticeable symptoms) and blastic (most aggressive with 20% myeloblasts or lymphoblasts (CTCA, 2020).

1.1.2 Epidemiology

According to the diagnosed cases in 2016, leukaemia is the 12th most common cancer in the UK, with 3% incidence of all new cancer cases, and having a distribution of predominance in males (60%), compared to females (40%). In the UK every year, around 10,100 new leukaemia cases are diagnosed, and 4700 leukaemia deaths recorded. Mortality rates for leukaemia in the UK are highest in people aged 90+. Over the last decade, mortality rates have decreased in the UK with rates of 9% and 7% in females and males respectively (Medinger *et al.*, 2016; Cancer Research, UK, 2017; IARC, 2014). In the UK, 12% of leukaemia cases are suggested to be preventable. The ten-year age-standardised net survival for leukaemia has increased from 7% (1971-1972) to 46% (2010-2011) in England and Wales, UK (IARC, 2014). It is predicted that >72%, >54% and >41% of people diagnosed with leukaemia in England survive their disease for ≥ 1 year, ≥ 5 years and ≥ 10 years respectively. However, leukaemia survival for females is

lower than for males at one year, and similar to males at five- and ten-years (Cancer Research, UK, 2017).

As documented by Swerdlow *et al.* (2016), the global incidence of ALL is approximately 3 cases per 100,000 population. AML sees around 3000 new cases in the UK every year. CLL exhibits an incidence rate of 4.2 cases per 100,000 population, while CML has an incidence rate of 1 case per 100,000 population (Swerdlow *et al.*, 2016). Every year, new cases and deaths due to individual subtypes are ALL 800, 230; AML 3200, 2600; CLL 3800, 990 and CML 830, 220 respectively. Excluding AML, all other subtypes collectively contribute to less than 1% of annual cancer deaths in the UK. In contrast, AML accounts for 2% of these deaths. Again, this notable difference underscores the significance of AML within the spectrum of leukaemia types, emphasising its pivotal role in contributing to leukaemia-related mortality. ALL incidence rates are highest in people aged <4 years and about 6% cases are in >75 year old people, whereas for AML both incidence and mortality rates are highest in people aged 85-89. CLL has the highest incidence rates in people aged 85-89 and mortality rates is highest in the 90+ age group. CML incidence and mortality rates are highest in ages above 85 (Cancer Research, UK, 2017; IARC, 2014).

In females it is the 12th most common cancer with ~4,000 new cases, while in males is the 10th most common cancer, with around ~5800 new cases in 2017. The prevalence of leukaemia is generally higher in white/black males compared to Asian males and more common in white females than in Asian or Black females. Age-specific incidence rates fall gradually from age 0-4 and remain stable throughout childhood and early adulthood, then rates rise sharply from around age 45-49. The highest rates are in the 85 to 89 year old age group for both females and males. Each year the highest incidence rate (38%) of new leukaemia cases is diagnosed in people aged over 85 in the UK (Cancer Research, UK, 2017; IARC, 2014).

Figure 1.2 illustrates substantial variations in the five most prevalent cancers among males (Fig. 1.2A) and females (Fig. 1.2B) across different age groups. Notably, the types of cancers diagnosed in children and young individuals differ significantly from those diagnosed in older populations. Leukaemia, however, stands out as the most frequently diagnosed cancer in children under 14 years, comprising 32% and 31% of all cases in males and females, respectively. Interestingly, as age surpasses 25 years, leukaemia ceases to be among the most common cancers. Despite this shift, AML emerges as the highest occurring cancer in adults

and the second highest in children. This observation prompts a compelling need for further research into the aetiology of AML as an important adult and paediatric leukaemia. The elevated prevalence suggests that AML may play a pivotal role across age groups, demanding a deeper exploration of its mechanisms and implications.

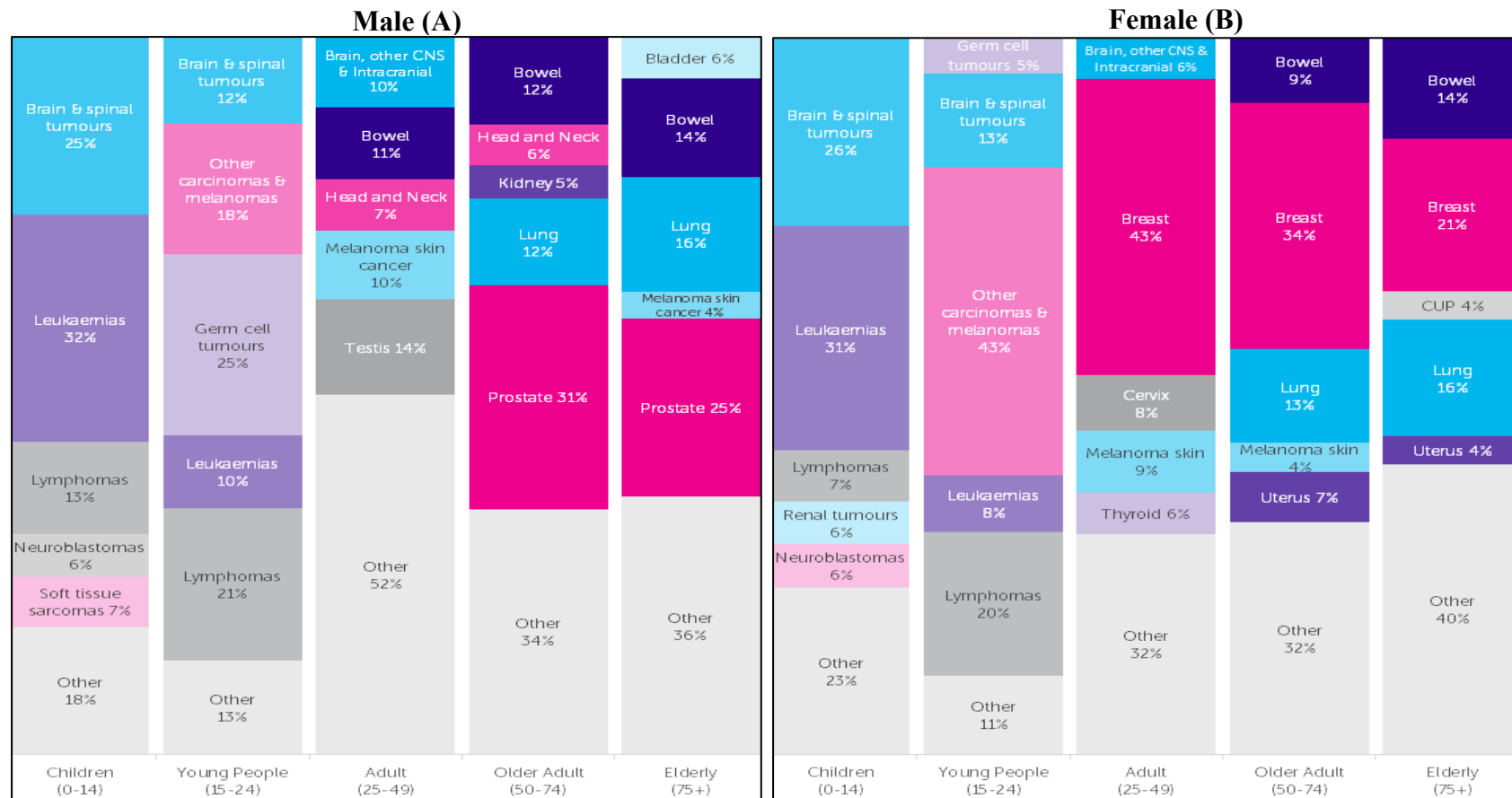


Figure 1. 2. Five most prevalent cancers by age. (A) Most common in males and (B) females. Leukaemia emerges as the predominant cancer diagnosis in the age group of 0-14 years, displaying a notable incidence of 31% in males and 32% in females. However, as individuals surpass the age of 25 years, leukaemia no longer maintains its status among the most prevalent cancers. Adapted from Cancer Research, UK (2017).

1.1.3 Aetiology and risk factors

Due to the heterogeneity of leukaemia, the aetiology remains unclear. It appears to have combinatorial risk factors including age, ethnicity, gender, chemotherapy, environmental factors, inherited syndromes, ionising radiation exposure and infections (Pokharel, 2012; Jin *et al.*, 2016). According to Cancer Research UK (2017), ionising radiation, smoking and workplace exposures cause 9%, 3% and less than 1% of leukaemia cases respectively. The risk of developing most types of leukaemia increases steadily with age and obesity. Leukaemia occurs more commonly in those of white ancestry compared to those of Asian, Hispanic and Black ancestry. Also, rates of ALL in Caucasian children are almost 2-fold rates of ALL in African-American children and in the first three years of life, the rate of AML in Caucasian children is around three times the rate of AML in African-American children (Jin *et al.*, 2016). Leukaemia also occurs more frequently in males than females (Pokharel, 2012). Within the spectrum of leukaemia, a subset known as therapy-related leukaemia (TRL; section 1.4) may arise following exposure to specific chemotherapeutic agents, including platinum agents, alkylating agents and topoisomerase inhibitors (Khalade *et al.*, 2010). Environmental factors also play a significant role, with documented increased risks associated with alcohol, cigarettes, and drug consumption during pregnancy, particularly in the context of childhood AML. Occupational exposure to benzene stands out as an established risk factor for leukaemia in adults, notably AML (Davis *et al.*, 2014; Jin *et al.*, 2016; Maele-Fabry *et al.*, 2019).

However, 30% of all paediatric cancers is leukaemia, and as such, is the most common cancer that is diagnosed in children that are less than 15 years old and children with Down syndrome have 20-fold increased risk of developing childhood leukaemia (Davis *et al.*, 2014), with higher incidence of AML than ALL (Jin *et al.*, 2016). Maele-Fabry *et al.*, (2019) demonstrated the highest AML risks for children aged ≤ 2 years who had been exposed to household pesticides such as mosquito repellents and insect pesticides, or exposed to them during pregnancy. Development of other leukaemia subtypes (e.g. TRL) arise from previous haematological malignancy history (Brenner & Hall, 2007). Persons exposed to ionising radiation, such as atomic bomb survivors, medical radiation workers and patients receiving radiation treatment, have an increased risk of developing different types of leukaemia. Young people show increased leukaemia risk following radiation from computed tomography (Kuznetsova *et al.*, 2016). Some studies found that populations that resided near the Sellafield nuclear plant in the UK have increased childhood leukaemia (Jin *et al.*, 2016). Infection with Human T-cell

Lymphotropic Virus-1 is linked to the development of adult T-cell leukaemia/lymphoma (Pokharel, 2012; IARC, 2014). Additionally, parental age (mothers >35 years, fathers >40) and higher birth weight lead to an increased risk of childhood leukaemia (Jin *et al.*, 2016).

1.1.4 Diagnosis

Acute leukaemia should be suspected when a peripheral blood smear or bone marrow specimen is overpopulated with blast cells. Classically, AML (M2 and M3) is characterized by the presence of auer rods on a peripheral smear. However, immune phenotyping by flow cytometry and cytogenetic testing are required to distinguish between acute leukaemia subtypes. Cytogenetic abnormalities have become an essential component of diagnostic protocols for AML, prompting significant alterations in both diagnostic approaches and treatment strategies. AML can now be diagnosed with fewer (<20%) myeloblasts in the BM if they carry a chromosomal aberration associated with AML (Swerdlow *et al.*, 2016). In the UK, cytogenetic analysis is performed because patients with certain abnormalities (~5% AML carry *TP53* deletion), have a worse prognosis and need to be treated differently (Davis *et al.*, 2014).

The diagnosis of CLL is based on a clonal expansion of B lymphocytes in the peripheral blood, confirmed by immuno-phenotyping. A BM specimen is not required for diagnosis of CLL but can be obtained to determine the extent of marrow involvement for prognosis. Malignant lymphocytes in CLL express CD5 and CD23 membrane antigens, so usually have a distinctive immuno-phenotype (Swerdlow *et al.*, 2016). However, some diagnosis requires fluorescent *in situ* hybridisation (FISH) or karyotyping for a specific abnormality called the Philadelphia chromosome (fusion of chr9-chr22; *BCR-ABL*) (Davis *et al.*, 2014; Pokharel, 2012).

BM biopsy is also examined for chromosomal abnormalities of haematopoietic cells (loss or gain of chr 7, 5, 21, 22 19, 11, 15, 17) (Hamerschlak, 2008; Stieglitz & Loh, 2013). Different genetic markers such as *FLT3* (FMS3-like tyrosine kinase 3; mostly internal tandem duplication), *KIT* (tyrosine protein kinase KIT; point mutation) and nucleophosmin (Baldus *et al.*, 2007) may also be examined depending on the type of leukaemia (Medinger *et al.*, 2016). In severe conditions, due to nodal infiltration, lymph node biopsy and a spinal tap or lumbar puncture is also examined (Pokharel, 2012). Other helpful initial laboratory tests include measurement of serum electrolyte and creatinine levels, liver function tests, and coagulation studies. If the patient appears ill or is febrile, the physician should evaluate for infection with urinalysis, urine culture and blood cultures. X-rays, magnetic resonance imaging (MRI), CT

scan, DEXA scan and ultrasounds may also be used to diagnose leukaemia (Pokharel, 2012; Davis *et al.*, 2014; CTCA, 2020).

1.1.5 Therapeutic regimens

The type of treatments varies depending on the leukaemia subtypes, cytogenetic analyses, patient age, and comorbid conditions. Therefore, in general, there are five major treatment approaches including chemotherapy, radiotherapy, immunotherapy, targeted therapy and haematopoietic stem cell transplantation (HSCT), which have greatly improved the prognosis of leukaemia in the last few decades (Medinger *et al.*, 2016; Fausel, 2007; Hoffbrand *et al.*, 2011). Chemotherapy is the mainstay treatment for leukaemia and refers to a wide range of drugs used alone or as combination treatments (Pokharel, 2012; Davis *et al.*, 2014).

Radiation therapy is one of the many tools used to combat leukaemia by utilising high-energy ionising irradiation to kill leukaemia cells. This modality can be applied independently or synergistically with other therapeutic approaches, aiming to achieve either a curative outcome or the stabilisation of the leukaemia cells (Pokharel, 2012). Ionising radiation is delivered in fractions to a final dose. Standard fractionation involves single daily doses of 1.8–2.0 Gray/day to a weekly dose of 9.0–10 Gray. Radiation can directly act on the DNA backbone, forming DNA strand breaks by ionising or exciting atoms in DNA, however radiation also can indirectly damage DNA by producing reactive oxygen species (ROS) from ionised water molecules, leading to oxidative DNA damage (Swift & Golsteyn, 2014). HSCT is considered as being a potentially curative option for leukaemia because it is an extremely aggressive and potentially life-threatening approach due to conditioning therapy (myeloablative or nonmyeloablative therapy) involving high dose chemotherapy and radiotherapy (section 1.3). Curative therapy regimens for AML and ALL are very intensive. Most patients will have severe side-effects; older patients are especially unlikely to tolerate myeloablative regimens, as are patients with unfavourable cytogenetic events. As an alternative, reduced intensity non-myeloablative therapy may be offered to this subset of patients (Swerdlow *et al.*, 2016).

Immunotherapy is a treatment that uses certain parts of the immune system to fight leukaemic cells. This can be done in a couple of ways; stimulating the natural defences of the immune system and/or creating substances that are just like immune system components which help to restore and improve immunity against cancer cells. The main types of immunotherapies used to treat cancer are checkpoint inhibitors, chimeric antigen receptor T-cell therapy, cytokines,

immuno-modulators, vaccines, and monoclonal antibodies (mAb) (American Cancer Society (2019; Medinger *et al.*, 2016). Targeted therapies are designed to target specific cancer biomarkers (certain cancer proteins and/or products of mutated genes) in cancer cells. There are many different types of targeted immunotherapies including; angiogenesis inhibitors (e.g. bevacizumab), mAb, proteasome inhibitors (e.g. bortezomib), signal transduction inhibitors (e.g. imatinib) (American Cancer Society (2019).

1.2 Chemotherapeutic agents and mechanisms of action

The discovery of a role in treating illness by genotoxic agents was noted in the early 1900's when the BM suppressive effect of nitrogen mustards was observed. Ever since, anticancer drug research activity has continued and the goal of treatment with chemotherapy has evolved from relief of symptoms to cancer cure.

A major advantage of chemotherapy is its ability to treat widespread or metastatic cancer, called systemic treatment whereas surgery and radiation therapy are limited to treating cancers that are confined to specific areas (Maltzman & Millar, 2012). Chemotherapies are varied in their chemical composition, effectiveness in types of cancer, how they are prescribed and the side-effects they might have. They can be used as a curative or palliative option or can be more effective as a combination treatment as chemo-radiation or neo-adjuvant chemotherapy, as well as several chemotherapeutics used concomitantly. Treatment may need multiple cycles (4-8) over a period of months, at specific time intervals. A series of cycles is called a course, which may take 3 to 6 months to complete (Maltzman & Millar, 2012).

Chemotherapy protocols for different types of leukaemia are categorised into distinct phases including induction, consolidation, and maintenance therapy. These approaches may cause complete or partial remission of leukaemia, where complete remission is considered to be less than 5% blasts remaining at day 28. Induction chemotherapy serves as the initial line of treatment, preceding higher-dose chemotherapy. This phase typically spans 4 to 6 weeks, aiming to maximise the destruction of leukaemic cells and induce a remission. Consolidation, also referred to as 'intensification treatment', constitutes post-remission therapy involving higher doses of chemotherapy administered subsequent to the initial treatment. The objective is to target any residual leukaemia cells within the body, preventing their resurgence. Maintenance therapy represents the concluding phase of treatment, designed to sustain

leukaemia remission. Typically, this involves the daily administration of low-dose chemotherapy, accompanied by brief courses of steroids over several days and periodic chemotherapy injections every 3 months (Cancer Research, UK, 2021).

Most chemotherapy targets fast-growing cells, including cancer cells and some healthy cells such as hair follicles, skin and the gastrointestinal tract leading to side-effects of hair loss, rashes and diarrhoea respectively. Each drug varies in its mechanism of action, but typically, chemotherapy either prevents the synthesis of new DNA or damages existing genetic material through genotoxic mechanisms, leading to prevention of cell replication and apoptotic cell death respectively. Combinations of agents that work differently, generally achieves the most tumour killing. Chemotherapeutic drugs can be grouped by chemical structure and mechanism of action. Hence, some drugs may belong to more than one 'group' (Higgins, 2014; Maltzman & Millar, 2012). The major categories of chemotherapy agents are shown in table 1.1.

Table 1. 1. Classes of chemotherapeutic agents (Maltzman & Millar, 2012; American Cancer Society, 2019; Swift & Golsteyn, 2014)
 However, the metal salts are not alkylating as they do not have alkyl groups, but they do create cross links in the DNA.

Alkylating agents	Topoisomerase inhibitors	Plant alkaloids	Antimetabolites	Antibiotics	Miscellaneous Antineoplastics
Nitrogen mustard Mechlorethamine Cyclophosphamide Chlorambucil Melphalan Ifosfamide	Topo-I inhibitors Irinotecan Topotecan	Vinca alkaloids Vincristine Vinblastine Vinorelbine	Folic acid antagonist Methotrexate	Anthracyclines Doxorubicin Daunorubicin Epirubicin Mitoxantrone Idarubicin	Ribonucleotide reductase inhibitor Hydroxyurea
Nitrosoureas Carmustine Lomustine Streptozocin	Topo-II inhibitors Mitoxantrone Amsacrine Etoposide Teniposide	Taxanes Paclitaxel Docetaxel	Pyrimidine antagonist 5-Fluorouracil Floxuridine Cytarabine Capecitabine Gemcitabine	Chromomycins Dactinomycin Plicamycin	Adrenocortical steroid inhibitor Mitotane
Ethylenimines Thiotepa Hexamethylmelamine		Podophyllotoxin Etoposide Teniposide	Purine antagonist 6-Mercaptopurine 6-Thioguanine	Miscellaneous Mitomycin C Bleomycin	Enzymes Asparaginase Pegaspargase
Metal salts Carboplatin Cisplatin Oxaliplatin <i>(Cross linkers but not alkylating)</i>		Camptothecan analogs Irinotecan Topotecan	Adenosine deaminase inhibitor Cladribine Fludarabine Nelarabine Pentostatin		Antimicrotubule agent Estramustine
Hydrazines and Triazines Altretamine Procarbazine Dacarbazine Temozolomide					Retinoids Bexarotene Isotretinoin Tretinoin (ATRA- all trans retinoic acid)

Briefly, plant alkaloids are known as mitotic inhibitors and are derived from natural plant products. They are cell-cycle M phase specific, and act on the mitotic spindles to prevent the formation of spindle fibres and disrupt the cytoskeleton of the cell, thereby inhibiting chromosome segregation and cell division. This group is also listed under topoisomerase inhibitors (Topo-I and II) due to the group's mechanism of action. Moreover, they can also interfere with replication in all phases by enzyme inhibition. The main side-effect of these drugs is that they may cause nerve damage (American Cancer Society, 2019; Pokharel, 2012).

Antitumour antibiotics act at multiple phases of cell cycle by intercalating themselves into the spaces between the nucleotides in the DNA to interfere with transcription, thus affecting growth and replication. The use of cumulative doses is often applied to these drugs as high doses can permanently damage the heart. Antimetabolites either have similar structure to nucleotides or have the capacity to inhibit enzymes involved in the pathways leading to nucleotide construction. They mainly act on S phase by incorporating into cellular metabolism and mimic the bio-molecular building blocks to ultimately interfere with replication and cell division (American Cancer Society, 2019; Pokharel, 2012).

Beyond the aforementioned types, many other types of chemotherapy exist including targeted therapy, immunotherapy and hormone therapy. However, due to the high genotoxicity activity (section 1.4) and key role in chemotherapy induced bystander effect (CIBE; section 1.6.3.2), an alkylating agent and topo-II inhibitor were used as chemotherapeutic agents in this study and these are discussed in subsequent sections 1.2.1 and 1.2.2.

1.2.1 Mechanism of action of alkylating agents

Alkylating agents were first used in the 1940's and are the most commonly used anticancer drugs, used to treat a wide range of cancers including both solid tumours and leukaemia (Ralhan & Kaur, 2007). All alkylating agents are high risk for causing secondary cancers but vary in their carcinogenic potential. The most common secondary cancer is AML (American Cancer Society, 2019). Prolonged use of these drugs will decrease sperm production, and lead to cessation of menstruation and permanent infertility (Maltzman & Millar, 2012; Ralhan & Kaur, 2007). Alkylating agents can act on both cycling and resting cells; proliferating cells are more sensitive to the drugs, especially in G1 and S phases. The drugs covalently bind to the bases and disrupt DNA through three classical mechanisms (Fig. 1.3); formation of crosslinks, mutations due to mismatch of nucleotides and DNA fragmentation due to the activity of DNA

repair enzymes, but they differ in their clinical efficacy (Ralhan & Kaur, 2007). Ultimately, steps leading to genetic material duplication (replication, transcription and base pairing) are significantly altered.

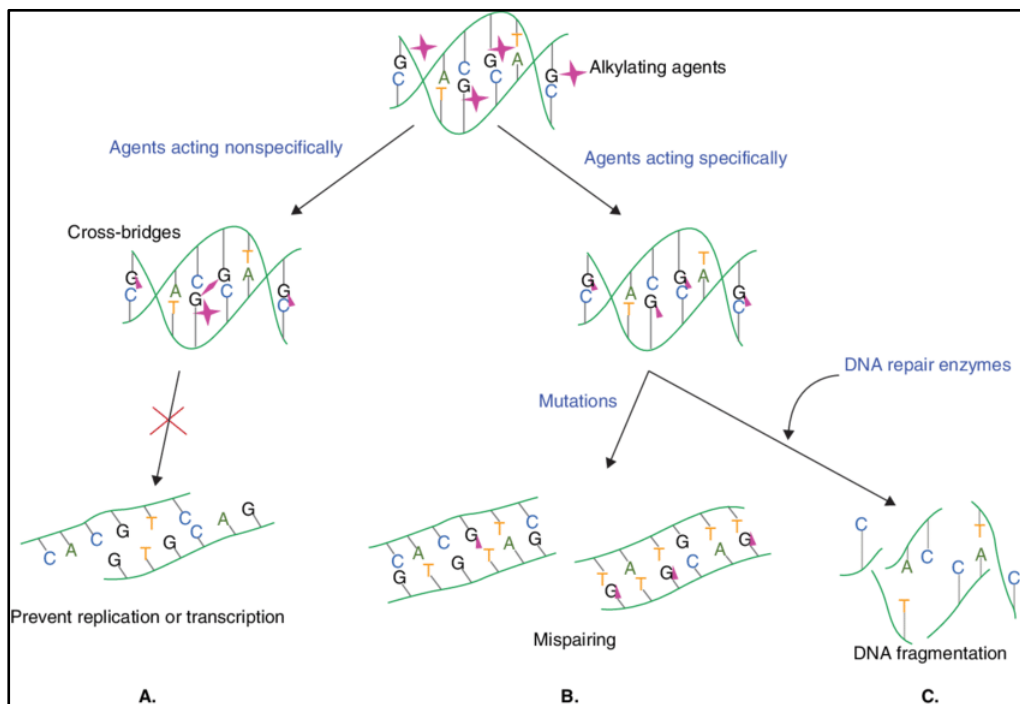


Figure 1. 3. Classical mechanisms of action of the alkylating agents. (A) Bi-functional alkylating agents form cross-bridges between atoms in two DNA strands resulting in prevention of strand separation, replication, and transcription. **(B)** Mono-alkylation of bases leading to mismatch can also cause permanent mutations if this is not repaired prior to replication. **(C)** DNA fragmentation might occur as a result of attempts to remove and replace alkylated bases by DNA repair enzymes. Taken from Ralhan & Kaur (2007) under the free creative common licence.

Alkylating agents attack the nucleophilic sites in DNA such as oxygen, nitrogen, phosphorous and sulphur atoms, either mono- or bi-functionally (e.g. nitrogen mustards, carmustine, platinum compounds, mitomycin and psoralen). Mono-functional agents possess only one reactive site which modify single bases (usually the N₇ of the purines adenine and guanine) causing bulky DNA adducts, whereas bi-functional alkylating agents have two independent reactive sites to cross-link with DNA bases, either residing within the same DNA strand (intrastrand) or opposite strands (interstrand) (Kondo *et al.*, 2010; Huang & Li, 2013; Noll *et al.*, 2006; Clauson *et al.*, 2013). Conversely, mono-functional agents can form base alkylation

(C_nH_{2n+1}) or methylation (CH_3) at any O- and N-atoms depending on the alkylating agent and whether the DNA is single or double stranded (Swift & Golsteyn, 2014).

The majority of nitrosoureas are mono-functional chloroethylating agents that add chloroethyl groups to the N^7 and O^6 of guanine. O^6 -chloroethylguanine adducts react with cytosine to generate guanine-cytosine interstrand crosslinks. Triazine compounds are mono-functional methylating agents linked to production of O^6 -methylguanine, are highly mutagenic and cytotoxic which accounts for <8% of the total DNA methyl adducts (Swift & Golsteyn, 2014; Kondo *et al.*, 2010). DNA polymerases frequently mis-pair O^6 -methylguanine with thymine which persists in the absence of the mismatch repair proteins leading to point mutation (Fig. 1.4). This leads to futile cycles of DNA repair and replication that eventually cause DNA single (SSB) and double strand breaks (DSB) (Swift & Golsteyn, 2014). Mono-alkylated bases can change the DNA code and depending on its position, can greatly alter protein production. This can lead to dysregulation of certain aspects of the cell leading to death or cancer (Georg & Weber, 2015; Kondo *et al.*, 2010). In contrast, the bi-functional agents are typically clastogenic rather than mutagenic and constitute an absolute block to DNA strand separation by crosslinking. They are extremely toxic because they affect both strands, leading to loss of template information. Blocking the replication machinery or DNA repair at interstrand crosslinks can lead to DSB, which can lead to insertions, deletions and chromosomal rearrangements if incorrectly repaired (Swift & Golsteyn, 2014; Georg & Weber, 2015; Huang & Li, 2013; Noll *et al.*, 2006). Alternatively, if the two modified bases are located in the same DNA strand, it leads to ‘limpet’ attachment of the drug molecule to the DNA (Ralhan & Kaur, 2007). Mono-alkylation and limpet attachment can also prevent the DNA replication fork and transcription by bending the DNA double helix but do not prevent the separation of the two DNA strands. They physically block the enzyme processing the DNA from accessing the bases, resulting in inhibition of cell growth or stimulation of apoptosis (cell suicide). However, comparative analysis of cross-linking agents’ genotoxicity showed *in vivo* TD50 (the total lifetime dose of carcinogen required to increase the probability of tumour formation to 50%) is 10- to 1000-fold less than mono-functional alkylating agents (Vogel *et al.*, 1996). Some natural metal derivatives, called platinum-based drugs are similar to alkylating agents due to similar crosslinking activity, yet they do not contain an alkyl group (Maltzman & Millar, 2012). Following the findings of the previous research group members (unpublished data), chlorambucil was focused on within this study.

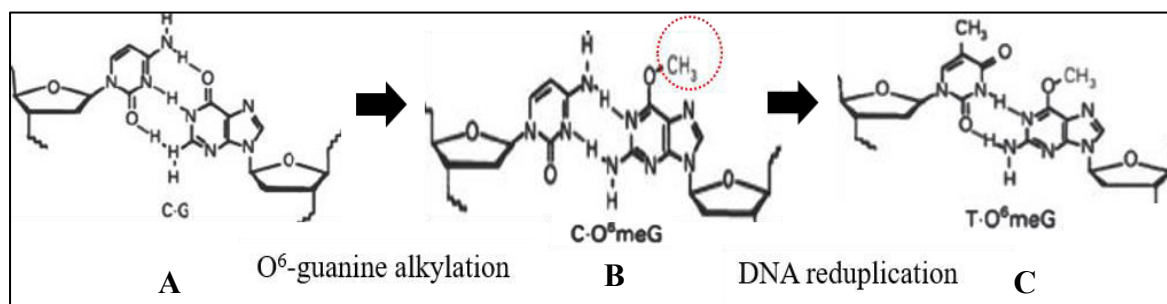


Figure 1. 4. DNA adducts caused by alkylating agents. Methylating the 6th oxygen on guanine results in O⁶-methylguanine (B). If it is left unrepaired, replication causes the base to be misread as an adenosine rather than a cytosine and paired with a thymine, resulting in T-O⁶MeG mismatch (C) or C-O⁶MeG ambiguous pair. In the next round of replication T-O⁶MeG becomes an A:T transition mutation and C-O⁶MeG may become T-O⁶MeG mismatch mutations. Adapted from Georg & Weber (2015) under the open access free common license.

1.2.1.1 Chlorambucil

Chlorambucil (CHL) is a bi-functional aromatic nitrogen mustard alkylating agent (Fig. 1.5A) and was developed in 1953 at the Chester Beatty Research Institute, England (Georg & Weber, 2015). This compound reacts through the formation of highly reactive ethyleniminium radicals which form interstrand cross-linkage between two DNA strands to interfere with RNA, DNA and protein synthesis. The electron withdrawing properties of the aromatic ring leads to slower reactions with serum and cellular constituents, therefore CHL is given orally in tablet form (Kondo *et al.*, 2010). Since it is the least toxic alkylating agent, it has been mainly used in the palliative treatment of CLL, Hodgkin/low-grade non-Hodgkin lymphoma, lymphosarcoma, giant follicular lymphoma and Waldenstrom's macroglobulinaemia (Noll *et al.*, 2006; Clauson *et al.*, 2013) but is replaced with fludarabine in paediatrics for the management of neural and BM toxicity (Huang & Li, 2013). CHL is usually given at 0.1–0.2 mg/kg/day for 3–6 weeks. The entire daily dose may be administered at one time. The pharmacokinetics of CHL demonstrates rapid and complete gastrointestinal absorption and blood clearance. After single oral doses, peak CHL levels in the blood are reached within 1 hour and the terminal elimination half-life is roughly 1.5 hours. The agent is extensively metabolised in the liver and bound to plasma and tissue proteins (99 %), specifically to albumin. Urinary excretion is below 1 % over 24 hours (Georg & Weber, 2015).

CHL forms covalent interstrand and intrastrand adducts through alkyl groups to nucleophilic groups in DNA. Within DNA and RNA, the most covalently targeted site is N⁷ guanosine to

form N⁷-alkylated guanine derivatives (Fig. 1.5). N⁷-alkylated guanines are to some extent unstable and can undergo a further reaction to create an abasic site in the DNA. It is apparent then that bi-functional alkylating agent reaction can lead to a variety of products of DNA (Huang & Li, 2013; Noll *et al.*, 2006). Other common DNA adducts are N¹, N³, N⁷ adenine and N³ cytosine, thus leading to DNA strand cross-linking, strand breaks and eventually cell death (Georg & Weber, 2015). CHL is typically a clastogenic agent that causes damage at the chromosomal level (gain, loss, rearrangement and sister chromatid exchanges) rather than at the DNA sequence level (Noll *et al.*, 2006; Clauson *et al.*, 2013). Cells have repair systems to remove these harmful lesions and thus preserve the integrity of their genomes. Intrastrand crosslinks can be readily removed by the nucleotide excision repair (NER) mechanism, whereas interstrand crosslinks are exceedingly genotoxic and cytotoxic DNA lesions, especially in dividing cells and require a combination of complex repair mechanisms (Drabløs *et al.*, 2004; Kondo *et al.*, 2010). Moreover, 20-40 unrepaired interstrand crosslinks could be fatal to mammalian cells (Noll *et al.*, 2006; Clauson *et al.*, 2013; Huang & Li, 2013). CHL engages in off-target alkylation due to poor DNA recognition properties, which make it carcinogenic and a risk for secondary malignancies (e.g. AML) (Georg & Weber, 2015). Secondary malignancies (e.g. TRL) refer to new cancers that develop in tissues or organs that were not originally affected by the primary cancer as a result of DNA damage in healthy cells induced by previous cancer treatments, e.g. chemotherapy and radiotherapy. Here, the second malignancy/ second primary malignancy refers to a new and independent cancer that develops in a person who has previously had cancer. These cancers are unrelated to the primary cancer and arise independently of each other due to different underlying causes. This is unlike secondary malignancies, which are not necessarily caused by cancer treatments but may arise due to shared risk factors, genetic predispositions (e.g., *BRCA* mutations), exposure to carcinogens, immune system dysfunction, or lifestyle factors (Eldridge, 2023).

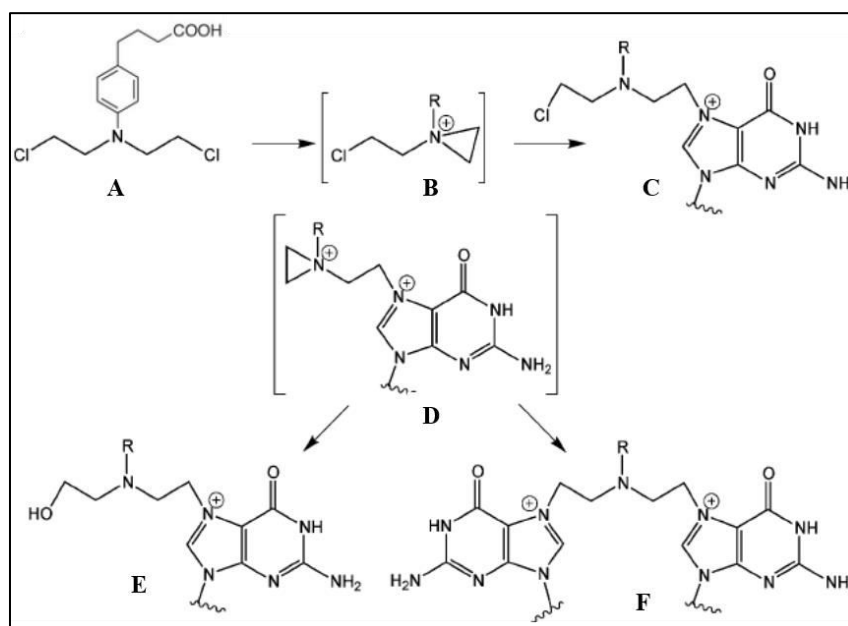


Figure 1. 5. DNA interstrand cross-link formation by chlorambucil ($C_{14}H_{19}Cl_2NO_2$), molar mass 304.212 g/mol. N=Nitrogen, Cl=Chlorine, O=Oxygen, R=Alkyl group. Chlorambucil reacts with guanine residues in DNA via the aziridinium intermediate (**B**) to form an N7-alkylated guanine derivative (**C**). This guanine mono-adduct can then form another reactive aziridinium intermediate (**D**), which can react either with water to form a 2-hydroxyethyl mono-adduct (**E**) or with a second guanine residue to form the interstrand cross-link (**F**). Copied from Noll *et al.* (2006) with copyright clearance license.

1.2.2 Mechanism of action of topoisomerase inhibitors

During vital cellular processes such as DNA replication, transcription, recombination and repair, topological constraints of DNA must be resolved in order to preserve the integrity of the genetic material. Topoisomerases are ubiquitous enzymes that control DNA supercoiling and entanglements by introducing transient SSB or DSB in DNA, thus being essential in maintaining the integrity and topology of DNA during replication and transcription processes (Maltzman & Millar, 2012; Rocha *et al.*, 2018; Kenneth, 2008; Nitiss, 2009).

In mammalian cells, there are key I-, and II-topoisomerases. Despite their differences in specificity, their catalytic mechanism is a common feature between the different types of enzymes. In all cases, this mechanism consists of a reversible nucleophilic attack of a DNA phosphodiester bond by a catalytic tyrosine residue from the topoisomerase to form phosphotyrosyl covalent bonds (Fig. 1.6B and E). Topo-I enzymes form a phosphotyrosyl bond at the 3' end of the break and cleave only one strand of DNA for catalysis to facilitate rotation

either side of the replication bubble, whereas topo-II removes knots and tangles and cleave both strands of DNA to overcome the entanglements or to avoid supercoiling by forming a phosphotyrosyl bond at the 5' end of the break. The intermediates formed in this process are commonly referred to as cleavable complexes (Nitiss, 2009; Binaschi *et al.*, 1995; Yves *et al.*, 2010; Maltzman & Millar, 2012; Swift & Golsteyn, 2014). Topo-II plays a vital role in transcription, replication and chromosomal segregation due to two isoforms α and β . Isoform α associates with replication forks mainly in G2/M and is essential for the survival during proliferation. However, isoform β is independent of proliferation and dissociates from chromosomes during mitosis (Rocha *et al.*, 2018).

A number of topoisomerase inhibitors have been proven to exhibit anticancer effects by stabilizing the cleavable complexes through specifically binding at the interface of topoisomerase-DNA complexes (Fig. 1.6C and F), hence preventing the DNA re-ligation, increasing cleavable complexes and inducing lethal strand breaks (Binaschi *et al.*, 1995; Kenneth, 2008; Yves *et al.*, 2010). Each of these drugs are able to stimulate DNA cleavage preferentially only at certain sites, but not at all sites recognized by the enzyme, thus suggesting that effective drug interactions in the ternary complex depend on the local base sequence (Binaschi *et al.*, 1995). Topo-I inhibitors first cause SSBs, which are converted to DSBs when they are met by a replication fork (Swift & Golsteyn, 2014). Currently available topo-I inhibitors include irinotecan and topotecan (Kenneth, 2008). Topo-II inhibitors are divided into two classes: the main and most widely clinically used class is topo-II poisons/drugs (e.g. doxorubicin, teniposide, daunorubicin and mitoxantrone) which lead to increased levels of topo II-DNA cleavage complexes and generate lethal lesions (SSB, DSB and covalently bound protein to DNA). Some poisons (e.g. etoposide) inhibit re-ligation of the DNA cleaved strands. The second class is presumed to act primarily by inhibiting the enzyme catalytic activity, preventing the enzyme attached to the DNA and are called topo-II catalytic inhibitors (Nitiss, 2009; Rocha *et al.*, 2016; Swift & Golsteyn, 2014). Following previous work within our research group (unpublished data), mitoxantrone was focused on in this study.

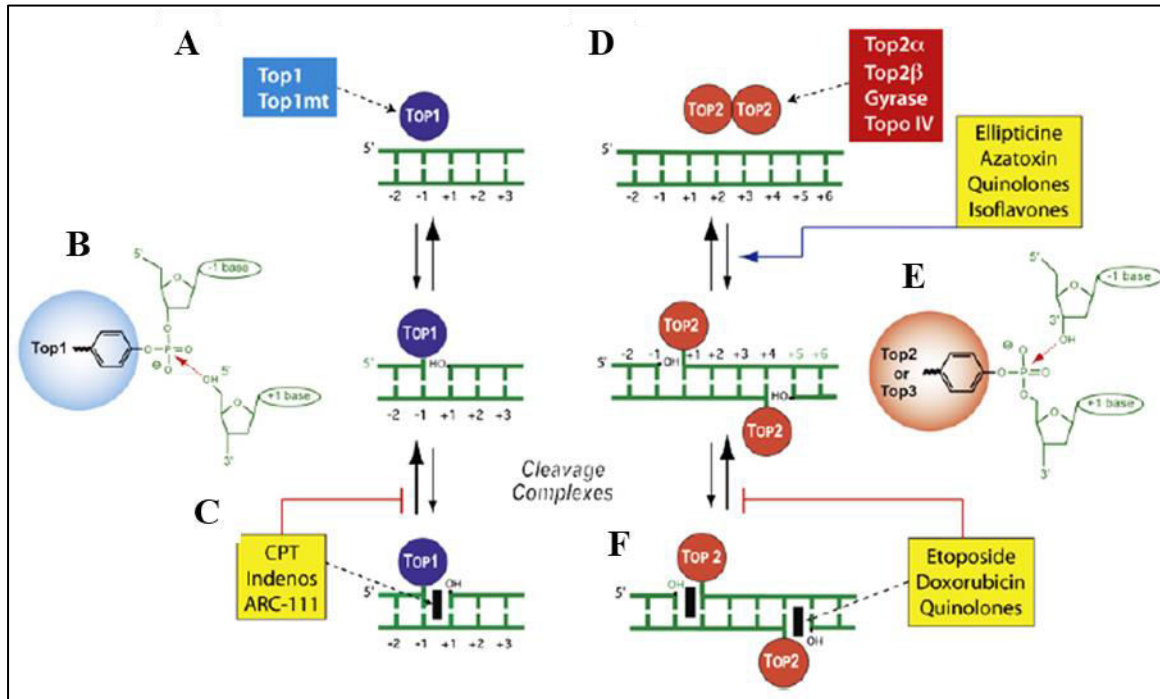


Figure 1.6. Mechanism of action of topoisomerase inhibitors. (A) Noncovalent binding of topoisomerase I enzyme. (B) Formation of 3'-phosphotyrosine covalent bond and cleavage of one strand of DNA segment. The arrow indicates the re-ligation reaction. (C) Trapping of the cleavage complex by camptothecin (CPT) and the topo-I inhibitors. (D) Noncovalent binding of topoisomerase II enzyme which act as homodimers to cleave both strands, (E) formation of a 5'-phosphotyrosine covalent bond to produce double strand breaks and inhibit the recombination process. The arrow indicates the re-ligation reaction. (F) Trapping of the cleavage complex by mitoxantrone, etoposide, doxorubicin, or quinolones. Some topoisomerase II poisons (ellipticines, azatoxin, quinolones and isoflavones) increase the cleavage by tightening the topoisomerase II complex with DNA. Adapted from Yves *et al.* (2010) with free creative common license.

The combination of alkylating agents with topoisomerase inhibitors have been claimed to be more effective in management and treatment of leukaemia and solid tumours including ovarian, lung, breast, colon and cervical cancer, whereas topoisomerase II inhibitors are used for lymphoma, testicular and lung cancer (Ralhan & Kaur, 2007; Kenneth, 2008; Evison *et al.*, 2016). The most important side effect of this drug group is cardiac toxicity (Maltzman & Millar, 2012). Secondary cancers have been reported in long term use of topoisomerase II inhibitors along with chromosome translocations t(9;11) (p21;q23) and several 11q23 breakpoints (Georg & Weber, 2015; Binaschi *et al.*, 1995). Topoisomerase generates transient SSB, and such lesions are converted into DSBs upon collision with replication forks, implying that DNA repair pathways could be involved in the repair of topoisomerase mediated DNA damage. Homologous recombination and non-homologous end joining (NHEJ) are the main pathways involved in the

removal of DSBs while NER is mainly characterised by the removal of lesions that lead to significant structural distortions in the DNA double helix. However, topo-II inhibitors induce other types of lesions, like DNA adducts, interstrand crosslinks and ROS (Ralhan & Kaur, 2007; Rocha *et al.*, 2018).

1.2.1.2 Mitoxantrone

Mitoxantrone (MTX) is a synthetic anthracenedione that resulted from a concerted effort in the late 1970s to develop a topoisomerase inhibitor with reduced cardiotoxicity and whose original structure maintained the planar polycyclic aromatic ring, and the diaminoalkyl groups which are crucial for the biological activity of these compounds (Fig. 1.7A) (Vollmer *et al.*, 2010; Parker *et al.*, 2004; Georg & Weber, 2015). It was approved by the FDA in 1996 for the treatment of prostate cancer and is used primarily as therapy for ALL, AML, melanoma, lymphoma and adult acute non-lymphocytic leukaemia, and is also second line therapy for breast and haematological malignancies (Kenneth, 2008; Evison *et al.*, 2016; Parker *et al.*, 2004). Even though MTX plays a valuable role in the treatment of relapsed or t-AML, its use as a frontline therapy is limited due to concerns regarding efficacy, cardiotoxicity, resistance, risk of secondary leukaemia, and the availability of alternative treatments. The dosage and timing of MTX is determined by the combination therapy regimen used. The recommended dose is 12–14 mg/m² for adults bearing solid tumours and is typically administered (every 3–4 weeks) via intravenous infusion, while 8-20 mg/m² for 5 days is given to acute leukaemia adults. The pharmacokinetics of MTX is characterized by a three-compartment distribution, with the mean α half-life being 5–15 minutes, the mean β half-life 1–3 hours, and the mean γ (terminal or elimination) half-life 1–10 days (median approximately 75 h) (Georg & Weber, 2015; Evison *et al.*, 2016).

MTX is extensively distributed to tissues and binds to endothelial surfaces and penetrates blood cells and tumour tissue. It is highly protein bound (78%) with a large volume of distribution 1000–4000 l/m² (Kenneth, 2008). The metabolites are composed of mono- and di-carboxylic acid derivatives (Georg & Weber, 2015). MTX appears to be excreted predominantly in the bile, ~11% within the urine and ~18% in the faeces either unchanged or in the form of inactive metabolites. MTX intercalates DNA forming a stabilized topo-II-DNA cleavable complex acting to exert its cytotoxic activity. This can generate strand breaks, DNA damage, and inhibition of DNA repair, which are critical signals for NF- κ B activation and induction of

apoptosis (Kenneth, 2008; Evison *et al.*, 2016). The effectiveness of MTX cancer treatment can be modulated by various mechanisms of action of the drug. Due to MTX's structure, it is able to intercalate between DNA bases, forming adducts, interstrand crosslinks and ROS (Fig. 1.7) besides acting as a topo-II poison (Parker *et al.*, 2004; Rocha *et al.*, 2018).

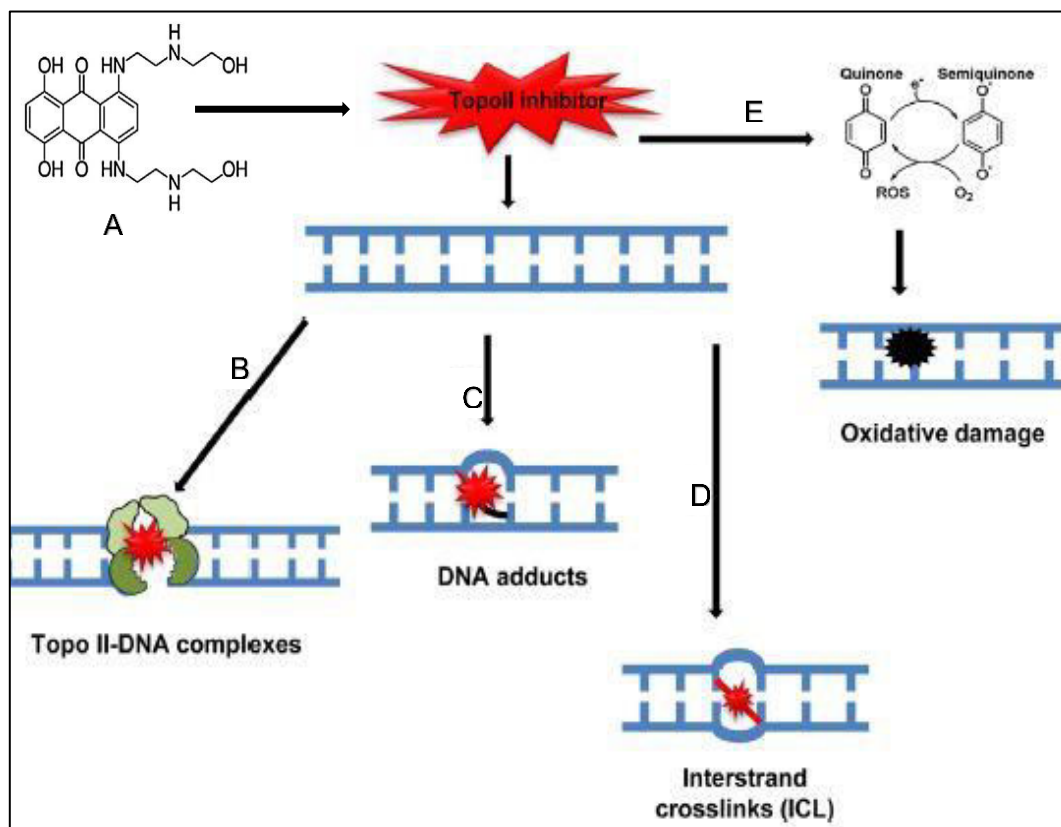


Figure 1. 7. Possible DNA lesions induced by mitoxantrone. (A) Mitoxantrone (C₂₂H₂₈N₄O₆), molar mass of 444.481 g/mol, O =Oxygen, N=Nitrogen, H=Hydrogen. **(B)** Topo-II-DNA stabilized complex induced by anthracyclines, mitoxantrone and etoposide. Anthracyclines and mitoxantrone can intercalate into DNA and be activated to form DNA-adducts **(C)** or interstrand crosslinks **(D)**. **(E)** Reactive oxygen species can be formed via enzymatic reduction of the quinone moiety of anthracyclines and mitoxantrone to a semiquinone, and subsequently can induce oxidative DNA damage. Adapted from Rocha *et al.*, (2016) under free creative license.

Further studies suggest the oxidation of MTX into an active metabolite (naphthoquinoxaline) that covalently binds RNA, thereby contributing to its cytotoxic effect (Parker *et al.*, 2004). This novel electrophilic metabolite is susceptible to intramolecular nucleophilic attack or may covalently interact with cellular nucleophiles (e.g. glutathione, DNA) (Evison *et al.*, 2016). MTX also produces immunosuppression by inhibiting B-cells, T-cells and monocytes, induces

apoptosis of dendritic cells, and decreases the secretion of the proinflammatory cytokines IL-2, TNF- α , and IFN- γ (Vollmer *et al.*, 2010). MTX hydrochloride, which was initially approved for the treatment of AML in 1987, intercalates into and cross-links DNA, thereby disrupting DNA reduplication and RNA synthesis (Evison *et al.*, 2016; Georg & Weber, 2015). High risk of secondary malignancies from drug-induced translocations (e.g. therapy related acute leukaemia, MDS) is an important side effect of MTX (Rocha *et al.*, 2018).

1.3 Haematopoietic stem cell transplantation

Haematopoietic stem cell transplantation (HSCT) in most cases is considered the only potentially curative option for haematological malignancies that may be incurable with conventional therapy, but there are clinical trials for HSCT in non-haematological disorders (Catacchio *et al.*, 2013). A record number of 40829 HSCT in 36469 patients (allogeneic 43%, autologous 57%) were reported by 656 centres in 47 countries to the 2014 survey by the European Society for Blood and Marrow Transplantation (Passweg *et al.*, 2016). Not surprisingly, the outcome of HSCT depends on many patient factors (age, comorbidities), disease factors (diagnosis, disease stage, prior therapy), donor factors (human leukocyte antigen [HLA], gender match) and transplantation factors (conditioning regimen, stem cell source, graft-versus-host disease: GvHD prophylaxis). HSCT consists of three stages of ‘therapy’; a conditioning phase, stem cell infusion and GvHD prophylaxis, the latter of which can be achieved through immunosuppressive medications or graft manipulation (T-cell depletion) (Antin & Raley, 2013).

Transplantation is performed after maximal reduction of leukaemic cells in the BM by conditioning regimens consisting of combinations of chemotherapy, total body irradiation and immunotherapy (Sweeney & Vyas, 2019). Conditioning regimens can vary considerably in intensity, ranging from high dose regimens that result in complete ablation of BM to reduced intensity regimens that cause milder myelotoxicity/myelosuppression (Antin & Raley, 2013). Intensive conditioning clears the BM of both the leukaemic clones as well as the entire blood system; this process is named ‘myeloablative’ and includes high dose chemotherapy/radiotherapy to achieve as deep a remission as possible. This can only be performed in relatively young patients in excellent general medical condition. Increased conditioning intensity may decrease relapse rates but usually increases non-relapse morbidity and mortality (Champlin, 2013). Unfortunately, myeloablation is prohibitively toxic for older

patients and more likely to have high risk cytogenetic abnormalities, severe early GvHD, as well as age itself conferring a poorer prognosis. This led to the development of reduced-intensity, non-myeloablative or 'mini' transplants that can be applied for diseases in remission or less severe cases but has largely revolutionised the treatment of the elderly patients and/or sicker patients which make up the major proportion of leukaemic patients.

Depletion of the leukaemia using chemotherapy can also lead to depletion of the haematopoietic stem cells (HSC) compartment of the BM, so replacement with donor stem cells is required to reconstitute normal haematopoietic and immune cells. Stem cells are primitive somatic cells with the capacity to self-renew (give rise to one/two daughter stem cells) and differentiate (develop into mature specialized cells). HSCs utilised for HSCT, can be obtained from bone marrow (BM), mobilised into the peripheral blood (PB) or collected from umbilical cord blood (UCB). BM-HSC samples are obtained by multiple needle aspirations from the iliac crest or sternum while the donor is under general anaesthetic and placed in a sterile container with anticoagulant and electrolyte solution. Cell suspension will be processed by passing through sterile filters to remove fat, bone particles and cellular debris before administered to the recipient intravenously. HSC migrate to the marrow within the recipient, where they adhere, expand, self-renew and differentiate into new blood cells which finally are released into the blood, restoring blood counts and immunity (Champlin, 2013). High dose of immunosuppression is administered early post-transplantation, which depletes allo-reactive T cells derived from the host and donor (Sweeney & Vyas, 2019). HSC can be stored in the refrigerator (<24 hr), vapour phase of liquid nitrogen (>48 hr) or liquid nitrogen (~10 years) depending on the infusion time required. Engraftment is defined as an absolute neutrophil count which is dependent on the used GvHD prophylaxis (Antin & Raley, 2013).

PB-HSC recover faster than BM-HSC, whereas UCB-HSC tends to be the slowest to engraft. PB-HSC is more commonly used for haematological malignancy due to potent graft versus malignancy/graft versus leukaemia (GvL) effect and the avoidance of anaesthetic risks. PB-HSC is collected by a leukapheresis procedure, usually after recombinant growth factor (granulocyte colony-stimulating factor: G-CSF/ granulocyte-macrophage colony-stimulating factor: GM-CSF) and chemotherapy administration (Antin & Raley, 2013; Catacchio *et al.*, 2013). Consequently, cell preparation that is infused back into patients is not pure HSCs, but a mixture of HSCs, progenitors, T cells and in the case of autologous transplants, quite possibly tumour cells as well. Highly purified HSCs as a graft is rare and it is labour and cost-effective

(Catacchio *et al.*, 2013). UCB-HSC obtained following infant delivery are then processed using 170- to 260-micron filters (removes red cells and plasma) immediately or within 48 hours of collection; cells are then infused or cryopreserved. UCB-HSC are used mainly for unrelated allogeneic HSCT, particularly in children, owing to a single cord blood unit transplant causing delayed engraftment in adults (>40 kg) due to a significantly lower haematopoietic progenitor count in UCB ($\sim 5 \times 10^6$) compared to other HSC sources (roughly 1×10^8) (Catacchio *et al.*, 2013). A combination of two cord units may be used but can cause higher rates of acute GvHD (Sweeney & Vyas, 2019; Antin & Raley, 2013).

The two distinct HSCT types are autologous (self-donation) and allogeneic (non-self-donation). The advantages of autologous transplantation are low complication risk (no GvHD), and no requirement of HLA matching or immunosuppression. It is mainly used to treat lymphoma and multiple myeloma, but is less commonly used for leukaemia, due to concern of reinfusion of occult tumour cells causing a higher risk of relapse. However, there is no GvL effect in auto-HSCT. Allogeneic transplantation uses stem cells from preferably fully matched donors (family member or HLA/ABO compatible unrelated donor), but HLA mismatch and/or other genetic incompatibility can lead to complications, such as GvHD and rejection, but survival from GvHD results in a low relapse risk (Sweeney & Vyas, 2019). The first allo-HSCT was reported by Thomas *et al.* (1957) and has been the most common and most effective cellular immunotherapy for myeloid malignancy. Conversely, allo-HSCT has dual tumour killing mechanisms; cytotoxicity from the conditioning regimen and the most important effect is alloreactivity of donor-derived immune system (T and B cells, NK) cells that can effect an immunologic attack against any mismatched minor histocompatibility antigens or antigens on leukaemic cells to create a GvL effect. For these reasons the use of tissue type matched, but non-identical siblings is generally the preferred choice for HSCT treatment of leukaemia (Sweeney & Vyas, 2019; Antin & Raley, 2013).

However, the recognition of a GvL effect in disease eradication led to the development of reduced-intensity conditioning/ non-myeloablative HSCT in older or medically infirm patients who are not eligible for myeloablation (Champlin, 2013). This approach is designed not to have direct antitumour activity, but rather to provide both sufficient host immunosuppression and a GvL effect through creating a 'mixed chimerism' between the host and donor lymphocytes. The consequent immune response resulting from the (non-HLA) genetic mismatches is tipped in favour of the donor cells, by chasing the HSCT with donor leukocyte infusions and this

promotes the GvL effect to kill the leukaemia. Adverse cytogenetic and molecular abnormalities are associated with a higher relapse rate, but disease-free survival exceeds that with standard chemotherapy (Champlin, 2013). This type of transplantation is most appropriate either for diseases in remission (e.g. AML) or for diseases that tend to be more indolent (e.g. CLL, follicular lymphoma, myelofibrosis) (Sweeney & Vyas, 2019; Antin & Raley, 2013). Nevertheless, GvHD is strongly associated with a GvL effect in CML and ALL, with GvL effect inferred from post-transplant relapse rates. In contrast, there is a weaker correlation between the GvL effect and GvHD in AML and MDS, suggesting that some mechanisms of GvL may be distinct from GvHD (Sweeney & Vyas, 2019).

However, immunoediting of tumour cells has been shown to lead to immune escape, evading the GvL response and subsequent relapse. AML may relapse post-transplant due to the rapid proliferation overwhelming the protective GvL response. Donor lymphocyte infusion is an effective cellular therapy to induce GvL effects in relapsed allo-HSCT or for failing donor chimerism even after non-myeloablative therapy (Sweeney & Vyas, 2019).

1.4 Post transplant complications

Chemotherapy was originally thought to ‘target’ cancers, but it also targets other dividing normal cells through damaging DNA, thereby resulting in many side-effects as described in section 1.2. Depending on the chemical composition of chemotherapy, the side-effects may also differ. Hair loss, skin rashes, fatigue, diarrhoea and infections are usual side-effects, while there are also rare and spontaneous complications after chemotherapy, immunosuppression or the leukaemia itself, such as tumour lysis syndrome (Davis *et al.*, 2014). Although HSCT is considered as the only curative therapy and last approach for most malignancies, it is a life-threatening treatment due to multiple complications. It is critical to have a solid understanding of the entire course of HSCT complications with consideration of mitigating factors including transplant type (autologous or allogeneic), stem cell source (BM, PB, UCB), donor match (related or unrelated, matched or mismatched), interval post-HSCT (early or late), GvHD prophylaxis, infectious prophylaxis, immune suppressive medications and conditioning regimen (ablative or non-myeloablative). However, these effects can be recognised as either common early complications or long-term severe complications. The time course is generally thought of as early – first 30 days, mid – day 15 to ~100 and late >100 days. There is often an overlap in timing of complications (Antin & Raley, 2013).

Most often, the recipient's cellular and humoral immunity is usually destroyed after myeloablative therapy leading to the most common early complications including infection, engraftment syndrome, GvHD, graft rejection and failure (Pokharel, 2012). Acute GvHD occurs when donor T cells recognise host antigens as foreign, resulting in T-cell stimulation and effector cell response (cytokine secretion, cytotoxic T cells, NK cells). Damaged tissue from the conditioning regimen, releases higher levels of inflammatory cytokines such as IFN- γ , IL-1, IL-6 and TNF- α which leads to 'cytokine storm' following cancer treatments, which will be discussed in more detail in section 1.6.2.1, section 4.1 and section 6.1. Mostly these patients are highly susceptible to life-threatening infection (*Neisseria meningitides*, *Haemophilus influenzae*, *Streptococcus pneumoniae*). Graft rejection is uncommon but occurs frequently in aplastic anaemia and occasionally in non-myeloablative transplantation (Antin & Raley, 2013; Sweeney & Vyas, 2019). Even though HSCT has been a very successful treatment, relapse of the original disease remains a problem in many cases (Walshauer *et al.*, 2014). A number of factors appears to influence the incidence of relapse including the stage of disease, conditioning regimen and GvHD prophylaxis. All of these relapses are a reflection of the original disease (McCann & Wright, 2003). Subsequently, long-term severe complications of HSCT include the relapse of leukaemia, development of secondary malignancies such as TRL and an entirely new form of malignancy, which may be host derived or leukaemia of transplanted donor cell origin (donor cell leukaemia; DCL) (Wiseman, 2011) which will be discussed in detail in the section 1.5.

In general, most chemotherapies are "genotoxic"; they directly or indirectly damage DNA, which is the precursor event to mutation and affects the cancer cell's ability to proliferate, leading to cell apoptosis and possible remission (Swift & Golsteyn, 2014). Whilst this DNA damage can be beneficial in therapy, due to impaired ability to detoxify chemotherapeutic drugs or repair drug-induced genetic damage caused by genetic polymorphisms in enzymes, these chemotherapies have been shown to lead to TRL, which has been highly associated with alkylating agents and topoisomerase inhibitors (Candelaria & Dueñas-Gonzalez, 2015; Baehring & Marks, 2012). Epidemiologic studies reported increased risks of secondary leukaemia after treatment with alkylating agents (3 to 8 years) including busulphan, chlorambucil, cyclophosphamide and topoisomerase II inhibitors (2 to 3 years) (Leone *et al.*, 1999). TRL may represent a model of leukaemogenesis for *de novo* leukaemia as it shares cytogenetic aberrations. Some of these may likewise represent incidental cases of MDS and

AML *de novo*; others may later turn out as recurrent but rarer cytogenetic abnormalities of therapy-related myeloid neoplasm (t-MDS and t-AML) (Pedersen-Bjergaard *et al.*, 2002). Clinical observations clearly indicate that administration of interstrand crosslinking drugs have a leukaemogenic effect, particularly exhibiting a high risk of haematopoietic malignancies, including therapy-related myeloid neoplasms (Candelaria & Dueñas-Gonzalez, 2015; Huang & Li, 2013).

Indeed, alkylators and topo-II inhibitors are two major distinct patterns of cytotoxic drugs associated with the risk of TRL (Wiseman, 2011). Roughly 10% and 20% of cases of AML and MDS are therapy related. Approximately 2/3 of TRL patients will present with clonal abnormalities including chromosomes 5, 7 13q-, der (17p) and -18 (Candelaria & Dueñas-Gonzalez, 2015). Deletions or loss of chromosomes 5 and 7 are present in 43%–87% of cases and closely associated with patients treated with alkylating agents (Baehring & Marks, 2012). Fotemustine, an alkylating drug, showed genotoxicity on *in vitro* cultured lymphocytes with chromosomal aberrations and sister chromatid exchanges (SCEs) (Celikler *et al.*, 2006). Defects of the long arm of chromosome 5 is the second most common cytogenetic abnormality of t-MDS/t-AML after alkylating agents therapy (Pedersen-Bjergaard *et al.*, 2002). Subsequently, a variety of balanced translocations such as t(9;11), t(19;11) or t(4;11) in t-MDS and t-AML were significantly related to therapy with topo-II inhibitors (Candelaria & Dueñas-Gonzalez, 2015; Wiseman, 2011; Leone *et al.*, 1999). Long-term use of immunosuppressive agents or G-CSF treatments are also risk factors for the development of TRL (Ma & Liu, 2016).

As opposed to actual relapse, many donor cell-derived leukaemias occur as an entirely new form of the disease. This phenomenon provides an insight into deciphering the mechanisms involved in leukaemogenesis of donor origin, which often present as more severe and aggressive than *de novo* leukaemia (McCann & Wright, 2003). This donor cell derived neoplasm has gained wider attention in the past decade, as its aetiology and pathogenic mechanism remains unexplained (Wiseman, 2011; Walshauer *et al.*, 2014).

1.5 Donor cell leukaemia

1.5.1 Clinical manifestation and epidemiology

Post-transplantation relapse was originally thought a re-enactment of primary disease due to therapy evasion and was frequently seen with varied incidence depending on the type of primary neoplasm (Wang *et al.*, 2011). Occasionally, relapses may display different phenotypic or cytogenetic features from the original disease. This may be because of a lineage switch (myeloid to lymphoid blast crisis), clonal evolution or emergence of latent surviving sub-clones but usually the relapse clone is host (patient) derived (Wiseman, 2011). However, Fialkow *et al.* (1971) described a 16-year-old acute lymphoblastic leukaemia female patient who relapsed following HSCT from her matched brother and the leukaemic clones were observed to be Y chromosome positive. This was the first description of the relatively rare *de novo* haematological malignancy called DCL which is genetically proven to be of donor cell origin, that develops in a recipient following transplantation of “healthy” donor cells. This intriguing entity is the subject of considerable interest for the unique insights into the mechanisms of leukaemogenesis it might provide (Wiseman, 2011). DCL appears to represent a heterogeneous cohort, with characteristics and transplant details broadly reflecting those for the general HSCT population. Common symptoms of DCL include anaemia, neutropenia and thrombocytopenia (Wang *et al.*, 2011). The paucity of reported cases suggested it to be a rare phenomenon because prior to current molecular biology testing, it may have frequently been mistaken for relapse and /or under-diagnosed (e.g. in sex-matched cases) (Wiseman, 2011; Cetin *et al.*, 2006), as well as the uncertainty of the neoplastic origin such as cases without clonal cytogenetic abnormality and overt leukaemia (McCann & Wright, 2003; Wang *et al.*, 2011). However, the recognition of sex-mismatched transplant cases demonstrating donor cell origin made investigators aware of DCL and thus formed the basis for the genetic determination of cell origin following SCT complication (Sala-Torra & Loeb, 2011; Ruiz-Argüelles *et al.*, 2007).

For many years, efforts to estimate the incidence of DCL have been hampered by the sporadic nature of reports and habitual difficulties in confirming the diagnosis. Overall rates of DCL are difficult to estimate but enhanced cytogenetic and molecular diagnostics of donor/host chimerism facilitate the identification and awareness of this rare entity, suggesting that DCL is more common than first thought (Majzner *et al.*, 2017; Ma & Liu, 2016; Wang *et al.*, 2011). About 6.6% of all post-HSCT relapses are considered to be DCL; remarkably >60 cases have

been reported by Wiseman (2011). Hertenstein *et al.* (2005) described 14 cases of DCL among 10489 allogeneic stem cell transplants in Europe, an estimated incidence of 124 DCL per 100,000 transplants. The largest DCL study to date was in Japan, where 40 DCL cases were identified after 2 years of 36,870 allogeneic BM transplantations with a higher incidence after UCB and in older donors (Kato *et al.*, 2016). The diagnosis of the majority of DCL manifest as AML (50%), ALL (23%) and MDS (20%) (Suárez-González *et al.*, 2018; Cetin *et al.*, 2006; Sala-Torra & Loeb, 2011). Other types of donor cell neoplasms have been reported including, multiple myeloma, gingival squamous cell carcinoma, B-cell immunoblastic sarcoma and granulocytic sarcoma. Very rarely DCL has been reported in recipients of solid organ transplants: donor-derived acute promyelocytic leukaemia after a liver transplant and IgA myeloma 7 years after a renal transplant (Walshauer *et al.*, 2014).

Incidence and diagnosis of DCL depends on the source of the HSC. Until 2005, the predominance of DCL was exclusively in allogeneic BM-HSCT, possibly due to differences in repopulation capacity and the response of replicative stresses (Flynn & Kaufman, 2007). However, there have now been more DCL cases reported with all stem cell sources including PB and UCB transplant recipients, from both related and unrelated donors, as well as after both myeloablative or non-myeloablative regimens, but there are still not enough data to draw definite incidence of these cases (Flynn & Kaufman, 2007, Majzner *et al.*, 2017). HSC source leading to DCL has been reported to be BM 70%, PB 24% and UCB 6% and details of conditioning regimens were 89% of myeloablative and 11% of non-myeloablative following HSCT (Wiseman, 2011; Cetin *et al.*, 2006). Surprisingly, some have observed higher DCL cases in HSCT-UCB than other cell sources, which may be due to more immunologically naïve cells and lower stem cell doses affecting immune reconstitution after HSCT and decreasing the immune surveillance in the transplanted patient (Suárez-González *et al.*, 2018).

DCL develops with a shorter latency period following malignant transplantation, than for benign conditions (Sala-Torra & Loeb, 2011). The latency period of DCL has been reported to range between 1 to 193 months (Ma & Liu, 2016), 2 to 164 (Ruiz-Argüelles *et al.*, 2007) and 4 to 164 months (Hertenstein *et al.*, 2005). It is noteworthy that most cases appeared in the first 30 months after transplantation (Ruiz-Argüelles *et al.*, 2007; Hertenstein *et al.*, 2005). However, the DCL diagnosis median time was statistically significant between UCB (15 months) vs PB (24 months) or BM (36 months) (Suárez-González *et al.*, 2018). In contrast, some exhibit slower DCL development following UCB-HSCT, which may be related to the

increased replicative stress and lower cell dose during engraftment and marrow regeneration (Sala-Torra & Loeb, 2011; Flynn & Kaufman, 2007; Wang *et al.*, 2011).

Suárez-González *et al.*, (2018) revealed that DCL mortalities were majorly due to severe cell depletion following chemotherapy or sepsis and other complications of HSCT. The median survival time of patients who succumb to the disease is 5.5 months following DCL diagnosis and the mean overall survival time for treated patients is 32.8 months. The median recipient age at primary transplantation of developing DCL was around 31-32 years old. Children appear to develop DCL more quickly than adults, although the reasons are unknown (Suárez-González *et al.*, 2018; Wiseman, 2011). So far, no significant sexual preponderance has been reported between donor and recipient, but gender mismatched DCL cases represented ~60% of cases (Suárez-González *et al.*, 2018). Intuitively, donor age might influence the risk of DCL. According to Suárez-González *et al.* (2018), the most frequent DCL donor type is matched related (59%) and in HSCT-UCB matched unrelated (9%), mismatched related (6.5%), mismatched unrelated (3%) and haploidentical (1.5%). The median donor age was 22.0 years in 17 of the 60 reports and donors were older than recipients in 9/16 cases (Wiseman, 2011; Ma & Liu, 2016).

1.5.2 Hypothesis of the aetiology of DCL

Based on the limited data available, any discussion regarding the mechanisms underlying donor cell transformation must be approached with caution, as it largely remains speculative. The diverse nature of documented cases prevents the identification of a singular mechanism or overarching hypothesis. Current literature has proposed various theories on the aetiology of DCL, representing a unique and scientifically intriguing model of leukaemia development (Fig. 1.8) (Wiseman, 2011). In this model, normal cells undergo oncogenic transformation within a previously diseased microenvironment. The oncogenesis of DCL likely involves a complex interplay of multiple factors, including both recipient and/or donor-related influences. These factors encompass a range of possibilities such as traditional effects, aberrant BM microenvironment, chemotherapy effects, impaired immune system, and viral integrations (Ma & Liu, 2016; Sala-Torra & Loeb, 2011). These putative theories are categorized as intrinsic features inherent in the donor stem cells and extrinsic factors provided by the regenerating marrow environment. However, existing research on DCL suggests that it is not solely attributable to one factor within the donor stem cells. Instead, it appears to involve the

convergence of multiple factors, possibly from the aforementioned list, thereby supporting a multi-hit theory in the development of DCL (Wiseman, 2011; McCann & Wright, 2003).

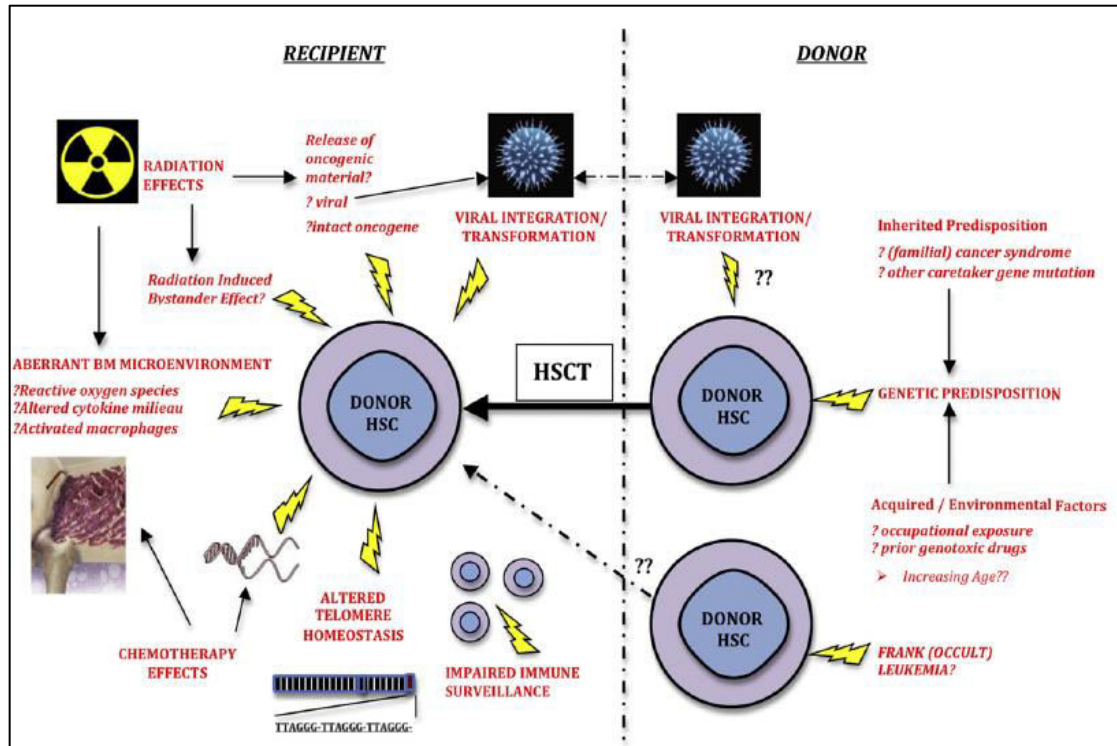


Figure 1. 8. Proposed aetiological factors influencing the development of DCL. A “multiple hit” hypothesis has been proposed, with DCL probably the convergent endpoint of numerous distinct pathways. Several mechanisms have been suggested to contribute critical “hits” for leukemogenesis. Donor genetic factors (occult leukaemia), recipient factors (impaired immune surveillance, viral transfection), therapy-specific factors (chemotherapy & radiation) and recipient bone marrow environment (reactive oxygen species; ROS & Cytokines). This figure is credited to Wiseman (2011) under the creative common license copyright.

1.5.2.1 Intrinsic donor factors

Genetic factors seem to play an important role in the development of DCL as most cases have been in the setting of an HLA-matched allo-HSCT (Cetin *et al.*, 2006). The most simplistic explanation is that the graft harboured an occult malignancy that is below the threshold of current screening at time of donation and over time develops into overt leukaemia (Walshauser *et al.*, 2014). Studies using whole-exome sequencing have shown that premalignant clones are present in up to 10% of people over 65 and 1% of those younger than 50, but they often remain silent over long periods of time (Majzner *et al.*, 2017).

Persistent antigenic stimulation of donor lymphoid cells, resulting from minor histocompatibility disparities between the host and donor, is proposed as a potential mechanism for lymphoid DCL development. In authentic DCL cases, it is crucial to unequivocally demonstrate the donor's sustained health during long-term follow-up (Ruiz-Argüelles *et al.*, 2007). This requirement underscores the possibility of an inherited or acquired predisposed donor clone evolving independently, acquiring additional influences from the post-transplant immunologic milieu, and transforming into leukaemia upon engraftment in an allogeneic environment (Sala-Torra & Loeb, 2011; Walshauer *et al.*, 2014).

Dickson *et al.* (2014) reported a DCL case emerging 14 years post-HSCT with trisomy 11 detected by FISH in both patient and donor peripheral blood at relapse. Despite the donor's continued good health, the explanation posited is that the initial hit in leukaemogenesis could occur in the donor, with subsequent 'hits' missing. Upon transplantation, donor cells encounter a milieu rich in extrinsic leukaemogenic factors, triggering malignant transformation. In instances where the underlying disease was a haematological neoplasia, the recipient's haematopoietic environment has already previously proven to be capable of triggering or facilitating malignant transformation (Ruiz-Argüelles *et al.*, 2007).

1.5.2.2 Host Extrinsic factors

Viral transfection/integration; The notion of a leukaemogenic virus has always been attractive. Viruses could be involved in transforming donated cells or promoting fusion of donor cells with residual leukaemic clones; the best-known example of post-transplant lymphoproliferative disorder (PTLD) in donor cells. In the HSCT setting, PTLD frequently occurs in donor cells and is not commonly classified as DCL but may provide clues into the development of DCL (Wiseman, 2011; Sala-Torra & Loeb, 2011).

Oncogenic activation; viral integration and transformation of the new donor cells in an impaired host immune system may contribute to oncogenic transformation. Some dominant oncogenes might be released by conditioning from residual leukaemia cells and directly transfect the genome of donor HSC (Sala-Torra & Loeb, 2011; Wiseman, 2011; Cetin *et al.*, 2006).

Impaired immune surveillance; Development of DCL may be the result of impaired immune surveillance and an acquired translocation due to immunosuppressant medications in HSCT.

The latter may spontaneously arise in a clone or may be induced by the impaired stem cell niche, disrupting the regulation of stem cell functions (Ma & Liu, 2016). Additionally, dysfunction of antigen-presenting cells, notably dendritic cells, persists post-transplant (Wiseman, 2011; Ruiz-Argüelles *et al.*, 2007).

Telomere shortening and replicative stress; Telomere shortening has been suggested to play a role in DCL induction (Wiseman, 2011; Cetin *et al.*, 2006). Interestingly, UCB recipients have significantly longer telomeres compared to PB-HSCT and it has been hypothesised that UCB-HSCT may provide the replicative reserve potential and a delay in the onset of haematologic disorders (Pipes *et al.*, 2006).

Residual effects of cancer therapy and bystander effect; Residual effects of therapeutic irradiation and conditioning has been linked to DCL leukaemogenesis via several mechanisms (Ruiz-Argüelles *et al.*, 2007; Cetin *et al.*, 2006; Walshouser *et al.*, 2014). Researchers hypothesised that radiation might have an enhancing effect on both oncogenic viruses, and materials might be physically released from BM cells by radiation damage and transfect into DNA of donor HSC. Although delayed HSC infusion intends to prevent direct exposure to genotoxic effects, engrafted HSCs might conceivably be exposed to previously administered chemotherapy either directly or via bystander effect (BE) via stromal elements within the patient (Wiseman, 2011). Both radiotherapy and chemotherapy can induce BE known as radiotherapy induce bystander effect (RIBE) and CIBE this will be discussed in more detail in section 1.6.3.

Defective marrow stroma/microenvironment; A compromised marrow stroma or microenvironment refers to a collection of cells and their products, encompassing extracellular growth factors, cytokines, and chemokines, capable of influencing target cell function (Barcellos-Hoff *et al.*, 2005). Following multiple rounds of chemotherapy, radiation, and subsequent immunosuppression, the microenvironment exhibits damaged niche structures, disrupting BM homeostasis. This disruption leads to alterations in cytokine production types and levels, triggering a cytokine storm (section 1.6.2.1, 4.1 and 6.1) and shows disturbances in the crosstalk between the niche and the HSC; all of which could contribute to leukaemogenesis (Suárez-González *et al.*, 2018). Therapy-induced damage to the microenvironment could support leukaemic transformation in the donor cells as has been shown in mouse models (Cetin *et al.*, 2006). These data may suggest that the intensive therapy exposure to the BM

microenvironment might trigger release of key soluble mediators such as ROS, RNS and mainly cytokines, which may alter the overall growth and phenotypic characteristics of non-treated donor stem cells and contribute to leukaemogenic potential and DCL. These observations reflect cell communication through secreted factors, supporting the idea that cytokines may play a role in CIBE and possibly in DCL.

1.5.3 Diagnosis and treatments of DCL

Diagnosis of DCL depends on accurate and unequivocal detection of donor derivation of the leukaemic clone (Flynn & Kaufman, 2007). Prior to the advent of molecular techniques, successful engraftment was detected by analysis of differences between sex-matched donor and recipient accessible to immunological or biochemical techniques. Such markers were erythrocyte antigens, leukocyte isozymes, immunoglobulin allotypes and red cell phenotypes among others (Ruiz-Argüelles *et al.*, 2007). No consistent pattern of cytogenetic abnormality is apparent among the reported cases of DCL; almost half are associated with a normal karyotype and the remainder include a heterogeneous mix of complex karyotypes including deletions, balanced or unbalanced chromosomal translocations, chromosome gains/losses with frequent cytogenetic alterations including whole or partial loss of chromosome 5/7 and rearrangement of the 11q23 locus containing the *MLL* gene (Suárez-González *et al.*, 2018; Flynn & Kaufman, 2007). Interestingly more than half of DCL cases showed a similar cytogenetic profile occurred in both t-AML and t-MDS, most commonly complete or long arm deletion of chromosome 7 together with anomalies of chromosome 5 or complex karyotypes (Ma & Liu, 2016; Wiseman, 2011, Leone *et al.*, 1999).

DCL was initially detected in cases of sex-mismatched transplants, and diagnosis relied on cytogenetic studies, particularly the detection of Y chromosome absence or presence. In sex-matched cases, monitoring of chimeric engraftment in the regenerating marrow is by polymerase chain reaction (PCR) amplification of tandem repeat sequences targeting variable number of tandem repeats (VNTRs) or short tandem repeats (STRs). These polymorphic stretches of DNA provide a sensitive marker for detecting a minor clone of residual host cells in a background of donor-derived marrow (Cetin *et al.*, 2006). Currently, a number of reliable molecular methods are available to confirm the sex-mismatched origin of donor cells, including FISH, restriction fragment length polymorphism (RFLP), YCS-PCR for detecting Y chromosome specific sequences, mini-satellite or (VNTRs), single nucleotide

polymorphisms (SNPs) and short inversion or deletion polymorphisms (SIDPs) while some limitations for XY-FISH may occur with gains and loss of sex chromosomes that can be seen in patients with leukaemia. Due to the high sensitivity and availability of commercial multiplex kits, STRs amplified by PCR are considered the gold standard technique for analyzing DCL cases (Wiseman, 2011; Sala-Torra & Loeb, 2011; Ruiz-Argüelles *et al.*, 2007; Flynn & Kaufman, 2007; Walshauer *et al.*, 2014; Wang *et al.*, 2011). Nevertheless, care must be taken in identification of the malignant clone, utilizing both cytogenetic and microsatellite analyses. The importance of this, is that the patient may spontaneously lose the Y chromosome and/or gain an X chromosome in the recipient cells, or hybridization of donor and recipient cells may result in a chimerical pattern of genetic markers (Spinelli *et al.*, 2000).

DCL as a rare disorder has a very poor prognosis, hence it is notoriously difficult to treat, and frequently resistant to treatment. Re-induction chemotherapy or/and reduced intensity second HSCT are the main treatments for DCL (Wiseman, 2011; Wang *et al.*, 2011). However, chemotherapy followed by IL-2 maintenance therapy indicates an effective approach for DCL maintenance therapy (Ma & Liu, 2016).

1.6 Bone marrow microenvironment

1.6.1 Haematopoiesis and supportive factors

Haematopoiesis is identified as a hierarchically orchestrated and highly regulated process from embryonic development to adulthood, to produce and replenish the whole blood system from the BM. The haematopoietic homeostasis relies on the division and self-renewing of the HSCs (CD34+), with enormous self-renewal capacities, that differentiate through the lineage-committed progenitors into the different mature blood cells including erythroid, megakaryocytic, granulocytic, monocytic and lymphocytic lineages (Robb, 2007). BM-MSC (BM mesenchymal stem cells) can express a variety of cytokines to support this expansion as well as the reconstruction of the haematopoietic microenvironment. These cytokines and chemokines have impacts on haematopoiesis, HSC differentiation, migration, and homing. Haematopoietic cytokines include interleukins (IL), colony-stimulating factors (CSF), interferons, erythropoietin (EPO) and thrombopoietin (TPO) (Kemp *et al.*, 2011; Robb, 2007).

As shown in figure 1.9A, specific subsets of these cytokines influence each step in the process. The haematopoietic cytokines are either constitutively present in the circulation (CSF-1, SCF,

FL, G-CSF, EPO and TPO) or appear in response to infection or inflammation (GM-CSF, IL-3, IL-5, IL-6 and IL-11). Original multipotent haematopoietic cells, which co-express different lineage-specific cytokine receptors at low levels, require a combination of cytokines for lineage commitment. As these cells differentiate, they lose receptors for some cytokines while increasing expression of receptors for the late-acting cytokines (Fig. 1.9A). When they reach the stage of committed progenitor cell, their further proliferation and differentiation is along one particular lineage and is regulated by more late-acting cytokines where non-dividing cells require specific cytokines for survival, activation, and function (Fig. 1.9A) (Pixley & Stanley, 2010).

The BM niches comprise the generally well-defined sub-compartments called endosteal and perivascular (arteriolar and sinusoidal) niches. HSCs show different behaviours between the different subniches (Zhang *et al.*, 2019). The endosteal niche contains quiescent HSCs with greater self-renewal capacity due to various cytokines, adhesion molecules and hypoxia, while the vascular niches comprise the stromal lineages (chondrocytes, osteoblast, adipocytes, myocytes fibroblast and endothelial cells) which are the key players in the maintenance of the BM acting to activate HSC cell cycle, initiate proliferation, differentiation, mobilisation and homing (Gleitz *et al.*, 2018; Zhang *et al.*, 2019). The two main cellular systems in the BM are the CD34⁺ haematopoietic and non-haematopoietic cell systems (Athanosou *et al.*, 1990; Catacchio *et al.*, 2013). HSCs are essential for the generation of the haematopoietic blood system including lymphocytes, erythrocytes, monocytes, granulocytes and platelets (Fig. 1.9B) thus producing nearly a trillion mature blood cells daily, while they can also transdifferentiate into non- haematopoietic cells. Normal haematopoiesis involves a complex interaction between the BM niche and haematopoietic cells to continuously regenerate and replace the blood pool under the influence of cytokines expressed by BM stromal cells. HSCs constitute only a small fraction of the BM population (1 in 10⁸ of BM nucleated cells) and the microenvironment provides signals for survival and external control of stem cell activity (Catacchio *et al.*, 2013). MSCs constitute a rare population of adherent, fibroblastic cells found mainly around the perivascular niche and are in direct contact with endothelial cells to play supportive roles for physiological features of HSCs; others are located in the endosteal niche adjacent to the bone (Gleitz *et al.*, 2018). MSC contain common surface receptors including CD29, CD44, CD49a-f, CD51, CD73, CD105, CD106, CD166, and Stro-1. MSCs show pluripotent properties and transdifferentiate into many different cells, including hepatocytes, endothelial cells, skeletal

muscle, myocardial cells, central nervous system neurons and glial cells (Cilloni *et al.*, 2000; Avots *et al.*, 2002) whilst also having capacity to transdifferentiate within the mesenchymal lineage into osteoblasts, adipocytes and chondrocytes (Fig. 1.9B) *in vitro* and into heterotopic osseous tissue when transplanted *in vivo* (Catacchio *et al.*, 2013; Fasouli & Katsantoni, 2021).

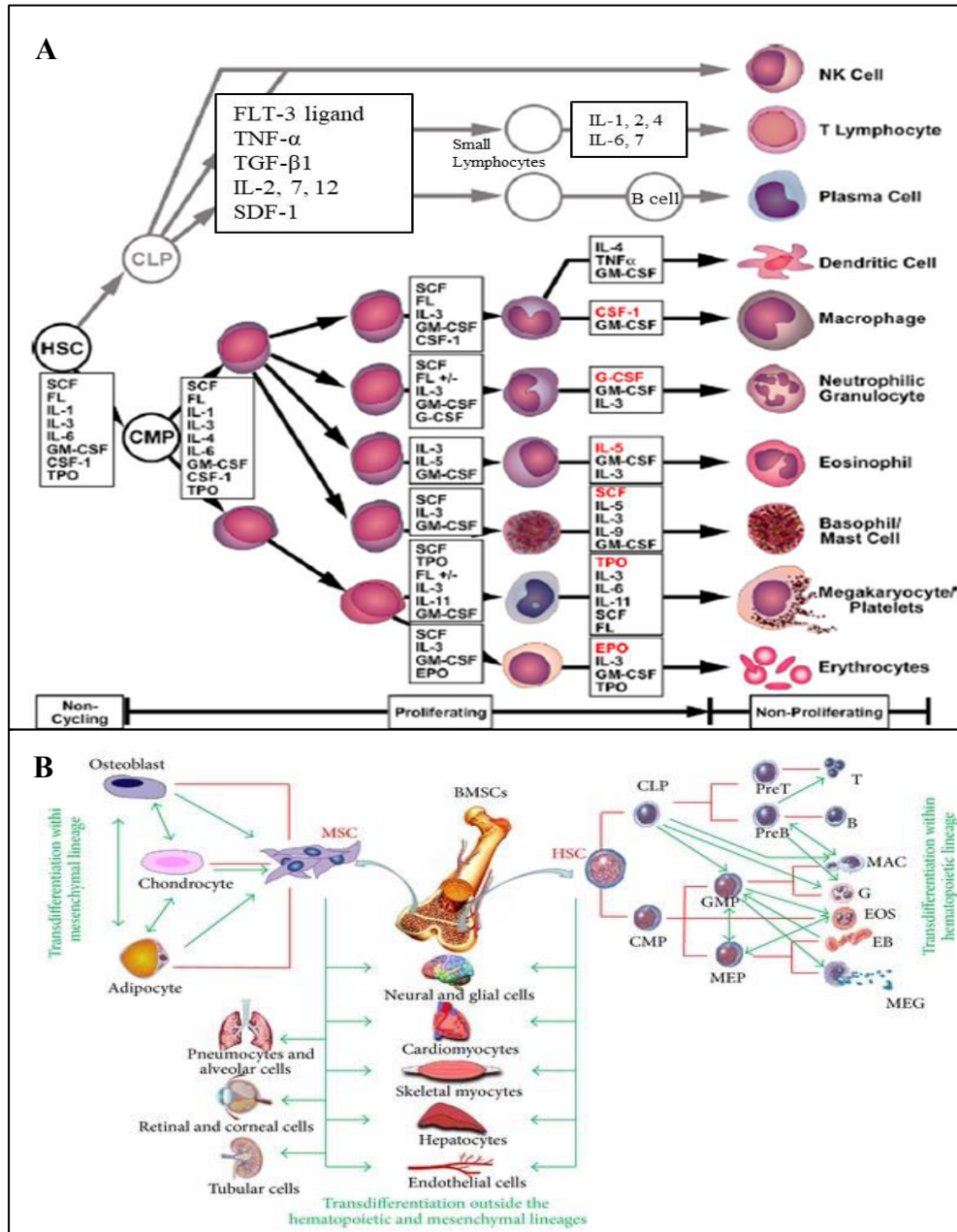


Figure 1.9. Cytokine regulation in bone marrow haematopoiesis and plasticity. (A) Many different cytokines in the BM microenvironment stimulate the development of cells of different lineages. These cytokines may be circulating or bound to either the surface of their producing cells or to the extracellular matrix. Progenitor cells can also proliferate and differentiate in semisolid culture under the influence of specific cytokines, to form macroscopic colonies of differentiated cells – hence the term colony-stimulating factor (CSF) for the responsible growth factor. **(B)** Bone marrow stem cells (BMSCs) are divided into mesenchymal stem cells (MSC) and haematopoietic stem cells (HSC). MSC differentiate into osteoblasts, chondrocytes and adipocytes whereas HSC differentiate into multipotent common myeloid progenitor cells (CMP) and common lymphoid progenitor cells (CLP). CMP cells are cells committed to the myeloid lineages, including megakaryocyte-erythroid (MEP) and granulocyte-monocyte lineages (GMP). These lineages differentiate into megakaryocytes (MEG), erythrocytes (EB), eosinophils (EOS), granulocytes (G) and macrophages (MAC). The CLP cells are committed to lymphoid lineages, including the T-cells and B-cells. Adapted from Pixley & Stanley, 2010; Catacchio *et al.* (2013) with permitted usage of the free creative common license.

1.6.2 Aberrant bone marrow and cytokines

In vitro studies on the functional integrity of the haematopoietic microenvironment in leukaemia have been controversial. There is increasing evidence indicating that there are alterations in the function of aberrant BM microenvironment from leukaemia (Flores-Figueroa *et al.*, 2002). The term ‘aberrant homeostasis’ covers a broad entity of phenomena and encompasses the absence, under-expression or over-expression of receptors and ligands involved in cell-to-cell signalling, which in turn might affect signalling amongst stromal, endothelial and haematopoietic precursor cells; but additionally, it might encompass aberrant, absent or excessive cytokine signalling within the haematopoietic milieu (Ruiz-Argüelles *et al.*, 2007). A potential method of immune evasion following HSCT is the modulation of pro- and anti-inflammatory cytokines (Sweeney & Vyas, 2019).

Investigations have shown that both non-transformed and malignant HSC precursors can transdifferentiate within the haematopoietic lineage (e.g. lymphoid-to-myeloid and myeloid-to-erythroid switches) and they can transform into leukaemia stem cells (LSC) dependent on BM stroma insoluble proteins, growth factors, transcription factor expression, numerous cytokines/chemokines, drug treatments or changes in environmental conditions. LSC contribute to propagation of leukaemia with impaired normal haematopoiesis. It has been hypothesised that HSCs are expelled from their niche and the resultant LSC microenvironment supports leukaemogenesis (Asada *et al.*, 2017; Fasouli & Katsantoni, 2021). The exact mechanism underlying the leukaemic transformation is currently unknown, but certain genetic and metabolic changes play a role. Recent studies were able to mechanistically elucidate how LSC and proinflammatory cytokines activate stromal cells in the BM, support their fibrotic and secretory activity, and influence their reduced haematopoiesis-supporting capacity (Gleitz *et al.*, 2018). LSCs can alter the BM normal dynamics through their expression of cytokines, especially SCF and form the malignant niche where LSC can proliferate and differentiate. LSC’s fate and survival is influenced by crosstalk within the BM microenvironment. Genetic deletion of key genes like *Rary* and disruption of miRNAs in a mouse model were shown to induce the development of DCL, demonstrating the first model of DCL from an abnormal BM (Raaijmakers *et al.*, 2010; Asada *et al.*, 2017). These findings support the fact that altered BM microenvironment indeed has the potential to promote primary malignancy and leukaemia patients undergoing HSCT can develop donor derived leukaemia directly initiated by an

abnormal HSC niche (Asada *et al.*, 2017). However, the process of leukaemogenesis in BM microenvironment still requires more investigation.

BM microenvironment cells can interact directly with target cells or by secreting regulatory molecules that stimulate or inhibit target-cell proliferation and differentiation. Many soluble signals such as cytokines, growth factors and chemokines have been shown to be induced in aberrant marrow in cancer patients. The most significant among them are epidermal growth factor (EGF), pro-inflammatory cytokines and fibroblast growth factor (FGF) (Barcellos-Hoff *et al.*, 2005). Abnormalities of the BM microenvironment might be an inherent feature, or chemo-/radiotherapy can inflict considerable damage on BM stromal elements even though the effects of endogenous and pharmacologic cytokines on the stromal equilibrium are not well understood (Flynn & Kaufman, 2007). As a consequence of the BE inflammatory response, radiation induced stroma can contribute to secondary cell damage in the microenvironment which also contributes towards selection and proliferation of leukaemic clones (Flynn & Kaufman, 2007; Wiseman, 2011). In addition, chemotherapy agents can also induce changes in potential of HSCs through disruption of the BM endothelium barrier and cause endothelial injury which allow cells, proteins and cytokines to move between the vascular space and the BM niche which have an impact on HSC migration and repopulation (Kemp *et al.*, 2011; Flynn & Kaufman, 2007). Local expressions of cytokines in tumours aids angiogenesis and protects the tumour from immune mediated elimination, suggesting that anti-cytokine therapy may prove efficacious for some cancer treatment (Langowski *et al.*, 2006).

1.6.2.1 Cytokine storm

Patients who have undergone conditioning therapy commonly display disruption of the marrow architecture and loss of stromal compartments. Importantly most of these patients demonstrate cytokine response to conditioning (dominated by IL-6, TNF- α , IL-1) representing the first step in the post-transplant cytokine storm (Melenhorst *et al.*, 2012; Gallet *et al.*, 2011; Tisoncik *et al.*, 2012). After infusion of the stem cell graft, donor T cells become activated due to host antigens, resulting in their proliferation and further cytokine production. The end result of this is a systemic cytokine storm, which is the hallmark of HSCT complications leading to GvHD. It is unclear how much the homeostatic drive to lymphocyte recovery and the production of cytokines from the engrafting donor immune system determine cytokine fluctuations in the peri- and immediate post-transplant period (Kemp *et al.*, 2010; Melenhorst *et al.*, 2012).

However, both donor and host cells, contribute to this proinflammatory cytokine milieu, which is generated as a response to tissue damage.

Cytokine storm (more detailed in section 6.1) also known as ‘cytokine release syndrome’, has been defined as a systemic inflammatory state that occurs due to robust and widespread immune activation induced by variety of factors such as infections, types of therapies such as radio-, chemo-, immune-mAbs and T cell-mediated therapy (Riegler *et al.*, 2019). Serum levels of TNF- α and IL-6 peaked in all patients with B-Cell CLL after onset of the anti-CD20 mAb infusion, rituximab (Winkler *et al.*, 1999). Serum samples after cell infusion showed marked increases in TNF- α , IL-6, IFN γ , GM-CSF, and IL-10, consistent with a cytokine storm (Morgan *et al.*, 2010). Most recently a cytokine storm was reported in all patients that were treated with anti-CD28 mAb TGN1412. Depending on their occurrence time, *in vitro* studies by Gallet *et al.*, (2011) detected significantly increased pro-inflammatory cytokines (IL-1a, TNF- α , IL-2, IFN- γ , IL-6) following irradiation. Early effects occur soon after irradiation and late effects can appear clinically months, or even years, later. However, the molecular mechanisms involved in the development of these effects remain unclear. Melenhorst *et al.*, (2012) identified two cytokine storms subsequent to allogeneic-HSCT; the first occurred following conditioning and the second concurrently with HSC reconstitution. Cytokine storm could occur throughout the body including the central nervous system (Clark & Vissel, 2017). Studies have classified the cytokine storm usually due to binding of the specific antibody or cell receptor to its antigen and subsequent activation of bystander immune- and non-immune cells through the cytokine signalling (section 1.6.3.3) (Shimabukuro-Vornhagen *et al.*, 2018). Activation of these bystander cells results in the massive release of inflammatory cytokines, such as IL-6, TNF- α , IFN γ , IL-2, and IL-10, by large numbers of activated lymphocytes (B cells, T cells, and/or natural killer cells) and/or myeloid cells (macrophages, dendritic cells, and monocytes) into the blood (Riegler & Jones, 2019). While the literature extensively describes RIBE and cytokine storms following radiation therapy, limited information is available regarding chemotherapy-induced cytokine storms.

The core cytokines IL-6, TNF- α , IL-10 and IFN γ as well as IL-1b, IL-2, IL-10, IL-8, IL-5, and CXCL1 are consistently found to be elevated in the serum of patients with cytokine storm (Shimabukuro-Vornhagen *et al.*, 2018; Yildizhan & Kaynar, 2018). A biomarker screen in ALL patients after T cell therapy found that peak levels of IL-6, sIL-6 α , IFN- γ , and sgp130 correlated with the risk of severe cytokine storm. As discussed in both *in vivo* and *in vitro*

studies (Flores-Figueroa *et al.*, 2002; Peled *et al.*, 1996; Lazutka, 1996; Blau *et al.*, 2007), the aberrant cytokine milieu resulting from these storms can profoundly impact BM cells, including the microenvironment, fostering the survival and proliferation of cancer cells in patients with AML and MDS. Moreover, evidence suggests that the stromal cell layer from AML patients frequently exhibits abnormal cytokine profiles (Wiseman, 2011). Additionally, the incidence and severity of GvHD is characterised by the production of cytokines that may negatively regulate marrow homing and proliferation of stromal cells (Cilloni *et al.*, 2000). Suppression of pro-inflammatory and elevation in anti-inflammatory cytokines are predicted to reduce effective GvL responses (Sweeney & Vyas, 2019). With the altered cytokine secretion, studies indicate that ROS, RNS, and inflammatory cells contribute to exacerbating this condition, leading to the induction of numerous DNA damages (Barcellos-Hoff *et al.*, 2005; Ewan *et al.*, 2002). The concept that cytokines can both promote mutations and replication of cells suggests that cytokines can also induce and prevent apoptosis of the mutant cells. Apoptosis inducing cytokines include TGF- β 1 and TNF- α whereas IL-6, G-CSF, GM-CSF or IL-3 inhibit apoptosis. For example, TGF- β 1 is a multifunctional mediator of both homeostasis and injury responses controlling both proliferation and apoptosis (Lorimore *et al.*, 2001).

An aberrant BM microenvironment might facilitate the expansion of the mutated clone but the dysregulation in cytokines and their mutual interactions become an essential factor in leukaemogenesis by playing a crucial role in self-renewal, proliferation, commitment and differentiation of normal HSC (Ruiz-Argüelles *et al.*, 2007). Most DCL cases present with an alteration of the homeostatic balance between the complex interactions of the BM cells, growth factors, cytokines and transplanted donor HSCs within the BM microenvironment (Flynn & Kaufman, 2007). The seminal “seed and soil hypothesis” of Paget in 1889 can be used as a model for DCL. Optimal development of engrafted HSCs (seeds) occurs when the seed and the soil (BM niche) are in equilibrium. Close physical interaction invariably occurs between the soil (the stroma) and seed (donor HSCs) essential for supporting healthy haematopoiesis. BM signals identified from irradiation that mediate bystander communication (section 1.6.3) between soil and seed are cytokines, chemokines, ROS, nitric oxide and miRNAs, which can be transferred between cells via gap junctions or the extracellular medium (Xu *et al.*, 2014; Song *et al.*, 2016; Morgan, 2003). However, most of the knowledge of mechanisms for BE results from observations from RIBE (Greenberger *et al.*, 1996; Leone *et al.*, 1999) and little

is known of the mechanisms for CIBE (discussed in sections 1.6.3.2). Perturbation of this BM microenvironment (the soil) equilibrium, thereby obstructing the usual homeostatic balance and crosstalk between the BM cells, cytokines and the transplanted donor HSCs (the seed) might play a role in leukaemic transformation and also facilitate accumulation of mutated HSC clones in the BM stoma (Flynn & Kaufman, 2007; Bydlowski *et al.*, 2013).

The above evidence suggests that LSCs occupying the HSC niche, remodel it into an oncogenic unit by self-reinforcing at the expense of normal haematopoiesis, with the help of extramedullary release of cytokines by the malignant haematopoietic clone. Therefore, BM niche deregulation is a key step in leukaemogenesis processes (Gleitz *et al.*, 2018; Asada *et al.*, 2017). However, there are currently no FDA-approved drugs that are able to directly target MSC remodelling. Thus, considering the importance of inflammatory cytokines involved in BM niche remodelling and AML development in murine models, it will be exciting to test the effect of blocking these specific cytokines (TNF- α and IL-6) with various suppressing, neutralizing and/or antagonizing antibodies that are currently available for clinical use (Chapter 6) (Gleitz *et al.*, 2018; Asada *et al.*, 2017).

1.6.3 Bystander effect

Recent radiobiological findings on a BE in non-irradiated progenitors provide insights into the potential mechanisms behind DCL (McCann & Wright, 2003). Ionising radiations exert their effect on rapidly dividing cells and as such, do not only affect the directly treated cells but also the unexposed/untargeted neighbouring compartments. When these non-treated cells show biological responses that mimic the direct effect, such a response is referred to as a ‘bystander effect’ (BE) (Morgan, 2003). Two mechanisms for signal transfer from irradiated to unirradiated cells are proposed: one involves cell-to-cell gap junction communication, and the other suggests irradiated cells secrete factors that may induce damage in unirradiated cells. Evidence links the NADPH oxidase/NF- κ B pathway to this effect. The contribution of BE to overall cellular responses, especially *in vivo*, remains unclear (Lorimore & Wright, 2003).

Surrounding bystander cells immediately respond, leading to multiple endpoints including DNA damage and mutations, chromosomal breaks, altered protein and enzyme levels, apoptosis, oncogenic transformation and reduced clonogenic efficiency in their progeny. Clearly, new transplanted donor cells could be similarly affected by these outcomes termed BE (Lorimore *et al.*, 2001; Wang *et al.*, 2018). Due to the bystander cells inherently responding to

DNA damage, the cells could activate inflammatory cytokines, death ligands and ROS/RNS (Dickey *et al.*, 2009).

1.6.3.1 Radiation-induced bystander effects

RIBE is a well-established phenomenon in DNA damage responses and is induced in the non-irradiated bystander cells through intercellular signal transmission (Banfi *et al.*, 2001). There is also considerable evidence that progeny of bystander cells, often several generations later may present with delayed gene mutations and a variety of chromosomal aberrations resulting in genomic instability and/or apoptosis due to failed repair attempts (Lorimore *et al.*, 2001). Clastogenic factors found in the medium of both *in vivo* and *in vitro* irradiated cells can induce chromosomal aberrations when co-cultured with non-irradiated cells (Morgan, 2003) and irradiated BM stromal co-culture with non-irradiated stem cells can increase the transformation frequency of non-irradiated stem cells (Barcellos-Hoff *et al.*, 2005). Proposed cytotoxic features include breakdown products of lipid peroxidation, inosine nucleotides, and secretion of various cytokines (Ruiz-Argüelles *et al.*, 2007; Morgan, 2003). Irradiated cells release growth-inhibitory molecules, with evidence of inducing leukaemic transformation in non-irradiated stem cells transplanted into syngeneic mice (Lorimore *et al.*, 2001; Duhrsen & Metcalf, 1990). Recent studies suggest small non-coding RNAs, especially miRNAs, and secretive exosomes may mediate bystander effects (Xu *et al.*, 2014; Song *et al.*, 2016). Potential mechanisms involve cytokine overproduction, ROS, and apoptosis-inducing factor (AIF) released into the extracellular microenvironment from irradiated cells, confirmed via extracellular medium or gap junctions (Song *et al.*, 2016).

ROS can cause various DNA lesions leading to potentially leukaemogenic mutations and can activate signalling pathways (p53; MAPK) in bystander cells (Wiseman, 2011). ROS might also induce a self-perpetuating cycle of oxidative stress and persistence of clastogenicity by stimulating the generation of further ROS. Alternatively, soluble clastogenic factors generated by irradiated host cells might persist and circulate to induce genotoxic effects on donor cells, contributing critical hits towards a leukaemic phenotype. However, evidence from medium transfer experiments for bystander effects confirm that dependence on physical interaction is not universal (Wiseman, 2011).

Although the mechanism of RIBE has been well described with multiple endpoints (chromosomal aberrations, micronuclei, mutations, DNA DSB and SCE), and the influence of

cytokines in bystander effect has been suggested, the mechanisms of CIBE remains to be elucidated. Thus, this research was interested in the impact and possible aetiology of CIBE.

1.6.3.2 Chemotherapy-induced bystander effects

The concept of chemotherapy-induced bystander effect (CIBE) has struck the attention of researchers in recent times. Rugo and colleagues (2005) have shown that mitomycin-C (a DNA-alkylating agent that can induce *in vivo* and *in vitro* paracrine factors that cause growth inhibition) not only directly induces recombination but also induces persistent hyper-recombination in bystander cells, and promotes the ability of these bystander cells to further induce a sequence rearrangement in other neighbouring cells (Rugo *et al.*, 2005). Demidem and colleagues (2006) demonstrated CIBE capacity of chloroethyl-nitrosourea agents *in vivo* and *in vitro* using a serum transfer experiment. In their study, *in vivo* cells showed cessation in tumour proliferation, metabolite alteration, reduced vessel formation and glutathione decrease. An *in vitro* co-culture model mimicked these results by showing *de novo* proteins secretion which resulted in growth inhibition, metabolite alterations and cytoskeleton disorders (Demidem *et al.*, 2006).

The results from Kumari *et al.* (2009) highlight that mitomycin C induced BE by killing hepatoma cellular models via FasL and TRAIL in the medium and this also occurred in co-cultured cells, implicating the involvement of soluble as well as membrane bound death effector molecules. Interestingly, with the treatment of FasL and TRAIL neutralising antibodies bystander killing was inhibited. Chhipa & Bhat (2007) demonstrated that the 5-fluorouracil and carboplatin induced cytotoxicity in co-cultured cell lines and target cells was due to the membrane bound Fas/FasL rather than soluble FasL. Di *et al.* (2008) evidenced the effects of adriamycin were related to telomere dysfunction in bystander breast cancer cells, whereas Proietti *et al.* (1998) suggested that cyclophosphamide produced bystander effects through immune cells. CIBE is not always detrimental, as Merle *et al.* (2008) experiments showed that cyclophosphamide, administered in a syngeneic tumour model, induced disturbance of tumour phospholipid metabolism and induced a protective effect against the development of secondary tumours.

Furthermore, Asur *et al.* (2009) showed that conditioned medium from mitomycin C and phleomycin exposed human lymphoblast cell lines produce soluble factors in the culture medium that could induce micronuclei in unexposed bystander cells. Subsequently,

Chinnadurai *et al.* (2011) suggested that bleomycin and neocarzinostatin can induce a bystander response in a co-culture system of WI-38, hBMSCs, NCI-H23, A-549 cell lines and peripheral blood lymphocytes using micronuclei as an endpoint, which is similar to that induced by radiation.

1.6.3.3 Cytokines and bystander effect

Cytokines are polypeptide hormones generally secreted by monocytes and lymphocytes in response to interaction with antigens, or non-specific soluble stimuli, but are also secreted by the BM microenvironment (Lazutka, 1996). Most cellular responses to cytokines are slow, occurring over a period of hours and require new mRNA and protein synthesis (Zhang & An, 2007). Cytokines, like other polypeptide hormones, initiate their action by binding to specific receptors on the surface of target cell types to activate complex cascades which usually balance the self-renewal, development and replication of the cells (Sica & Bronte, 2007). Cytokines may act on the cells that secrete them (autocrine action), on nearby cells (paracrine action), or in some instances on distant cells (endocrine action). The range of cytokines includes: pro-inflammatory, anti-inflammatory, interferons, chemokines, interleukins, growth factors etc. (Zhang & An, 2007). The role of cytokines in HSCT is currently an area of intense research. However, it is known that MSCs can produce several early acting cytokines which maintain HSCs in a state of quiescence or can promote their self-renewal. A variety of BM stroma cytokines, chemokines, receptors and intracellular signalling molecules act on haematopoietic progenitors to influence which lineage should develop (Peled *et al.*, 1996).

Over the years, various soluble mediators including ROS, nitric oxide and cytokines have been implicated in BE (Di *et al.*, 2008). Genotoxic effects induced by BE involve the formation of clastogenic factors, inosine nucleotides, lipid peroxidation and cytotoxic cytokines (McCann & Wright 2003). Lorimore *et al.* (2001) have shown that *in vivo*, BM macrophages are activated by exposure to radiation, leading to increased phagocytic cell activity with release of pro- and anti-inflammatory cytokines. Furthermore, McCann & Wright (2003) detailed that irradiated BM stromal cells release cytokines and enhance the frequency of haematopoietic growth factor-dependent cell transformation, when cells were co-cultured with irradiated stromal cell lines or transplanted into irradiated mice. Also, induction of inflammatory responses could increase the radiation-induced AML incidence (McCann & Wright, 2003). As evidence of chemotherapy induced cytokine production, Proietti *et al.* (1998) showed that

cyclophosphamide can induce cytokines and growth factors, and sustain the proliferation, survival, and activity of T lymphocytes during BE. Notably, the production of IFN- α/β is responsible for proliferation and long-term persistence of memory CD8⁺ T cells *in vivo*. The finding that antibodies to IFN markedly inhibit the response of the recipient to the combined therapy, highlights the importance of these cytokines in supporting antitumour activity of the transferred immune cells.

There is evidence that genetic instability in the progeny of HSC can be induced by an indirect bystander-type mechanism both *in vivo* and *in vitro* in a manner consistent with an inflammatory-type mechanism involving oxidative stress usually with superoxide and nitric oxide (McCann & Wright, 2003). Fibroblasts and macrophages can permanently arrest in an activated state, continuously generating ROS, probably mediated by TGF- β , which itself promotes survival and proliferation of AML cells *in vitro* (Wiseman, 2011). There are reports demonstrating involvement of ROS, RNS and cytokines such as TGF- β that promote bystander cell killing in sparsely populated cell cultures (Kumari *et al.*, 2009). Iyer & Lehnert (2000) found that TGF- β 1 capably induces intracellular ROS, decreases cellular levels of p53 and proliferating cell nuclear antigen in bystander cells. This can be mimicked by the addition of low concentrations of TGF- β 1. According to Morgan (2003), following the production of cytokines and free radicals, which again could stimulate cytokine production, more free radicals could be produced creating an environment conducive to stimulating and perpetuating the unstable phenotype (Fig. 1.10). Lorimore & Wright (2003) also pointed out that radiation induced intercellular signalling, high cytokine production and free radicals, have the potential for both BE and persistent damage which may contribute to the genomic instability and increased leukaemia incidence. Barcellos-Hoff *et al.* (2005) further supports the idea that the prolonged exposure to these signals plays a crucial role in the development of genomic instability and subsequent cancer initiation.

However, certain cytokines are implicated in repair or the induction of DNA damage. Interestingly, in some instances, the same cytokine plays a dual role in both repair and DNA damage induction, and the underlying theory behind this dual functionality remains elusive and warrants further understanding. Currently, there is no satisfactory explanation for the direct genotoxicity of cytokines themselves, and the potential mechanisms of cytokine genotoxicity remain unclear. To date, the published literature on the genotoxicity of cytokines primarily suggests an indirect mechanism through immune cells and ROS. If indeed this indirect pathway

established cytokine storms following chemotherapy, it is reasonable to suggest that chemotherapy might similarly induce a BE through cytokine-mediated mechanisms, and this is worthy of investigation as a possible aetiology of DCL. Several researchers have discussed that both radio- and chemotherapy could induce cellular immunity and release many cytokines/chemokines to cause an inflammatory condition which directly and/or indirectly contribute to the BM homeostasis, haematopoiesis and BE, and may affect transplant rejection depending on the genetics of the individuals. This untargeted effect on immunity requires an in-depth understanding of the phenomenon, especially the aspect of its biological significance and associated non-targeted effects which could clearly pose a major contribution to DCL mechanisms and development. While it is not yet clear how BE contributes to the overall cellular responses *in vivo*, it has opened up avenues of investigation with potential relevance to understanding leukaemic relapse in donor cells. Based on these premises, using models of BM- MSC (HS-5) and HSC (TK6) cell lines, this research explored the genotoxicity of cytokines in CIBE.

1.7 Hypothesis

Physiologically relevant doses of chemotherapy can induce a cytokine storm from the BM which has the capacity to induce a bystander effect in neighbouring unexposed cells.

1.8 Aims

- 1. To confirm *in vitro* cytokine expression by a BM-MSK line at baseline and cytokine storm following chemotherapy exposure.**
 - Cytokine upregulation was confirmed and measured post-exposure to chemotherapy using cytokine arrays in the HS-5 human BM-MSK cell line.
 - One alkylating agent (CHL) and one topoisomerase inhibitor (MTX) were selected and exposed to HS-5 at a clinically relevant dose. Changes in cytokine expression were measured using the Abcam cytokine array (80 targets). Five cytokines that were up-regulated in the presence of both drugs were further explored in the following aims.
- 2. To confirm the selected candidate cytokines and to measure the expression level of each candidate, in-house ELISA assays were developed.**
 - Using the in-house developed ELISA, cytokine levels were quantitated for both chemotherapy treatments.
 - Cytokine expression within the *in vitro* cell line models (HS-5 and TK6, alone and in co-culture) were quantitated in this study using these ELISA assays.
- 3. To explore the capacity for candidate cytokines to induce DNA damage and cytotoxicity.**
 - Recombinant proteins of selected cytokines (aim 1) were directly exposed to the lymphoblast cell line (TK6) with a range of single and combination doses at normal and cytokine storm levels.
 - Previously identified genotoxicity endpoints (micronuclei) in the bystander assay were assessed following direct exposure of cells to the selected cytokines.
 - The IL-6 cytokine signalling pathway was focussed on and inhibited in TK6 using chemical inhibitors and assessed for changes in micronuclei formation compared to the uninhibited TK6.
- 4. To confirm the role of cytokines in the bystander effect.**
 - IL-6 within the culture medium conditioned by the HS-5 was reduced using siRNA knockdown (k/d) approaches and using chemical inhibitors; the co-culture was then assessed for ablation of the bystander effect genotoxicity.

CHAPTER 2

MATERIALS AND METHODS

2.1 Materials

All reagents that were used in this research were purchased from Sigma-Aldrich (Dorset, UK) except where otherwise stated. All protocols were performed according to the regulations for the Control of Substances Hazardous to Health (COSHH), which encompasses all risk assessments and control measures for the use of reagents involved in this study.

2.1.1 Cell lines

The following cell lines were used as an *in vitro* model to mimic the BM compartment and its cellular crosstalk between the compartments. To act as the BM microenvironment, the mesenchymal stromal cell line HS-5 was used, and as the haematopoietic stem cell compartment, the lymphoblastoid cell line TK6 was used.

2.1.1.1 Mesenchymal stromal cell line; HS-5.

As a model of the BM-MSK, this study has used the human stromal cell line HS-5, purchased from ATCC (American Type Culture Collection, US). HS-5 is the only human fibroblastic mesenchymal stem cell line available, which is derived from long-term BM culture transformed with amphotrophic retrovirus vector. HS-5 is a male adherent cell line, which expresses similar genes to a typical BM and secretes cytokines that support growth and proliferation of committed haematopoietic cells when co-cultured in serum-deprived media. Secreted cytokines include G-CSF, GM-CSF, macrophage-CSF (M-CSF), Kit ligand, macrophage-inhibitory protein-1 α , IL-1 α , IL-1 β , IL-1RA, IL-6, IL-8, IL-11, and stem cell factor, which play a key role in proliferation of progenitor cells (Roecklein and Torok-Storb, 1995; Schmidmaier *et al.*, 2006). The STR profile includes: Amelogenin - X,Y; D16S539 - 10,11; CSF1PO - 10,11; D5S818 - 12; D7S820 - 12; D13S317 - 11; TH01 - 7,9; TPOX - 8; vWA - 18, 19 (ATCC).

2.1.1.2 Lymphoblastoid cell line; TK6

The thymidine kinase heterozygote cell line TK6 isolated from the lymphoblastoid line HH4 was kindly supplied by Professor Ann Doherty (AstraZeneca Genotoxicology Laboratory,

Cambridge, UK). The STR profile includes: Amelogenin - X,Y; D16S539 - 11,12; CSF1PO - 11,12; D13S317 -11; D5S818 - 12,13; D7S820 - 9,11; TH01 - 8,9,3; TPOX - 8,11; vWA - 17,20 (Cellosaurus, 2023). TK6 is widely used in genotoxicity testing of chemical substances due to its p53 competency, it is positive for the cell surface markers CD19, CD20 and CD22 and is reported negative for bovine viral diarrhoea virus (Fowler *et al.*, 2012; Yasui *et al.*, 2019).

2.1.2 Chemotherapeutic agents

Chemotherapeutic drugs were chosen from each of the two drug groups (alkylating agents and topoisomerase inhibitors) which are linked to therapy-related malignancies and were used at doses equivalent to clinically relevant or *in vivo* observed plasma concentrations (Table 2.1) (Candelaria & Dueñas-Gonzalez, 2015; Swift & Golsteyn, 2014). The chemotherapeutic agent stocks were made up in the recommended solvent (100% ethanol) at a 100x concentrates, stored in small aliquots and frozen at -80 °C. Working concentrations were prepared fresh on the day of the assay, with dilutions made in culture medium. For assessment of cytokine expression in cytokine arrays and knockdown (k/d) bystander models, HS-5 cells were treated with chlorambucil (CHL; alkylating agent) and mitoxantrone (MTX; topoisomerase II inhibitor) at relevant doses for one hour at 37 °C with 5% CO₂. After one hour these agents were washed off the cells twice in phosphate buffered saline (PBS) (1x) with a further wash with culture medium. The half-lives are suggested to be 1.5 hours (CHL) and 15 minutes to 10 days for α , β and γ (MTX) (Georg and Weber, 2015; Evison *et al.*, 2016).

Table 2. 1. Plasma concentrations of chemotherapeutic agents.

Drug name	Solubility	Concentration used this study	Human plasma Concentration	Clinically relevant dose	References
Chlorambucil (CHL)	Ethanol	4 μ M (40 μ M only for cytokine array)	2 – 6 μ M	0.6 mg/kg, 0.2 mg/kg (oral)	Hong <i>et al.</i> , 2010; Ganta <i>et al.</i> , 2008; Ganta <i>et al.</i> , 2010
Mitoxantrone (MTX)	Ethanol	1.12 μ M	500 ng/ml (1.12 μ M)	12 mg/m ² (IV)	Smyth <i>et al.</i> , 1986 Van Belle <i>et al.</i> , 1986

2.1.3 Recombinant cytokines

Recombinant cytokines were used to detect genotoxicity (micronuclei) induced by each cytokine in TK6 cells at both single dosage and combination treatments using both healthy and storm levels as shown in table 2.2. All recombinants used in this study were human proteins and the choice of these recombinant cytokines are justified in the sections 2.2.2 and chapter 4. TNF- α , IL-6, and GM-CSF were obtained from BD Biosciences, and G-CSF and TGF- β 1 were purchased from Peprotech EC Ltd. Stock and working solutions of each cytokine were prepared according to the manufacturer’s instructions.

Table 2. 2. Cytokine concentrations used to treat TK6 cells.

A literature search (Appendix II) was performed to ascertain the range of cytokine concentrations measured in healthy individuals versus cytokine storm events. A panel of test concentrations was then established to cover these ranges. Due to genetic polymorphism in cytokine genes, there are no clear threshold divides between ‘high’ or ‘low’ in cytokine concentrations within individuals.

	Blood levels and storm levels (pg/ml)							
TNF-α	50	250	500	-	1000 [†]	2000↔	3000 [†]	4000
IL-6	50	250	500	-	1000 [†]	2000↔	3000	4000 [†]
GM-CSF	100	250	500	750	1000 [†] ↔	2000	3000 [†]	4000
G-CSF	100	250	500	750	1000 [†] ↔	2000	3000 [†]	4000
TGF-β1	100	250	500	750	1000 [†] ↔	2000	3000 [†]	4000

↔ Indicates the overlap between the upper end of the healthy doses and the lower end of cytokine storm doses.

† Indicates the doses used for the cytokine combinations in the micronucleus assay.

2.1.4 Mitomycin C

Mitomycin (MMC) was used as a positive control (10,000 pg/ml; 30 nMol) in comparison to the cytokines in the micronucleus assay and was dissolved in dimethyl sulphoxide (DMSO; final concentration 0.01%) (Thermo Fisher Scientific).

2.2 Methods

2.2.1 Cell culture

All the cell culture procedures were carried out in a class II biosafety cabinet working with aseptic technique to prevent cell culture contamination, guided by the use of an appropriate COSHH assessment.

2.2.1.1 Standard culture conditions

HS-5 stromal cells

HS-5 cells were cultured at 1×10^6 cells/175 cm² flask in high glucose Dulbecco's Modified Eagles medium (DMEM-HG) supplemented with heat inactivated foetal bovine serum (FBS; 10%), L-glutamine (2 mM), penicillin (100 U/ml) and streptomycin (100 µg/ml; complete culture medium (DMEM-CCM)) at 37 °C in a humidified atmosphere with 5% CO₂. Cells were maintained in a 75 cm² vent cap Corning culture flask and had a medium change every 2-3 days with new DMEM-CCM (≤ 10 ml) without touching the adherent layer. When cells were at 70-80% confluence, they were trypsinised (section 2.2.2.4) and counted by light microscopy using trypan blue exclusion (section 2.2.1.5) and re-seeded at the same density (2nd passage). HS-5 cells were maintained between 4×10^3 and 2.4×10^4 cells/cm² (37 °C, 5% CO₂) and cells in passages 6-10 were used for experiments.

TK6 lymphoblast cells

TK6 is a suspension cell line which is cultured in Roswell Park Memorial Institute culture medium (RPMI-1640) supplemented with heat inactivated FBS (10%), L-glutamine (2 mM), penicillin (100 U/ml) and streptomycin (100 µg/ml; complete medium (RPMI-CCM)) at 37 °C in a humidified atmosphere with 5% CO₂. Cells had a culture medium change every 1-2 days. Cell pellets were obtained after centrifugation at 300x g for 10 minutes, re-suspended in 1 ml of fresh RPMI-CCM and viability was determined by trypan blue exclusion (section 2.2.1.5). Cells were re-seeded at 3×10^5 cells/ml. TK6 cells were maintained in culture between 3×10^5 and 1×10^6 cells/ml and cells in passages 3-9 were used for experiments.

2.2.1.2 Thawing of cryopreserved cell lines

Cells were removed from the liquid nitrogen and immediately thawed by carefully agitating the cryovial in a pre-warmed water bath at 37 °C until a small ice lump can be seen. The vial was wiped with tissue soaked in 70% ethanol before transfer into the class II biosafety culture hood.

Thawing medium (TM; 20% heat inactivated FBS and 80% basal culture medium) was added to the vial dropwise whilst mixing until the cryo-vial was full. The contents were transferred into a 15 ml falcon tube and TM was added 1 ml at a time, up to 10 ml, whilst gently mixing over a 10-minute period. Cell suspensions were centrifuged at 230 x g for 5-10 minutes and the supernatants were discarded. Cells were washed for a second time by adding sequential 1ml TM aliquots with mixing up to 10 ml, then centrifuged to ensure the removal of DMSO as the cryopreservant, from the cells. The cells were resuspended in 1 ml of the relevant CCM and viability was determined by light microscopy before seeding the cells at the appropriate densities.

2.2.1.3 Cryopreservation of cells

Cryopreservation was performed to maintain a master stock of early passage cells. Both cell lines were frozen in a solution containing 25% FBS, 10% DMSO and 65% basal culture medium. DMSO acts as a cryoprotectant through a partial solubilisation of the cell membrane thereby making it less prone to puncture and by hindering the formation of intra- and extra-cellular ice crystals (formed as the suspension of cells freezes) (Berz *et al.*, 2007). TK6 and HS-5 cells were centrifuged at appropriate seeding densities (TK6; 3×10^6 cells/ml and HS-5; 1×10^6 cells/ml) and resuspended in 50% FBS: 50% basal culture medium. A solution of 20% DMSO: 80% basal medium was added dropwise at an equivalent volume to the resuspended cells, thus achieving the final concentrations. Mixing of DMSO is exothermic, and so should be done on ice. One ml of cell mixture was aliquoted into each cryovial and placed into a holding chamber ('Mr Frosty'; Sigma-Aldrich), containing isopropanol, which enables gradual freezing at a rate of approximately 1 °C per minute. The freezing chamber was placed in a -80 °C freezer for 2-3 hours, then the cells were transferred to vapour phase liquid nitrogen for longer storage.

2.2.1.4 Detachment of HS-5 adherent cells by trypsinization

Trypsinisation was performed using a 1 x solution containing 0.25% trypsin and 1 mM ethylenediaminetetracetic acid (EDTA). First, the culture medium was discarded, and the HS-5 cells washed with 10 ml of 1x sterile PBS (1x PBS at concentration of 10 mM PO₄⁻, 137 mM NaCl, and 2.7 mM KCl). Trypsin was added to just cover the surface area of the flask (5 ml per T75 cm² flask), which was placed in an incubator for 3-5 minutes. A gentle tap facilitated the detachment process and then the flask was observed under a microscope to ensure all cells had detached from the flask. The cell suspension was transferred into a 15 ml tube and fresh DMEM-CCM was added to deactivate the trypsin. Cells were centrifuged at 300 x g for 10 minutes, re-suspended in 1 ml DMEM-CCM and counted by Luna FL Automated Cell Counter Dual Fluorescence (Labtech).

2.2.1.5 Manual cell counting; trypan blue exclusion assay

Cytotoxicity of chemotherapeutic drugs on HS-5 was determined by trypan blue exclusion assay, based on the principle that dead cells absorb trypan blue dye due to the loss of cell membrane selectivity whereas viable cells, who have an intact cell membrane, actively extrude the dye. Once the cells were re-suspended with 1 ml of culture media, 10 µl of cells was mixed with an equal volume of 0.4% trypan blue. A haemocytometer counting chamber was cleaned with ethanol and a cover slip was applied. The cell suspension was applied under the cover slip without forming air bubbles and overflow. Under the microscope, unstained (viable) and stained (non-viable) cells in 1 mm² square (middle/corner) were counted to obtain the cell viability and density in the original suspension. Manual cell counting was followed during standard cell cultures and other experimental assays, apart from micronuclei.

2.2.1.6 Automated cell counting; fluorescent image-based automated cell counter

The trypan blue exclusion assay was made less subjective using the LUNA fluorescent automated cell counter (Labtech, UK). A 1:10 dilution of cell suspension was made and 20 µl of sample was loaded onto the disposable haemocytometer. Protocols were set into the counter specifically accommodating the ranges of cell line size used in this study. The machine analyses this sample to produce values of total, viable and dead cells within seconds and a visual mark up of live versus dead cells is also produced. Automated cell counting was used in all micronuclei assays.

2.2.1.7 Bystander co-culture model

HS-5 cells were seeded at 7×10^4 cells/well into a 12 well plate with 1ml of RPMI-CCM. Co-culture experiments were set up in RPMI-CCM medium which was the optimised culture media as described in section 3.2.1. Following 24 hours incubation, HS-5 cells were treated with clinically relevant doses of CHL ($4 \mu\text{M}$) and MTX ($1.12 \mu\text{M}$) (Table 2.1) for 1 hour at 37°C and 5% CO_2 atmosphere. Of note is that during IL-6 siRNA or chemical inhibition assays, k/d reagents or resatorvid were added 24 hours before drug treatment as discussed in section 2.2.6.1 and 2.2.6.2 respectively.

Each well was washed three times with PBS to ensure complete removal of the excess drug and then was filled with 1 ml of RPMI-CCM. To allow time for the induction of cytokine secretion, cells were incubated for 48 hours (highest level of cytokine secretion) after drug treatments, then culture media were changed in all wells. Subsequently, $0.4 \mu\text{m}$ polyethylene terephthalate (PET) hanging culture inserts (Merck Millipore, UK) containing 3×10^5 TK6 cells in 1 ml RPMI-CCM were transferred into the HS-5 seeded wells using sterile forceps (Fig. 2.1). After 24 hours incubation, aliquots of 20,000 bystander cells per slide were harvested for the MN assay (section 2.2.4) and the remaining TK6 cells were allowed to recover in a

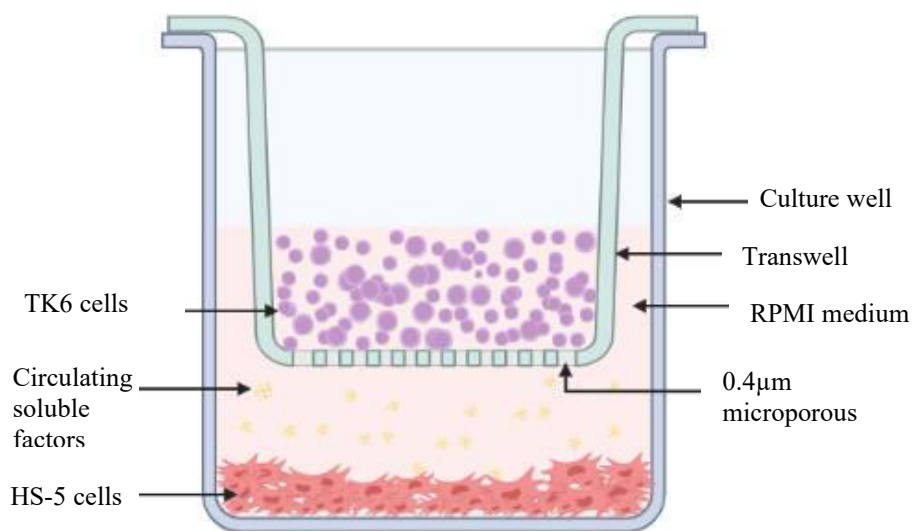


Figure 2. 1. Co-culture model to determine the bystander effect. HS-5 cells were seeded at 7×10^4 cells/well and exposed to IL-6 knockdown reagents for 24 hours. HS-5 cells were exposed to chemotherapy for 1 hour, then washed with PBS before adding new media. Following 48 hours incubation, 3×10^5 TK6 cells in a culture insert were transferred into the HS-5 seeded well with 1ml of media. Bystander TK6 cell line was co-cultured with HS-5 at 37°C at 5% CO_2 for 24 hours. TK6 cells and culture medium were harvested for micronuclei and ELISA analysis. (Figure created by author via BioRender.com)

fresh 12-well plate for 24 hours and then following counts, relative population doubling (RPD) was calculated. Also, complete medium (CM) in the co-culture wells was collected for IL-6 ELISA analysis (section 2.2.3).

2.2.2 Cytokine array analysis of drug treated HS-5 cells

2.2.2.1 Establishing the HS-5 culture for drug treatment

According to previous research data (Kelechi Okeke, personal communication), maximal genotoxic bystander effects were detected after 2 and 3 days for MTX and CHL exposure respectively. Thus, the assays focussed on cytokine secretion on 2- and 3-days post-chemotherapy exposure for MTX and CHL respectively. In order to ensure there were enough cells for cytokine secretion and that they had time to adhere, cells were seeded at 50% confluence, such that after 72 hours they would have reached 70% confluence. HS-5 cells from confluent 75 cm² flasks were counted to determine the number of cells per cm² and a seeding density was estimated to equate to 50% confluence. This was then cultured for 2-3 days to ensure 70% confluence at the time that the drug treatment would start. Thus, 5.6×10^4 cells/cm² was determined as a seeding density on day 0. Figure 2.2A and B shows the HS-5 cell density between 50% (at seeding) and 70% (72 hours of seeding) confluency in 75 cm² flask. Using this cell count, cells were seeded at 5.6×10^4 / cm² into 25 cm² flasks.

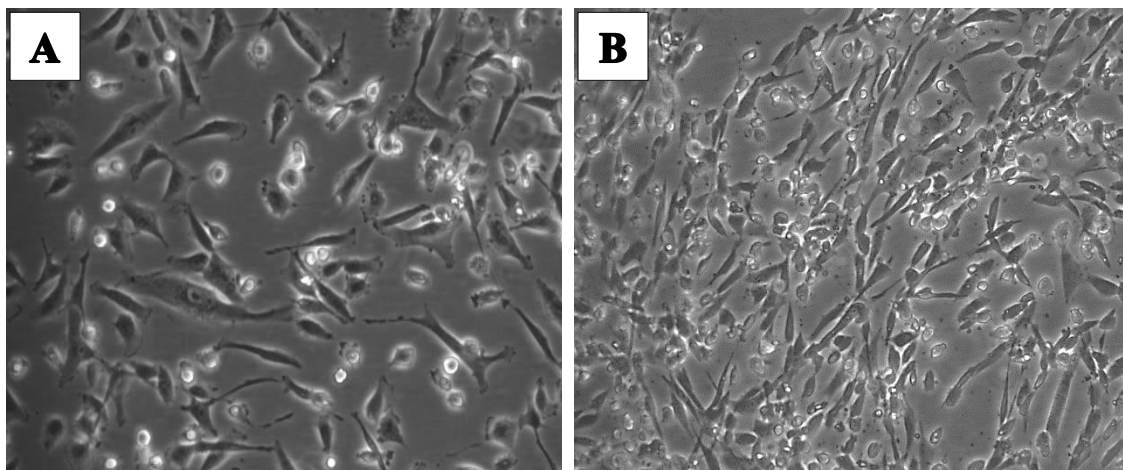


Figure 2. 2. HS-5 cells confluence assay (A) shows 50% surface area coverage by HS-5 at seeding (5.6×10^4 cells/cm²) under 40x magnification and **(B)** shows HS-5 at 70% confluence after 72 hours of culture at 10x magnification by inverted light microscope. Chemotherapy treatment was started when the cells became 70% confluent to avoid unnecessary cell death due to the toxicity of the drugs. HS-5 cells at 70% will have enough growing space until conditioned medium collection 2-3 days following drug treatment, which was 120 hours after seeding.

2.2.2.2 Abcam cytokine microarray protocol

To ascertain candidate molecules for the induction of CIBE through the production of cytokines released by HS-5, the Abcam 80 targets cytokine array (ab133998) was used. On day one, three culture flasks (25 cm²) were seeded with 5.6 x 10⁴ cells/cm² with DMEM-CCM. Cells were allowed to adhere under normal culture conditions. Once the cells were 70% confluence by 72 hours, one flask was treated with 40 µM of CHL. After 1 hour incubation, this flask was washed with PBS 3 times and fresh DMEM-CCM was added before leaving in the incubator for 48 hours. Twenty-four hours later, a further flask was treated for 1 hour with 1.12 µM of MTX. The flask was washed 3 times with PBS and replaced with fresh medium before incubating overnight (24 hours). During treatment with CHL and MTX, an untreated control flask was also washed 3 times with PBS to replenish medium and undergo the same manipulation of treated flasks.

In order to collect the cytokines only produced within the 24-hour period on day 2 (MTX) and day 3 (CHL), all the media were removed from the flasks and replaced with 5 ml of fresh DMEM-CCM. One flask with only culture medium (no cells) was also prepared as a negative control to negate any natural cytokines in the FBS in the medium when compared with the untreated control. The four flasks were placed into the incubator for 24 hours at 37 °C, 5% CO₂ and this medium (conditioned medium) would be collected for cytokine analysis.

The Abcam cytokine array was performed according to the manufacturer's instructions. Briefly, all array reagents and membranes were prepared immediately prior to use and before the collection of conditioned media from flasks. Membranes were placed (printed side up) into a plastic well tray provided with the kit. Membranes were blocked with 2 ml of 1 X blocking buffer for 30 minutes at room temperature (RT) with rocking motion. Blocking buffer was removed from each well and replaced with 1 ml of conditioned medium from each separate flask into the respective wells as shown below in figure 2.3. The plate was incubated on a rocker for 2 hours at RT.

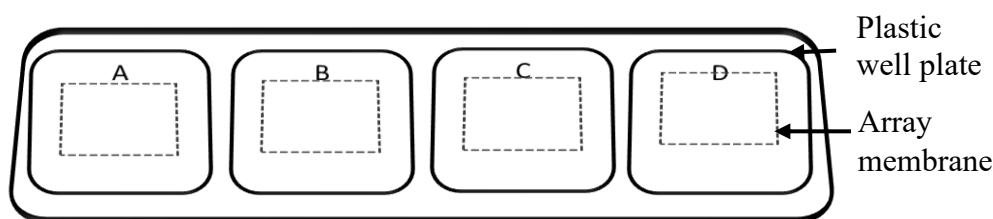


Figure 2. 3. Incubation of array membranes with conditioned medium. A; membrane in culture medium from negative (no cell) control, B; membrane in conditioned medium from untreated cell control, C; membrane in conditioned medium from cells treated with 40 μ M CHL and D; membrane in conditioned medium from cells treated with 1.12 μ M MTX.

Medium samples were aspirated from each well and the membranes were individually washed 3 times with 2 ml of 1X washing buffer I for 5 minutes. Membranes were washed with 2 ml of 1X washing buffer II twice at RT for 5 minutes each. One millilitre of 1 X biotin-conjugated anti-cytokines reagent was pipetted into each well and aspirated after incubation for 2 hours at RT. As described above, washing steps were repeated with 2 ml of I and II washing buffer thrice and twice respectively. Each well had 2 ml of 1 X horse radish peroxidase-conjugated streptavidin added and was incubated overnight at 4 °C with rocking motion.

After 24 hours, reagents were removed from the membranes and the washing steps were performed as described above. Each membrane was placed onto tissue paper and excess wash buffer was removed using another piece of tissue. The membranes were placed printed side up onto a plastic sheet provided with kit. Detection buffer was prepared prior to use by mixing (1:1) buffer C and D, and 500 μ l was gently pipetted onto each membrane and incubated for 2 minutes at RT. Another plastic sheet was placed on top of the membranes and gently rolled over the membranes to remove air bubbles. The plastic sheets containing the membranes was inserted into the Li-cor reader (Bioscience UK Ltd) on a tray and membranes were read simultaneously at 2 minutes.

2.2.2.3 Cytokine microarray results analysis

The Li-cor demonstrated that array membranes were emitting different intensities depending on the amount of cytokine which was captured by antibody coated on each spot (Fig. 2.4). Appendix I shows the layout of the cytokines as arranged on the plate. A positive control normalisation factor (P/C) was determined using the ‘average positive control IgG spots’ on

all four array membranes. Using this P/C normalisation factor it is possible to compare the relative differences in cytokine expression levels among or between more array repeats as described in the manufacturer's instructions. Thus, using the respective correction factor for a given membrane, cytokine spots on each array were normalised for comparison of results across four array membranes. The array was repeated three times for each treatment and results were analysed using 'Image Studio Lite'. Background intensities (medium alone) were subtracted from untreated cells to determine baseline HS-5 cytokine secretion. To obtain the absolute secretion levels for drug treated cells, background intensities were subtracted from cytokine array spot in drug treated samples (section 4.3.1.2).

Cytokine secretion was also analysed for fold-change by dividing the absolute change by the baseline expression of each respective cytokine (section 4.3.1.3). Cytokines were also determined for which cytokines were 'switching on or off' post-drug exposure (section 4.3.1.4). Five cytokines were selected for later investigation, based on both highest absolute expression and fold up-regulation in drug-treated relative to untreated cultures (section 4.3.1). Cytokines were also selected based on a possible role in promoting myeloid differentiation, as commonly observed for TRL and DCL (section 1.6 and 1.7).

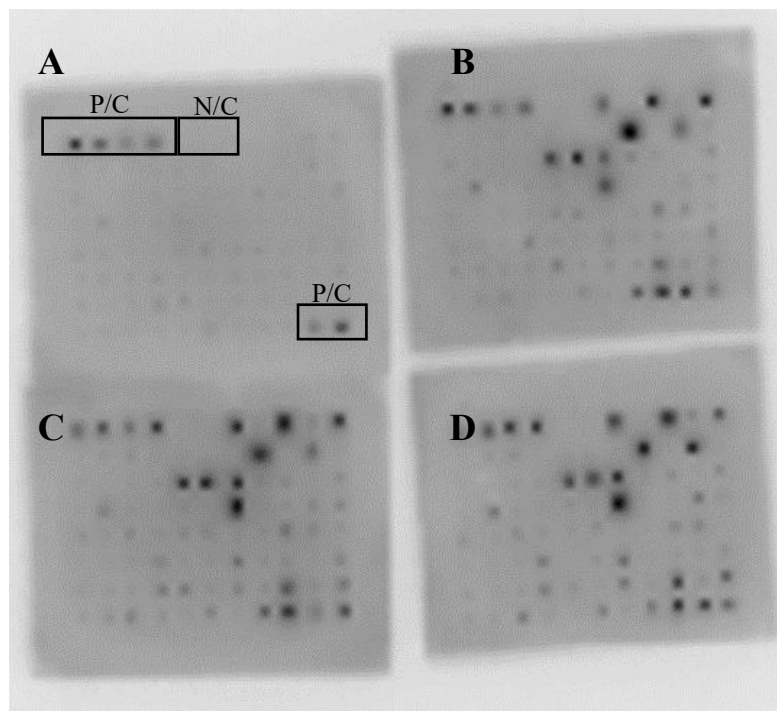


Figure 2. 4. Cytokine membranes after chemiluminescence detection. (A) Culture media (CM), **(B)** CM from untreated cells, **(C)** CM from cells exposed to CHL, **(D)** CM from cells exposed to MTX. As shown, drug treated membranes (C and D) give high intensity spots when compared to both culture media (A) and cells with culture media (B) membranes. There were six positive control (P/C) spots and two negative control (N/C) spots in each membrane as shown in membrane A.

2.2.3 Enzyme-linked immunosorbent assay (ELISA)

2.2.3.1 In-house ELISA assay for TNF- α , IL-6, GM-CSF

For the purpose of this research, five ELISA assays were utilised to assess the possible role of candidate cytokines in chemotherapy induced bystander effect. To validate the cytokine array results and to quantitate cytokine expression in bystander assays, this research developed and/or optimised ELISAs for the selected cytokines. For each ELISA assay, samples were collected from distinct treatment assays and promptly stored at -80 °C until analysis. Given the proteinaceous nature of cytokines, aliquots were carefully prepared in small volumes to facilitate accurate measurement, mitigating the need for multiple freeze-thaw cycles to preserve sample integrity. Out of the five cytokines used in this research, TNF- α ELISA was pre-optimised by the Director of Studies (DoS), IL-6 had been started by another student but required final optimisation, but TGF- β 1, GM-CSF, G-CSF were entirely developed as part of

this research and will be discussed more fully in section 3.2.2. Both capture and detection antibodies for all the cytokines were purchased from BD Biosciences, UK. Table 2.3 illustrates the concentrations of each capture and detection antibody for each cytokines' ELISA after optimisation.

Table 2. 3. Capture and detection antibody concentrations to detect the cytokines analysed in this study. The solvents for these preparations was bicarbonate buffer and PBS/ 1% BSA for capture and detection antibodies respectively.

	TNF-α	IL-6	GM-CSF	G-CSF	TGF-β1
Capture antibody	2 μ g/ml	3.5 μ g/ml	2.5 μ g/ml	4 μ g/ml	3.5 μ g/ml
Catalogue no		(554543)	(554502)	(551342)	(555052)
Detection antibody	1.5 μ g/ml	1.75 μ g/ml	0.75 μ g/ml	1.25 μ g/ml	1.25 μ g/ml
Catalogue no		(554546)	(554505)	(554670)	(555053)

To prepare the plate, capture antibodies were prepared in freshly made bicarbonate buffer (pH 9.6) at the concentrations shown in table 2.3. Nunc immunosorbent plates (96 well; Thermo Thermo Fisher, UK) were coated with 50 μ l antibody solution per well using a multichannel pipette. The plate was gently tapped to ensure the antibody solution spread evenly to cover the base of the well. Plates were covered with lids or sealing strips and left to incubate at 4°C for at least 24 hours. Plates could be stored for at least 3 months at 4°C without loss of activity. At the start of an assay, wells were washed twice with PBS/0.1% Tween-20 and twice with PBS. The plate was blocked by adding 200 μ l PBS /1% BSA per well at room temperature for 1 hour. Plates were washed twice with PBS /0.1% tween, and then a further twice with PBS. If the samples were not ready to add (e.g. still defrosting), PBS was left in the plates to prevent them drying.

Before adding the samples into the plate, the top concentration for the standard curve and high and low concentration quality controls were prepared using the relevant recombinant protein for each cytokine diluted with PBS/1% BSA. The top standard for TNF- α recombinant protein was 30000 pg/ml while all the other cytokines were 8000 pg/ml. Their high (HQ) and low quality (LQ) control samples were: TNF- α was HQ; 1500 pg/ml and LQ; 500 pg/ml and for

rest of the cytokines were HQ; 750 pg/ml and LQ; 75 pg/ml. Further details of setting up the ELISA plate are presented in section 3.2.2.2. The first wells (A1 and B1) of the top two rows of the plate were filled with 100 µl of top standards and the remaining wells of these rows were filled with 50 µl of PBS/1% BSA. Using a multichannel pipette, 50 µl was removed from the first two wells and double diluted across the plate up to last wells, then the excess 50 µl was discarded from the final wells (A12 and B12).

Two wells for each HQ and LQ were pipetted with 50 µl of prepared quality controls. Negative control (N/C) wells were filled with 50 µl of PBS/1% BSA and complete culture media to negate the 'vehicle' for the standards/HQ/LQ, and the samples respectively. Finally, duplicate samples from three biological repeats were added to the plate at 50 µl per well and the completed plate was then incubated for 2 hours at RT. After performing the washing steps described above, 50 µl of detection antibody solution was pipetted into each well using a multichannel pipette (table 2.3). Plates were incubated for 1 hour at RT and the plate washed as previously described. Then the plate was incubated for 30 minutes at RT with 50 µl of streptavidin, or poly-streptavidin, horseradish peroxidase (HRP or poly-HRP respectively; Fisher Scientific UK) diluted in PBS/1% BSA. The concentration of the HRP or poly-HRP were decided according to the candidate cytokine as mentioned in section 3.3.2.3. Following the washing steps, substrate was prepared by adding 100 µl of 10 mg/ml TMB (3,3',5,5' – tetramethylbenzidine) into 10 ml phosphate/citrate buffer with 3 µl of 30% H₂O₂ and mixed well before adding to the plate at 100 µl per well with a multichannel pipette. When the blue colour started to develop in the penultimate standard, 50 µl of 2M sulphuric acid (H₂SO₄) was added to stop the reaction. This 'stop time' also varied depending on which cytokine was being analysed, due to some being secreted at higher or lower levels (section 3.3.2.3). Plates were read on a Fluostar Optima spectrophotometer (BMG Labtech, UK) at 450nm.

2.2.3.2 ELISA commercial kits

TGF-β1

In accordance with the manufacturer's recommendations, the initial step involved the dilution of samples at a ratio of 1:10 with Assay Buffer (1x) following a specific scheme: 20 µl of sample was combined with 180 µl of Assay Buffer (1x). Subsequently, 20 µl of 1N HCl was introduced to a 200 µl portion of the prediluted sample, followed by an incubation period of 1

hour at room temperature. The samples were then neutralised with the addition of 20 µl of 1N NaOH, and vortexed for 5 minutes to ensure thorough mixing.

Microwell strips underwent a two-time wash using approximately 400 µl of Wash Buffer per well, with meticulous aspiration of microwell contents between washes. Wash Buffer was allowed to incubate in the wells for approximately 10 – 15 seconds before aspiration, and the strips were used promptly after washing. Standard dilutions were prepared on the microwell plate by duplicating the addition of 100 µl of Assay Buffer (1x) to all standard wells. Then, 100 µl of Human TGF-β1 standard was pipetted into the first two standard wells (section 3.2.2.2), denoted as A1 and B1. The contents of these two wells were mixed and subsequently 100 µl were transferred to wells A2 and B2 to double dilute the standards. This procedure was repeated five times until wells A7 and B7, generating two rows of human TGF-β1 standard dilutions spanning concentrations from 2000 to 31 pg/ml. The excess of the last microwells were discarded. Blank wells were covered with 100 µl of Assay Buffer (1x) in duplicate. Additionally, 60 µl of Assay Buffer (1x) was added to the sample wells, and this was combined with 40 µl of pre-diluted sample in duplicate. The plate, covered with the provided adhesive film, was incubated at RT for 2 hours on a microplate shaker. Subsequently, all microwell strips were washed, as previously described, and the wells were treated with 100 µl of biotin-conjugate for 1 hour at RT on a microplate shaker. Following the instructed washing procedure, 100 µl of streptavidin-HRP was added to all wells, and the plate underwent a 1 hour incubation at RT. Post-incubation, the plate was treated with 100 µl of TMB substrate solution in all wells and incubated at RT for approximately 30 minutes. As per the manufacturer's guidance, 100 µl of stop solution was promptly added to the plate when the highest standard developed a dark blue colour. It was crucial to add the stop solution quickly and uniformly across the microwells to completely inactivate the enzyme. Absorbance measurements for both samples and standards were determined using a spectrophotometer at a wavelength of 450 nm.

The averaged absorbance for each set of duplicates was computed, and a standard curve was constructed by plotting absorbance against standard concentrations using GraphPad Prism. In accordance with the protocol, the samples were diluted 1:30 (20 µl sample + 180 µl Assay Buffer + 20 µl 1N HCl + 20 µl 1N NaOH and 40 µl pretreated sample + 60 µl Assay Buffer), and concentrations were calculated by multiplying the values read from the standard curve by the dilution factor (x 30).

G-CSF

The G-CSF ELISA assay was conducted following the manufacturer's protocol. Distilled water was added to standard wells (see section 3.2.2.2; A1-A7 and B1-B7) and blank wells. In duplicate sample wells, 125 µl of distilled water was added, and 25 µl of each sample were combined with the contents in the designated wells. The plate was covered with a plate cover, and incubated at RT for 3 hours on a microplate shaker. Subsequently, microwell strips were subjected to six washes with approximately 400 µl of wash buffer per well. Thorough aspiration of microwell contents between washes was ensured, and the wash buffer was allowed to incubate in the wells for about 10 – 15 seconds before aspiration. The strips were used immediately after washing. The plate was treated with 100 µl of TMB substrate solution in all wells, including blank wells, and incubated at RT for about 10 minutes.

In accordance with the manufacturer's recommendations, 100 µl of stop solution was added to the plate when the highest standard exhibited a dark blue colour. Absorbance measurements for both samples and standards were determined using a spectrophotometer at a wavelength of 450 nm. The averaged absorbance for each set of duplicates was computed, and a standard curve was constructed by plotting absorbance against standard concentrations using GraphPad Prism. Following the protocol's instructions, a common dilution factor for samples was considered due to the conjugate, which needed inclusion in the calculation. The samples contributed 100 µl to the final volume per well, composed of 75 µl of sample diluent plus 25 µl of the sample, resulting in a 1:4 dilution. The remaining 50 µl, contributing to a total of 150 µl, was due to the addition of 50 µl conjugate to all wells. Consequently, the concentrations read from the standard curve were multiplied by the dilution factor (x 4).

2.2.4 *In vitro* micronucleus assay

The micronucleus assay (MN) has become one of the most common methods to assess genotoxicity of different chemical and physical factors, including ionising radiation-induced DNA damage. MN has been most widely used for *in vivo* assay as the most reliable test to assess the induction of chromosomal aberrations, which is one of two major endpoints of mutagenicity (Sommer *et al.*, 2006; Hayashi, 2016). As a multi-target genotoxic endpoint, the MN assay was used in this research to detect the genotoxicity of the five cytokine candidates. The investigation was prompted by prior research within the team, which had established the induction of MN by CIBE.

On day one (0 hr), TK6 were seeded at 1.5×10^5 cells/ml in RPMI-CCM medium and incubated overnight in a CO₂ incubator. On day two (24 hr), a 10 µl aliquot of TK6 from each flask was counted for baseline measurements. Then TK6 cells were directly exposed to recombinant cytokine using three different treatment approaches representing single cytokine treatment at healthy reference range, single cytokine treatment at cytokine storm doses and combination of two cytokines treatment at ‘high’ baseline plus ‘high’ storm doses with reference to the cytokine concentrations listed in the table 2.2. Alongside the cytokines, TK6 were treated with MMC (section 2.1.4) and PBS at the same volume of PBS as the cytokine treatments, as a positive control and negative control respectively. The MMC dose was determined from previous work with doses of MMC to choose a dose with RPD > 50% and statistically significant MN induction; MMC was used at 30 nM (10ng/ml) (Vernon *et al.*, 2022).

On day 3 (48 hr), TK6 cells were washed, counted and reseeded into fresh culture medium at the baseline cell count determined on day 2, for a further 24 hours recovery. On day four (72 hr), cell counts were performed to determine RPD.

2.2.4.1 Cytotoxicity detection

According to the Organisation for Economic Co-operation and Development (OECD) 487 (micronucleus assay) guidelines, in order to accurately assess MN for genotoxicity testing, doses used must result in cell viability, measured as RPD, of $> 55\% \pm 5\%$. Therefore, cell counts were also taken of 24 hours pre- and post-treatment.

The trypan blue exclusion assay was used to determine cytotoxicity of the TK6 cells during execution of the MN assay. The cytotoxicity assay was performed to enumerate total, live and dead cells, and calculate percentage viability parameters using the automated Luna-FLTM cell counter (Labtech International Ltd), which maximised accuracy and reproducibility (section 2.2.1.6).

2.2.4.2 Genotoxicity detection

After confirming the cell cytotoxicity (section 2.2.4.1) is within the $55\% \pm 5\%$ requirements for RPD, 2×10^4 TK6 cells were harvested per slide and two slides were prepared for each treatment category including control flasks. They were pipetted into microcentrifuge tubes and centrifuged (MicroCentaur SANYO) at $200 \times g$ for 5 minutes. The supernatant was decanted, and the pellet resuspended in 150 µl of PBS. Cell suspensions were dispensed into Shandon

cytofunnels attached onto a clean grease free microscope slide and centrifuged at 800 rpm (300 x g) for 8 minutes onto each glass slide using a Cytospin 4 (Thermo Fisher). Cells were fixed using 90% methanol for 10 minutes at RT and air dried for 5 minutes. Cytospun slides were stained whilst maintaining them in the dark, by dipping in fresh phosphate buffer (0.66% w/v potassium monobasic + 0.32% w/v sodium phosphate dibasic; pH 6.4), followed by staining for 1 minute with 12% (w/v) acridine orange in phosphate buffer and washing twice with fresh phosphate buffer for 10 and 15 minutes respectively. Slides were air dried at room temperature and stored in the dark until scoring to avoid fading.

Slides were wet mounted with phosphate buffer and cover-slipped immediately before analysis. MN were detected and scored using a fluorescent microscope (Nikon Eclipse 80i TE300) with an attached Nikon Digital Sight DSF1 camera Nikon Coolpix 950 camera (Nikon Instruments Europe) at x40 magnification using triple band pass (standard excitation and emission wavelength range of 435-660nm for DAPI, FITCs and Texas Red filters). Images were visualised with NIS Elements software and pictures were captured with a Nikon Digital Sight DSF1 camera. Aberrant cells were identified through the distinctive properties of acridine orange where the cytoplasm stains orange and nuclear material (including MN) appear green. Slides were scored for mononucleated cells (normal); mononucleated, binucleated and multinucleated cells with or without MN; lobed cells; apoptotic and necrotic cells (Fig. 2.5). The criteria for scoring the MN are: a) must be about 1/16th to 1/3rd the size of the main nucleus, (b) must be distinct from artefacts and non-refractile, (c) must have the same staining intensity as the main nucleus/nuclei and (d) can touch the main nucleus but must not be linked or overlap it (Fenech, 2000). A total of 2000 cells were scored per treatment. For all concentrations, three biological replicates were performed, data was averaged and presented per 1000 mononucleated cells. RPD was compared relative to the vehicle (PBS) and positive (MMC) control in line with the OECD guidelines. Doses which induced an RPD <50%, were not scored for MN.

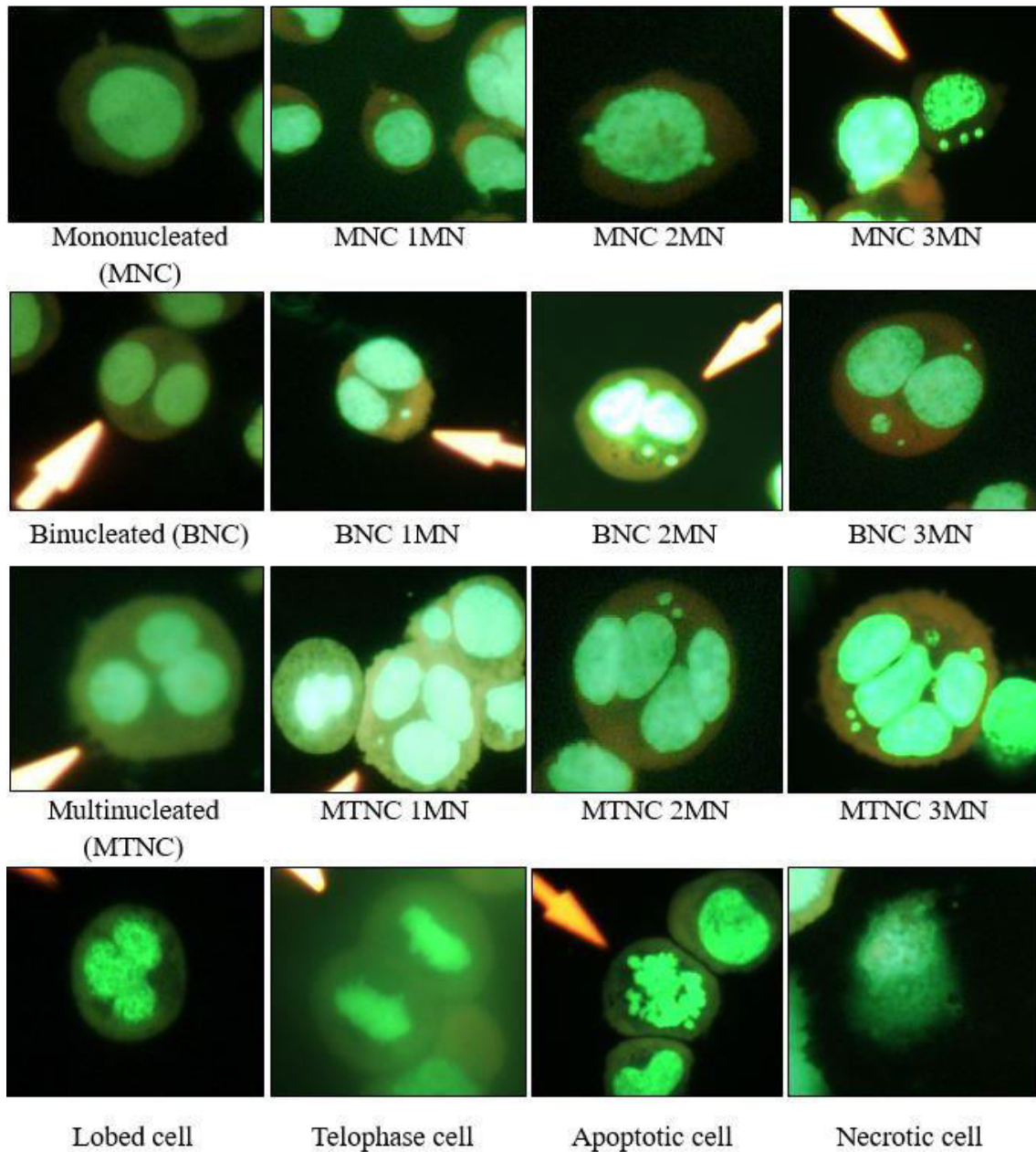


Figure 2. 5. Visual presentation of micronuclei (MN) following recombinant cytokine treatments. Micronuclei formed by nuclear envelope deposition around fragments or lagging chromosomes during mitosis as a result of nuclear damage. Both the main nucleus and MN are stained green against an orange cytoplasmic background. According to recommended criteria of size ($1/16^{\text{th}}$ to $1/3^{\text{rd}}$ of main nuclei), appearance and similar staining intensity to the main nucleus/nuclei, MN were scored. Different parameters were observed during the MN scoring including, mononucleated cells (MNC), binucleated (BNC) and multinucleated cells (MTNC) with/without micronuclei, lobed cells, apoptotic and necrotic cells.

2.2.5 Cytokine signalling pathway inhibition

According to the results of chapter 4 and 5 in this research, IL-6 proved to be the most interesting cytokine to pursue further. Using two chemical inhibitors, the IL-6 signalling pathway was blocked in TK6 and attempted to explore its role in MN induction (section 5.2.3.2). As chemical inhibitors, FLLL-32 and BAY-293 were used to inhibit IL-6 signalling pathways in isolation. According to the manufacturer's instructions, both inhibitors were analysed for the optimum doses with respect to cell lines used in this study (section 5.2.3.1).

2.2.5.1 FLLL-32

FLLL-32, a synthetic analogue of curcumin with antitumour activity, is currently known to induce melanoma apoptosis and inhibit tumour growth in various cancers (FLLL 1). FLLL-32 is a potent JAK2/STAT3 inhibitor with IC₅₀ of <5 µM, which specifically reduced STAT3 phosphorylation at Tyr705 (pSTAT3) by IL-6 in breast cancer cells (FLLL-32, Selleckchem.com, 2023). After dose response optimisation in section 5.3.3.1, the working solution concentration was 5 µM in every treatment.

2.2.5.2 BAY-293

BAY-293 (compound 23) selectively inhibits the k-RAS–SOS1 interaction with an IC₅₀ of 21 nM. Son of Sevenless 1 (SOS1) is the guanine nucleotide exchange factor (GEF) and activator of RAS (BAY-293, Selleckchem.com). The optimal concentration for BAY-293 from the optimisation study (section 5.3.3.1) is 2 µM.

TK6 were seeded in 12-well plates at 1.5×10^5 cells/ml in RPMI-CCM and plates were incubated at 37 °C overnight. Control wells were prepared as follows: untreated (without either inhibitor or IL-6), IL-6 alone (4000 pg/ml), and inhibitor alone (FLLL-32 at 5 µM or BAY-293 at 2 µM). Samples were prepared in duplicate wells to incubate cells with IL-6 in the presence and absence of inhibitors at their respective doses; a further two wells were prepared to incubate cells with and without IL-6 in the presence of both inhibitors. Following 24-hour incubation, aliquots were taken from each sample and cell counted. Then respective samples were treated with inhibitors of FLLL-32 at 5 µM or BAY-293 at 2 µM. Plates were incubated at 37 °C in a humidified atmosphere with 5% CO₂ air for 2 hours. IL-6 at 4000 pg/ml was then added to the respective wells of controls and sample duplicates and incubated for 24 hours,

after which cell counts and viability were determined. Then cells were reseeded into new RPMI-CCM media for another 24 hours to calculate RPD. On the following day, aliquots of 20,000 cells were sampled from each control and test well, and MN slides prepared as described in section 2.2.4.2 providing the viability for the respective well was $\geq 50\%$.

2.2.6 Cytokine expression inhibition in co-culture models

Utilising bystander models previously developed to analyse MN formation following chemotherapy exposure, IL-6 secretion from the HS-5 compartment was knocked down using siRNA or inhibited using a chemical inhibitor to further explore the role that IL-6 plays in inducing genotoxicity in bystander TK6 cells. It is relevant to remember that HS-5 are exposed to the drug and secrete the cytokines, but the genotoxicity is measured in the bystander cells (TK6), thus the IL-6 secretion/synthesis needs to be inhibited in the HS-5, but the consequences are measured in the TK6 bystander cells.

2.2.6.1 IL-6 siRNA knockdown

RNA interference (RNAi) is a means of silencing genes by way of mRNA degradation. Gene knockdown (k/d) by this method is achieved by introducing small double-stranded interfering RNAs (siRNA) into the cytoplasm. Small interfering RNAs can originate from inside the cell or can be exogenously introduced into the cell. IL-6 k/d was done according to the manufacturer's instructions (Thermo Fisher, UK) and recommended procedure to transfect Human Silencer® Select IL-6 siRNA into human MSC using Lipofectamine™ transfection reagent. As a negative control, the Silencer™ Select Negative Control No. 1 siRNA was used with Opti-MEM™. Only forward transfection has been used for IL-6 k/d in HS-5 cells in this research. All volumes are given on a per well basis as illustrated by the manufacturer's MSC transfection protocol.

A day before the transfection, the HS-5 cell line was seeded at 3.5×10^4 cells per well in a 24-well plate with 500 μ l RPMI-CCM. For each well to be transfected, RNAi duplex-Lipofectamine™ complexes was prepared by adding 6 pmol RNAi in 50 μ l Opti-MEM and mixed gently. Lipofectamine™ was gently mixed before use, then diluted by adding 1 μ l into 50 μ l Opti-MEM and mixed gently. After combination of the diluted RNAi duplex with the diluted Lipofectamine™, the mixture was incubated for 20 minutes at RT. RNAi duplex-Lipofectamine™ complexes was transferred into each sample well. The plate was gently mixed

on a plate rocker for 10 minutes for equal distribution of the k/d reagents to every cell in the well. The plate was incubated with the transfected HS-5 cells at 37 °C in a CO₂ incubator for 24 hours and then followed with the chemotherapy treatments and washes as described in section 2.2.1.7. Plates were incubated for another 48 hours (72 hours after k/d treatments), and bystander assay was performed as described in section 2.2.1.7. The RPD was calculated and the MN assay performed on the bystander cells. This time period correlates with the highest bystander genotoxicity detected by a previous PhD team member (Kelechi Okeke) and also the lowest IL-6 expression by the HS-5 cells following the IL-6 siRNA k/d (section 6.3.1.2). The same protocol was performed to prepare the scramble control using Silencer™ Select Negative Control No. 1 siRNA (Thermo Fisher, UK).

2.2.6.2 IL-6 chemical inhibition by resatorvid

Resatorvid (TAK-242) is a drug which acts as a selective antagonist to inhibit the Toll-like receptor 4 (TLR4). Resatorvid downregulates the expression of the TLR4 downstream signalling molecules, which inhibit the production of lipopolysaccharide and damage-associated molecular patterns-induced inflammation, mainly IL-6 and TNF- α (resatorvid, Selleckchem.com, 2023). Its anti-inflammatory effects may show potential as an additional treatment alongside conventional chemotherapy drugs (Matsunaga *et al.*, 2011; Suzuki *et al.*, 2012).

Resatorvid was tested for the optimal working dosage and inhibition timeline in HS-5 (section 6.2.2). According to the manufacturer's information (resatorvid, Selleckchem.com, 2023) and following optimisation results, 3 μ M was selected to use in this research. HS-5 cells were seeded at 7×10^4 cells in a 12-well plate and left to incubate for 24 hours at 37 °C in a 5% CO₂ atmosphere. Cells were treated with 3 μ M resatorvid and placed in the incubator for 2 hours. After that, HS-5 cells were treated with CHL (4 μ M) and MTX (1.12 μ M) for 1 hour in the incubator (table 2.1). Following incubation with the chemotherapies, cells were washed with PBS three times and fresh RPMI-CCM was added into each well. HS-5 cells were incubated for 48 hours at 37 °C in a 5% CO₂ atmosphere. On the next day, the culture media were changed in all the wells and TK6 cells in a culture insert were added to each well (Fig. 2.5) and the bystander assay was performed as described in section 2.2.1.7.

2.2.7 Statistical analysis

All statistics and graphical illustrations were done using GraphPad Prism software v. 8.2.1 for Windows (GraphPad Software, Inc., La Jolla, California, USA). Except for where otherwise stated, the mean, standard deviation and standard error of the mean were calculated using GraphPad prism software. The unpaired Student t-test was used to determine direct significance between treated and untreated (control) samples, while one-way or two-way ANOVA was used for group comparisons followed by a Dunnett's, Tukey's or Šídák's multiple comparison test.

All error bars are expressed as mean \pm standard deviation (SD) of three independent biological repeats unless otherwise stated. Statistical significances were performed using analysis of variance and are represented as (*) for $p \leq 0.05$, (**) for $p \leq 0.01$, (***) for $p \leq 0.001$ and (****) for $p \leq 0.0001$.

CHAPTER 3

METHOD DEVELOPMENT

3.1 Introduction

Cell culture

Mammalian cell culture technology has revolutionized biological research by providing a controlled environment for studying cellular behaviour. This controlled environment allows researchers to manipulate various factors and observe cellular responses under tightly regulated conditions, which may not be feasible or easily achievable *in vivo*. One of the primary advantages of cell culture is that it enables researchers to study cell behaviour *in vitro*, which can sometimes transcend what occurs *in vivo*. This is particularly important when investigating specific aspects of cell physiology or pathophysiology, as it allows for a more controlled and detailed examination of cellular processes (Joseph *et al.*, 2018).

Cell culture has found applications across a wide range of fields within life sciences and medicine. These applications include assessing drug efficacy and toxicity, studying reproductive technologies, and producing vaccines and biopharmaceuticals. Each of these areas benefits from the ability to control and manipulate cell behaviour *in vitro*. While cell culture offers numerous advantages, it also comes with challenges. These challenges include issues related to the culture environment, such as hyperoxic conditions or improper mechanical settings. These factors can influence cell behaviour and, if not controlled, may lead to data misinterpretation (Yao and Asayama, 2017).

To ensure the reliability and reproducibility of experimental results, it is essential to optimise cell culture conditions. Several factors contribute to optimal cell growth, including substrate for cell attachment, incubator conditions (pH, osmolality, temperature), and the choice of growth medium. Among these factors, the choice of the culture medium stands out as critical. The culture medium provides essential nutrients, growth factors, and other components necessary for cell survival and proliferation. Selecting the right medium tailored to the specific cell lines used in research is paramount for success.

Later in this study, the research will be working with co-culture models, thus the development of an *in vitro* co-culture model involving the BM cell line HS-5 and TK6 lymphoblast bystander cell lines required careful consideration. Ensuring that both cell lines thrive in the same culture environment is essential for maintaining experimental consistency and generating reliable data. The use of various media and their optimisation for both cell lines are not only about growth but also serves as a quality control measure. Consistency in culture conditions minimises variability in experimental outcomes and ensures that any observed effects are due to the experimental manipulations rather than fluctuations in the culture environment.

Doubling time refers to the amount of time it takes for a quantity to double in size or value. This concept is often used in the context of population growth, cell culture, and financial investments. The doubling time of any cell lines can be calculated using the following formula by monitoring their growth over time: Doubling Time = $(t_2 - t_1) * \log(2) / [\log(N_2) - \log(N_1)]$ (<https://toponlinetool.com/cell-doubling-time-calculator/>). For a meaningful doubling time calculation, one may need to extend the time period of observation or adjust the initial cell seeding density to ensure the population doubles within that time frame. The doubling time of cells is a versatile and essential parameter with broad applications in biology, medicine, biotechnology, and research. It aids in experimental design, quality control, and the understanding of various biological processes, making it a fundamental concept in the life sciences. Therefore, monitoring the growth of relevant cell line over time and calculating the doubling time is recommended for accurate results in different assays.

Enzyme-Linked Immunosorbent Assay (ELISA)

From the cytokine array data (Chapter 4), five key cytokines were identified for further investigation: tumour necrosis factor-alpha (TNF- α), interleukin-6 (IL-6), granulocyte colony-stimulating factor (G-CSF), granulocyte-macrophage colony-stimulating factor (GM-CSF) and transforming growth factor beta 1 (TGF- β 1). This research demands the quantification of these cytokines under various experimental conditions, encompassing different treatments and time points. To accomplish this, a reliable method was required for cytokine detection. Cytokines can be detected through various techniques, each with its own merits. Among these methods, the Enzyme-Linked Immunosorbent Assay (ELISA), a widely adopted biochemical technique, has had a profound impact on the fields of immunology and molecular biology.

ELISA is a cornerstone technique in biomedical research and clinical diagnostics, primarily due to its sensitivity, specificity, and versatility. A comparison among different assays, such as PCR, loop-mediated isothermal amplification (LAMP), radio immune assay (RIA) and ELISA cleared that ELISA has multiple advantages (Alhajj *et al.*, 2023). Its high specificity and sensitivity allow for the early detection of disease markers, enabling prompt treatment for better patient outcomes. ELISA assays play a pivotal role in various applications including diagnosis of infectious diseases, autoimmune disorders, screening tests for human immunodeficiency virus (HIV), detection of other viruses, bacteria, fungi, blood typing, presence of the pregnancy hormone hCG, laboratory and clinical research, forensic toxicology and identifying biomarkers for various cancers. The evolution of the ELISA has played an important role in the detection of contaminants, allergens, and pathogens in food products and the environment (Mousavi *et al.*, 2016; Alhajj *et al.*, 2023).

The ELISA encompasses various types, each tailored to specific purposes. Among these, the primary categories are direct, indirect, sandwich, and competitive ELISA (Fig. 3.1). These ELISA variants distinguish themselves based on their intended applications, sensitivity levels, and procedural intricacies. The selection of the appropriate ELISA type hinges upon factors such as the nature of the target antigen, the desired level of sensitivity, and the available resources.

There are four main general steps to completing an ELISA immunoassay including coating (either antigen or antibody), blocking, detection, and final read. In the most common approach to using the ELISA technique, an aliquot of sample or calibrator containing the antigen to be quantified is added to the plate and allowed to bind with a solid-phase antibody. After washing, an enzyme-labelled antibody is added and forms a sandwich complex of solid-phase Ab-Ag-Ab enzyme (Fig. 3.1C). Unbound antibody is then washed away, and enzyme substrate is added. This step can generate a colour signal visible to the naked eye, with a blue or yellow colour depending on the substrate and HRP or alkaline phosphatase respectively. The amount of product generated is proportional to the quantity of antigen in the sample (Alhajj *et al.*, 2023). A primary detection antibody is a specific antibody that only binds to the protein of interest. In contrast, a secondary detection antibody is a second enzyme-conjugated antibody that binds to a primary antibody that is not enzyme-conjugated (Mousavi *et al.*, 2016).

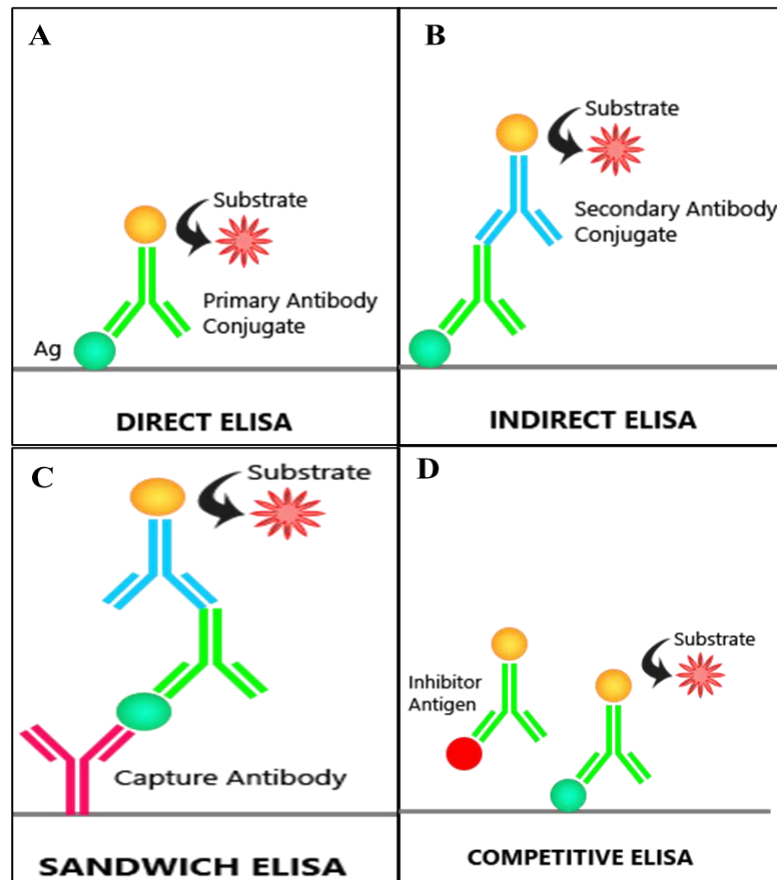


Figure 3. 1. Different types of ELISA. (A) Direct ELISA, a single antibody (monoclonal or polyclonal) linked to an enzyme is used to detect the target antigen. This enzyme-conjugated antibody directly binds to the antigen. It is a simple and quick method but may have limitations in sensitivity and specificity. (B) Indirect ELISA, the antigen is immobilized on the solid phase (usually a microtitre plate). A primary antibody specific to the antigen is added, followed by an enzyme-conjugated secondary antibody that binds to the primary antibody. This ELISA is more versatile and sensitive compared to the direct method. It allows the use of a wide range of primary antibodies and can amplify the signal. (C) Sandwich ELISA, the antigen to be detected is bound between two antibodies - a capture antibody (usually immobilised on the solid phase) and a detection antibody (enzyme-conjugated). If the antigen is present, it will form a "sandwich" between the two antibodies. This ELISA is highly specific and sensitive, making it suitable for detecting low concentrations of antigens, including cytokines and other biomarkers. (D) Competitive ELISA is used to measure the concentration of small antigens that may not have multiple epitopes for antibody binding. In this assay, the sample antigen competes with a labelled antigen (conjugated to an enzyme) for binding to a limited amount of immobilized antibody. This ELISA is valuable for quantifying the concentration of antigens like hormones and drugs.

Specific antibodies in a sample can also be quantified using an ELISA procedure in which antigen instead of antibody is bound to a solid phase. The second reagent is an enzyme-labelled antibody specific to the analyte antibody. In addition, enzyme conjugates coupled with substrates that produce visible products have been used to develop ELISA-type assays with results that can be interpreted visually. Such assays are very useful in screening (Alhajj *et al.*, 2023). In the case of cytokine detection, ELISA has the ability to selectively detect and quantify cytokine concentrations in complex biological samples such as serum, plasma, or culture media depending on their antigen-antibody interaction.

The ELISA can be conducted in either a qualitative, quantitative or semiquantitative format. In a qualitative setup, the assay yields a straightforward positive or negative result of a particular antigen/antibody in a sample, with the determination of the cutoff point of the analysis. Typically, this border is established by employing two or three times the standard deviation to differentiate between positive and negative samples. On the other hand, quantitative ELISA involves a more detailed analysis. In this approach, the optical density of the sample is compared to a plotted standard curve consisting of known values, usually created through a serial dilution of the target molecule. The semiquantitative results compare the intensity of the signals, which allow for comparison of relative antigen levels in a sample (Alhajj *et al.*, 2023). Thus, the development of an ELISA and the generation of a standardised concentration curve is the best tool to comprehensively analyse TNF- α , IL-6, G-CSF, GM-CSF, and TGF- β 1 under varying experimental conditions and across different time frames.

3.2 Methods

3.2.1 Cell culture medium optimisation

The growing capacity of HS-5 and TK6 was determined and compared in three culture media in order to select the most suitable environment for co-culture experiments: DMEM-HG, DMEM-low glucose (LG) and RPMI-1640.

3.2.1.1 Media selection assay for HS-5

HS-5 were seeded at 1×10^5 per flask in three media in 25 cm² vent cap Corning cell culture flasks (Fisher Scientific) and incubated in a humidified culture chamber with a 5% CO₂ atmosphere as described in chapter 2, section 2.2.1.1. Media was changed every 2-3 days, and cell morphology was determined under a microscope every 24 hours up to 120 hours and documented as pictures.

All three flasks were trypsinised, as soon as one flask achieved confluence (5-7 days/ ≥ 120 hours). Live cell counts and percentage viability were determined using the Luna counter (section 2.2.1.6). Each flask was re-seeded (2nd passage) at a 1:3 ratio in three different media and again trypsinised and recounted when one flask achieved confluence. The same procedure was repeated until 3rd passage.

3.2.1.2 Media selection assay for TK6

TK6 cells were seeded at 3×10^5 cells/ml in a 6 well plate containing 2 ml of the three different media (DMEM-HG, DMEM-LG and RPMI-1640) and kept in an incubator until the next day. Live cell counts, percentage viability and TK6 cell size were analysed every 24 hours for five days using the Luna counter (section 2.2.1.6).

3.2.1.3 TK6 growth curve development

TK6 cells were seeded at three different seeding densities as following: 0.5×10^5 cells/ml, 1.5×10^5 cells/ml and 2.5×10^5 cells/ml into a 6-well plate with 2 ml of RPMI-CCM. The following day, live cell counts were taken for every well and repeated every 24 hours over 5 days (120 hours). Using the live cell counts in respective samples, a TK6 growth curve was developed and the TK6 doubling time was analysed using the following formula:

$$\text{Doubling Time} = (t_2 - t_1) * \log(2) / [\log(N_2) - \log(N_1)]$$

(t1 is the initial time (in hours) when the growth experiment starts, t2 is the final time (in hours) when the growth experiment ends. N1 is the initial cell count at time t1, N2 is the final cell count at time t2)

Each cell media selection assay was conducted with three biological replicates with HS-5 and TK6 to ensure robustness and reliability of the results. During culturing, a minimum of three wells or three flasks were included to represent each sample, thereby mitigating the impact of outliers. Cell count averages were calculated to minimise errors in the data analysis process.

The data analysis utilised GraphPad Prism software version 8.2.1, employing two-way ANOVA for group comparisons, followed by Tukey's multiple comparison test. The results are presented as mean \pm SD for three independent biological replicates, with significance levels denoted as follows: (*) for $p \leq 0.05$, (**) for $p \leq 0.01$, (***) for $p \leq 0.001$, and (****) for $p \leq 0.0001$.

3.2.2 ELISA development

This study focused on five cytokines. The TNF- α ELISA assay has been successfully completed and well-established by the DoS. For the cytokine IL-6, preliminary work was initiated by a previous student; however, further work was needed to optimise the assay's sensitivity. In contrast, the development of ELISA assays for GM-CSF, G-CSF, and TGF- β 1 was an integral part of this PhD research.

The development of an ELISA assay typically involves several key steps, which include the optimisation of both capture and detection antibody concentrations. Additionally, standard curve development is a crucial aspect of assay development. Finally, streptavidin peroxidase and poly-HRP to increase sensitivity were important components in the assay methodology. This approach ensures the accuracy and reliability for these cytokines.

3.2.2.1 Capture and detection antibodies optimisation

In this study, the development of an optimised ELISA assay involved a systematic approach to determine the ideal concentrations of capture and detection antibodies for precise quantification of cytokines. The method entailed the use of two microtitre plates, referred to as "plate one" and "plate two," containing high-quality (HQ) and low-quality (LQ) controls for recombinant

cytokines, and negative controls of PBS and RPMI-CCM. A "checkerboard" approach was employed to establish the most effective antibody concentrations. Both capture (CAP) and detection (DET) antibodies were titrated against each other to determine which combination of concentration produces the best signal-to-background ratio when comparing HQ and LQ against the negative controls.

A range of CAP antibody concentrations (ranging from 2 to 5.5 $\mu\text{g/ml}$) was applied to the plates with incrementing concentrations vertically from rows A to H and filling every well with that dose in a horizontal orientation from columns 1 to 12 (Fig. 3.2). These concentrations were in accordance with the manufacturer's recommendations, with specific ranges for GM-CSF (2 to 5.5 $\mu\text{g/ml}$), G-CSF (0.5 to 4 $\mu\text{g/ml}$), and TGF- β 1 (0.5 to 4 $\mu\text{g/ml}$). The plates were subsequently incubated at 4°C for at least 24 hours. The plates were washed to remove any unbound antibodies and were then blocked with 200 μl of PBS/1% BSA per well at RT for 1 hour. After another round of washing, recombinant cytokines (HQ or LQ; see section 2.2.3.1 for doses) and negative controls (PBS or RPMI-CCM), were added to the plates as indicated in Figure 3.2.

The ELISA plates were divided vertically into two halves: columns 1 to 6 (orange or blue) and columns 7 to 12 (yellow or green). The first half of plate one (orange; columns 1 to 6) was treated with GM-CSF HQ (750 pg/ml), while the second half (yellow; columns 7 to 12) was treated with PBS. Plate two followed a similar pattern, with the first half (blue; columns 1 to 6) treated with GM-CSF LQ (75 pg/ml) and the second half (green; columns 7 to 12) with RPMI-CCM. Both plates were incubated for 2 hours at RT. The selection of HQ and LQ concentrations was based on the cytokine's standard curve, with HQ being 2-3 points from the highest plateau and LQ being 2-3 points from the lower detection limit. The same approach was attempted for G-CSF and TGF- β 1.

Following recombinant protein incubation, the plates were washed again, and a range of DET antibodies (0.5 to 1.75 $\mu\text{g/ml}$) were applied to 'columns' from 1 to 6 vertically and 7 to 12, spanning rows A to H. These DET antibody concentrations were with specific ranges for GM-CSF (0.5 to 1.75 $\mu\text{g/ml}$), G-CSF (0.5 to 1.75 $\mu\text{g/ml}$), and TGF- β 1 (0.5 to 4 $\mu\text{g/ml}$) in accordance with the manufacturer's recommendations. The plates underwent a series of washing steps to eliminate unbound antibodies as instructed above. To amplify the signal, HRP was applied to each well for 30 minutes incubation, alternatively poly-HRP was employed during

3.2.2.2 Standard curve optimisation

The process of standard curve development involved the utilisation of predetermined concentrations of both CAP and DET antibodies for each cytokine, as established in section 3.2.2.1. In tandem with this, duplicate samples of HQ and LQ positive controls, as well as negative controls consisting of PBS/CCM were included. These controls can be used to assess the accuracy of the standard curve as well as intra- and inter-assay variability as soon as the standard curve was established.

Having determined the optimal CAP antibody concentrations for GM-CSF as 2.5 µg/ml, G-CSF as 4 µg/ml, and TGF-β1 as 3.5 µg/ml, the standard curve development for these cytokines commenced. The ELISA plate was coated with GM-CSF CAP antibody at a concentration of 2.5 µg/ml and incubated at 4°C for 24 hours before the experiment. Similar plates were set up for G-CSF and TGF-β1. As depicted in figure 3.3, the ELISA plate was divided horizontally into two sections, denoted as AB and EF, to act as distinct plates. This division facilitated the generation of two separate standard curves, enabling the subsequent analysis of intra-assay variability.

The first two rows in both sections (AB and EF) were reserved for standard curve development with recombinant proteins. Based on the knowledge of normal cytokine levels in the circulation during typical immune function, as well as following exposure to chemotherapy, a standard curve was constructed to encompass the expected concentration range for the samples. For GM-CSF, G-CSF, and TGF-β1, the standard curve concentrations were established as 8000, 4000, 2000, 1000, 500, 250, 125, 62.5, 31.25, 15.62, 7.81, and 3.91 pg/ml. The wells designated for the standard curve (wells 2 to 12 in rows A, B, E, and F) were filled with 50 µl of PBS/1% BSA and the top standard (8000 pg/ml) prepared in PBS/1% BSA was introduced into wells A1, B1, E1, and F1 at a volume of 100 µl. Double dilution was performed across the plate, spanning wells from 1 to 12 for each of rows A, B, E and F, using a multichannel pipette by removing 50 µl from well 1, and mixing with well 2, then moving sequentially across the plate.

Employing pre-diluted recombinant cytokines, GM-CSF HQ (750 pg/ml) and LQ (75 pg/ml) were prepared in PBS/1% BSA. HQ was added to the plate to cover wells from C1 to C6 and G1 to G6, while LQ was introduced to wells from C7 to C12 and G7 to G12. Subsequently, negative controls, represented by PBS, were incorporated into wells from D1 to D6 and H1 to H6, while RPMI-CCM was applied to wells from D7 to D12 and H7 to H12. The plate was

then incubated at room temperature for a duration of 2 hours. The same approach was used for G-CSF and TGF- β 1.

Subsequent to the washing steps, the plate was subjected to incubation with GM-CSF DET antibody at a concentration of 0.75 μ g/ml for 1 hour at RT. In the case of G-CSF and TGF- β 1, the DET antibody concentration employed was 1.25 μ g/ml. This step was followed by further washing and subsequent incubation with HRP for 30 minutes. It is noteworthy that during optimisation, as was detailed in section 3.2.2.1, poly-HRP was utilised as an alternative to HRP, and the optimal concentration was determined in accordance with the specific cytokine's standard curve development. The substrate solution was introduced to each well, followed by the addition of H₂SO₄ to stop the reaction. The precise termination timing was established by visual assessment of colour development in the final wells of each standard curve. Finally, the plates were read at 450 nm by spectrophotometer.

Optimisation performed with the standard curve,

- Vary the dilution of streptavidin HRP and/or poly-HRP
- Vary the 'stop' time for development of the colour change relative to the streptavidin HRP and poly-HRP dilutions

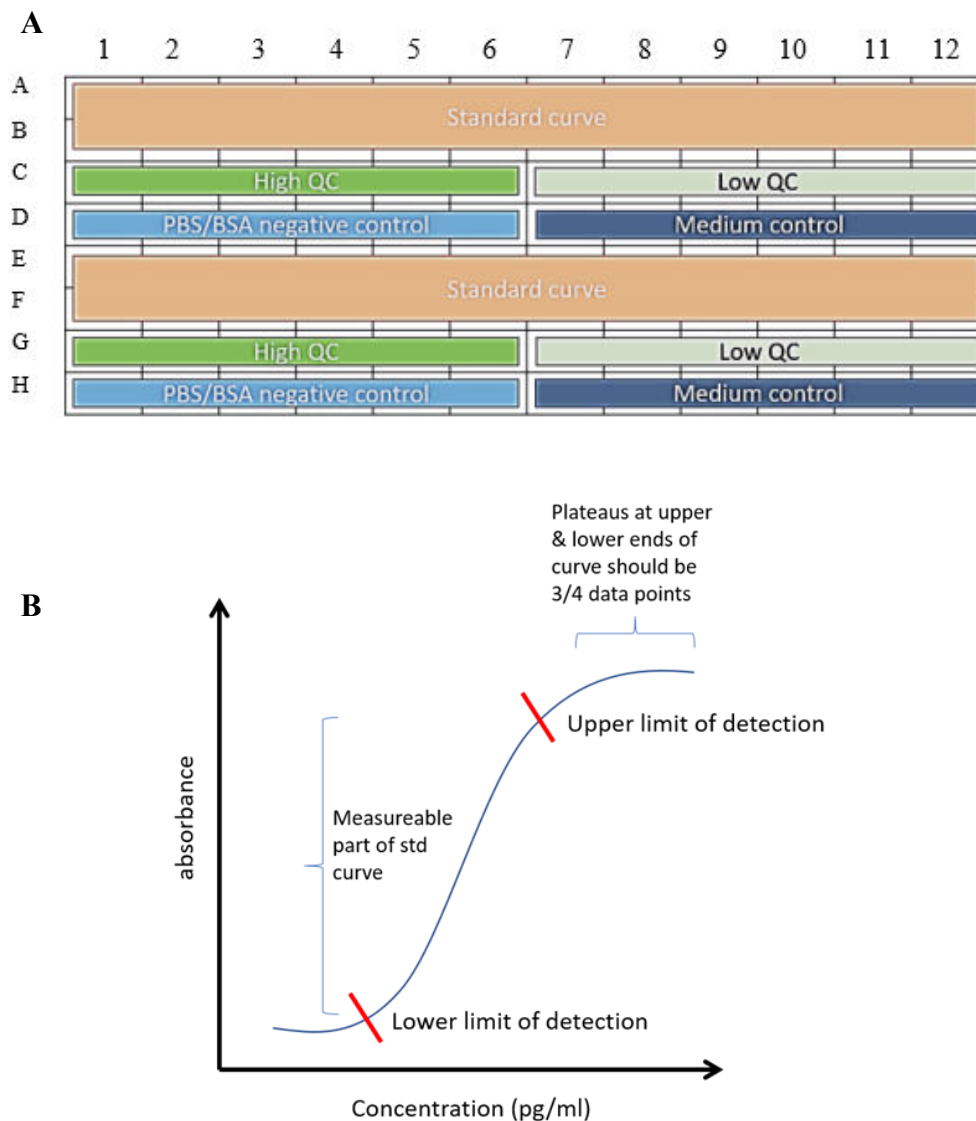


Figure 3. 3. ELISA standard curve development. (A) ELISA plate plan. The plate was split into half to produce two distinct standard curves, QCs, and negative controls for intra-assay analysis. (B) ELISA standard curve. The standard curve should be sigmoidal in shape (like an ‘S’ shape). There is little differentiation between the colours at the lower end of the curve, and it is largely saturated at the top end, thus it is difficult to differentiate concentrations between the top standards, represented as plateaus.

3.2.2.3 Sensitivity optimisation

The cytokines selected are expressed at quite low concentrations and necessitated an additional layer of sensitivity optimisation. In order to achieve this, the ELISA was performed to compare the absorbance outcomes when using avidin modified with several HRP molecules (“poly-HRP”) relative to absorbances for a standard HRP-avidin molecule, with the former increasing the sensitivity of the assay. Sensitivity can also be improved by modifying the amount of substrate added to the plate, and time allowed for the colour reaction to develop. The data presented shows a range of approaches incorporating all three development approaches (poly-HRP utilisation, substrate manipulation & time adjustment) with the aim of achieving a standard sigmoidal curve where the expected cytokine concentrations lie within the linear part of the curve (validated by appropriate placement of the high and low QC controls). This validation was accomplished by ensuring the appropriate positioning of both HQ and LQ samples within the curve.

The steps above (antibody titration, standard curve and sensitivity development) were performed in order. However, under specific circumstances where the colour change was insufficiently sensitive to elicit the desired absorbance within the standard curve, these steps needed to be revisited and re-evaluated. This iterative process was particularly relevant for certain cytokines where antibody titration required further adjustment in response to sensitivity enhancements achieved through substrate concentration modifications or the use of poly-HRP instead of standard HRP-avidin. To obtain the optimum standard curve, all cytokines, including IL-6, GM-CSF, G-CSF, and TGF- β 1, were optimized using HRP and poly-HRP at various time periods. If nothing produced a good sigmoidal curve for the standard curve, a combination of HRP and poly-HRP was applied.

3.2.2.4 Intra- and Inter-assay reproducibility

Following the establishment of a satisfactory standard curve, it becomes imperative to perform an assay reproducibility assessment. This procedure serves multiple purposes: it evaluates the consistency of the standard curve, the reproducibility of QCs and N/Cs, and it identifies the limits of sensitivity within the standard curve, particularly at the lower and upper concentration extremes. This analysis enables the user to discern points beyond which the standard curve can no longer effectively detect analytes.

To conduct this assessment, each well containing QCs (HQ and LQ) and N/Cs (PBS and CCM) was compared against the respective standard curves. The analysis determined whether the QCs fell within the predefined acceptable range and provided background readings for the N/Cs. Subsequently, the data from the six concentrations were averaged, and the standard deviation was calculated for each set of wells.

It is noteworthy that in this experimental setup, two separate standard curves were used within the same plate. Consequently, these are treated as distinct plates for the purposes of the analysis. The averaged QCs and N/Cs were compared within the same plate to assess intra-assay reproducibility and perform a comparison between plates to determine inter-assay reproducibility. This comprehensive evaluation ensures the reliability and consistency of the ELISA assay across multiple runs.

Calculating the coefficient of variation (CV) was determined by dividing the standard deviation by the mean and was computed for both intra- and inter-assay ELISA runs. CV for the inter-assay %CV should be less than 15%, while the intra-assay %CV should ideally be less than 10%.

3.3 Results

3.3.1 Evaluation of optimum culture conditions for cell lines

The cell lines used in this study were cultured in different culture medium and growth was monitored until about 80-90% confluent. The culture medium that propagated the best healthy cell growth and proliferation for both cell lines was used in the *in vitro* co-culture model. HS-5, and TK6 cells were grown in different culture medium over 120 hours. Photographs of the HS-5 cell morphology were taken and cell viability was assessed for both the cell lines at three passages.

3.3.1.1 Mesenchymal stem cell line; HS-5

The growth potential of HS-5 in different culture media was investigated to work out the best culture medium that works for both cell lines. HS-5 morphology was observed every 24 hours up to 5 days in all three different culture media (Fig. 3.4). The HS-5 cell line displayed consistent adherence to the culture flask within a mere 24 hours, regardless of the specific culture medium employed. When it came to cell morphology, HS-5 cells maintained a fibroblast-like appearance in most of the culture media tested. Notably, in the presence of DMEM-LG supplement, these cells appeared comparatively smaller. A comparison to the typical morphology of primary MSCs revealed that HS-5 cells cultured in RPMI 1640 medium exhibited fibroblast-like projections that closely resembled stromal cells, setting them apart from other media where the cellular morphology leaned more towards endothelial cells. In terms of growth patterns, the initial 24-hour period saw all cells thriving, with some firmly adhering to the culture flask. As time progressed, most cells in alternative media experienced a noticeable increase in number, expanding to cover a greater surface area as they proliferated and divided. Interestingly, a contrasting pattern emerged with cells in DMEM-LG medium, which exhibited a decreased cell count to cover the culture flask surface area at from 48- to 120 hours. Finally, at 120 hours, all media except DMEM-LG exhibited cell confluence. DMEM-HG stood out with the highest cell population, albeit with shorter fibroblast projections compared to RPMI-1640 cells, which displayed a spindle fibroblast phenotype akin to stromal cells. These observations underscore the significant impact of the choice of culture medium on the morphology and growth characteristics of HS-5 cells, with RPMI-1640 emerging as the preferred medium for maintaining a fibroblast-like phenotype.

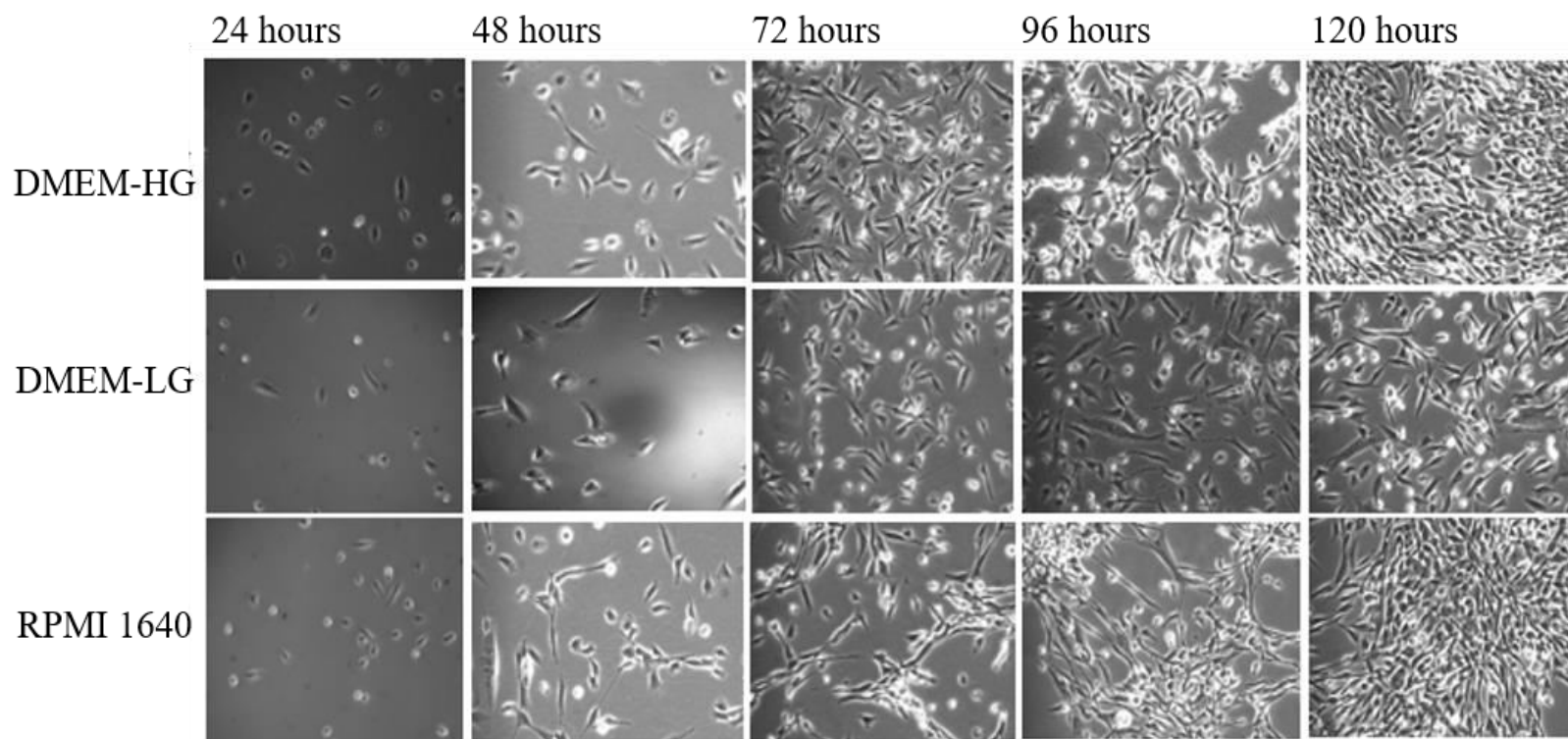


Figure 3. 4. Morphology of HS-5 in different culture media (40x). Photomicrographs were taken every 24 hours for five consecutive days when HS-5 were cultured in complete DMEM-HG, DMEM-LG and RPMI 1640 media. Seeding density was $1 \times 10^5 / 25 \text{ cm}^2$ flask with 5 ml of different media and images were taken with an inverted light microscope every 24 hours over 120 hours at 40x magnification. HS-5 cells showed gradual adherence, dividing, and multiplying to cover the cell surface area and showing good cell growth of the HS-5 cells over time. Data show n=3.

Quantitatively, all cultures were assessed for total live cell numbers (Fig. 3.5A) and percentage viability at each trypsinization (Fig. 3.5B) plotted over cell passages until 3rd passage. First, it is noteworthy that cells cultured in DMEM-HG (6×10^5 , 6×10^6 , 6×10^7) and RPMI-1640 (6×10^5 , 7×10^6 , 4×10^7) exhibited similar expansion rates, achieving a 6-10 fold increase between passages 1 and 2. However, a slight drop in expansion rate was observed in RPMI-1640 from passage 2 to passage 3. In contrast, DMEM-LG displayed a substantially lower expansion rate of approximately 5-fold over the three passages.

By the third passage (P3), it became evident that both DMEM-HG and RPMI-1640 significantly differed from DMEM-LG in terms of live cell numbers ($p < 0.0001$). Moreover, DMEM-HG was found to have a significantly higher live cell count than RPMI-1640 ($p < 0.0001$) at P3. This indicates that DMEM-HG and RPMI-1640 are superior to DMEM-LG in supporting cell growth over multiple passages. Furthermore, when considering cell viability (Fig. 3.2B), it was observed that all media maintained cell viability above 50% at each passage, with the exception of DMEM-LG. RPMI-1640 displayed the highest viabilities at P1 (89%) and P3 (91%), while DMEM-HG exhibited the highest viability at P2 (83%). However, DMEM-LG consistently had the lowest viability throughout all three passages, with a significant difference observed in comparison to the other media.

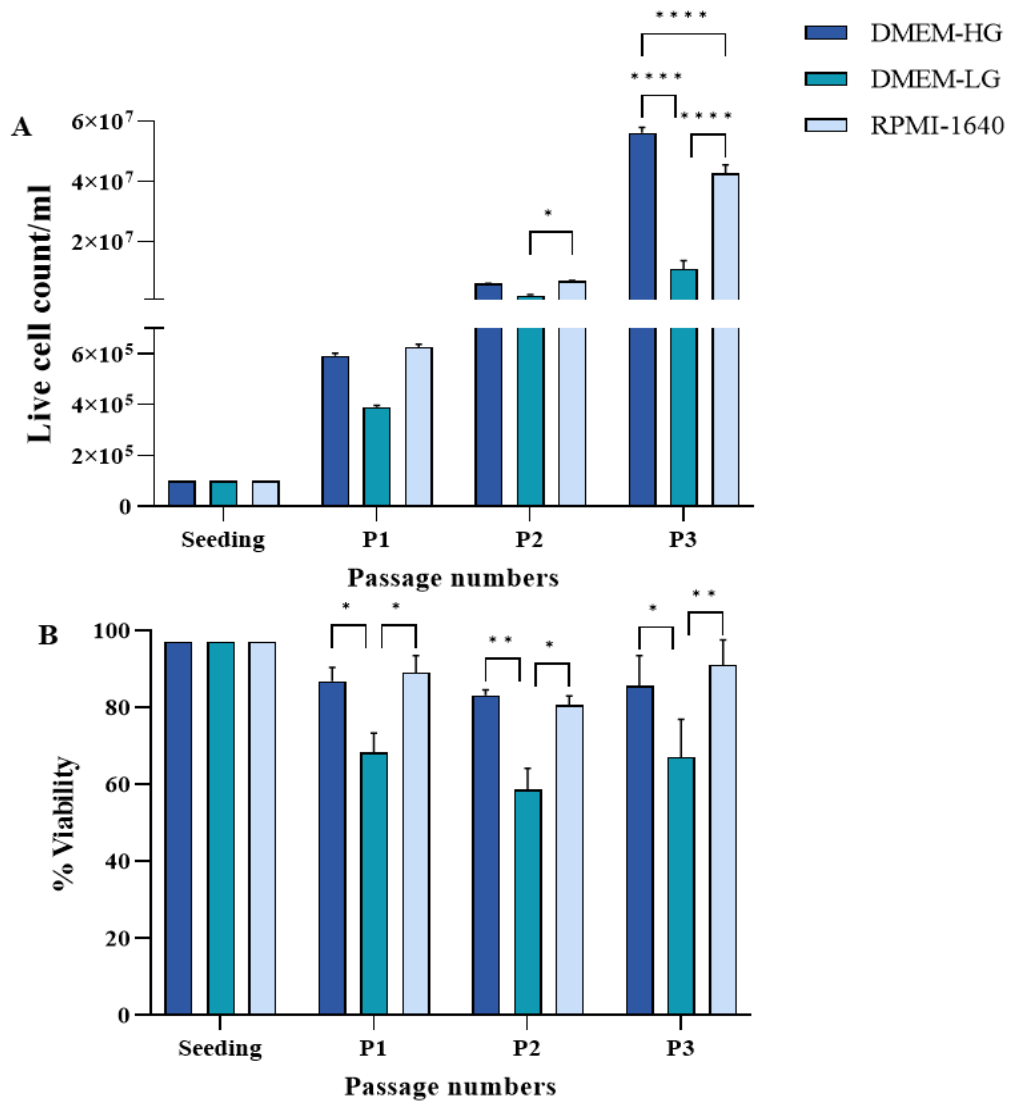


Figure 3. 5. HS-5 live cells count (A) and viability (B) in different media. Cells were seeded at $4 \times 10^3 / \text{cm}^2$ and were trypsinized after 120 hours when they looked confluent. Cells were estimated for total live cells (A) and percentage viability (B) by the Luna counter. When the cells were split into each passage, a 1:3 ratio was followed in each culture media. Data shows the mean \pm SD (n=3) and significant difference is shown as * $p \leq 0.05$, ** $p \leq 0.01$ and **** $p \leq 0.0001$ as determined by two-way ANOVA, Tukey's multiple comparisons test.

3.3.1.2 Lymphoblast cell line; TK6

Using an initial cell seeding density of 3×10^5 cells/ml, the TK6 cells were quantified for their total number of live cells, percentage viabilities and cell size in the three different culture media and at different time points (Fig. 3.6).

Figure 3.6A shows the TK6 live cell count analysis over 120 hours. Initially, it was observed that cells seeded in DMEM-HG and RPMI-1640 exhibited a gradual increase in live cell count at a comparable expansion rate. In contrast, DMEM-LG consistently had the lowest live cell count, and this disparity became statistically significant from 72 hours onwards. Interestingly, at 24 and 48 hours, TK6 cells in all three culture media displayed similar cell numbers at approximately 5×10^5 and 1×10^6 cells/ml, respectively. However, at 72 hours, RPMI-1640 demonstrated a notable surge in live cell count, while the other two media maintained relatively stable counts. Subsequently, between 96 and 120 hours, DMEM-LG lagged behind in cell count, while DMEM-HG and RPMI-1640 continued to exhibit an upward trend. Significant differences in cell counts were noted at 96 and 120 hours, with each medium showing variations at different levels of statistical significance.

Surprisingly, despite the observed differences in cell counts over time, there were no significant variations in percentage viability between the samples at any time point (Fig. 3.6B). This indicates that the culture media did not induce cell death but rather influenced the rate of cell growth. RPMI-1640 and DMEM-HG displayed similar viability results, whereas DMEM-LG consistently exhibited the lowest viability over the 120-hour duration. The highest viability, at 93.6%, was recorded in RPMI-1640 after 96 hours, while the lowest viability, at 77.5%, was observed in DMEM-LG after 120 hours of seeding.

Moreover, over the 120-hour period, DMEM-HG and RPMI-1640 yielded similar cell sizes for TK6 cells, although DMEM-HG was slightly smaller than the cell size achieved in RPMI-1640 (Fig. 3.6C). The maximum cell size, $12.9 \mu\text{m}$, was observed in RPMI-1640 at 48 hours, while the smallest cell size, $11 \mu\text{m}$, was recorded in DMEM-LG at 24 hours. Furthermore, DMEM-LG consistently exhibited significantly smaller cell sizes compared to both other media throughout the study, except at the 96-hour time point.

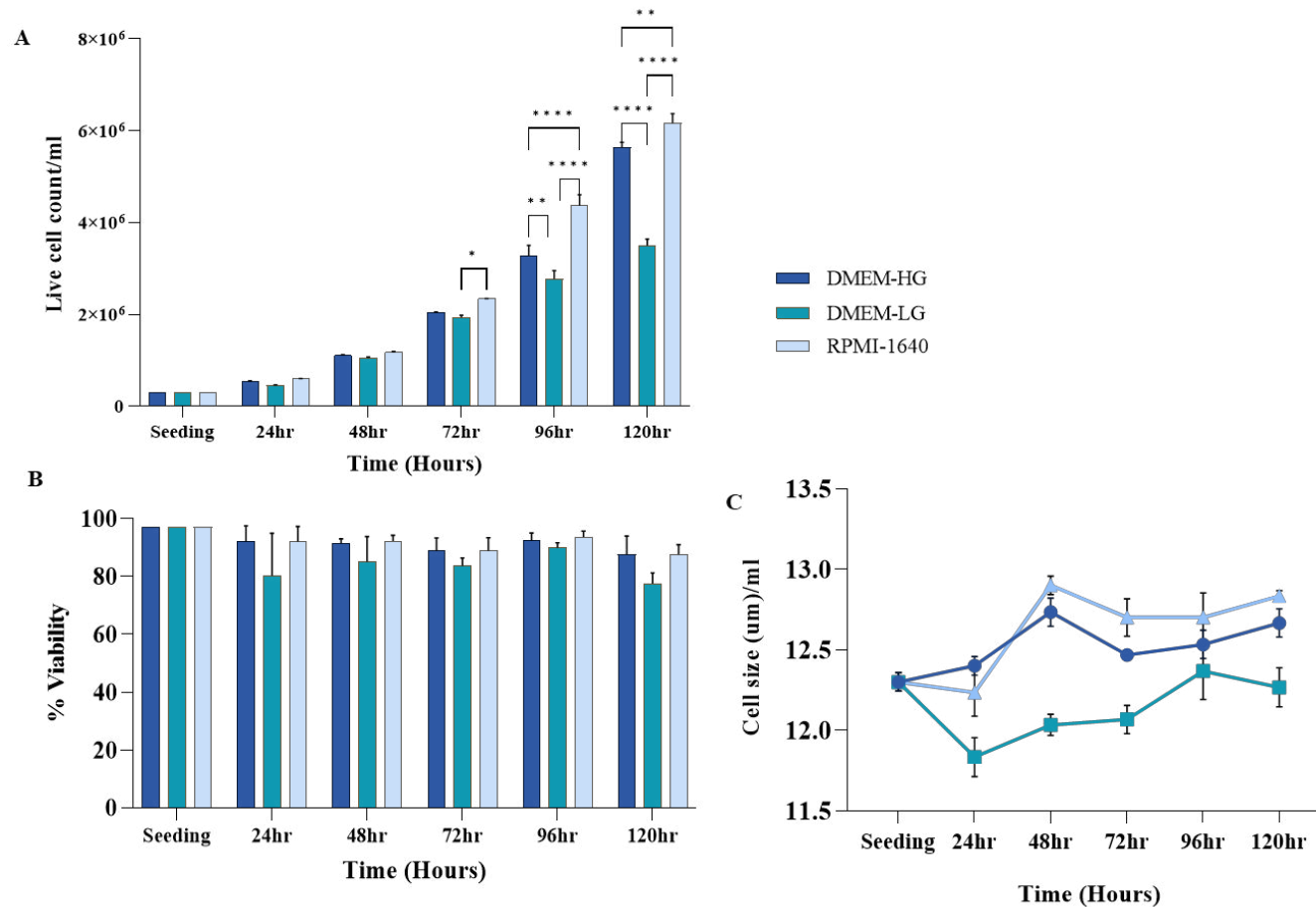


Figure 3.6. TK6 live cell count (A), viability (B) and size (C) in different media. Cells were seeded at 3×10^5 /ml in three different culture media and were assessed by the Luna counter for total live cell count per ml (A), percentage cell viability (B) and cell size (C) every 24 hours until 120 hours (5 days). Data shows the mean \pm SD (n=3) and significant difference is shown as * $p \leq 0.05$, ** $p \leq 0.01$ and **** $p \leq 0.0001$ as determined by two-way ANOVA, Tukey's multiple comparisons test.

3.3.1.3 TK6 growth curve

It is important to note that doubling times of any cell line can vary depending on various factors, including how the cells are being cultured, the growth conditions, medium, cell density and protocols used in a laboratory. Monitoring the cell growth over time and calculating the doubling time by the following equation is recommended for accurate results in research.

$$\text{Doubling Time} = (t_2 - t_1) * \log(2) / [\log(N_2) - \log(N_1)]$$

As shown in figure 3.7, the TK6 growth curve experiment was conducted to investigate the impact of various seeding densities on the doubling time of TK6 cells. Over a span of 5 days, the live cell counts exhibited variability when different seeding densities were employed. However, an intriguing and consistent observation emerged from this experiment: the calculated doubling time for TK6 cells at all seeding densities remained remarkably stable, consistently hovering around 16-17 hours.

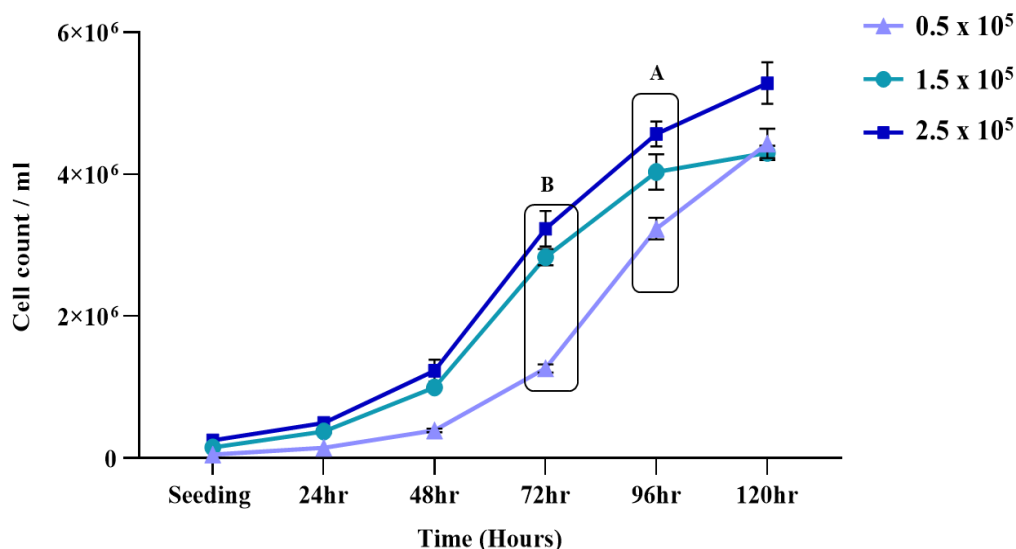


Figure 3. 7. TK6 growth curve development. Cells were seeded at three different densities as 0.5×10^5 cells/ml, 1.5×10^5 cells/ml and 2.5×10^5 cells/ml into a 6-well plate with 2 ml of RPMI-CCM. Cell counts were taken every 24 hours until day 5 (120 hours). Cell numbers were plotted according to their time scale and the growth curve and doubling time was calculated. Data shows the mean \pm SD (n=3).

3.3.2 ELISA assay development

3.3.2.1 Development of optimum signal-to-background ratio

Following the completion of three repeats of GM-CSF experimentation, the signal-to-background ratio was determined using the formula below. Specifically, the absorbance of HQ and LQ samples was divided by the absorbance of PBS and RPMI-CCM respectively. The top 10 values with the highest ratios were identified in figure 3.8. Those with the highest ratios were considered to have low background interference but a strong signal and were subsequently selected for the development of standard curves.

e.g. GM-CSF

Calculations were performed as follows:

Highest signal to background ratio	=	$\frac{\text{Absorbance of HQ or LQ}}{\text{Absorbance of PBS or CM}}$
	=	ratio value

Based on the data in figure 3.8A, it was decided to use CAP and DET antibody concentrations of 4.5 µg/ml and 1.75 µg/ml respectively, for GM-CSF. As for G-CSF and TGF-β1, the chosen concentrations were CAP 2 µg/ml, DET 1.75 µg/ml, and CAP 2 µg/ml, DET 1.5 µg/ml, respectively. However, during standard curve development, it was observed that the generated curves were not optimal. It was explained that any ratio less than 1 implied that the absorbance of HQ or LQ samples was lower than the background, indicating that the assay was not sensitive enough. Consequently, the signal-to-background ratio was revisited by introducing poly-HRP and sensitivity optimisation steps. This refined antibody titration process led to the identification of new CAP and DET antibody concentrations for GM-CSF (Fig. 3.8B; 2.5 µg/ml and 0.75 µg/ml), G-CSF (4 µg/ml and 1.25 µg/ml), and TGF-β1 (3.5 µg/ml and 1.25 µg/ml) cytokines.

A	HQ:PBS						HQ:PBS						HQ:PBS							
	0.5	0.75	1	1.25	1.5	1.75	0.5	0.75	1	1.25	1.5	1.75	0.5	0.75	1	1.25	1.5	1.75		
2	4.03	4.85	5	5.14	3.7	5.97	2	5.42	4.99	5.4	3.03	4.71	5.38	2	2.48	2.598	3.39	4.24	5.2	3.11
2.5	6.79	6.51	4.2	4.5	6.3	6.87	2.5	4.43	5.18	5.1	2.41	4.81	4.53	2.5	2.89	5.367	1.85	4.62	4.7	1.65
3	5.43	0.83	4.9	6.65	7.9	9.14	3	6.94	4.65	4.6	2.73	4.95	4.31	3	3.27	6.436	5.61	5.41	2.9	4.17
3.5	5.35	5.45	5.8	5.27	8.5	7.96	3.5	5.7	4.49	4.8	2.78	4.74	7.85	3.5	6.09	3.797	3.3	5.2	5.5	4.21
4	4.67	6.9	5.1	7.81	8.6	10.3	4	3.58	3.67	4.9	2.27	7.09	7.72	4	5.94	2.91	2.27	3.39	4.7	8.67
4.5	5.25	5.97	4.8	4.62	9.3	8.94	4.5	3.65	3.56	3.9	3.11	7.96	7.06	4.5	6.77	3.824	4.17	5.26	4.4	10.8
5	4.47	4.4	7.3	9.62	8.4	10.6	5	3.4	4.03	6.5	5.35	8.48	5.6	5	5.52	4.509	5.82	9.86	7.7	10.5
5.5	9.57	5.89	6.2	7.36	8.1	6.11	5.5	3.67	4.51	8.1	6.25	8.15	7.66	5.5	4.94	5.91	5.86	7.41	7.6	9.47
LQ:CM						LQ:CM						LQ:CM								
0.5	0.75	1	1.25	1.5	1.75	0.5	0.75	1	1.25	1.5	1.75	0.5	0.75	1	1.25	1.5	1.75			
2	0.8	1.05	1.3	1.73	0.7	2.19	2	0.94	0.72	1.7	2.1	0.98	2.05	2	2.57	1.152	0.91	1.23	2.4	2.33
2.5	1.34	1.05	1	1.35	2	2.5	2.5	0.45	0.54	2.3	1.54	1.46	1.76	2.5	0.9	1.532	1.34	1.6	2.1	2.79
3	1.12	1.04	1.3	1.51	1.6	2.13	3	0.63	1.76	3.1	4.07	1.37	1.3	3	0.9	1.218	1.05	1.69	1.4	1.9
3.5	1.14	0.86	1.2	0.96	1.6	1.22	3.5	0.73	1.49	1.8	3.77	1.52	1.88	3.5	0.66	0.816	1.05	1.15	1	2.74
4	0.62	1.07	1.4	0.9	1.2	1.75	4	0.78	1.66	1.7	1.82	1.42	1.97	4	1.41	0.989	0.75	0.82	2.8	2.38
4.5	1.75	1.37	1.5	1.46	0.6	1.88	4.5	1.35	0.91	2	2.61	1.95	1.89	4.5	0.85	0.783	1.62	2.37	2.2	3.27
5	1.22	0.92	1.6	0.56	3.1	2.02	5	1.25	1.55	1.5	2.19	2.07	1.32	5	1.49	1.193	2.04	1.82	2.3	2.62
5.5	1.1	1.49	2	1.79	1.5	1.77	5.5	0.75	3.67	0.8	1.84	1.95	2.65	5.5	1.04	1.3	1.13	1.48	1.4	2.83

B	HQ:PBS						HQ:PBS						
	0.5	0.75	1	1.25	1.5	1.75	0.5	0.75	1	1.25	1.5	1.75	
2	15	16.1	14.2	13.7	12.9	13.903	2	9.11	17.04	20.89	13.2	9.87	9.548
2.5	16	18.7	15.8	15.7	11.5	12.703	2.5	11.9	13.36	11.39	9.55	10.9	7.07
3	14	15.1	10.3	15.2	13.5	14.78	3	12.1	16.33	12.25	9.38	9.66	13.2
3.5	15	11.8	10.8	11.8	14.2	13.442	3.5	13.4	15.75	13.64	13.6	13.4	12.17
4	14	13.6	13.1	13.1	13.1	10.766	4	7.24	9.255	11.49	9.73	7.54	11.29
4.5	11	14.8	12.7	14.2	13.3	14.425	4.5	7.69	10.19	9.48	7.59	3.61	8.767
5	11	13.5	11.9	13	13.2	11.339	5	7.09	10.35	7.073	10.2	6.5	12.81
5.5	12	15.1	15.3	13.1	12.6	12.221	5.5	11.6	13.56	13.74	12.2	10.1	10.87
LQ:CM						LQ:CM							
0.5	0.75	1	1.25	1.5	1.75	0.5	0.75	1	1.25	1.5	1.75		
2	9.6	11.3	9.45	10.2	9.26	9.0241	2	6.53	9.26	5.815	5.46	7.1	6.926
2.5	12	10.8	9.52	10.4	9.09	9.3333	2.5	5.26	8.492	5.177	7.84	6.21	6.486
3	9.9	10.7	11	11	9.31	8.9655	3	5.11	9.806	8.771	6.99	6.21	5.611
3.5	12	11.7	9.29	7.85	8.86	8.0204	3.5	2.36	8.959	8.415	7.18	7.31	7.083
4	12	9.2	10.3	9.22	9.71	8.4138	4	8.12	6.692	7.187	5.88	9.93	7.141
4.5	8.5	10.4	11.8	8.57	8.99	9.8608	4.5	3.49	5.667	7.238	6.85	8.07	6.41
5	9.3	9.55	9.18	7.67	10.1	7.5392	5	5.5	6.19	6.26	6.73	7	7.508
5.5	9	9.73	10.7	8.59	7.4	6.4825	5.5	9.08	13.65	10.27	4.95	6.97	7.066

Figure 3. 8. Signal to background ratio for GM-CSF antibody titration. (A) Signal to background absorbance ratio for GM-CSF with standard streptavidin (HRP). HQ with PBS and LQ with RPMI-CCM was analysed. The best concentration pair for CAP; 4.5 µg/ml and DET; 1.75 µg/ml. **(B)** Signal to background absorbance ratio for GM-CSF with poly-streptavidin (poly-HRP). The optimal antibody was changed into CAP; 2.5 µg/ml and DET; 0.75 µg/ml.

3.3.2.2 Development of standard curve

Upon achieving satisfactory results with CAP and DET antibodies for all target cytokines GM-CSF, G-CSF, and TGF- β 1, the development of standard curves was performed, as detailed in section 3.2.2.2. Initially, standard curves were generated using standard HRP. Figure 3.9 illustrates the evolution of the standard curve at various time intervals of HRP incubation.

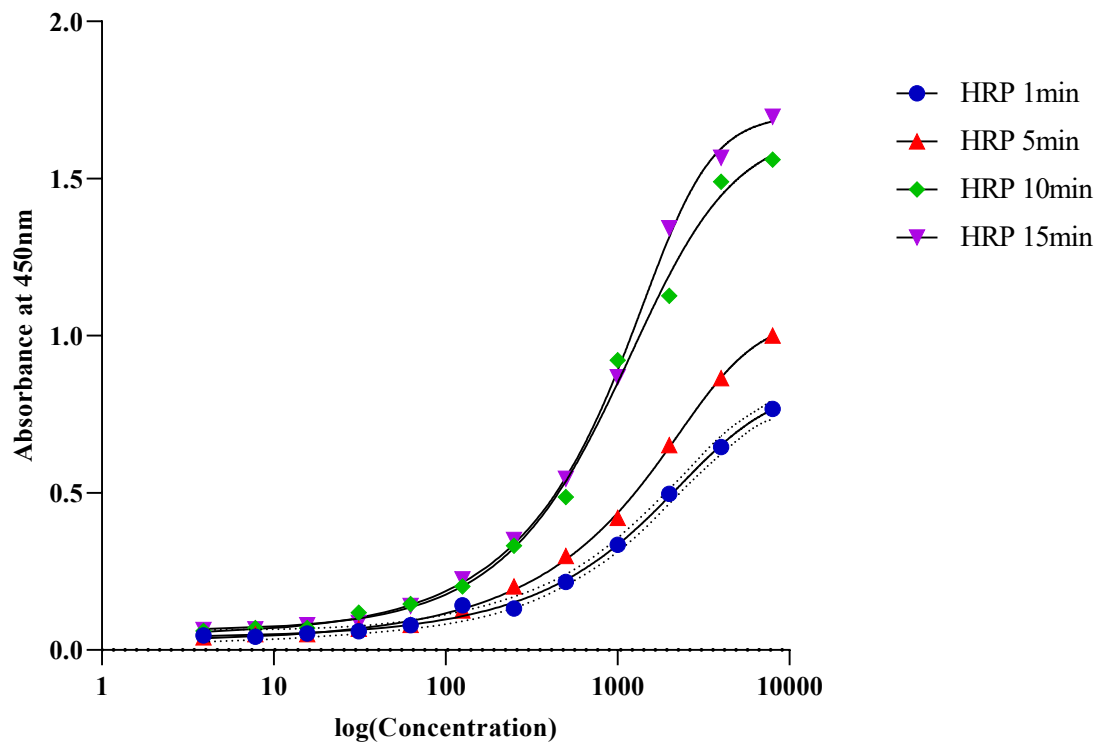


Figure 3.9. Standard curve development using horseradish peroxidase. The GM-CSF assay involved treating the plates with horseradish peroxidase (HRP), which was diluted at a ratio of 1:1000 with a solution of phosphate-buffered saline (PBS) containing bovine serum albumin (BSA). Upon reaching the conclusion of the experiment, substrate was uniformly added to each plate at a consistent concentration, initiating the process of colour development. Subsequently, the colour development was halted for each plate by introducing sulphuric acid (H_2SO_4) at specific time intervals, including 1 minute, 5 minutes, 10 minutes, and 15 minutes once the colour development was observed. This protocol was followed consistently with all the candidate cytokines and the results analysed.

The assessment of the standard curve's quality was contingent on it displaying a sigmoidal S-shaped curve. Additionally, QC and N/C wells were compared against the standard curves to validate the accuracy of values. The acceptance criteria for QCs, ideally falling within $\pm 10\%$

of the expected values, were established. Consequently, for HQ samples (750 pg/ml), values within the range of 675-825 were considered acceptable, while for LQ samples (75 pg/ml), values within 67.5-82.5 were deemed acceptable.

The results from ELISA plates treated with HRP and subjected to substrate incubation for varying durations (1, 5, 10, and 15 minutes) exhibited promising curves during the initial attempts. However, despite the correct placement of quality controls on certain plates (as shown in Fig. 3.9), the signal did not reach a sufficiently high level to reach the plateau phase of the curve. Furthermore, the limited linear range of data acquisition was attributed to the use of streptavidin peroxidase.

Nevertheless, extending the incubation time of the plate demonstrated the potential for signal improvement when employing HRP. In response to these findings, there was consideration of switching to the use of 'poly-HRP streptavidin' to enhance the signal in future experiments.

3.3.2.3 Sensitivity optimisation

GM-CSF

The HRP step for GM-CSF was performed with 5ul of poly-HRP mixed with 5ml of PBS/BSA (1:1000) to improve sensitivity of the plate. The reaction was then stopped by adding H₂SO₄ at different time points as shown in figure 3.10A. The signal development process exhibited a more rapid response when utilising poly-HRP in comparison to the standard HRP-treated samples. Initial incubation periods of 1-2 minutes did not yield a substantial signal. Consequently, a decision was made to extend the incubation time. As the incubation period approached 4-5 minutes, colour development became notably intense, and precipitates began forming in the first few wells containing high-concentration standards within the standard curve. Therefore, it was deemed necessary to terminate the reaction at 4- and 5-minute intervals. Analysis of the resulting data revealed that the standard curves generated from the 4–5-minute incubation plates displayed a favourable linear trend and were close to reaching the plateau phase. However, due to observed declines in signal intensity at higher concentrations at 5 minutes incubation (Fig. 3.10A), further extension of the incubation time was not considered viable. This led to the exploration of alternative strategies for signal development that could enhance sensitivity without inducing the observed precipitation, presumably arising from the combination of high poly-HRP concentration and prolonged

incubation. Consequently, experiments were initiated involving different dilutions of HRP with poly-HRP at various time points to optimise the sensitivity of the assay.

In figure 3.10B, the GM-CSF standard curve development is presented, which involves varying concentrations of HRP with poly-HRP over a timescale. It is evident that the curve generated with a combination of 4 μ l poly-HRP and 1 μ l HRP exhibited a notably steeper slope compared to the other samples. However, due to the rapid rise in signal, the quality control values for this curve slightly deviated from the predefined range. In contrast, the samples treated with 2.5 μ l (poly-HRP and HRP) and 1 μ l of poly-HRP with 4 μ l HRP demonstrated QC values that fell within the acceptable range, even though their slopes were slightly less steep than the curve treated with 4 μ l poly-HRP and 1 μ l HRP. Subsequently, additional iterations of this experiment were conducted, exploring various combinations of HRP and poly-HRP at different time intervals (ranging from 7 to 10 minutes). Although this thesis includes only select portions of the data, the overall findings led to opt for the combination of 2.5 μ l HRP and 2.5 μ l poly-HRP for the establishment of the GM-CSF standard curve.

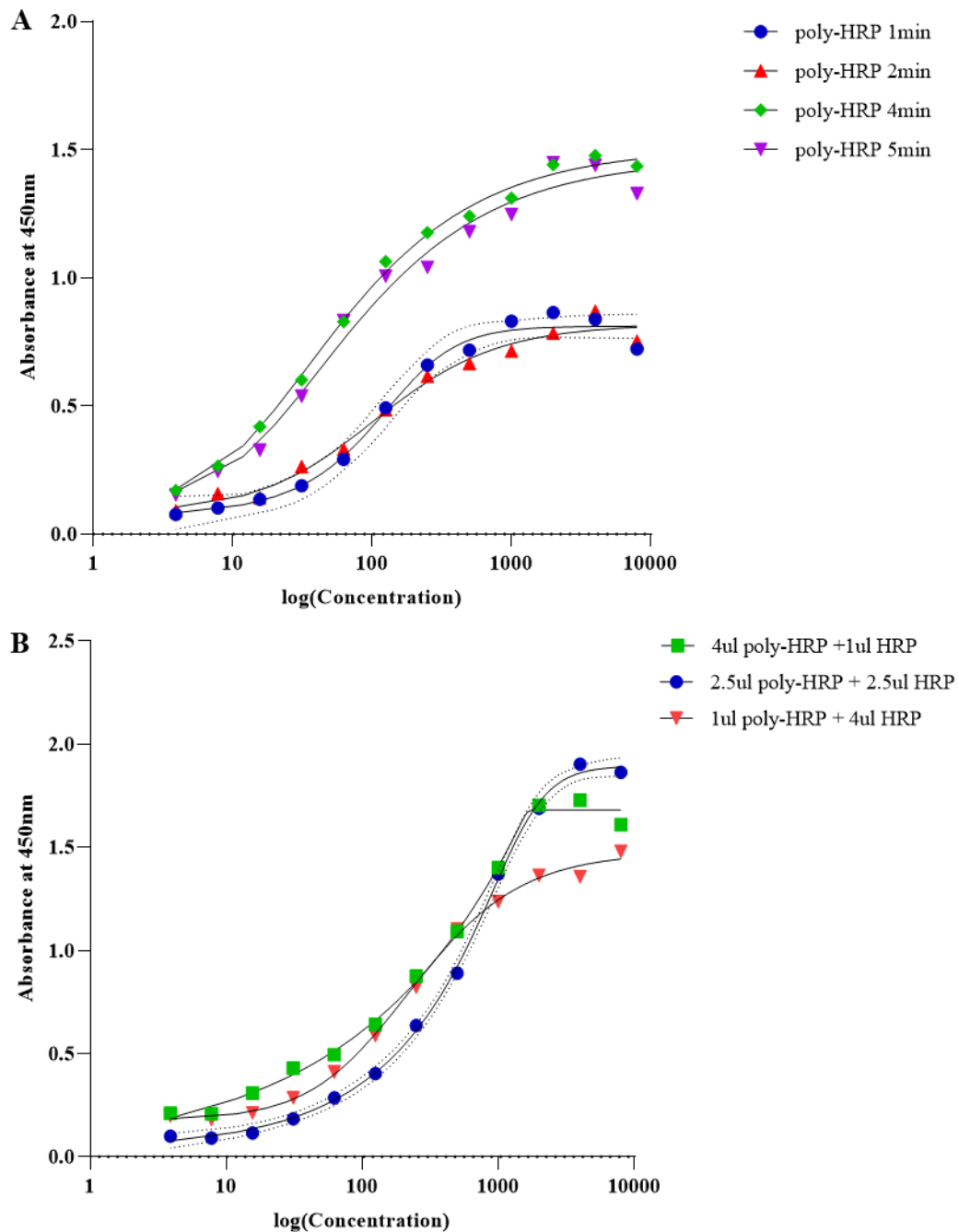


Figure 3. 10. Sensitivity development for GM-CSF ELISA. The GM-CSF assay involved treating the plates with poly-horseradish peroxidase (poly-HRP), which was diluted at a ratio of 1:1000 with PBS/1% BSA. **(A)** Standard curve development with poly-HRP at different time points before adding stop solution (H₂SO₄) at specific time intervals, including 1 minute, 2 minutes, 4 minutes, and 5 minutes. **(B)** Standard curve development with poly-HRP at different dilutions and at different time points. The ELISA plate was treated with HRP with poly-HRP at different dilutions with different stopping time points.

IL-6

For the IL-6 standard curve development, a need arose for sensitivity optimisation. Figure 3.11A displays the process where the IL-6 ELISA assay was conducted with varying durations of HRP treatment, followed by the analysis of the resulting standard curves. It is noteworthy that all HRP treatment durations exhibited the capacity to enhance the standard curve, even though not all of them reached the plateau phase of the curve. Only the sample incubated for 15 minutes succeeded in reaching the plateau; however, its low concentration samples clustered closely together, requiring a more distributed spread along the curve.

Subsequently, an alternative approach was explored involving the treatment of samples with 5 μ l poly-HRP at different time points, as depicted in figure 3.11B. The results indicate that all samples treated with poly-HRP effectively elevated the standard curve. The sample incubated for 2 minutes appeared to require additional time for colour development and reaching the plateau phase, while the sample incubated for 5 minutes exhibited a more pronounced upward trend but also required further time to reach the plateau phase, surpassing the 2-minute sample. Ultimately, the optimal treatment was determined to be the incubation of the ELISA plate with poly-HRP for 10 minutes, as it resulted in the highest elevation of the standard curve and a well-defined plateau, particularly for the three to four highest concentrations at the upper end of the curve.

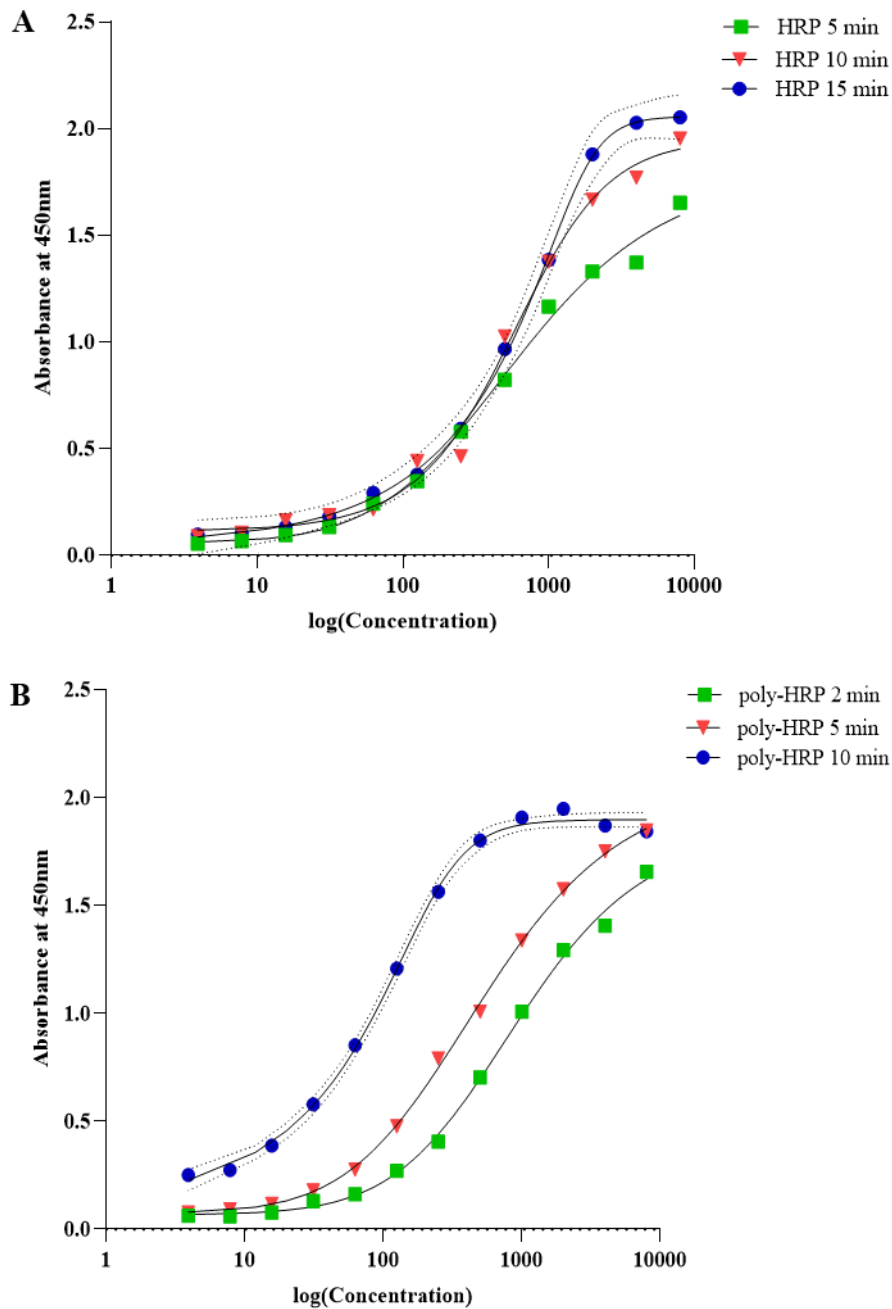


Figure 3. 11. Sensitivity development for IL-6 ELISA. This sensitive development was done with HRP and poly-HRP which was diluted with PBS/BSA. **(A)** Standard curve development with HRP at 1:1000 ratio and the reaction was stopped at 5 minutes, 10 minutes, 15 minutes. **(B)** Standard curve development with poly-HRP at 2 minutes, 5 minutes, 10 minutes.

G-CSF

It was observed that treatment with standard HRP did not yield favourable results, as the resulting standard curve remained predominantly parallel to the x-axis (data not shown). Consequently, the assay was transitioned to poly-HRP without further exploration of HRP at different time points. In the context of G-CSF sensitivity development with poly-HRP, two phases were undertaken. In figure 3.12A, the initial phase involved utilising poly-HRP at various time intervals. Unfortunately, even when poly-HRP was employed at the typical dilution of 1:1000 across different incubation durations ranging from 5 to 15 minutes, the standard curve development did not exhibit a positive trend. This was evident in the fact that the curve remained parallel to the x-axis until reaching the 6 to 7th well of the standard curve. Furthermore, even after a 15-minute incubation, the curves failed to approach a well-defined plateau phase.

Given the suboptimal outcomes with poly-HRP at the standard 1:1000 dilution, higher concentrations were explored; specifically, 1:500 and 1:250, in conjunction with modifications to the substrate concentration, as detailed in figure 3.12B. Upon evaluating the elevation of the standard curves, it became evident that the concentration of poly-HRP exerted a significant influence. However, it remained disappointing that, even after incubation periods extending to 17-20 minutes, a distinct plateau phase could not be achieved in any of the four treatment variants. Changing the substrate concentration from 100 μ l to 200 μ l did not make a significant change in the curve development. Furthermore, the quality controls did not align as expected in these standard curves because of the poor slope of the curve. Notably, the LQ consistently resided in the plateau region of the lower detection limit, rendering these graphs unsuitable for sample detection purposes.

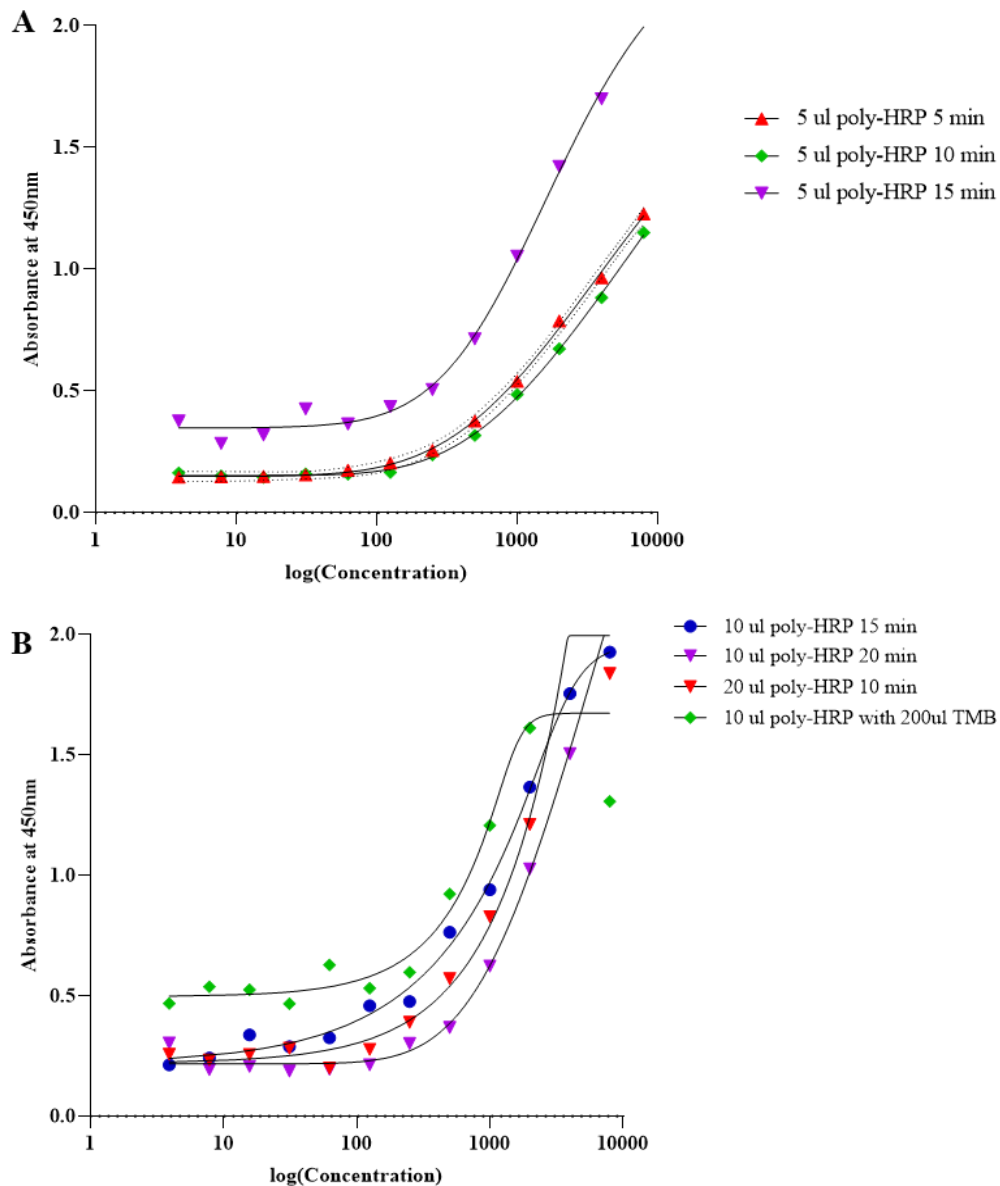


Figure 3. 12. Sensitivity development for G-CSF ELISA. The ELISA plate was treated with poly-HRP at different dilutions and time points. **(A)** Standard curve development with poly-HRP at 1:1000 diluted with PBS/1% BSA, and the reaction was stopped at 5 minutes, 10 minutes, 15 minutes. **(B)** Standard curve development with poly-HRP at different dilutions - 1:500 (10 μ l in 5ml PBS/1% BSA) at 15 minutes and 20 minutes. With 1:250 (20 μ l in 5ml PBS/1% BSA) stopped at 10 minutes. The last attempt was 1:500 diluted poly-HRP with modified concentration of substrate; 200 μ l TMB.

TGF- β 1

The sensitivity development of TGF- β 1 presented considerable challenges and demanded significant effort. In figure 3.13A, the poly-HRP treated ELISA was conducted with varying incubation times. Observations revealed that both the 5- and 10-minute incubations produced comparable results, while the 15 minute incubation exhibited higher absorbance values at each concentration. Nevertheless, none of these datasets managed to reach the plateau phase of the standard curve, indicating that saturation at high concentrations remained elusive. Consequently, the application of higher poly-HRP concentrations was explored along with adjustments to the substrate concentration, as depicted in figure 3.13B.

The utilisation of 10 μ l poly-HRP demonstrated an enhanced uplift in the standard curves in comparison to the 5 μ l treated samples. However, employing two different substrate concentrations (100 and 200 μ l) did not yield significant alterations in the resulting standard curves. It remained a consistent challenge that a substantial portion of data points clustered within the lower plateau phase, while none of the curves succeeded in reaching the upper plateau phase.

Given the persistently unfavourable outcomes and in the interest of optimising time and resources, the decision was made to discontinue further work on the ELISA development for G-CSF and TGF- β 1 and to use commercial kits. This allowed to redirect focus towards the development of other cytokines and achieve more promising and productive results for them.

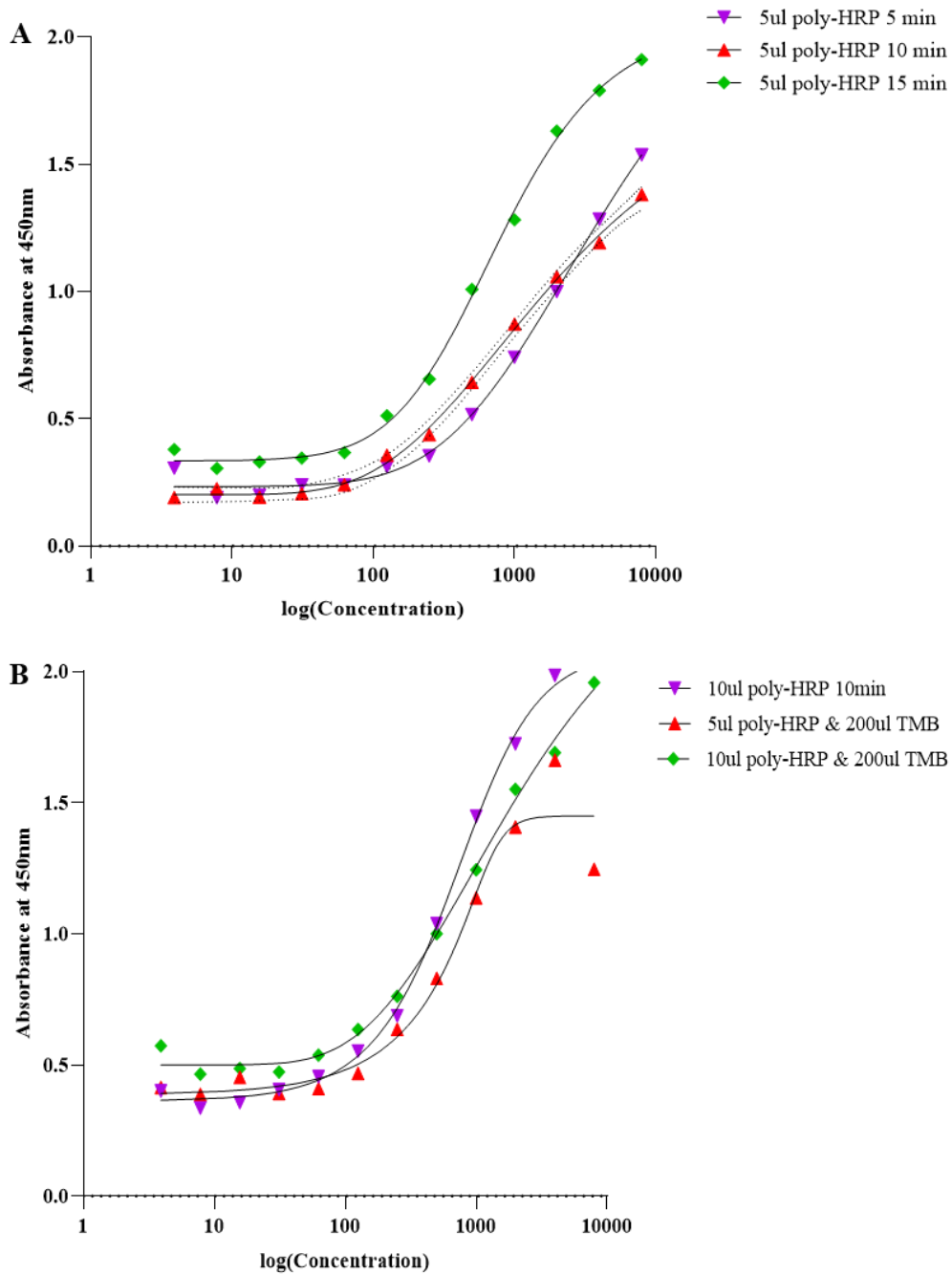


Figure 3. 13. Sensitivity development for TGF-β1 ELISA. The ELISA plate was treated with poly-HRP at different dilutions and time points. **(A)** Standard curve development with poly-HRP at 1:1000 diluted with PBS/1% BSA, and the reaction was stopped at 5 minutes, 10 minutes, 15 minutes. **(B)** Standard curve development with poly-HRP at different dilutions. With 1:500 (10 μl in 5ml PBS/1% BSA) stopped at 10 minutes, 1:1000 diluted poly-HRP with modified concentration of substrate (200 μl TMB) and 1:500 diluted poly-HRP with 200 μl TMB.

3.3.2.4 Intra- and inter-assay reproducibility

This analysis aimed to determine whether the individual QCs fell within the predefined acceptable range (HQ between 675-825, LQ between 67.5-82.5) and comparing their averages and standard deviations within and between the plates.

Intra-assay reproducibility was assessed by comparing the QC and N/C concentrations within two assays from standard curve 1 (upper) and standard curve 2 (lower) within the same plate. For GM-CSF and IL-6, intra-assay reproducibility demonstrated that the six quality controls (HQ and LQ) and six negative controls (PBS and CM) were all within the acceptable limits. For GM-CSF, as illustrated in figure 3.14A, in standard curve 1 (top), the average concentrations for HQ and LQ were 764.3 pg/ml and 76 pg/ml, respectively, with standard deviations of 7.4 and 7.9 for HQs and LQs, respectively. In standard curve 2 (bottom) on the same plate, the average concentrations for HQs and LQs were 731 pg/ml and 75.6 pg/ml, respectively, with standard deviations of 15.7 and 3.3 for HQs and LQs, respectively. Most of the absorbance values for PBS and RPMI-CCM were below the limit of detection, resulting in non-calculable concentrations for these controls.

In terms of inter-assay reproducibility, both IL-6 and GM-CSF consistently exhibited positive reproducibility across multiple ELISA runs, with the exception of potential issues related to recombinant cytokine quality or pipetting errors, such as the presence of air bubbles. Comparing the inter-assay reproducibility, the average concentrations for GM-CSF HQs were 737.9 pg/ml, and for LQs, it was 74.2 pg/ml, with standard deviations of approximately 9.2 and 1.9 for high and low-quality controls, respectively, as illustrated in figure 3.14B. These findings affirm the robustness and reliability of the assay under different experimental conditions and across multiple assays runs.

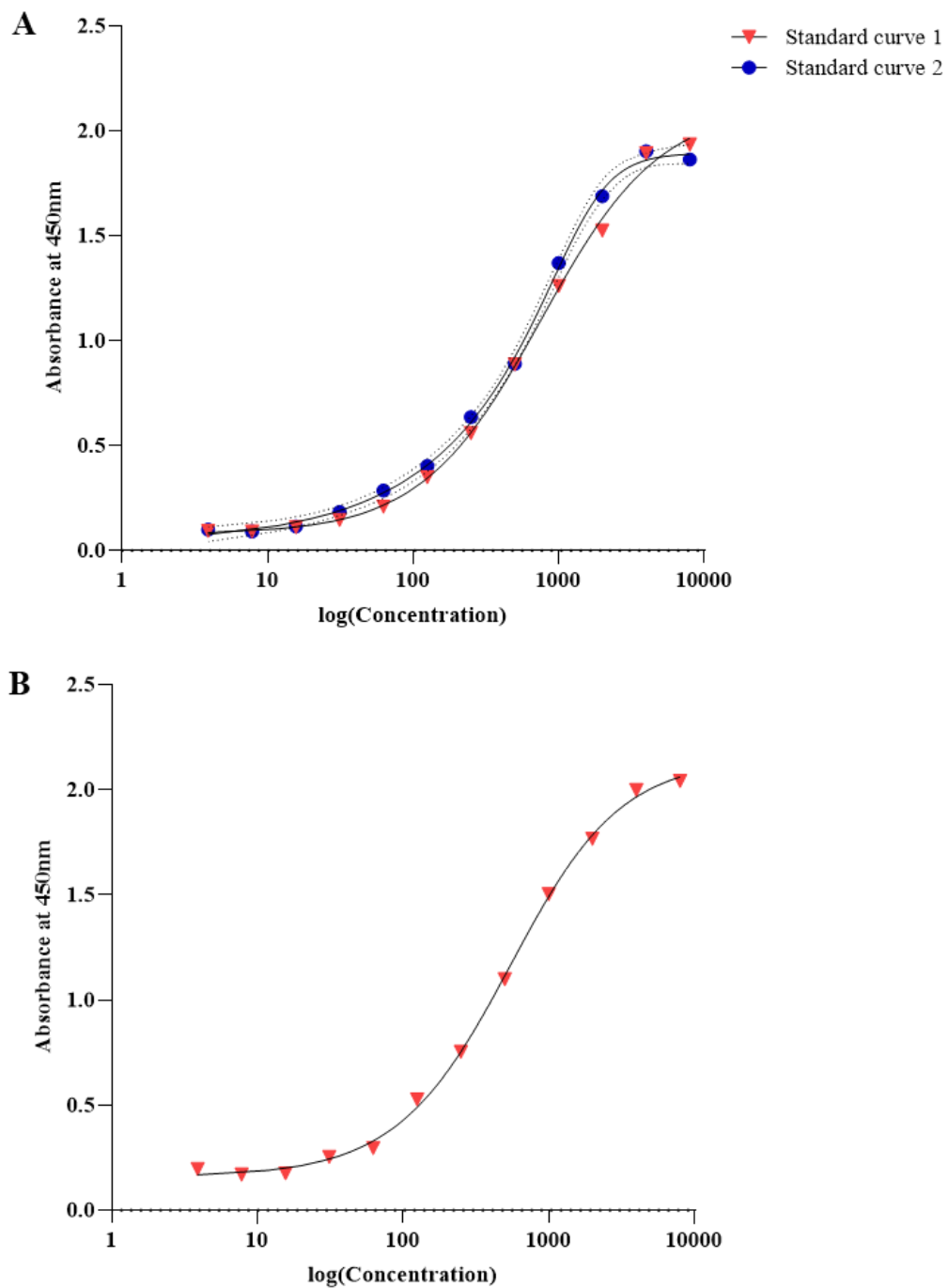


Figure 3. 14. Intra- and inter-assay reproducibility for GM-CSF. To evaluate the reproducibility of the assay, both intra-assay and inter-assay analysis were conducted. **(A)** GM-CSF intra-assay reproducibility with standard curve one (top) and standard curve two (bottom). **(B)** GM-CSF inter-assay reproducibility standard curve. All the quality controls and negative controls were within their respective limits for both reproducibility assay. Comparison of averages between curves was within 738-764 pg/ml for HQ and 74-76 pg/ml for LQ.

3.4 Discussion

Cell culture optimisation

In the context of this study, cell culture conditions played a pivotal role in ensuring the relevance and success of this research, particularly as it aimed to investigate the co-culture of HS-5 and TK6 cell lines. Although these immortalised cell lines normally multiply and succeed in different culture conditions, no common culture medium has been developed for these cell types in co-culture models yet. So, there was a requirement to culture cell lines using the conventional media in order to find a common denominator that would benefit both cell types. To address the cytokine bystander genotoxicity hypothesis, this study embarked on an optimisation journey for each cell line using various culture media, focusing on factors such as morphology, cell growth, and viability over the time. The three media under analysis were DMEM-HG, RPMI-1640, and DMEM-LG, which are conventional choices for these cell lines. Findings as detailed in section 3.3.1, demonstrated that RPMI-1640 emerged as the most favourable medium for both the cell lines in this study.

HS-5 is an alternative cell source for BM-MSC to facilitate the work with BM stromal cells which have been used for researchers' *in vitro* and *in vivo* models (Schmidmaier *et al.*, 2006). Figure 3.4 shows the investigation of the HS-5 variable morphology, plasticity and proliferation in different media including DMEM-HG, RPMI-1640, and DMEM-LG, over three consecutive passages. The cells' morphologies appeared to be similar in all media used. However, RPMI-1640 stood out due to its ability to induce highly elongated fibroblastic projections in the cells, possibly attributable to the specific medium supplementation. Both RPMI-1640 and DMEM-HG demonstrated themselves as the most promising culture media in terms of cell expansion and maintenance of high cell viability levels throughout the experiment. Cells reached over 80% viability in RPMI-1640 and DMEM-HG in every passage (Fig. 3.5B) but live cell count was always high in RPMI-1640 (Fig. 3.5A). This may be due to the DMEM-HG cultured HS-5 adhering to the flask quickly but taking less growing space than other media. HS-5 turns the medium acidic, which may control the cell growth and prevent exceeding the space they have to adhere to (Schmidmaier *et al.*, 2006). In contrast, DMEM-LG exhibited the lowest cell count and consistently lower cell viability, potentially due to its low glucose content, which may not be conducive for maintaining healthy cell cultures over extended periods. Additionally, doubling times were calculated for HS-5 in DMEM-HG (approximately

36 hours), RPMI-1640 (approximately 40 hours), and DMEM-LG (approximately 61 hours). This information underscored that RPMI-1640 and DMEM-HG are the most reliable choices for optimal growth and viability of HS-5 cell cultures among the considered options. Turning the attention to the TK6 cell line, comprehensive assessment in three different culture media was conducted: DMEM-HG, RPMI-1640, and DMEM-LG, over a period of 120 hours. The results provided valuable insights into the suitability of these culture media for TK6 cell expansion in co-culture models.

When considering TK6 cell live count, viability and cell size in figure 3.6, RPMI-1640 emerged as the most suitable medium for promoting the growth of TK6 cells. This conclusion was supported by consistent live cell counts (Fig. 3.6A), viabilities (Fig. 3.6B), and larger cell sizes (Fig. 3.6C) achieved in RPMI-1640. Although TK6 exhibited similar proliferation rates and viabilities in DMEM-HG, the literature favoured RPMI-1640 for *in vitro* co-culture research, which made it a more favourable choice in this study. In contrast, DMEM-LG consistently demonstrated lower cell counts, reduced viabilities, and smaller cell sizes, making it less suitable for promoting the growth of TK6 cells. Lymphoblasts have variable sizes between 10 to 20 μ m (Rozenberg, 2011) and larger lymphocytes have more dividing capability than smaller cells (Meer *et al.*, 2007). Interestingly, Tzur *et al.* (2009) have examined that growth and proliferation rates are influenced by both cell size and cell age using populations of lymphoblasts, implying that cultures containing the smallest cells (DMEM-LG) reduce the cell proliferation rate and give minimal cell numbers compared to the other two media. TK6 proliferated well in DMEM-HG and RPMI-1640 and increased at a similar rate. The highest and lowest doubling time was for DMEM-LG (~47 hours) and RPMI (~25 hours) respectively. DMEM-HG doubling time was slightly higher than ~35 hours. The TK6 growth curve was analysed (Fig. 3.7) to determine its doubling time using the equation, which is needed in future experiments in this research. The consistent doubling time of approximately 16-20 hours for TK6 cells in different seeding densities implies that TK6 cells reach a stable growth phase with relatively uniform growth rates. These findings align with existing literature, despite slight variations possibly attributed to experimental conditions (Liviak, 2010).

Importantly, these results lay the groundwork for co-culture conditions and medium development for HS-5 and TK6. Considering the critical role of HS-5 in leukaemia and biomedical research, it is worth noting that this finding aligns with recent co-culture studies that utilised RPMI-1640 as a supplement medium (Guan *et al.*, 2018; Podszywalow-Bartnicka

et al., 2018). Therefore, it was concluded that RPMI-1640 is the most suitable environment for the co-culture model in this study, supported by both this study data and prior research. This outcome further reinforces the credibility of the results obtained by colleagues within the research team.

ELISA

Enzyme immunoassays use the catalytic properties of enzymes to detect and quantify immunologic reactions. Among these assays, the ELISA serves as a heterogeneous immunoassay technique extensively employed in clinical analyses. Depending on the specific ELISA type, testing requires a primary and/or secondary detection antibody, antigen, coating antibody/antigen. This assortment of ELISA types includes direct (utilising an antigen-coated plate and a screening antibody), indirect ELISA (employing an antigen-coated plate and a screening antigen/antibody), sandwich ELISA (involving an antibody-coated plate and a screening antigen) and competitive ELISA (screening antibody) variants (Alhajj *et al.*, 2023). In the context of this study, the utilisation of sandwich ELISA emerged as the most suitable technique to achieve the research objectives. This choice was informed by the prevalent use of ELISA in previous cytokines studies, where it has been employed both quantitatively and qualitatively. Notably, investigations by Kim *et al.* (2011) focused on the analysis of 22 cytokine concentrations through commercially available multiplex bead-based sandwich immunoassays. Arican *et al.* (2005) evaluated serum proinflammatory cytokines in psoriasis (TNF- α , IL-6, IFN- γ , IL-8, IL-12, IL-17, and IL-18) using sandwich ELISA. Moreover, Winkler *et al.* (1999) measured cytokines including IL-6, TNF- α , IL-2, IL-4, IL-10, IL-12, IFN γ , IL-1a, levels in serum samples by ELISA. Inspired by the example these investigations set, sandwich ELISA was developed for candidate cytokines IL-6, GM-CSF, G-CSF, and TGF- β 1. This strategic selection aligns with the established efficacy of ELISA in cytokine research and underscores the relevance of chosen methodology.

During the ELISA development process, a series of steps were meticulously followed. Initially, identification of the optimal antibody pair, comprising a capture and detection antibody, for each cytokine under investigation was performed. The assessment of the signal-to-background ratio proved instrumental in this endeavour, with the highest value signifying the most favourable antibody pair concentration. This assessment was conducted with both high-quality and low-quality control samples. To enhance the robustness of the ELISA, the assay was executed using both HRP and poly-HRP for all targeted cytokines (except TNF- α , which is

naturally expressed at higher levels). Data indicated that poly-HRP consistently out-performed HRP, resulting in a higher signal-to-background ratio for all the detected cytokines (Fig. 3.8). As a result, optimal antibody pairs were identified for GM-CSF (CAP 4.5 µg/ml and DET 1.75 µg/ml), G-CSF (CAP 2 µg/ml, DET 1.75 µg/ml), and TGF-β1 (CAP 2 µg/ml, DET 1.5 µg/ml).

Upon measuring colour changes using a spectrophotometer at 450 nm, the resulting absorbance data were analysed and plotted using GraphPad software. A standard curve was generated from the serial dilution data, with concentration plotted on the x-axis using a logarithmic scale and absorbance on the y-axis using a linear scale. Typically, this graph illustrates the relationship between optical density and the logarithmic concentration of cytokines, yielding a sigmoidal curve. Known concentrations of recombinant cytokines are employed to construct this standard curve, facilitating the determination of unknown sample concentrations by comparing them to the linear segment of the graphed standard curve, typically between the HQ and LQ. This process was performed using the 'Interpolate standard curve, asymmetric sigmoidal concentration' option within GraphPad software.

Given the initial challenge of low baseline expression levels for target cytokines, the standard curve maintained the range from 0 to 8000 pg/ml. This decision was influenced by literature evidence (Arican *et al.*, 2005), that minimum detectable concentrations of TNF-α and IL-6 were 4.8 pg/ml and 1.1 pg/ml respectively. To ensure accuracy and reliability, high and low-quality control concentrations were tailored to the sensitivity of each ELISA assay, aiming for values within ± 10% of the respective reference values. This approach is crucial because samples falling below the assay's lower limit of detection cannot be reliably measured using the standard curve or assigned the values at the midpoint between the lower limit of detection and zero, as suggested by Melenhorst *et al.* (2012). Furthermore, in instances where values exceeded the limit of detection, entering the plateau phase, dilution strategies were implemented as necessary to bring them within the linear range of the assay. For IL-6, GM-CSF, G-CSF, and TGF-β1, HQ and LQ were set at 750 pg/ml and 75 pg/ml, respectively, allowing for detection within the ranges of 675 – 825 and 67.5 – 82.5, respectively. Ideally, the standard curve was designed to consistently position approximately 2-3 standard deviations within the plateaus at both ends of the curve. This deliberate design ensured that quality controls consistently resided within the linear, measurable segment of the curve.

However, as illustrated in figure 3.9, the standard curve with HRP did not provide the desired outcome and the quality controls did not align as expected. This was particularly noticeable

with G-CSF and TGF- β 1, which were not demonstrating positive uplifts of the curve. As a result, alternative avenues were explored by incorporating poly-HRP at different incubation times, as demonstrated in figure 3.10 to 3.13, relating to each cytokine. Nevertheless, even with poly-HRP, only GM-CSF and IL-6 met the established criteria for the proper standard curve. In the case of G-CSF, varying the poly-HRP concentration over time did not lead to the desired curve shape. Consequently, it was decided to increase the poly-HRP concentration and modify the substrate concentration, as shown in figure 3.12. For TGF- β 1, increasing the poly-HRP concentration did elevate the curve within the linear phase, however, it failed to reach the plateau phase under any of the conditions tested in this study.

Developing a satisfactory standard curve for G-CSF and TGF- β 1 posed significant challenges, consistently yielding unexpected results throughout the experimentation. Notably, the alignment of quality controls did not meet the anticipated outcomes, leading to multiple attempts with varied parameters at different time points. However, a study by Wakefield *et al.* (1995) successfully quantified TGF- β 1 and TGF- β 2 in acid-ethanol extracted samples from breast cancer patients, employing isoform-specific ELISA assays.

Considering the challenges encountered to develop a robust ELISA for G-CSF and TGF- β 1, it is noteworthy that alternative methodologies have been employed by other researchers. For instance, some investigators utilised quantitative sandwich enzyme immunoassay kits, following the manufacturer's instructions to detect various cytokines in plasma, including G-CSF and GM-CSF, as well as IL-6, TNF- α , and IFN γ . Additionally, for cytokines that prove challenging to analyse using ELISA, alternative techniques such as quantitative microarrays have been employed (Lee *et al.*, 2008; Morgan *et al.*, 2010). Despite the persistent efforts, the optimal development of the ELISA for G-CSF and TGF- β 1 remained elusive, even after extensive modifications to key components like HRP, poly-HRP, TMB, H₂O₂, and the coating buffer. Considering the demonstrated success of ELISA kits in detecting these two cytokines in various studies, the adoption of commercially available ELISA kits for G-CSF and TGF- β 1 may be performed in future research endeavours, ensuring reliable and validated measurements of these crucial cytokines.

The attention was then focussed on IL-6 and GM-CSF for further assay development and still there were some inconsistencies noted across repeated experiments. These inconsistencies could be attributed to factors such as pipetting errors, sampling order variability, inadequate washing, and incomplete mixing. It is essential to acknowledge that various factors can

interfere with ELISA testing at any stage of the process, beginning with specimen collection. The quality and integrity of the assay plate, coating buffer, capture antibody, blocking buffer, target antigen, detection antibody, enzyme conjugate, washes, substrate, and signal detection can all interfere with proper ELISA testing (Alhajj *et al.*, 2023). Therefore, it is imperative to maintain strict adherence to standardised laboratory procedures to ensure the accuracy, reliability, and reproducibility of outcomes. Attention to detail, in line with the optimised protocol, proved instrumental in achieving a high degree of reproducibility in each assay. For instance, during the sampling process, care was taken to introduce PBS/1% BSA into the standard curve rows first, followed by the placement of high and low-quality controls in six separate wells. Single pipettes were employed, not multichannel pipettes, for the precise pipetting of quality controls into each well. This approach enhanced the confidence in the integrity of the subsequently obtained data, facilitating the determination of intra- and inter-assay reproducibility. Finally, the 100 µl of the high standard being added into the first wells of standard rows as duplicates and starting the double dilution accordingly using a multichannel pipette ensured wells did not dry out. It is essential to have standards and all the samples in duplicate for averaging outcomes before the concentration analysis with standard curve (Lee *et al.*, 2008; Winkler *et al.*, 1999), then to compare the value of high and low QCs against the standard curve and determine if the correct concentration is established consistently. Moreover, meticulous washing steps using a buffer, such as PBS, and a non-ionic detergent were executed between each assay step to remove unbound materials. This thorough approach was essential to achieving proper ELISA testing. Notably, GM-CSF and IL-6 assays demonstrated enhanced intra- and inter-assay reproducibility, consistently yielding the expected results and alignment of HQs and LQs, as exemplified in figure 3.14. It is important to underscore that positive and negative controls were integral to the validity of the ELISA test results, and they were included in every ELISA test run. These controls served to validate the standard curve outcomes and the positivity of the test results, as emphasized by Alhajj *et al.* (2023).

3.5 Conclusion

In conclusion, this chapter highlights the critical aspects of assay development, optimisation, and revalidation for both cell culture and ELISA experiments, emphasising their pivotal role in generating reproducible and reliable data in the laboratory. In standard culture media optimisation, RPMI-1640 was identified as the optimal choice to provide an ideal environment for the *in vitro* HS-5 and TK6 bystander co-culture model.

The meticulous and iterative process involved in developing ELISAs, specifically for quantifying cytokines like IL-6 and GM-CSF, is discussed. The strategic selection of the sandwich ELISA technique, supported by its proven efficacy in cytokine research, is highlighted. Despite facing challenges, particularly in achieving a satisfactory standard curve for G-CSF and TGF- β 1, commitment to method optimisation and careful consideration of alternative methodologies were integral to the development process.

Throughout the development process, priority was given for the identification of optimal antibody pairs, standard curve utilisation of both HRP and poly-HRP and quality control measures. The incorporation of poly-HRP proved instrumental, especially for GM-CSF and IL-6, leading to consistent and reproducible results, but challenges persisted with G-CSF and TGF- β 1, ultimately leading to their exclusion from full optimisation. Despite encountering challenges, the developed assays can be used for future studies when analysing respective test samples while the lessons learned from unsuccessful assays will notify future considerations.

The importance of method validation cannot be overstated, thus there should be potential consideration of alternative methods as undertaken by other studies; for example, the Luminex multiplexing platform to analyse two cytokine fluctuations (storm) in peri- and post-myeloablative HSCT (Melenhorst *et al.*, 2012) and magnetic bead-based multiplex immunoassay (Kleiner *et al.*, 2013). Nonetheless, these diverse approaches will be based on factors such as the number of candidates to analyse, sample types, assay time, and cost-effectiveness.

In summary, the ELISA development chapter underscores the complexities and nuances involved in optimising assays for cytokine quantification. While challenges were encountered, the strategic adoption of sandwich ELISA and continuous method refinement, guided by insights from previous literature, positioned this study for reliable cytokine analysis, particularly for IL-6 and GM-CSF.

CHAPTER 4

ARRAY ANALYSIS OF CYTOKINE SECRETION FROM HS-5 EXPOSED TO CHEMOTHERAPY

4.1 Introduction

The BM microenvironment comprises a variety of cells, including HSC, MSC, macrophages, fibroblasts, and osteoblasts in the BM cavity, and adhesion molecules, chemokines, cytokines, and soluble or membrane-bound factors present in the BM stroma, which combine to form the so-called BM niche (Chen *et al.*, 2021). Haematopoiesis is regulated by many cytokines that are present in the BM microenvironment (section 1.6.1). In addition to maintaining steady-state haematopoiesis, cytokines and their corresponding receptors play a significant role in mediating the intricate, regulatory paths that control both basal and emergency haematopoiesis such as systematic infections (sepsis or chronic inflammatory disease), injuries or external inflammatory signals (long term radiation or chemotherapy) (Robb, 2007; Wang *et al.*, 2022). Sustained exposures to aberrant inflammation have detrimental effects on the haematopoietic system, leading to increased proliferation, DNA damage, different forms of cell death (apoptosis, pyroptosis and necroptosis) and BM microenvironment modifications. Together, all these changes can cause premature loss of haematopoiesis function and tend to increase leukaemogenesis. Especially in individuals with inherited chronic inflammatory signals (cytokine polymorphism) which may exacerbate inflammation and accelerate disease progression (Wang *et al.*, 2022).

Chemotherapy is known to damage BM stromal cells *in vitro*, but the extent to which marrow MSCs are damaged by conditioning therapy *in vivo* is largely unknown. As explained in section 1.6.2, aberrant BM niche promotes leukaemogenesis with the help of supporting factors expressed following conditioning therapy, the precise process by which they occur as yet is unclear. However, among the various responses following conditioning therapy, the cytokine storm (section 1.6.2.1 and section 6.1) emerges as a predominant concern due to its potential to induce numerous complications.

Cytokine storm was first coined in 1981 when the anti-T-cell antibody muromonab (okt3, anti-CD3) was first introduced into the clinic as an immunosuppressive treatment for solid organ

transplantation and it caused increased cytokine levels and systemic reaction (Shimabukuro-Vornhagen *et al.*, 2018; Yildizhan & Kaynar, 2018). Cytokine storm is a toxic condition caused by the extreme levels of pro-inflammatory cytokines released with the activation of the cellular immune response independent of the antigen (Yildizhan & Kaynar, 2018). Conventionally, TNF- α , IL-6, IFN- γ , and IL-1 β serve as prominent proinflammatory cytokines. However, divergent investigations propose that LIF, IFN- α , IL-6, and TGF- β 1 can be designated as either anti-inflammatory or proinflammatory cytokines under various circumstances (Zhang & An, 2007). Consequently, the intricate pathophysiology of cytokine storm remains obscure and incompletely understood due to the dual activity of some cytokines and their expression level which differ between individuals' genotypes.

Cytokine storm is associated with a wide variety of infectious and non-infectious diseases including GvHD, multiple sclerosis, pancreatitis, or multiple organ dysfunction syndrome (Tisoncik *et al.*, 2012). Also, many studies have investigated the tissue concentrations of cytokines, mainly in lungs, gut, or brain following irradiation or immunotherapy (Melenhorst *et al.*, 2012; Gallet *et al.*, 2011; Tisoncik *et al.*, 2012). Cytokine secretion in BM after irradiation is also well described (Greenberger *et al.*, 1996; Lorimore *et al.*, 2001). But only limited data is available about how chemotherapy exposure affects cytokine secretion or the release of other bystander mediators from the BM microenvironment. Therefore, as a prospective mechanism underlying CIBE, this chapter aims to ascertain the *in vitro* expression of cytokines at baseline and during cytokine storm (section 1.6.2) by a model of BM-MSCs following exposure to the alkylating agent; CHL (section 1.2.1) and the topoisomerase II inhibitor; MTX (section 1.2.2).

To mimic the BM compartment, this study used an *in vitro* model comprising the HS-5 cell line as it is the only human fibroblastic mesenchymal stem cell line available (section 2.2.2.2). Utilising an array capable of detecting a broad panel of cytokines allowed for the selection of candidates based on various criteria, including baseline expression in the BM, increased expression following drug exposure, fold change, and cytokines influencing myeloid differentiation, as well as those expressed in response to chemotherapy exposure. However, a drawback of the array analysis was that it only presented relative changes, as the measurements were conducted via chemiluminescence. To address this limitation, an ELISA, including both in-house developed assays and commercial kits, was employed in the subsequent section 4.3.2

to quantitatively validate the candidate cytokines selected from the array, particularly in relation to chemotherapy treatments.

4.2 Methods

4.2.1 Cytokine array

The cytokine array experiment was replicated three times using fresh membranes, maintaining consistent procedural parameters. Each replication utilised independent biological samples, ensuring the experimental conditions were applied across distinct biological contexts. Two chemotherapeutic drugs linked to TRL were used at doses equivalent to clinically relevant or *in vivo* observed plasma concentrations (section 2.1.2). CHL (alkylating agent) and MTX (topoisomerase II inhibitor) were assessed for induction of cytokine secretion in the human BM stromal cell line HS-5. CHL was used at 40 μM , which was equivalent to plasma levels measured in mouse pharmacokinetic studies. MTX was used at 1.12 μM (500 ng/ml), aligning with levels measured in human plasma following *in vivo* administration. A profile of candidate cytokines released by HS-5 with and without drug exposure was performed using the Abcam 80 targets cytokine array (ab133998) as detailed in section 2.2.2. Data analysis was done according to the instructions in the Abcam protocol using the Li-cor reader (Bioscience UK Ltd) to measure the intensity of the respective cytokine spots. Layout of the cytokines on the array is listed appendix II. Each array experiment was repeated three times, and results were analysed using 'Image Studio Lite' and averaged for each cytokine. The density of each spot was measured using the same size circle (drawn with the software) that is roughly the size of one of the largest spots. To validate data, all four arrays (medium alone, and medium from untreated and treated cells) were visualised concomitantly on the Li-cor.

Utilising the densitometry data, a positive control normalisation factor was determined using the 'positive control IgG spots' on all four array membranes and was used to normalise signal responses for data comparison. Cytokine spots on each array were similarly corrected for the respective correction factor for a given array and could be compared within and between repeats as described in the manufacturer's instructions. The signal intensity for each spot is proportional to the relative concentration of the cytokines in that sample. Thus, comparison of signal intensities for individual cytokines (between cytokines) and among arrays (treated vs untreated and CHL vs MTX) were done to determine relative differences in expression levels. Background intensities (medium alone) were subtracted from cytokine expression in untreated

cells to find baseline expression (cytokines that are typically expressed from the HS-5 cells) and also from each cytokine array spot in drug-treated samples to obtain the absolute changes in cytokine secretion due to drug exposure. Cytokine secretion was also assessed for fold change in secretion, as well as to determine which cytokines were only expressed prior to, or following, drug exposure. Five cytokines were selected for further investigation based on the highest absolute expression and/or fold up-regulation in response to both drugs relative to untreated cells. The selection of some cytokines was also based on some important factors as follows:

- Cytokines which trigger myeloid lineage differentiation (e.g. IL-1, 3, 6, GM-CSF and SCF)
- Cytokine storm candidates (e.g. TNF- α , IFN- γ , IL-1 β , 2, 4, 6, 8)
- Cytokines which are known to be involved in post-HSCT malignancy.

4.2.2 Array validation ELISA

Following cytokine array, five cytokine candidates were selected for further studies according to the three considerations mentioned above. Because the cytokine array showed only relative secretion, to validate array results and confirm selected cytokines, ELISA assay was performed to quantify the levels of the selected cytokines over five days following chemotherapy exposure. TK6 cells were measured alongside HS-5 to assess any contribution to cytokine secretion which would be relevant to the bystander assays described in chapter 6. For each TNF- α , GM-CSF and G-CSF assay iteration, three independent ELISA plates were utilized. Within each plate, a minimum of 2-3 replicate wells were dedicated to each sample. Subsequently, average readings were obtained whenever feasible, ensuring comprehensive data analysis. The inability to establish in-house ELISA assays for TGF- β 1 and G-CSF necessitated the procurement of ELISA kits for conducting these assays as required. Due to cost constraints associated with ELISA kits, a single repetition of TGF- β 1 ELISA (Fig. 4.6) and two repetitions of G-CSF ELISA (Fig. 4.9) were undertaken for sample analysis.

HS-5 and TK6 cells were seeded in a 12-well plate at their appropriate seeding density 24 hours before the experiment. Three separate HS-5 wells were treated with 4 μ M and 40 μ M of CHL and 1.12 μ M MTX for 1 hour and washed with PBS before adding new media. Alongside treated HS-5, untreated HS-5 and TK6 were also prepared and incubated at the same time. Then every 24 hours over 5 days (120 hours), supernatant was collected for cytokine measurement

from every treated well and replaced with new RPMI-CCM. For untreated HS-5 and TK6, only 24- and 120 hours collections were done. Collected supernatants were stored at -80 °C for ELISA analysis. As described in section 3.2.2 and section 2.2.3.1, in-house developed TNF- α , IL-6 and GM-CSF ELISA assays were performed. G-CSF and TGF- β 1 were measured using commercially available ELISA kits from Thermo Fisher according to the manufacturer's protocols (section 2.2.3.2).

ELISA assays were performed according to the protocol described in section 2.2.3. Briefly, after coating and blocking the plates, samples were incubated, followed by the addition of biotinylated secondary antibodies. Subsequently, HRP or/and poly-HRP was added, and the substrate solution was introduced to the wells. The reactions were halted at appropriate time points specific to each cytokine. Cytokine concentrations were determined by interpolation from a standard curve and expressed in pg/mL. Samples exceeding the detection limit were appropriately diluted. To ensure accuracy and repeatability, all samples were analysed in the same run with 2-3 replicates, including duplicate standards. Calculations of these assays indicated that the intra-assay and inter-assay CV were also lower than 10%.

For ELISA analysis, statistical analyses were performed using analysis of variance (2-way ANOVA) and group comparisons followed by a Tukey's multiple comparison test to evaluate the significant differences, where (*) for $p \leq 0.05$, (**) for $p \leq 0.01$, (***) for $p \leq 0.001$ and (****) for $p \leq 0.0001$ was considered significant. Error bars are expressed as mean \pm standard deviation (SD) of three independent experiments except for where otherwise stated. All statistics and graphical illustrations were done using GraphPad Prism software v. 8.2.1.

4.3 Results

4.3.1 Cytokine Array

4.3.1.1 Profile of cytokine secretion from HS-5 cells

The results from the cytokine array data using untreated, 40uM CHL and 1.12uM MTX treated HS-5 are described in Asurappulige *et al.* (2023).

Cytokine expression from untreated HS-5 cells represents cytokines that are typically expressed in the BM. Out of 80 cytokines on the array, there were 54 cytokines expressed at baseline untreated HS-5 cells. Most of the cytokines expressed from untreated HS-5 are listed in the literature and thus validate the HS-5 mesenchymal features of the BM (section 4.4). Figure 4.1 presents the cytokines that were consistently positive in all three repeats after correcting for the negative and positive controls, and when the ‘culture medium alone’ values were subtracted. The baseline secretion profile reveals that IL-6, TNF- α , GM-CSF, IL-8, ENA-78, MCP-1, TIMP-2, MCP-2, MCP-3, and GRO- α rank among the top ten cytokines with the highest levels. FGF-7 was positive on all three membranes but was the lowest detected cytokine at 0.01 absorbance. Therefore FGF-7 was considered as a ‘threshold’ of cytokine presence, with anything below this absorbance to be considered as not expressed. There were 11 cytokines that were not expressed at baseline, but interestingly they were all expressed following drug treatments (section 4.3.1.4). Due to negative absorbances in at least one membrane repeat, the remaining 15 cytokines were considered to not be expressed; these were IL-4, IL-7, TNF- β , EGF, Angiogenin, PDGF-BB, BDNF, IGFBP-1, LIGHT, NT-4, PARC, PIGF, TGF- β 2, TGF- β 3 and HGF. However, some of the cytokines among these fifteen were positive in two membranes out of 3 repeats, with an absorbance greater than the set threshold of 0.01 absorbance value of FGF-7. Therefore, these cytokines (IL-4, IL-7, TNF- β , EGF, Angiogenin, PDGF-BB, BDNF, IGFBP-1, PARC, and HGF) should be taken into consideration in further research.

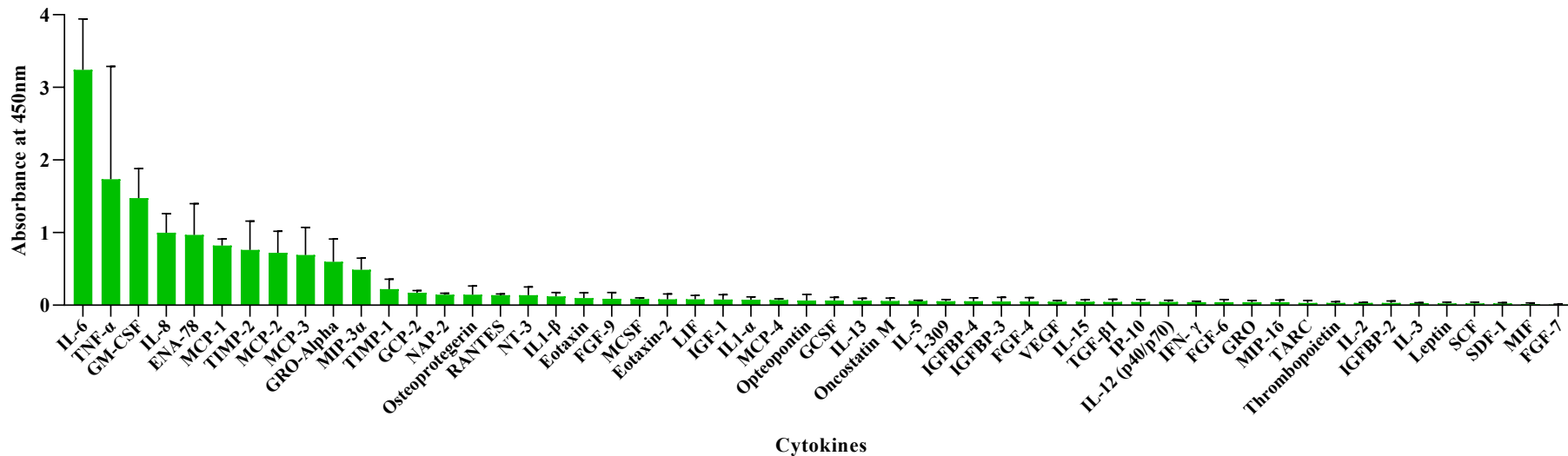


Figure 4. 1. Profile of cytokine secretion by untreated HS-5 cells. Out of 80 cytokines tested, 54 cytokines were expressed in untreated HS-5. Normalisation was performed using positive control signals on each array. Cytokines were detected utilising absorbance values of each cytokine spot on the membrane at 450nm and corrected for background cytokines from the culture medium. Data shows mean \pm SD (n=3). This figure was adapted from Asurappulige *et al.* (2023).

4.3.1.2 Absolute change of cytokine expression following drug exposure

A direct comparison of cytokine secretion due to drug exposure was compared with untreated cells' cytokine secretion levels. Treated samples generally showed a noticeable increased expression of cytokines following exposure to both of the drugs. As a change from very low to higher levels may be more biologically relevant, as well as absolute changes in secretion, (Fig. 4.2) the fold change in secretion (Fig. 4.3) was also explored.

Even though there were no significant differences in absorbances between each cytokine from untreated cells compared with exposure to either drug, treated samples showed higher overall expression of cytokines than untreated. Out of the 54 cytokines expressed from untreated cells, 24 cytokines were up-regulated for both drugs following treatment (Fig. 4.2A). Similar to the baseline data, the highest cytokines expressed by HS-5, whether treated or untreated, were IL-6, TNF- α and GM-CSF. FGF-7 again was the lowest cytokine to be both positive in all three membranes and also up-regulated by both drugs. Some cytokines were positive at baseline secretion, but slightly down-regulated following exposure to both drugs; Figure 4.2B shows the 10 cytokines common to both drugs which were down-regulated following drug exposure. Two cytokines were increased after exposure to MTX, but not by CHL (ENA-78 and GRO- α ; Fig. 4.2C) whereas 18 cytokines were increased by CHL but decreased by MTX (Fig. 4.2C). Of the 44 cytokines up-regulated by the drugs, 42 were more highly expressed following CHL exposure.

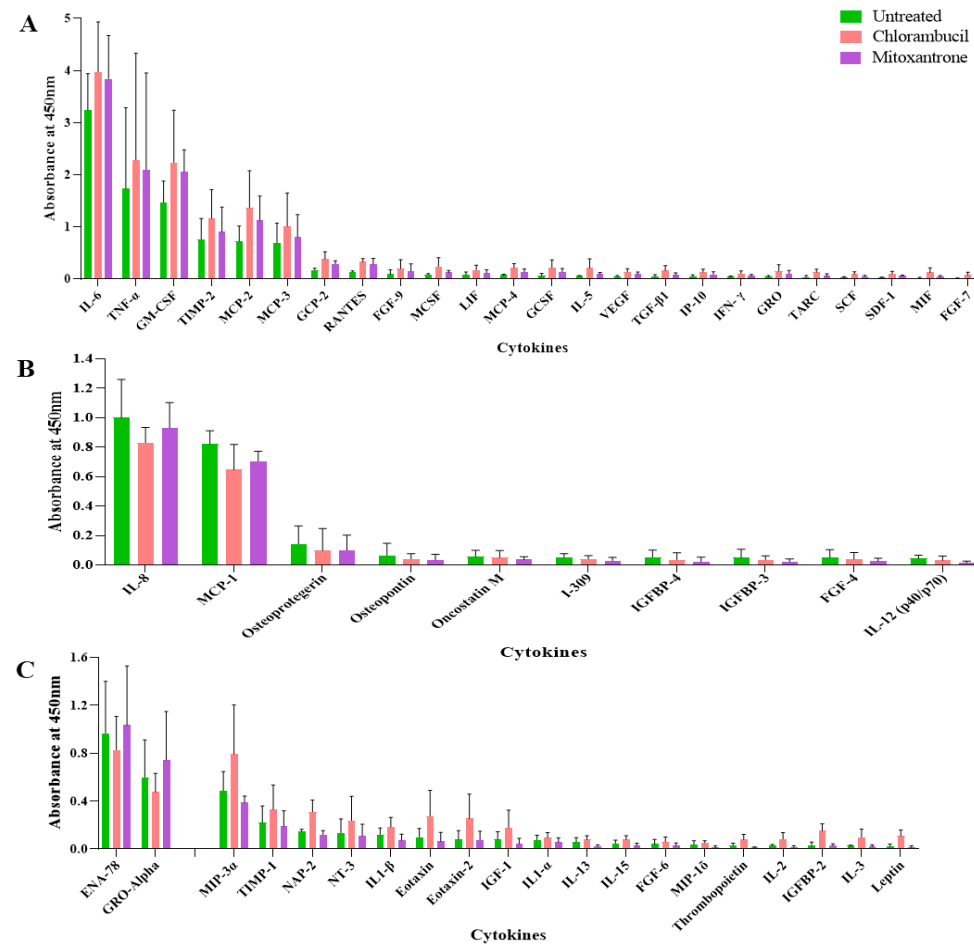


Figure 4. 2. Cytokine expression from HS-5 cells following chemotherapy treatments. HS-5 cells were exposed to CHL and MTX for 1 hour and then measured for change in cytokine secretion at 72 and 48 hours respectively after exposure. Cytokine secretion is arranged in the order of magnitude for CHL. (A) Cytokines which were up-regulated by both drugs in comparison to untreated HS-5 cells. (B) Cytokines which were down-regulated by both drugs relative to untreated HS-5 cells. (C) Cytokines which were up-regulated by one drug, but down-regulated by the other; ENA-78 and GRO-Alpha were upregulated by MTX, whereas the remaining cytokines were upregulated by CHL. Data shows mean \pm SD (n=3). CHL; chlorambucil, MTX; mitoxantrone. This figure was adapted from Asurappulige *et al.* (2023).

4.3.1.3 Fold change of cytokine expression following drug exposure

It was acknowledged that there was no significant difference between untreated and drug treated cells for absolute cytokine expression and that some cytokines might only be expressed due to drug exposure. Thus, the data was explored for this outcome and also investigated for fold increase in expression, as potentially being more relevant than absolute expression in driving a bystander/mutagenic profile. Each cytokine was then compared to the untreated control for fold-change in expression. Figure 4.3A demonstrates the descending order of fold change for 24 cytokines which were increased following exposure to both drugs. Out of the 24 upregulated cytokines, the top 10 highest fold change cytokines with CHL treatment were SCF, SDF-1, MIF, TGF- β 1, G-CSF, IL-5, GRO, IP-10, VEGF, and MCP-4, whereas for MTX the highest were MIF, SCF, GRO, SDF-1, G-CSF, IP-10, TGF- β 1, VEGF, RANTES, and MCP-4. Thus, the common cytokines in the top 10 for both drugs were SCF, SDF-1, MIF, TGF- β 1, G-CSF, GRO, IP-10, VEGF, and MCP-4.

The order of the cytokines in the graphs were different when the descending order of absolute change was compared with the fold change analysis. Briefly, on reviewing the fold difference in expression, the order of the cytokine position in the graphs has almost reversed from lowest to highest compared to the absolute expression data. When considering IL-6, which was the highest absolute expressed cytokine in figure 4.2A, whilst there was a large increase in secretion following drug exposure, the fold change was actually the lowest compared with the other cytokines (Fig. 4.3A). Similarly, both TNF- α and GM-CSF were placed towards the end of the fold change graphs, whereas they were in the first couple of cytokines in the absolute expression (Fig. 4.2A). This is to be expected as mathematically, the fold change can be more marked when the untreated secretion is low, even with modest changes in secretion. Thus, and expectedly, cytokines which had low secretion at baseline such as SCF, SDF-1 and MIF had much higher fold difference following drug treatment in figure 4.3A. Of note, is that the relatively lower absorbance values allow for more variability between repeats compared with the higher absorbance values, and this is reflected in the wide error bars decreasing in size as fold change decreases. For all of these cytokines, CHL created a higher fold increase than MTX, reflecting the higher absolute secretion levels post-drug exposure. In figure 4.3B, ten cytokines demonstrating decreased secretion following exposure to both drugs are represented as decreased fold change. Nine out of the 10 cytokines showed higher fold reduction with CHL than MTX; only FGF-4 was reduced more by MTX.

The fold change of cytokines which were up-regulated due to only one drug and down-regulated by the other drug is illustrated in figure 4.3C. The order of placement of cytokines have rearranged when compared with the absolute secretion levels. GRO-alpha and ENA-78 demonstrate the lowest fold difference, whereas they both were the highest absolute secretion levels (for MTX only) in figure 4.2C. Similarly, for CHL only, more highly expressed cytokines had the lowest fold change (e.g. MIP-3 α , TIMP-1), whereas the less highly expressed had the highest fold change (e.g. IGFBP-2, Leptin, IL-3). Nevertheless, this pattern did not follow for all cytokines. Thus, a consideration of whether absolute levels or fold change might be more biologically significant warrants further investigation.

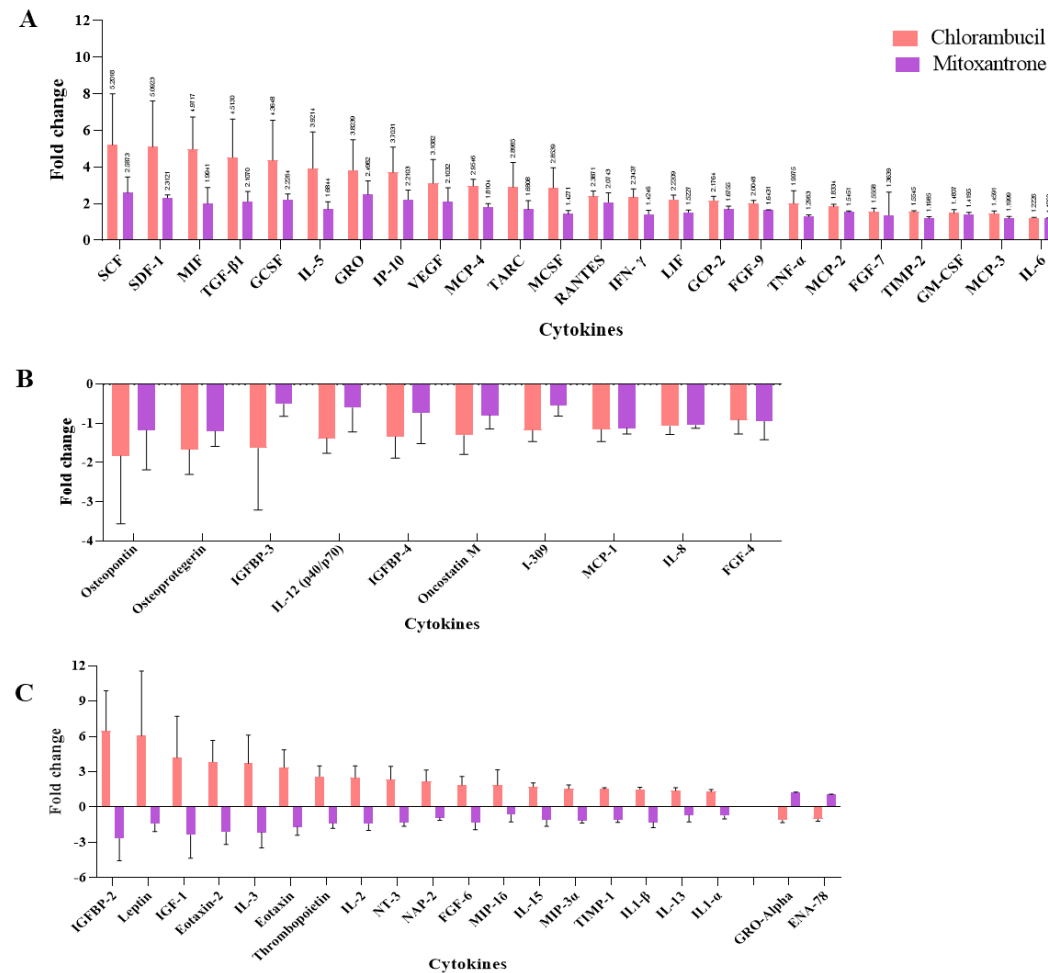


Figure 4. 3. Fold change of cytokine expression following chemotherapy treatments. Cells were exposed to CHL and MTX for 1 hour, then measured for cytokine secretion after 72 and 48 hours respectively. Fold change in secretion was calculated to determine the largest relative changes in cytokine secretion following drug exposure. Cytokines are arranged in order of magnitude of fold change for CHL. **(A)** Cytokines which have positive fold change by exposure to both CHL and MTX. **(B)** Cytokines which have negative fold change common to both drugs. **(C)** Cytokines which were positive for one drug, but negative fold change for the other. Data shows mean \pm SD (n=3). CHL; chlorambucil, MTX; mitoxantrone. This figure was adapted from Asurappulige *et al.* (2023).

4.3.1.4 Cytokine secretion due to drug treatment; switching on gene expression

There were eleven cytokines either at or below the set threshold of 0.01 absorbance or negative on at least two membranes and therefore deemed to not be expressed by untreated HS-5 cells. However, all these 11 cytokines were detected following drug exposure. All 11 were more highly expressed by CHL than MTX and are presented in descending order of secretion in figure 4.4, alongside FGF-7 as a comparator cytokine which was the lowest cytokine to be detected on all three membranes at baseline and following drug exposure.

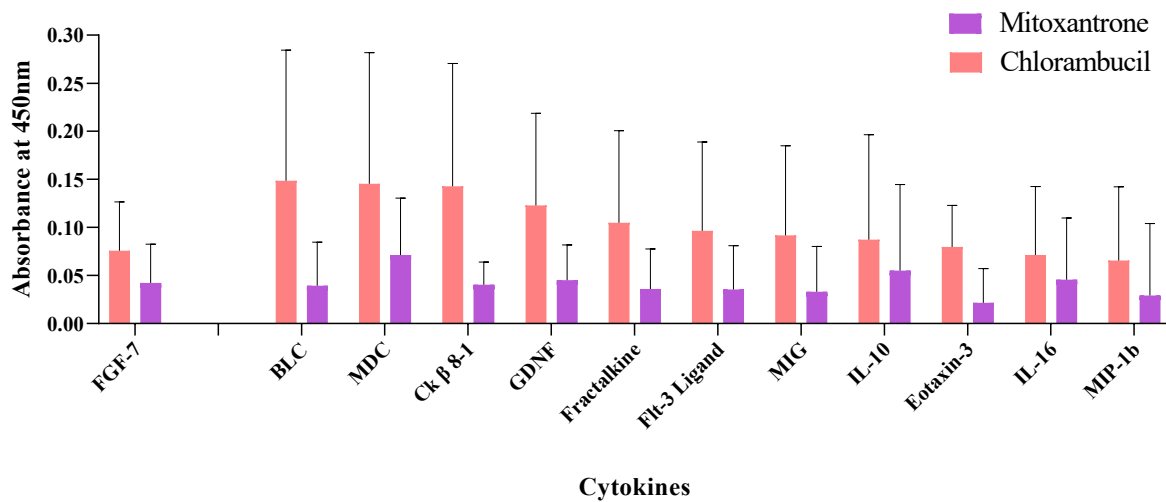


Figure 4. 4. Detection of cytokines secreted only in response chemotherapies. HS-5 cells were exposed to CHL and MTX for 1 hour then cytokines were measured after 72 and 48 hours respectively. Cytokines were identified for being absent in untreated HS-5 (negative absorbance values on untreated membranes) but then detected following drug exposure. Out of 80 cytokines, 11 cytokines were not expressed from untreated HS-5 cells however, all were detected following drug exposure. FGF-7 as the lowest detected cytokine both in untreated and drug treated HS-5 cells is presented for comparison of relative secretion levels. Data is presented as mean \pm SD (n=3). Figure was adapted from Asurappulige *et al.* (2023).

Based on the array cytokine expressions and the three cytokine selection factors mentioned in section 4.2.1 five candidate cytokines were selected out of the 80 candidates on the array. By considering documented literature and as representatives of high overall secretion or high fold increase, as well as contribution to myeloid differentiation, TNF- α , IL-6 and GM-CSF were chosen from the absolute change cytokines, and G-CSF and TGF- β 1 were selected from fold change to explore their potential role in genotoxicity (Chapter 5) and in the bystander assays (Chapter 6).

4.3.1.5 Functional assessment of cytokine profile

A literature review was performed on all 80 cytokines to explore their main functionality and to study how the HS-5 cells respond to chemotherapy. Table 4.1 describes the overall function of the BM cytokines when untreated and how the function might change with drug treatment.

Table 4. 1. Cytokine functionality table with respect to expression pattern in the cytokine array. The overall response inferred an upregulation of pro-inflammatory cytokines, supported by an increase in chemotactic factors, promotion of angiogenesis and proliferation. There appeared to be a balance in control of pro- and anti-apoptotic factors, with an overall sway towards promoting apoptosis. These observations align with the clinical picture of a cytokine storm in patients following chemotherapy. Thus, these data support the use of HS-5 as a model of the BM microenvironment.

Cytokine		Functions
Upregulated by both drugs (Fig. 4.2A & Fig. 4.3A)		
1)	IL-6	Pro- and anti-inflammatory depending on the situation, induces HSC proliferation and differentiation, induces pro-inflammatory cytokine production and costimulatory action. Synergizes with TGF- β to drive Th17.
2)	TNF- α	Pro-inflammation and inflammatory cytokine production, cell proliferation, apoptosis, anti-infection.
3)	GM-CSF	Proliferation of myeloid precursors, pro-inflammation, macrophage activation, increase neutrophil and monocyte function, growth and differentiation
4)	TIMP-2	Involved in degradation of the extracellular matrix. In addition to its inhibitory role against most of the known matrix metalloproteinases, the encoded protein is able to promote cell proliferation in a wide range of cell types and may also have an anti-apoptotic function.
5)	MCP-2	All monocyte chemoattractant proteins are strong chemoattractant activity for monocytes. Moreover, they display overlapping chemoattractant activity on basophils and eosinophils in humans.
6)	MCP-3	
7)	GCP-2	Granulocyte chemotactic protein 2, also known as CXCL6, is a chemoattractant for neutrophilic granulocytes.
8)	RANTES	Regulated upon Activation, Normal T cell Expressed and Secreted is a pro-inflammatory chemokine, proliferation and activation of monocyte/macrophage and certain NK cells
9)	FGF-9	Involved in cell growth, tumour growth and invasion
10)	M-CSF	Involved in the myeloid cell proliferation, differentiation, and survival of monocytes, macrophages, and bone marrow progenitor cells
11)	LIF	Induces cancer progression and cell survival
12)	MCP-4	Chemokine, MCP-1, MCP-3, and MCP-4 have been noted in the airways of asthmatic subjects
13)	G-CSF	Pro-inflammatory, differentiation and activation of granulocytes, act on myeloid cell differentiation
14)	IL-5	Pro-inflammatory, proliferation and activation; hallmark of Th2 effector cells
15)	VEGF	Pro-inflammatory, signalling proteins involved in vasculogenesis

Understanding the chemotherapy- induced bystander effect; an evaluation of the role of cytokine storm in an in vitro model of the human bone marrow

16)	TGF-β1	Multifunctional mediator of both homeostasis and injury responses controlling both proliferation and apoptosis in many cell types and is rapidly activated after ionising radiation in the microenvironment. Synergizes with IL-6 to promote Th17 cells
17)	IP-10	Interferon gamma-induced protein-10- chemotaxis, promotion of T cell adhesion to endothelial cells, antitumour activity, apoptosis, cell growth and angiogenesis. Alterations of IP-10 levels have been associated with infectious diseases, immune dysfunction and tumour development
18)	IFN- γ	Pro-inflammation, innate, adaptive immunity anti-viral, increased class I and II MHC
19)	GRO	GRO (growth-regulated oncogenes) or CXCL1 is a small peptide chemokine which acts as a chemoattractant for immune cells, especially neutrophils or other non-haematopoietic cells to the site of injury or infection and plays an important role in regulation of immune and inflammatory responses.
20)	TARC	Chemokine, sometimes attracts T-regulatory cells allowing for some cancers to evade an immune response, it more often helps the human body fight cancer
21)	SCF	HSC activation and growth in the bone marrow
22)	SDF-1	Strong chemotactic factor for lymphocytes. During embryogenesis, it directs the migration of haematopoietic cells from foetal liver to BM and the formation of large blood vessels. Involved in angiogenesis
23)	MIF	Pro-inflammatory, cell migration, delayed hypersensitivity response
24)	FGF-7	Possesses broad mitogenic and cell survival activities, and is involved in embryonic development, cell growth, morphogenesis, tissue repair, tumour growth and invasion.
Downregulated by both drugs (Fig. 4.2B & Fig. 4.3B)		
25)	IL-8	Pro- inflammation, chemotaxis, angiogenesis
26)	MCP-1	Chemokine, CCL2 is implicated in pathogenesis of several diseases characterized by monocytic infiltrates, such as psoriasis, rheumatoid arthritis and atherosclerosis
27)	Osteoprotegerin	Plays an important role in bone metabolism. Also been shown to bind and inhibit TNF-related apoptosis-inducing ligand which is responsible for inducing apoptosis in tumour, infected and mutated cells
28)	Osteopontin	OPN is an anti-apoptotic factor in many circumstances. OPN blocks the activation-induced cell death of macrophages and T cells as well as fibroblasts and endothelial cells exposed to harmful stimuli.
29)	Oncostatin M	Pro-inflammatory, pleiotropic cytokine that belongs to the IL-6 group. Of these cytokines it most closely resembles LIF
30)	I-309	Small glycoprotein that belongs to the chemokine family. Involved in inflammation through leukocyte recruitment, regulates apoptosis and plays a role in angiogenesis
31)	IGFBP-4	Autocrine and paracrine growth factors, either inhibit or stimulate growth and developmental rates by binding to IGF. Promote several oncogenic processes in solid tumours and multiple cancer signalling pathways. IGFBP family influences cell responses to DNA damage suggesting they are important mediators of p53 actions
32)	IGFBP-3	
33)	FGF-4	Possesses broad mitogenic and cell survival activities, and is involved in a variety of biological processes, including embryonic development, cell growth, morphogenesis, tissue repair, tumour growth and invasion.
34)	IL-12 (p40/p70)	Pro-inflammation, cell differentiation, activates NK cells, promotes Th1 cells
Up or Downregulated by one of either drug (Fig. 4.2C& Fig. 4.3C)		
35)	MIP-3α (CHL - up)	Macrophage Inflammatory Protein 3 alpha is mainly a chemokine
36)	TIMP-1 (CHL - up)	Involved in degradation of the extracellular matrix and may also have an anti-apoptotic function.

Understanding the chemotherapy- induced bystander effect; an evaluation of the role of cytokine storm in an in vitro model of the human bone marrow

37)	NAP-2 (CHL - up)	Chemokine activity
38)	NT-3 (CHL - up)	Activity on certain neurons of the peripheral and central nervous system
39)	IL-1 β (CHL - up)	Pro-inflammation, proliferation, apoptosis, differentiation
40)	Eotaxin (CHL - up)	Chemotaxis mainly in eosinophils. Chemotactic for resting T lymphocytes, basophils and the release of histamine and leukotriene C4 that had been primed with IL-3
41)	Eotaxin-2 (CHL - up)	Known as myeloid progenitor inhibitory factor 2. Chemokine receptor CCR3 to induce chemotaxis in eosinophils
42)	IGF-1 (C - up)	Insulin-like growth factor 1 is a primary mediator of the effects of growth hormone and anti-inflammatory activity
43)	IL-1 α (CHL - up)	Costimulatory molecule. Activation (inflammation). Acute phase reactant
44)	IL-13 (CHL - up)	B-cell growth and differentiation. Inhibits pro-inflammatory cytokine production. Works together with IL-4 associated with allergic inflammation and against parasites.
45)	IL-15 (CHL - up)	Pro-inflammatory, acts on T cells and activated B cells. It causes the proliferation of both B and T cells. It causes NK cell memory and CD8 ⁺ T cell proliferation
46)	FGF-6 (CHL - up)	Possesses broad mitogenic and cell survival activities, and is involved in embryonic development, cell growth, morphogenesis, tissue repair, tumour growth and invasion.
47)	MIP-1 α (CHL - up)	Pro-inflammatory chemokine
48)	Thrombopoietin (CHL - up)	Stimulates the production and differentiation of megakaryocytes
49)	IL-2 (CHL - up)	Pro- & anti-inflammatory, proliferation; enhancement of cytotoxicity, IFN- γ secretion, and antibody production
50)	IGFBP-2 (CHL - up)	Autocrine and paracrine growth factor. These key roles make this candidate promote several key oncogenic processes in solid tumours & multiple cancer signalling pathways.
51)	IL-3 (CHL - up)	Growth, differentiation, and survival of lymphoid and myeloid compartment
52)	Leptin (CHL - up)	Pro-inflammatory. Regulation of adipose tissue mass through central hypothalamus mediated effects.
53)	ENA-78 (MTX - up)	CXCL5 is a small cytokine belonging to the CXC chemokine family

54)	GRO-Alpha (MTX - up)	Chemoattractant for neutrophils and non-haematopoietic cells to the site of injury or infection
Cytokine secretion due to both drug treatments (Fig. 4.4)		
55)	BLC	Chemotactic for B cells belonging to both the B-1 and B-2 subsets
56)	MDC	T cell-mediated allergic airway inflammation and atopic dermatitis, and may play a role in chronic inflammation
57)	Ck β 8-1	Chemokine activity
58)	GDNF	Glial cell line-derived neurotrophic factor; promotes the survival of neurons
59)	Fractalkine	Unique ligand for the chemokine receptor CX3CR1 expressed on monocytes, NK cells and T cells. Mediates migration, adhesion, and proliferation
60)	Flt-3 Ligand	Differentiation and proliferation; synergises with SCF
61)	MIG	Monokine induced by IFN- γ plays a role in inducing chemotaxis, promotes differentiation and multiplication of leukocytes, and causes tissue extravasation
62)	IL-10	Anti-inflammatory, immune suppression; decreases antigen presentation and MHC class II expression of dendritic cells; down- regulates pathogenic Th1, Th2, and Th17 responses
63)	Eotaxin-3	Chemotactic for eosinophils and basophils
64)	IL-16	Pro-inflammatory causes CD4+ T cell chemoattraction
65)	MIP-1 β	Stimulated with bacterial endotoxin or proinflammatory cytokines such as IL-1 β . Induces the release of pro-inflammatory cytokines IL-1, IL-6 and TNF- α .
Negative absorbances in at least one membrane		
66)	IL-4 (2/3)	Anti-inflammatory, T-cell and B-cell proliferation, B-cell differentiation Differentiation into a TH 2 cell
67)	IL-7 (2/3)	Pro-inflammatory, acts on pre-B and T cells. It causes B-cell and T-cell proliferation
68)	TNF- β (2/3)	Pro- & anti-inflammatory, inhibition of pro-inflammatory cytokine production
69)	EGF (2/3)	Pro-inflammatory, stimulates the proliferation of fibroblasts and epithelial cells
70)	Angiogenin (2/3)	Anti-apoptosis, key protein implicated in angiogenesis in normal and tumour growth
71)	PDGF-BB (2/3)	Role in blood vessel formation and growth. Mitogenesis and proliferation of mesenchymal cells
72)	BDNF (2/3)	Acts on certain neurons of the CNS and the peripheral nervous system, supports survival of neurons, and growth and differentiation of new neurons and synapses.
73)	HGF (2/3)	Acts as a multi-functional cytokine on epithelial origin cells. Stimulates mitogenesis, cell motility, and has a role in angiogenesis and tissue regeneration
74)	IGFBP-1 (2/3)	Promotes several key oncogenic processes in solid tumours and multiple cancer signalling pathways.

75)	LIGHT (1/3)	Costimulatory; promotes cytotoxic T lymphocytes activity
76)	NT-4 (2/3)	Activity on peripheral and CNS
77)	PARC (2/3)	Pulmonary and activation-regulated chemokine effects on the adaptive immune system
78)	PIGF (2/3)	Promotes endothelial cell growth, placental vasculogenesis and development
79)	TGF- β 2 (1/3)	Anti-inflammatory, TGF- β 1 is a multifunctional mediator of both homeostasis and injury responses controlling both proliferation and apoptosis in many cell types
80)	TGF- β 3 (2/3)	

CHL – up, indicates the cytokines which were up-regulated due to chlorambucil but down-regulated due to mitoxantrone treatments. MTX – up, indicates the cytokines which were up-regulated due to mitoxantrone but down-regulated due to chlorambucil treatments. (2/3), indicates the cytokines which were positive at baseline in at least two membranes out of three repeats and (1/3), is positive at baseline in at least one membrane out of three repeats.

The functions and information in the table 4.1 are from Danzer *et al.*, 1994; Barcellos-Hoff *et al.*, 2005; Lazutka, 1996; Flores-Figueroa *et al.*, 2002; Chua *et al.*, 2015; Neta & Oppenheim, 1991; Langowski *et al.*, 2010; Pixley & Stanley, 2010; Zhang & An, 2007; Markey & Hill, 2017; Kikuchi *et al.*, 1996; Riegler & Jones, 2019; Shimabukuro-Vornhagen *et al.*, 2018; Yildizhan & Kaynar, 2018; Winkler *et al.*, 1999; Morgan *et al.*, 2010; Melenhorst *et al.*, 2012; Gallet *et al.*, 2011; Tisoncik *et al.*, 2012; Clark & Vissel, 2017; Fathi *et al.*, 2019; Robb, 2007; Chen *et al.*, 2021; Cheleuitte *et al.*, 1998; Wang *et al.*, 2022; Kleiner *et al.*, 2013; You *et al.*, 2012; Lee *et al.*, 2008; Kim *et al.*, 2011; Khan & Ali, 2014; Robak *et al.*, 1998; Fernandez-Real *et al.*, 2001; Zou *et al.*, 2018; Noori *et al.*, 2017; Arican *et al.*, 2005; Bhattacharya *et al.*, 2015; Kawakami *et al.*, 1990; Matsubara *et al.*, 1999; Wakefield *et al.*, 1995.

4.3.2 Array validation ELISA

To validate the cytokine array data and to support the candidate cytokine selection, in-house developed ELISAs were performed. Important to note, is that subsequent to performing the array data at CHL 40 μ M (mouse plasma level from Ganta *et al.* (2008); Ganta *et al.* (2010)), literature was discovered from Hong *et al.* (2010) which suggested that the human plasma level of CHL is around 4 μ M. Thus, cytokines were measured at both concentrations to assess whether the 10-fold lower dose of CHL would have significantly altered the data presented with the cytokine array.

4.3.2.1 TNF- α expression by TK6 and HS-5

Figure 4.5 illustrates TNF- α expression from both untreated TK6 and HS-5, as well as HS-5 cells following treatment with CHL (4 and 40 μ M) and MTX (1.12 μ M) over 5 days. The untreated TK6 and HS-5 cell lines exhibited consistently low levels of TNF- α expression over a 5-day period. The range of TNF- α expression in both untreated TK6 and HS-5 cells fluctuated between 2-6 pg/ml throughout the observed timeframe, with no discernible significant differences in TNF- α expression between the two cell lines during this specified period.

As might be expected, 4 μ M CHL (human relevant) treated HS-5 showed lower TNF- α secretion compared to the CHL 40 μ M treatment (mouse relevant). However, TNF- α was below the limit of detection at 24 hours of 4 μ M CHL treatment. HS-5 treated with 40 μ M CHL exhibited increasing TNF- α expression to a peak at 96 hours followed by a reduction at 120 hours. MTX treated HS-5 showed a large increase of TNF- α when comparing 48 to 72 hours, however large error bars at 72 hours meant this was not significantly different. TNF- α secretion then slightly decreased until the 5th day. Nevertheless, the highest secretion of TNF- α was at 120 hours, 96 hours and 72 hours for 4 μ M, 40 μ M CHL and MTX treatment respectively, which is in line with previous unpublished data from the supervisor, and the timelines used for the array.

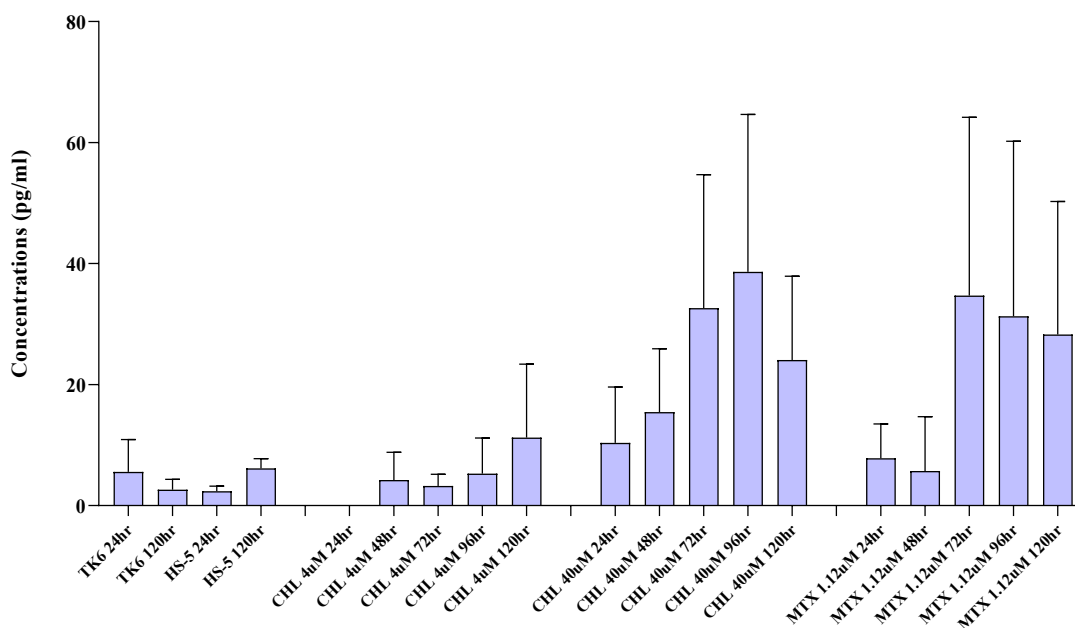


Figure 4. 5. ELISA analysis of TNF- α from TK6 and HS-5 cells. Untreated TK6 and HS-5 cells were cultured, and media samples were collected to detect TNF- α expression after 24 hours and 120 hours post-seeding. HS-5 cells were exposed to either CHL or MTX and the supernatant collected every 24 hours after treatment up to 120 hours post-exposure. For comparison, HS-5 were treated with CHL at 4 μ M (equivalent to human plasma levels) and 40 μ M (equivalent to mouse plasma levels) in the same plate. MTX was used at 1.12 μ M (equivalent to human plasma concentrations). Data is presented as mean \pm SD (n=3).

4.3.2.2 TGF- β 1 expression by TK6 and HS-5

Figure 4.6 exhibits the TGF- β 1 expression by TK6 and HS-5, with and without chemotherapy treatments; important to note is that in using an ELISA kit from Thermo Fisher, it was only possible to perform one repeat of the samples. Untreated TK6 and HS-5 stably expressed about 350 - 450 pg/ml of TGF- β 1 over 5 days. TGF- β 1 levels following 4 μ M CHL showed considerably lower expression levels (range 1400–1900 pg/ml) compared to 40 μ M CHL treated samples (range 2000-2900 pg/ml). However, both CHL doses showed the highest TGF- β 1 expression at 72 hours following treatment and reduced to stable lower secretion at 96 and 120 hours. These periods aligned with the timeline of array performed in section 4.2.2. MTX treatment showed HS-5 to have irregular TGF- β 1 expression over the observed period. At 24 and 72 hours, HS-5 showed highest secretion (~2300 pg/ml) but dropped to around 1700 pg/ml

at 48, 96 and 120 hours. With the exception of the samples from MTX at 24 and 72 hours, TGF- β 1 secretion showed similar levels of secretion at human relevant concentrations (CHL at 4 μ M and MTX at 1.12 μ M), whereas secretion was higher at mouse levels for CHL (40 μ M), so the data for TGF- β 1 from the array, needs to be treated with caution.

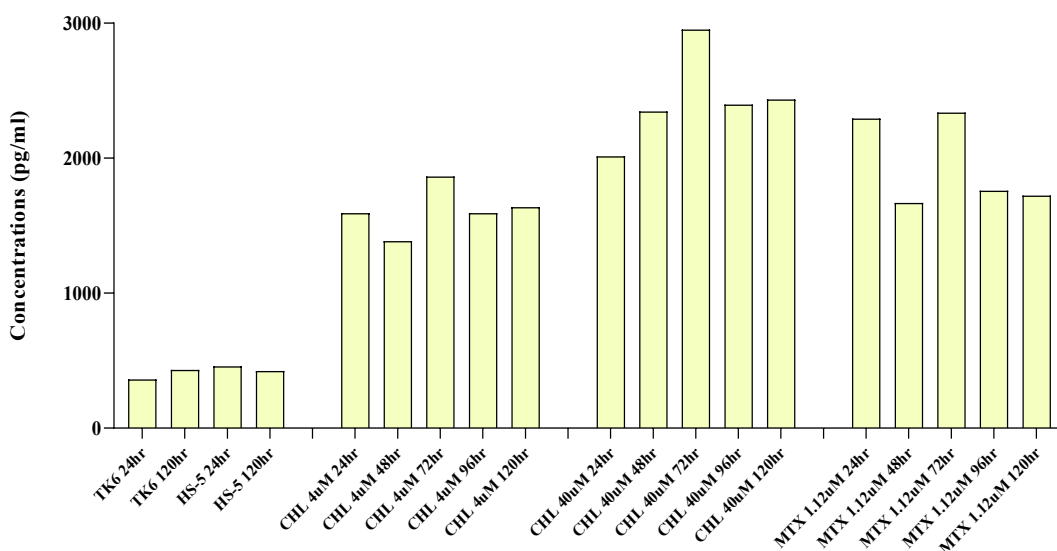


Figure 4. 6. ELISA analysis of TGF- β 1 from TK6 and HS-5 cells. TK6 and HS-5 cells were seeded, and supernatant was collected to detect TGF- β 1 expression using an ELISA kit (Thermo Fisher). HS-5 cells were exposed to either CHL or MTX and the supernatant was collected every 24 hours after treatment up to 5 days post-exposure. For comparison, HS-5 were treated with CHL at 4 μ M and 40 μ M in the same plate. MTX was used at 1.12 μ M. Data is presented as mean \pm SD (n=1).

4.3.2.3 IL-6 expression by TK6 and HS-5

The IL-6 expression profiles of untreated TK6 and HS-5 cells, with and without drug exposure, are presented in figure 4.7. Untreated TK6 cells demonstrated markedly low IL-6 expression, particularly when compared with the expression levels observed in untreated HS-5 cells. The IL-6 expression between 24- and 120-hours in untreated TK6 cells was around 120 pg/ml, whereas untreated HS-5 cells exhibited levels around 2600 pg/ml. Notably, a significant difference (** $p \leq 0.01$) in IL-6 expression between untreated TK6 and HS-5 cells was evident at the 120-hour timepoint. The quantitative ELISA assay enabled the detection of significant differences in IL-6 expression at 72 hours from HS-5 cells treated with CHL (40 μ M; $p \leq$

0.0001) and MTX ($p \leq 0.01$). Even though it was not quantifiable through array analysis, this reflects the highest IL-6 absolute expression by both drug treatments (Fig. 4.2).

Remarkably, HS-5 cells treated with a lower dose of CHL (4 μM) exhibited higher IL-6 expression (range 5800–9400 pg/ml) compared to cells exposed to a tenfold greater dosage of CHL (40 μM) (range 3200–3700 pg/ml). This difference was statistically significant ($****p \leq 0.0001$) at the 72-hour timepoint. Notably, HS-5 cells treated with MTX displayed a distinct pattern characterised by an increase in IL-6 levels at 48 hours, followed by a subsequent decline over time. Given that IL-6 demonstrated the highest absolute secretion in the array data for both drug treatments, the chosen 48- and 72-hour timepoints for array analysis appears optimal for capturing the peak IL-6 secretion following MTX and CHL treatment respectively.

Despite the lower IL-6 level in HS-5 cells treated with CHL (40 μM) compared to the 4 μM treatment, this might not impact the cytokine arrangement in the array results, as IL-6 remained the highest secretor among the selected candidate cytokines.

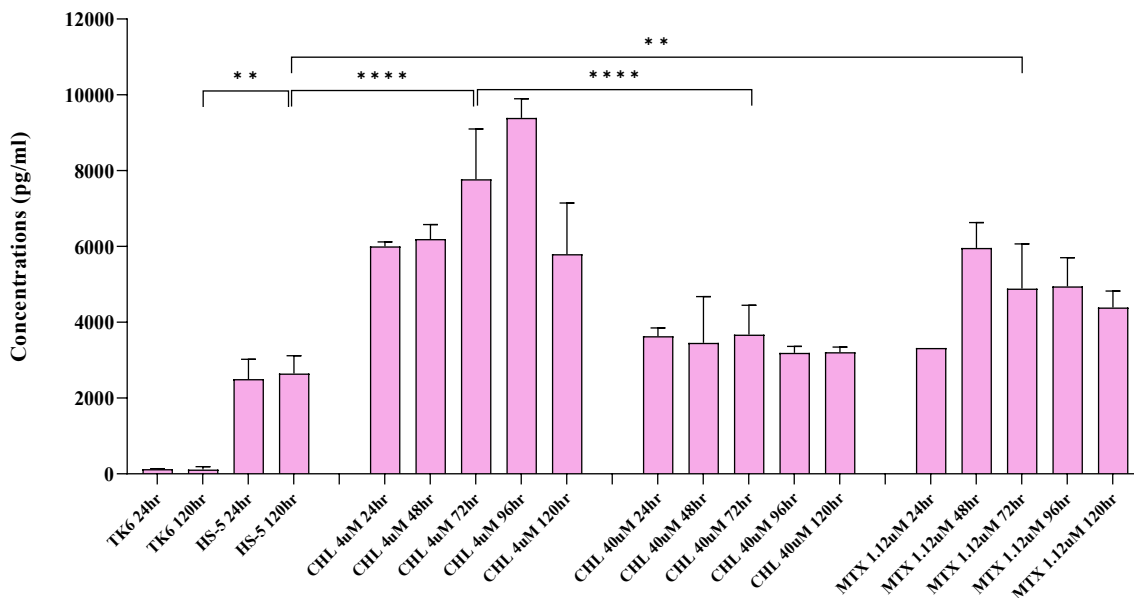


Figure 4. 7. ELISA analysis of IL-6 from TK6 and HS-5 cells. TK6 and HS-5 cells were initially seeded, and supernatants were collected at 24-hour and 120-hour timepoints from untreated culture flasks. In the case of HS-5 cells, exposure to CHL and MTX occurred separately, with supernatants collected every 24 hours post-treatment up to 120 hours. To facilitate comparison, HS-5 cells were treated with CHL at concentrations of 4 μM (reflective of human plasma levels) and 40 μM (equivalent to mouse plasma levels) within the same plate. MTX was administered at 1.12 μM , representing concentrations found in human plasma. The presented data is expressed as mean \pm SD ($n=3$), and statistical significance is denoted by $**p \leq 0.01$ and $****p \leq 0.0001$, as determined by two-way ANOVA, Tukey’s multiple comparisons test.

4.3.2.4 GM-CSF expression by TK6 and HS-5

Figure 4.8 depicts the expression patterns of GM-CSF following treatment. When comparing the expression of untreated HS-5 and TK6 cells, no significant differences were observed, although there was a slight change in untreated HS-5 GM-CSF expression (~350 pg/ml) and also untreated TK6 expression, (80 pg/ml) at the 120-hour time point in comparison to secretion at 24 hours. The overall profile of CHL 4 μ M treated samples reveals a consistent GM-CSF expression over the 5-day period, peaking at 72 to 96 hours (~500 pg/ml) and followed by a reduction at 120 hours. In contrast, the 40 μ M-treated samples exhibit a gradual increase over time, reaching its peak at 96 hours (600 pg/ml). However, the two CHL treated samples did not show a significant difference from each other at any time point. Consequently, the utilisation of 40 μ M CHL during array experiments is not expected to substantially impact GM-CSF expression or the arrangement of data in cytokine array graphs. Moreover, HS-5 cells treated with MTX also maintain steady levels of GM-CSF across time, with the highest expression occurring at 72 hours (500 pg/ml). Despite the similar secretion levels of GM-CSF for both

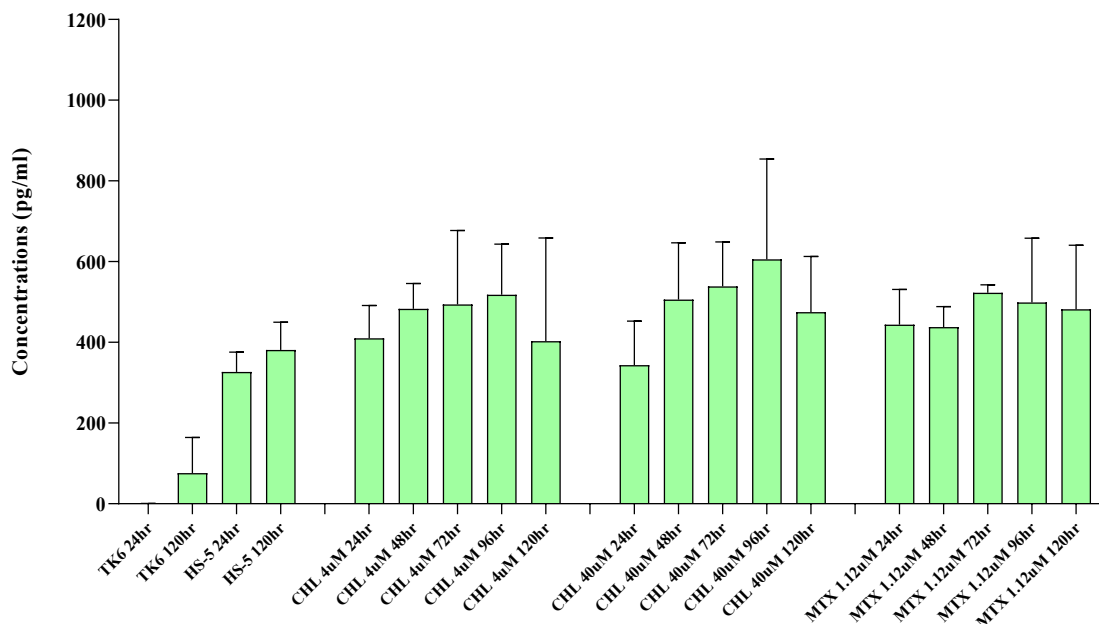


Figure 4. 8. ELISA analysis of GM-CSF from TK6 and HS-5 cells. Supernatants from untreated TK6 and HS-5 cells were collected at 24-hour and 120-hour intervals following seeding at their optimal density. HS-5 cells were exposed to CHL at concentrations of 4 μ M (reflective of human plasma levels) and 40 μ M (equivalent to mouse plasma levels) in the same plate, while MTX was administered at 1.12 μ M (equivalent to human plasma concentrations). Subsequently, supernatants from each of these cultures were collected at 24-hour intervals up to 120 hours. The presented data is expressed as mean \pm SD (n=3).

CHL and MTX at 72 hours, the data aligns with the expression levels obtained from array data analysis.

4.3.2.5 G-CSF expression by TK6 and HS-5

Figure 4.9 shows the G-CSF expression in HS-5 cells following two different chemotherapies and in untreated HS-5 and TK6 cells. Due to the use of the ELISA kit from Thermo Fisher, only two repeats of the ELISA plates were feasible. In contrast to every other ELISA detection, G-CSF maintains a consistent expression pattern throughout the course of therapy. Notably, in comparison to untreated samples, there is minimal response to both chemotherapies. TK6 cells exhibit robust G-CSF expression at both time periods (2300-2700 pg/ml), a finding particularly intriguing as it closely resembles the G-CSF expression by untreated HS-5 cells (2550-2750 pg/ml). In the context of CHL and MTX treated cells compared to untreated HS-5, there is a slightly elevated expression of IL-6, although this difference is not statistically significant. The highest G-CSF secretion is observed at 96 hours for CHL (4 μ M and 40 μ M) but at 72 hours for MTX-treated cells. Surprisingly, there is no discernible distinction between HS-5 cells treated with CHL at 4 μ M or 40 μ M at any time point. Thus, the variation in dosage is not anticipated to induce significant changes in G-CSF representation in the array data.

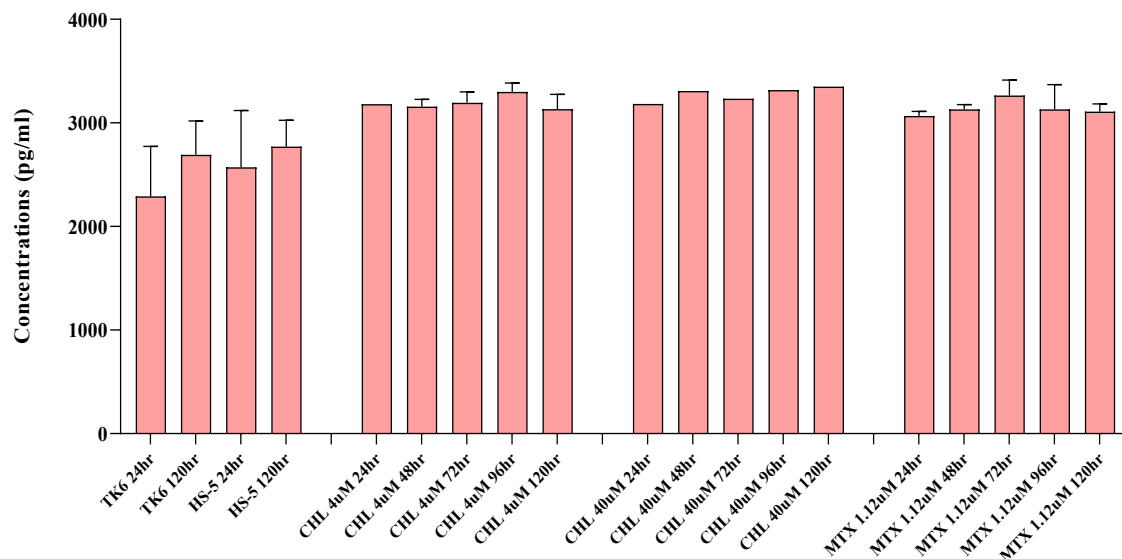


Figure 4. 9. ELISA analysis of G-CSF from TK6 and HS-5 cells. Following cell seeding, supernatants from untreated samples were collected at 24- and 120-hour time points to assess G-CSF expression. HS-5 cells were exposed to CHL at concentrations of 4 μ M (reflective of human plasma levels) and 1.12 μ M of MTX (equivalent to human plasma concentrations), while CHL at 40 μ M (equivalent to mouse plasma levels) was also administered separately to HS-5 cells in the same plate for comparative purposes. Supernatants from all treated samples were collected every 24 hours post-treatment up to 120 hours, and quantification was conducted using an ELISA kit from Thermo Fisher. The presented data is expressed as mean \pm SD (n=2).

4.4 Discussion

Human BM stromal cells secrete a range of cytokines, such as IL-6, GM-CSF, and IL-1 (Cheleuitte *et al.*, 1998). These cytokines play a crucial role in influencing the development of immature HSC and ensuring the overall homeostasis of the BM. Given the significance of maintaining a balance between pro- and anti-inflammatory mechanisms for immune homeostasis, the absence or dysregulation of one or more of these regulatory mechanisms could potentially lead to outcomes contributing to a cytokine storm (Tisoncik *et al.*, 2012).

Following chemotherapy treatment and conditioning therapy for HSCT it is observed that there is a 'cytokine storm' in response to the drugs (Döring *et al.*, 2015; Henden & Hill, 2015; Dickinson & Charron, 2005). Following HCST, Melenhorst *et al.* (2012) identified two cytokine storms; the first storm involved predominantly haematopoietic and lymphopoietic homeostatic cytokines, whereas the second involved inflammatory and anti-inflammatory cytokines/chemokines. A publication on GvHD in 1993 was the first to describe the concept of a "cytokine storm" which conjures up vivid pictures of an immune system lacking regulation and an uncontrolled inflammatory reaction. The idea of an excessive or uncontrolled release of proinflammatory cytokines is generally understood, but a precise description of a cytokine storm is lacking (Markey & Hill, 2017; Tisoncik *et al.*, 2012).

As recorded by many studies TNF- α , IFN- γ , IL-1 β , 2, 4, 6, 8, are examples of some key cytokines involved in the cytokine storm after a surge of the immune system following either toxic insult or transplantation (Döring *et al.*, 2015; Henden & Hill, 2015; Dickinson & Charron, 2005). As shown in the table in appendix II, the levels of these cytokines can become extremely high during the storm. In brief, You *et al.* (2012) found cytokine storm in six volunteers following mAb infusion and IL-6 (4000 pg/ml) and TNF- α (4500 pg/ml) peaked in first 24 hours of infusion. Winkler *et al.* (1999) revealed the serum cytokines which peaked vs baseline were TNF- α (500 vs 20 pg/ml) and IL-6 (280-25 pg/m) following anti-CD 20 mAb infusion. Another study Morgan *et al.* (2010) discovered that from undetectable levels before the infusion of humanised mAb, TNF- α reached 380 pg/ml, GM-CSF at 10,191 pg/ml, IL-6 at 34,467 pg/ml, and IFN- γ at 456 pg/ml. Peri- and post-myeloablative allogeneic-HSCT by Melenhorst *et al.* (2012) found dynamic changes in the expression levels of IL-6 (1.72-3524 pg/ml), G-CSF (0.12-38310 pg/ml), TNF- α (1.26–186.6 pg/ml) and IFN γ (0.34–1677 pg/ml). However, quantitative G-CSF ELISA analysis by Kawakami *et al.* (1990) found in the acute

stage of infection, a G-CSF level of 731.8 pg/ml, which could increase to 3199 pg/ml (Kikuchi *et al.*, 1996). Despite being a well-known pro-inflammatory cytokine, some studies indicate that G-CSF may stimulate tumour growth in mouse models when it interacts with host factors (TNF- α).

Clinical trials have shown that BE may occur through the immune system, such as T cells and different cytokines (Wang *et al.*, 2018). There is evidence for cytokines inducing a BE following radiation exposure (section 1.6.2.1 and 1.6.3.1) (Song *et al.*, 2016; Peled *et al.*, 1996)

In response to radiation, BM fibroblasts and macrophages continuously secrete cytokines (IL-1, IL-6, TNF- α and TGF- β 1), chemokines, ROS and RNS which promote survival and proliferation of AML cells *in vitro* (Barcellos-Hoff *et al.*, 2005; Peled *et al.*, 1996). These observations suggest that cytokines may have distinct way of playing a role in genotoxic BE from irradiation, but the role of cytokines in CIBE and the influence of such high levels produced during cytokine storm post-chemotherapy have not been previously studied. Some studies have shown that TGF- β , GM-CSF, IL-4, and IL-13 activate downstream signalling pathways and increase the expression of cytokines/growth factors, resulting in high levels of ROS by the co-cultured HSC in response to bystander signal (Sica & Bronte, 2007; Barcellos-Hoff *et al.*, 2005).

Thus, this study hypothesised that cytokines expressed at ‘storm’ levels from the BM could be a contributing factor to the development of DCL in donated cells that were unexposed to chemotherapeutics. The patterns of cytokine production by the culture may provide insight into the nature of cytokine storm and the relationship between the haematopoietic (TK6) and BM- MSC (HS-5) populations. Therefore, as a possible mechanism of CIBE, this research compared the profile of expressed cytokines in a cell line model of the human BM (HS-5) with and without chemotherapy exposure.

The alkylating agent CHL (nitrogen mustard) (Kondo *et al.*, 2010), and the topoisomerase II inhibitor MTX (anthracenedione) (Parker *et al.*, 2004) were chosen as ‘model’ drugs as these are both implicated in TRL (Georg & Weber, 2015; Binaschi *et al.*, 1995; Leone *et al.*, 1999). The cytokine array utilised in this study covers documented BM-expressed myeloid-focused cytokines/ storm from the literature, to determine candidate cytokines possibly playing a role in CIBE. As a model of the BM, HS-5 have been shown to ably support TK6 cells (Asurappulige *et al.*, 2023; Vernon *et al.*, 2022). Additionally, Fathi *et al.* (2019) highlights the

special interest of MSC due their potential clinical use in cell-based therapy in cancer treatment. A multitude of growth factors and cytokines secreted from these cells are known to provide multifunctional properties, but details of their role in cancers are yet to be absolutely demonstrated. (Döring *et al.*, 2015; Henden, & Hill, 2015; Dickinson & Charron, 2005; Cheleuitte *et al.*, 1998; Leuning *et al.*, 2018; Shi *et al.*, 2018)

All normalisations of the array data were carried out as described in section 2.2.2 before proceeding with the analysis of the results. For this analysis, FGF-7 was chosen as an arbitrary threshold for the limit of detection of the array because it was the cytokine with the lowest levels of secretion consistently found on all three repeat membranes. This cytokine was used as a point of comparison in the graphs to see the expression changes after drug exposure, and also allowed for the assignment of ‘presence’ versus ‘absence’ of the cytokines.

For the first time this study established a BM-MSK cytokine profile for the HS-5 cell line. There were 54 cytokines expressed by untreated HS-5 out of 80 candidate cytokines on the array. The information obtained for the cytokines released by untreated cells in array investigation (Fig. 4.1) is consistent with the literature and supports the use of HS-5 to reflect the mesenchymal characteristics of the BM (Park *et al.*, 2009). High baseline expression of IL-6 and GM-CSF suggested their role in haematopoiesis and supporting myeloid progenitors’ differentiation in BM-MSK. Fathi *et al.* (2019) detected only two cytokines (TIMP-1 and CINC-1) out of 24 candidates when BM-MSKs were co-cultured with the CML cell line (K562) suggesting that co-culture interaction has an affect towards the cytokine profile secreted by BM-MSK. However, a cytokine study suggested that IL-1 β , IL-5, IL-15, IL-1 α , IL-3, IL-12(p40), IFN- α , LIF, MCP-3, β -NGF, and TNF- β were not detected in baseline serum of any analysed age group, either because they are not produced at baseline, or they were lower than the limit of detection. Most of the cytokines measured by Kleiner *et al.* (2013) were not significant amongst the groups but TNF- α , IL-6, IFN- γ , PDGF-BB, IL-4, and IL-13 were upregulated in children between 7 to 17 years of age. Nevertheless, except for TNF- β , many of cytokines from the above list were positive in this study using *in vitro* HS-5.

After defining the HS-5 baseline cytokine profile, the data were evaluated as absolute and fold change because it was speculated that to create a physiologically relevant bystander effect, that candidate molecules should be present or upregulated following drug exposure.

Out of 54 baseline cytokines (absolute levels; figure 4.2), 24 were upregulated (Fig. 4.2A) whereas 10 were downregulated (Fig. 4.2B) by both chemotherapy drugs. The remaining 20 cytokines were up- and/or down-regulated separately by the two drugs (Fig. 4.2C). IL-6, TNF- α , GM-CSF, TIMP-2 and MCP-2 were the top five cytokines for absolute change in drug treated vs untreated HS-5 (Fig. 4.2A), but only IL-6, TNF- α and GM-CSF were the highest common cytokines for both drugs during baseline as well as after treatments. The fold change analysis (Fig. 4.3) was plotted to identify those cytokines which may have been more highly upregulated as a result of drug exposure. Figure 4.3A showed increased fold change due to both drugs including SCF, SDF-1, MIF, TGF- β 1, G-CSF and others, whereas figure 4.3B indicates the cytokines which were decreased by both drugs. Figure 4.3C shows cytokines which were upregulated by one drug, whilst downregulated by the other.

For this study, it was important to focus on candidates which relate to post-HSCT malignancies, in particular DCL. Of interest, both TRL and DCL predominantly follow the myeloid lineage, mainly presenting as AML and myelodysplasia (Suárez-González *et al.*, 2018; Guillermo *et al.*, 2007). Because cytokines and their cognate receptors are central to directing stem cells to develop into specific lineages, it was speculated that cytokines involved in myeloid lineage development would play a role in DCL aetiology and support the development as an AML. Therefore, cytokines associated with the myeloid progenitor lineage were considered during this analysis, including IL-1, 3, 6, GM-CSF and SCF. Notably, HS-5 cells had the largest fold change in SCF (Fig. 4.3A) at 5.2- and 2.6-fold after CHL and MTX treatment respectively. SCF is an early-acting cytokine in the propagation of haematopoiesis (Vladislav *et al.*, 2009) and demonstrated the essential role in human myeloid development using *in vivo* study by Takagi *et al.* (2012). IL-6 and GM-CSF also produced relatively high amounts of expression (untreated Fig. 4.1 and treated Fig. 4.2A), which justify the choice of HS-5 for these experiments. According to Chen *et al.* (2021), disruption of the BM microenvironment contributes to the development of a number of myeloid malignancies. Myeloid malignant cells can stimulate MSC to overproduce functionally altered osteoblastic lineage cells and accumulate in the BM cavity as inflammatory myelofibrotic cells, which favours the proliferation of leukaemic stem cells. Abnormally proliferating cells might stimulate normal haematopoietic cells and stromal cells in the BM niche to secrete more proinflammatory cytokines, which further aggravates the inflammation inside the niche (Chen *et al.*, 2021).

The data presented here, suggests IL-6 to be a major candidate expressed by MSC in both baseline cytokine secretion as well as following both drug treatments. Recently, Markey & Hill (2017) confirmed that IL-6 is the major cytokine detectable in patient plasma early after HSCT and that it appears to play a dominant role in conditioning-related pathology. According to Melenhorst *et al.* (2012), cytokines including IL-6 and G-CSF reached a peak within 1 week after transplantation. Shimabukuro-Vornhagen *et al.* (2018) also supports a key role for IL-6 in cytokine storm pathophysiology as highly elevated IL-6 was detected in every patient with cytokine release syndrome. It could be that as IL-6 has both anti- and pro-inflammatory properties, it may be an essential mediator in the signalling cascade of cytokine storm (Riegler & Jones, 2019). The current study supports increased IL-6 secretion followed both drug treatments, with slightly higher expression shown in CHL treatment compared to MTX. However, IL-6 demonstrates an almost 1.5-fold increase follow exposure to both drugs. Results of post-HSCT cytokine response by DiCarlo *et al.* (2014) showed high levels of IL-6 in children with HCST-complications. IL-6 produced by MSC can affect the HSC through paracrine or juxtacrine interactions and has a role in regulating human myeloma cell growth in the cultures (Cheleuitte *et al.*, 1998).

Out of key inflammatory cytokine storm candidates, IL-6 holds significance as its concentrations are often utilised to measure the intensity of systemic cytokine responses, given that integrated signals from TNF- α and IL-1 β can stimulate IL-6 production (Tisoncik *et al.*, 2012). However, in the current research findings, it is noteworthy that while IL-1 β was upregulated by only one drug (CHL), the increase was approximately 1.5-fold. Conversely, MTX resulted in a downregulation of IL-1 β , showing a decrease of 1.3-fold (Fig. 4.2C and 4.3C). Another interesting finding of Flores-Figueroa *et al.* (2002) was the demonstration that stromal cell layers from AML patients produce 2-fold higher levels of IL-6 and 22-fold higher levels of TNF- α . Indeed, the prognosis for AML can be predicted by measuring patient cytokine levels, with high IL-6 and TNF- α , alongside low IL-10, indicating a poorer outcome (Flores-Figueroa *et al.*, 2002).

TNF- α is another pivotal pro-inflammatory cytokine which is responsible for many different signalling processes including cellular proliferation, survival, differentiation or apoptosis in the cell (Wang *et al.*, 2022). This is the best known and most intensely studied proinflammatory cytokine which plays a prominent role in the cytokine storm literature associated with many chronic inflammatory and autoimmune diseases (Tisoncik *et al.*, 2012). The tumorigenesis role

of TNF- α was identified firstly in 1975 as a cytotoxic serum factor capable of inducing tumour regression in mice (Tisoncik *et al.*, 2012). The current research showed that TNF- α is the second highest cytokine expressed for both drugs (Fig. 4.2A) demonstrating a 2-fold increase with CHL and 1.5-fold increase with MTX. The importance of TNF- α following cancer therapy is also supported by Markey & Hill, (2017) who found that higher TNF- α levels secreted within recipients following conditioning therapy correlated with severe GvHD conditions. Crucially, the elevated TNF- α levels can persist for over one year after irradiation (Gallet *et al.*, 2011). This poses a considerable risk, as prolonged elevation of TNF- α may lead to substantial damage to the recipient. While the functions of TNF- α in inflammation are well-characterised, its roles in haematopoiesis and HSC homeostasis are inadequately described and remain controversial. However, a study conducted by Wang *et al.* (2022) unveiled that TNF- α plays a role in promoting HSC survival and myeloid differentiation.

Dysregulation of TNF- α production has been related to direct inhibition of growth and induction of apoptosis of HSCs, as well as indirectly changing the BM microenvironment which is critical for HSC homeostasis. After long-term exposure, clonal evolution may eventually progress into myeloid leukaemia. TNF- α induced accumulation of ROS and oxidative DNA damage leads to premature senescence in HSCs and progenitor cells of mice (Wang *et al.*, 2022). Data from the literature supports that TNF- α has a genotoxic capacity via immune reactivity, resulting in chromosome aberrations, MN and SCE in cultures (Lazutka, 1996; Sica & Bronte, 2007). Furthermore, TNF- α treated mice showed chromosomal aberrations together with impaired oxidative DNA damage repair pathway. TNF- α has also been associated with systemic genotoxicity in mice *in vivo* which was potentiated by IL-1 β and decreased by IL-10. These findings may suggest a genotoxic role of TNF- α in the cytokine storm following HSCT. Therefore, it needs to be taken into consideration that all these inflammatory signals can also lead to DNA damage, promoting the depletion of donor HSCs and manifesting as secondary malignancy, and potentially as DCL. Indeed, syndromes like aplastic anaemia and Fanconi Anaemia have also been found with overexpressed TNF- α and IFN- γ (Wang *et al.*, 2022). IFN- γ signalling through STAT1 activates T cells to produce other proinflammatory cytokines, particularly TNF- α (Markey & Hill, 2017). Conversely, a contrasting study by Melenhorst *et al.* (2012) researching conditioning therapy and induction of inflammatory cytokines detected no change of TNF- α levels and decreased IFN- γ during conditioning.

IFN- γ is recognized for its role as an antiproliferative and apoptotic mediator across various cell types (Wang *et al.*, 2022). Besides its protective effects, Riegler & Jones (2019) found IL-6 and IFN- γ significantly increased in patients with severe cytokine release syndrome. Kleiner *et al.* (2013) indicated IFN- γ was around 300 pg/ml in healthy individuals but according to You *et al.* (2012) it reached over 10-fold the normal range. These findings support observations in this study regarding IFN- γ , where both drugs (CHL: 0.1 and MTX: 0.06) demonstrated a modest increase in absolute changes. However, the fold change was notably higher, with CHL at 2.34-fold and at 1.42-fold increases. IFN- γ can induce activation of tissue, which can then produce many proinflammatory cytokines such as IL-6, TNF- α , and IL-10 (Shimabukuro-Vornhagen *et al.*, 2018). Danzer *et al.* (1994) showed that release of IL-6 and TNF- α could be completely blocked by addition of anti-IFN- γ antibody in mixed lymphocyte culture. Coates *et al.* (2008) suggest that BM derived macrophages' cytokine (IFN- γ) expression is an indirect (bystander) effect of tissue response after radiation. Moreover, while the induction of DNA damage during interphase can activate the cGAS-STING inflammatory response, releasing more IFNs (Fenech *et al.*, 2020; Decout *et al.*, 2021), which might be speculated to exacerbate the problem, IFN- α has been shown to reduce MN induction in gamma-irradiated *in vivo* mouse models (Fomenko *et al.*, 1997). Despite not focusing on IFN- γ as a primary candidate in this study, it is still a significant cytokine that plays a crucial role in inflammation, cytokine storm, HSCT complication and DNA damage.

Even though GM-CSF and G-CSF are mainly associated with HSC proliferation, differentiation and with a particular capacity to mobilise stem cells, there is evidence that CSF may be part of a mutually dependent proinflammatory cytokine network that includes TNF- α and IL-1 β (Tisoncik *et al.*, 2012). The third highest in absolute data (Fig. 4.2A) was GM-CSF with 1.4-fold differences for both CHL and MTX.

G-CSF is the 5th highest fold difference common to both drugs, showing a 4.36 higher fold change with CHL, whereas for MTX treatment it was 2.22-fold. G-CSF is a glycoprotein that stimulates the BM to produce granulocytes and stem cells and releases them into the bloodstream. G-CSF driven granulocyte expansion leads to the secretion of proteases, which then disrupt adhesion molecules and chemokine receptors (VCAM-1, CXCL12) that control maintenance of stem cells within the BM (Markey & Hill, 2017). By this mechanism, high dose G-CSF results in stem cell mobilisation from the BM into the peripheral blood. BM damaged

by conditioning therapy can be restored by injecting G-CSF to reduce the risk of infection and stimulate the production of granulocytes.

The fourth highest fold change expression in this study was TGF- β 1, which is one isoform of a multifunctional cytokine comprising 5 different isoforms (TGF- β 1 to - β 5) (Zhang & An, 2007). TGF- β controls cell growth, proliferation, differentiation and apoptosis in many cell types during haematopoiesis (Barcellos-Hoff *et al.*, 2005; Gallet *et al.*, 2011) and TGF- β 1 is essential for rapid p53-mediated apoptosis and inhibition of proliferation (Ewan *et al.*, 2002). However, this has been seen to contribute to haematopoietic suppression in Fanconi Anaemia and MDS (Wang *et al.*, 2022). TGF- β operates synergistically with TGF- α in inducing cellular transformation. TGF- β 1 is rapidly activated after oxidative stress following ionising irradiation but its specific role in cellular responses to DNA damage remains unidentified.

Gallet *et al.* (2011) found high levels of TGF- β 1, at 2.2- and 2.7-fold following 6 weeks and 6 months of irradiation; at one-year TGF- β 1 was still significantly increased but to a lesser extent. Indeed, some authors found an induction of TGF- β 1 during the first 24 hours after irradiation. Given the well-established understanding of cytokine storms and BE following irradiation therapy (section 1.6.2.1 and 1.6.3.1), it is plausible to speculate that the elevated levels of TGF- β 1 may also play a role in cytokine storm and BE induction following chemotherapy. However, a contrasting study by Yamada *et al.* (2001) suggested a chemoprotective mechanism, as TGF- β 1-deficient cell lines exhibited increased sensitivity to cell killing by alkylating agents due to the lack of DNA repair enzyme expression. With these interesting pieces of evidence about TGF- β 1 supporting the higher fold changes of CHL at 4.5-fold and MTX at 2.1-fold higher seen here, this suggests that TGF- β 1 could be an important candidate for further exploration.

It was interesting to note that all the cytokines that were not discovered at baseline were detected after drug administration. Interestingly, the data from this study and published in Asurappulige *et al.* (2023) is the first to report that 11 cytokines which were undetectable in untreated HS-5 cultured media (baseline) were detected in both CHL and MTX treated HS-5 supernatant (Fig. 4.4) including BLC, MDC, Ck β 8-1, GDNF, Fractalkine, Flt-3 ligand, MIG, IL-10, Eotaxin-3, IL-16 and MIP-1 β . However, overall, the picture of cytokine secretion seems to promote a pro-inflammatory and chemotactic environment within the model used in this study, which aligns with the clinically observed cytokine storm. This suggests an intense BM inflammatory process in myeloproliferative neoplasm patients; indeed Chen *et al.* (2021) found

significantly higher G-CSF, I-309, I-1b, IL-1ra, IL-12p40, IL-15, IL-16, M-CSF, MIG, PDGF-BB, and TIMP-1 in BM supernatants. Also, a panel of circulating inflammatory cytokines in PB including BLC, M-CSF, Eotaxin-2, and TIMP-1 reflected the inflammatory status in the BM niche. Although the current study did not detect PDGF-BB in HS-5 baseline cytokine profile, some studies have found PDGF-BB from 5000 to 20,000 pg/ml in healthy serum and 1000 to 5000 pg/ml in the BM supernatant in myeloproliferative neoplasm patients (Kleiner *et al.*, 2013; Chen *et al.*, 2021). However, cytokines including IL-16, Eotaxin-3, Fractalkine, MIG, and BLC, which support the overall chemotaxis are required to home the incoming stem cells, as well as Flt3 ligand, GDNF, MDC, and MIP-1b, which support inflammation, cellular survival, and differentiation (section 4.3.1.5).

Utilising the cytokine array in this study, a 'cytokine functionality table' (table 4.1) was developed, detailing the main physiological roles of all 80 cytokines based on their expression patterns by HS-5 (section 4.3.1.5). In brief, key functions encompass cytokines driving cell-mediated immunity (TNF- α , IFN- γ , IL-1 β , IL-12p70, IL-18, LIF, IL-17, IL-9) and humoral immunity (IL-2, IL-4, IL-5, IL-10, IL-13). Additionally, chemokines (RANTES, MCP-1, IL-8, Eotaxin, MIP-1 α , and -b), cytokines with inflammatory (IL-6, TNF- α , IFN- γ), and chemotactic functions (IL-8, IL-17), as well as homeostatic and tissue repair cytokines (GM-CSF, G-CSF, SCF, SCGF, HGF, FGF-basic, IL-7, IL-15, IL-6, VEGF, HGF), were identified according to the references listed in the table description. However, cytokines have multiple and sometimes unrelated functions that depend on the target cell or on the presence or absence of other cytokines. Some have limited sequence similarity and engage distinct receptors yet transduce signals through common intracellular pathways. Because of this diversity of structure and overlapping function, the classification of cytokines has been a challenge (see section 4.3.1.5). However future functional studies are warranted to investigate the underlying mechanisms of the cytokines' roles in leukaemia induction and the development of DCL.

MTX has been shown to be a highly immunosuppressive drug, which may explain the overall lower response with MTX where CHL shows a generally higher cytokine secretion. However, it was mindful that CHL was used at a 10-fold dose higher than was (human) clinically relevant, as pharmacokinetic studies in mice reveal plasma levels of CHL of 40 μ M (Ganta *et al.*, 2008), whereas subsequent literature searching suggests that plasma levels in patients may be closer to 4 μ M (Newell *et al.*, 1983; Silvennoinen *et al.*, 2000). While this highlights disparity following the dosing of rodents, which may be important in toxicity testing extrapolations

between rodent and man, further research is required to explore if a 10-fold lower dose of CHL would have significantly altered the data presented here.

Following the acquisition of these categorisation and secretion data, three criteria were considered when selecting candidate cytokines out of the 80 on the array as contributing to the development of DCL:

1. Cytokines which promote myeloid lineage differentiation (IL-1 [family], IL-3, IL-6, GM-CSF, G-CSF, and SCF)
2. Cytokine storm candidates (TNF- α , IFN- γ , IL-1 β , IL-2, IL-4, IL-6, and IL-8)
3. Cytokines previously implicated in malignancy or mutagenesis (GM-CSF, IFN- γ , TNF- α , IL-6, G-CSF, IL-3, and TGF- β 1).

By considering all the results from the array and documented literature, TNF- α , IL-6 and GM-CSF were selected from the absolute change data and TGF- β 1 and G-CSF were selected from the fold-change data for future experimentation in this research. The higher expression of these cytokines in the HS-5 cell line treated with CHL and MTX suggests that these cytokines could be involved in the cytokine storm following chemotherapy *in vivo* and contribute to the post-HSCT malignancy. Moreover, many of these candidate cytokines are implicated in the bystander effect following radiotherapy induction. Consequently, this research hypothesised that the induction of these cytokines due to chemotherapy exposure may also trigger BE analogous to RIBE.

Very often, cytokine and growth factor expression are analysed using immunochemistry or mRNA expression analyses. Also, some studies use western blot and the protein array technology to detect expression of proinflammatory, profibrotic, proangiogenic and stem cell mobilising cytokines (Gallet *et al.*, 2011). However, an ELISA assay (in-house or kit) remains the most frequently employed method in numerous studies, as evidenced by the following references; Winkler *et al.* (1999); Morgan *et al.* (2010); Robak *et al.* (1998); Zou *et al.* (2018); Noori *et al.* (2017); Arican *et al.* (2005); Kawakami *et al.* (1990); Matsubara *et al.* (1999) and Wakefield *et al.* (1995). Given that cytokine array data are a relative assessment (intensity) of the results, the data for candidate cytokines were subjected to quantitative analysis using ELISA to validate the results. The ELISA results in section 4.3.2 for the five selected candidates demonstrates the expression differences between two dosages of CHL. It also shows the expression of key cytokines by TK6 and HS-5 intermediately and over 5 days; this may be

important in the co-culture experiments (chapter 6), as cytokine secretion for TK6 is largely unknown.

It is more accurate to assume the cytokine response network as a collection of overlapping complex systems, each exhibiting distinct activities based on the presence or absence of other cytokines. This is supported by Gallet *et al.* (2011), which revealed both positive and negative correlations between cytokines when studied in isolation or in combination. Moreover, Cheleuitte *et al.* (1998) demonstrated that the induction of IL-6, IL-11, and GM-CSF from marrow stromal cells can be controlled by IL-1 β in the microenvironment. Consequently, the cytokine levels measured in this study using ELISA may differ when assessed in the *in vivo* setting (serum and BM) surrounding the immune system compared to their levels in an *in vitro* co-culture with HSC (TK6).

In this study cytokine concentration was assayed by three in-house developed sandwich ELISA (TNF- α , IL-6, GM-CSF) and two commercially available ELISA kits in accordance with the manufacturer's instructions (Thermo Fisher; TGF- β 1, G-CSF). Figure 4.5 to Figure 4.9, shows the ELISA measurements of candidate cytokine from TK6 and HS-5 +/- chemotherapies.

The expression of TNF- α by TK6 (Fig. 4.5) remained statistically unchanged over 120 hours, and TNF- α exhibited the lowest expression among the analysed cytokines. Although GM-CSF was initially undetected, it was later observed with no substantial changes over time. Intriguingly, G-CSF emerged as the cytokine with the highest expression from TK6 throughout the detection period. However, this is a much lower value to contribute to cytokine storm compared to the G-CSF levels release by *in vivo* BM after HSCT (38310 pg/ml) (Melenhorst *et al.*, 2012). TGF- β 1 expression by untreated TK6 was not changed over 5 days but remained between 360 – 431 pg/ml. Because limited research has been conducted on TGF- β 1 expressed during HSCT or cytokine storms, it is difficult to comment on the potential contribution of TGF- β 1 levels from HSC within the cytokine storm in the *in vivo* setting. IL-6 released by untreated TK6 was not changed over the time period and this was statistically significantly different to the IL-6 expression by untreated HS-5. Because TK6 is a B lymphoblastoid cell line, it may release a variety of cytokines. However, there are very few studies describing TK6 expressing cytokines in literature. According to Glover *et al.* (2015), IFN, IL-29, LIF, and TNFSF4 are a few cytokines released by TK6. To the PhD candidate's knowledge, the current study is the first study to report quantitated cytokine expression in TK6.

The expression of cytokines in untreated HS-5 ELISA data was mostly consistent with the array results found in chapter 4. Based on the ELISA findings, the baseline expression intensity order of candidate cytokines, as determined by the array order (IL-6, TNF- α , GM-CSF, G-CSF, TGF- β 1), has been revised to G-CSF, IL-6, GM-CSF, TGF- β 1 and TNF- α . However, it must be kept in mind that G-CSF and TGF- β 1 were only repeated once due to the high cost of the ELISA kit. The untreated HS-5 cells did not exhibit any significant changes in the expression of their respective cytokines over the detection time. Nevertheless, G-CSF was the highest expressed cytokine in untreated HS-5 at both detected time points where IL-6 was the second-highest cytokine produced across 5 days. Unexpectedly, TNF- α exhibited the lowest cytokine secretion among the untreated HS-5 cells in ELISA, despite being the second highest in baseline expression in the array, as shown in figure 4.1.

Following the chemotherapy treatments, all of the cytokines were elevated as expected. The CHL 40 μ M treated HS-5 exhibits greater results than the MTX treated HS-5, which is consistent with the array findings. However, cytokine expression at 4 μ M CHL was comparably lower than measurements at 40 μ M CHL in TNF- α and TGF- β 1 whereas for G-CSF and GM-CSF there was only a slight increase between the two doses, but it is largely unchanged. The most noteworthy ELISA data originated from IL-6 ELISA (Fig. 4.7), revealing numerous significant differences. Specifically, IL-6 expression in untreated HS-5 cells was significantly different from HS-5 cells treated with both CHL and MTX at 72 hours, with p-values of $p \leq 0.01$ and $p \leq 0.0001$, respectively. There was also a significant difference in IL-6 expression between two CHL doses (40 μ M vs. 4 μ M) for treated HS-5 cells at $p \leq 0.0001$. Interestingly, this distinction reveals a higher expression of IL-6 from HS-5 treated with 4 μ M compared to those treated with 40 μ M. This highlights the importance of further investigation into IL-6 in subsequent studies to elucidate the implications and influences of these differences in co-culture models.

During the array, cytokine secretion mainly focussed on 2 and 3-days post-chemotherapy exposure for MTX and CHL respectively since a senior research team member demonstrated maximal genotoxic bystander effects at these time points following 1 hour of drug exposure with respect to these two drugs. Therefore, this ELISA data supported the observations by the previous PhD students, showing that higher cytokine secretion correlated with the highest BE on the same days.

The selection of a 5-day window was driven by the intention to capture the timeline that could transpire between conditioning therapy and the last possible moment that stem cells might be infused. The objective was to explore if there might exist a "safe" window for transplantation when cytokine levels closely resemble normal (untreated) conditions. Upon analysing the current ELISA data over this timeline, the G-CSF levels showed no substantial difference across the 5 days, reflecting levels similar to untreated cells (Fig. 4.9). For GM-CSF treatment, non-significant lower levels were observed at 24 hours of 40 μ M CHL treatment compared to untreated HS-5 expression at 120 hours (Fig. 4.8). In the case of TNF- α , only the human-relevant concentration of CHL (4 μ M) approached untreated levels until day 4 (96 hours) and then started to increase. However, these were not statistically significant at any time point (Fig. 4.5). Both TGF- β 1 (Fig. 4.6) and IL-6 (Fig. 4.7) consistently remained substantially higher than untreated levels, with IL-6 showing significant elevation at 72 hours for both CHL (4 μ M) and MTX treatments. Based on these findings, there is no discernible period identified as a safer timeframe for HSC infusion without the risk of cytokine storm interruption.

Since there is not a good understanding of the molecular events that lead to cytokine storm, or the contribution that the storm makes to pathogenesis, understanding of the roles of key inflammatory signalling and their interactions in haematopoiesis could open attractive novel ways to develop therapies aimed at modulating the inflammatory immune response to prevent cytokine storm following HSCT. Although the understanding of the inflammatory roles in DCL remains limited, antagonising proinflammatory cytokines including TNF- α , IL-6 and IFNs by either neutralizing antibodies or silencing the genes, may have negative effects on inflammatory factors on HSCs' proliferation. This may lead to restoring the ability of the progenitor cells to reconstitute impaired BM and prevent severe cytokine storm following cancer therapies thus avoiding fatal consequences derived from TRL or DCL. Inhibitors for TNF- α have been approved for the treatment of inflammatory bowel disease, psoriasis, and rheumatoid arthritis (Tisoncik *et al.*, 2012; Clark & Vissel, 2017). However, given that significant changes in IL-6 ELISA data (HS-5 vs TK6 and untreated vs treated; Fig. 4.7), IL-6 appears to play a significant role in the pathogenesis of cytokine storm. This is supported by the many studies that have blocked IL-6 (Siltuximab) and its receptor (Tocilizumab) using mAbs to inhibit IL-6 signalling in effector cells which then reduced its effect during cytokine storm and prevented inflammatory conditions (Riegler *et al.*, 2019; Shimabukuro-Vornhagen *et al.*, 2018; Yildizhan & Kaynar, 2018). Therefore, later in this thesis, IL-6 signalling

pathways will be blocked in the lymphoblast cell line, TK6 (Chapter 5), as well as knocking down the IL-6 gene in the BM-MSC line, HS-5 (Chapter 6) to understand the contribution of IL-6's inflammatory effects in cytotoxicity and genotoxicity during bystander co-culture models.

4.5 Conclusion

To the author's knowledge, this is the first study that has directly revealed and compared extensive profiles of cytokines, including chemokines and growth factors expressed by the BM- MSC line, HS-5, and alteration in expression with regards to chemotherapies; CHL and MTX. This array model reflects the panel of cytokines in the HS-5 cell line, to be capable of modelling the cytokine storm status of the BM microenvironment following chemotherapy *in vivo*. While HS-5 represents a good model for CIBE in these experiments and clearly only reflects the cytokine profile of the recipient of origin, the profile measured within following study reflects that seen in clinical settings following toxic insult as described above. Furthermore, confirmation of the presence of cytokines known to be associated with a cytokine storm support the validity of the model employed for BE analysis. It is important to acknowledge that all the data from the cytokine array has already been published by Asurappulige *et al.* 2023.

The ELISA data largely supported that these key cytokines are expressed by HS-5 and increased their levels following drug treatments. When considering the cytokine storm levels from the literature, cytokine data following drug exposure implies what might happen to the patient in an *in vivo* setting when these cytokines act synergically. With regards to the time framing, detection confirmed that both CHL and MTX showed their highest expression at day 2 and/or 3, which reflect the bystander genotoxicity results that the senior research team member noticed with respect to these two drugs. This is the first study to measure these candidate cytokines expressed by TK6 cells, where they indicated some expression which did not change with time. However, the levels expressed by untreated TK6 cells were more like the untreated HS-5 expression, except for IL-6 and GM-CSF. However, further studies are required to establish the TK6 cytokines' profile and understand the co-culture communication between BM (HS-5) and HSC (TK6) compartment to mimic the cytokine signalling system *in vivo*.

CHAPTER 5

EVALUATION OF CYTOTOXICITY AND GENOTOXICITY IN AN *IN VITRO* CULTURE MODEL

5.1 Introduction

This chapter focuses on the ability to induce genotoxicity, measured as the induction of micronuclei, by the candidate cytokines selected in the chapter 4. Genotoxicity also describes the property of chemical agents that damages the genetic information within a cell leading to mutations. DNA or chromosomal damage in a somatic cell may result in a somatic mutation, which may lead to malignant transformation and development of cancer cells. Nearly 20 types of well-described *in vitro* or *in vivo* genotoxicity tests are presently used. *In vitro* assays are used to investigate the potential genotoxic effect of pharmaceuticals, medical materials, physical and chemical factors including poisons. *In vivo* tests allow for investigating the impact of environmental factors on humans or biota. The most often used *in vitro* assays include induction of nucleotide mutation and more complex genome changes by cytogenetic methods, such as the SCE assay, analysis of chromosomal aberration frequency, comet assay and different kinds of micronucleus assay (MN) (Sommer *et al.*, 2020). Also, the other types of abnormalities detected in cells affected by a genotoxic substance are chromatid and chromosome gaps, chromosome breaks, chromatid deletions, fragmentation, translocation and complex rearrangements (Kondo *et al.*, 2010; Swift & Golsteyn, 2014).

The micronucleus (MN) assay is used widely to test genotoxicity *in vitro*, because it is faster than many other assays and easy to perform. Micronuclei result in the daughter cell which has lost a part or all of a chromosome (Fig. 5.1). There is a chance of more than one micronucleus forming when more genetic damage has happened. Using FISH with probes targeted to the centromere region, it can be determined if a whole chromosome, or only a fragment is lost (Sommer *et al.*, 2020; Hayashi, 2016).

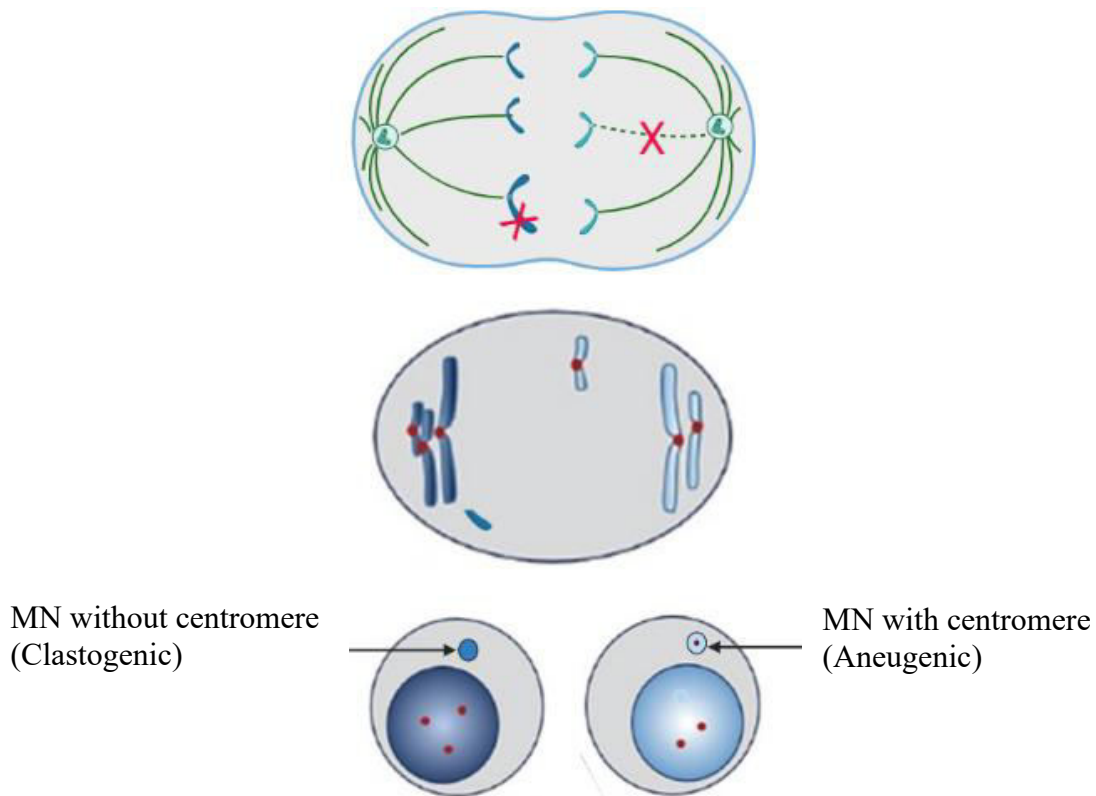


Figure 5. 1. Micronucleus formation during mitotic cell division. Micronuclei primarily result from acentric chromosome fragments or lagging whole chromosomes that are not included in the daughter nuclei produced by mitosis because they fail to correctly attach to the spindle during the segregation of chromosomes in anaphase. These full chromosomes (Aneugenic) or chromatid fragments (Clastogenic) are eventually enclosed by a nuclear membrane. Aneugens induce mis-segregation of chromosomes into daughter cells while clastogens break the DNA/ chromosome. Structurally they are similar to conventional nuclei but smaller in size. This small nucleus is referred to as a micronucleus. (Figure created by the author via BioRender.com)

As discussed in section 1.6.2.1, there is no proper explanation about how or why cytokines might act as genotoxic inducers and why there are high levels of expression during cancer treatments. Studies suggest different theories that could explain how these cytokines induce indirect genotoxicity through other chemical messengers (Barcellos-Hoff *et al.*, 2005; Morgan, 2003). Lazutka (1996) documented that TNF- α , IL-2 and IFN- α have the ability to induce different genetic endpoints in human peripheral blood lymphocytes *in vitro*. Genotoxic effects of cytokines may be mediated through the induction of ROS or may occur following exposure to inflammatory cytokines such as TNF- α and IL-6 (Danzer *et al.*, 1994; Sica & Bronte, 2007). Genotoxic analysis of human cytokines has shown that IFN α , - β , - γ , TNF- α and IL-2 can induce

chromosome aberrations, MN and SCE in cultures (Sica & Bronte, 2007). *In vitro* experiments demonstrated higher frequencies of chromosome and chromatid breaks in cell lines treated with TNF- β (Lazutka, 1996). This evidence suggests that the genotoxicity of cytokines is related to the induction of ROS and RNS from immune cells in both *in vitro* and *in vivo* settings, although the exact underlying mechanism remains unclear.

It is therefore vital to understand the activities and genotoxic potential of cytokines to explore the possible implications in bystander cells (chapter 6), because they could be involved in the potential mechanism of some secondary malignancies including DCL (section 1.5). Because there is no proper investigated knowledge on cytokine genotoxicity or the genotoxicity mechanism, the main purpose of this chapter was to focus on the genotoxicity of TNF- α , TGF- β 1, IL-6, GM-CSF and G-CSF by the micronucleus assay to evaluate structural and/or numerical chromosome aberrations.

Due to the notable upregulation of IL-6 expression observed in HS-5 cells subsequent to drug treatment (Chapter 4) and considering the evidence suggesting the potential for IL-6 to induce genotoxic effects under various recombinant treatments (Chapter 5), IL-6 was chosen to be investigated further to assess its involvement in signalling pathways and its pivotal role in genotoxicity. To achieve this, chemical inhibitors FLLL-32 and BAY-293 were used to inhibit IL-6 signalling pathways.

IL-6 signalling pathway

Functionally, IL-6 is an important factor in acute and chronic inflammatory diseases. To transmit information IL-6 binds to cells via a specific receptor complex which consists of the IL-6-specific α receptor IL-6R α (gp80, CD126) and the signal transducing subunit glycoprotein 130 (gp130, CD130). The receptor gp130 is located in the cell membrane. The IL-6R α exists in two forms: one form is integrated in the cell membrane of the target cell (mIL-6R α), the other occurs in soluble form in the blood serum (sIL-6R α) (Reeh *et al.*, 2019; Manore *et al.*, 2022; Neurath & Finotto, 2011).

Pro- and anti- inflammatory signals are transmitted by soluble- and membrane-bound IL-6R α respectively where this process is known as trans- and classic- signalling pathways correspondingly (Sansone & Bromberg, 2012). While all cells in the body express gp130, the expression of IL-6R α is restricted to hepatocytes and leucocyte subtypes where they could respond to both trans- and classic signalling. However classic signalling (mIL-6R α) is

restrained to a small subset of cells (hepatocytes, macrophages, neutrophils, and T cells) which express the mIL-6R α receptors, whereas all somatic cells are targets of trans-signalling (sIL-6R α). The response towards IL-6 trans- or classic signalling is determined depending on the availabilities of these receptor types and IL-6 molecules. However, membrane bound gp130 can also be cleaved into soluble form which can be found in human plasma. Soluble-gp130 reacts with IL-6/sIL-6R α complex with the same affinity as membrane bound gp130, thus antagonising IL-6 trans-signalling without affecting classic-signalling. However, soluble-gp130 levels are almost negligible when compared to sIL-6R α ; also soluble-gp130 does not affect IL-6 or mIL-6R α , and it can be used as an experimental tool to specifically inhibit the IL-6 trans-signalling pathway (Fasouli & Katsantoni, 2021; Manore *et al.*, 2022). During signal transmission, IL-6 first binds to IL-6R α with low affinity and then the IL-6:IL-6R α complex subsequently builds a high affinity complex with gp130. Association of gp130-IL-6R α complex promotes gp130 dimerization and formation of a heterohexameric complex consisting of IL-6:IL-6R α :gp130 in a 2:2:2 ratio. IL-6 activates trans-signalling through sIL-6R α . This mediates pro-inflammation and thus is referred to as the primary mechanism promoting tumorigenesis in multiple cancers (Manore *et al.*, 2022).

More recently, a third mechanism of IL-6 signalling has been reported where IL-6 signals between two interacting cells termed, trans-presentation or “cluster signalling”. IL-6 binds mIL-6R α on one cell (transmitting cell) and is able to bind a gp130 receptor on another cell type (receiving cell) for signal transduction. Co-culture experiments identified that gp130 receptors on T cells responded to IL-6/IL-6R α complexes on the membrane of dendritic cells resulting in robust activation of STAT3 (Manore *et al.*, 2022). However, the formation of either classic or trans ligand-receptor complexes leads to subsequent intracellular signalling pathways mainly JAK/STAT and RAS/MAPK, as well as PI3K/AKT and the MEK-ERK5. In general, these pathways lead to IL-6-dependent gene expression and result in cellular responses such as proliferation, migration, or metabolic changes (Bill *et al.*, 2010; Reeh *et al.*, 2019).

JAK/STAT

Janus kinase/Signal transducer and activator of transcription-3 (JAK-STAT) is important in developmental and homeostatic processes including stem cell maintenance, regulating haematopoiesis and immune cell development. It can be activated in response to cytokines (IL-6, IL-10 family, G-CSF, leptin, IL-21, IL-27), growth factors and hormones, as well as receptor

tyrosine kinases and non-receptor tyrosine kinases (Abl, Src, Syk) (Sansone & Bromberg, 2012; Vainchenker & Constantinescu, 2013; Yu *et al.*, 2009).

IL-6 binding activates JAK2/STAT3 in either classic or trans signal pathways allowing communication between the extracellular environment and the nucleus. As shown in figure 5.2, formation of IL-6/IL-6R α /gp130 hexameric complex recruits the JAK family tyrosine kinases (JAK1, JAK2, and TYK2) to the membrane which associate leading to phosphorylation of five tyrosine residues (Y759, Y767, Y814, Y905, and Y915) at the cytoplasmic tail of gp130 (Manore *et al.*, 2022). These phosphorylated gp130 tyrosine residues serve as binding sites for the transcription factors, particularly SH2 domain of STAT3 monomers that are subsequently phosphorylated by JAK2 at Y705. Notably, IL-6 activates STAT3 more potently when compared to STAT1. Phosphorylated STAT3 then undergoes a conformational homodimer change and detaches from the receptor complex to translocate into the nucleus to activate transcription of genes containing STAT3 response elements (Manore *et al.*, 2022). STAT3 is essential for gp130-mediated cell survival and G1 to S cell-cycle-transition signals.

In addition to upregulating numerous genes involved in cell proliferation, migration and survival, STAT3 induces the gene expression of many cytokines, chemokines and other mediators which in turn further activate STAT3, thus forming autocrine and paracrine circles. This condition may result in a stable change to the genetic programme and associate with cancer-promoting inflammation (Yu *et al.*, 2009). Therefore, negative regulators of Jak/STAT signalling through the tyrosine phosphatases, suppressor of cytokine signalling 3 (SOCS3) or direct protein inhibitors of activated STATs (PIAS) are important to prevent excessive inflammation (Fasouli & Katsantoni, 2021; Reeh *et al.*, 2019).

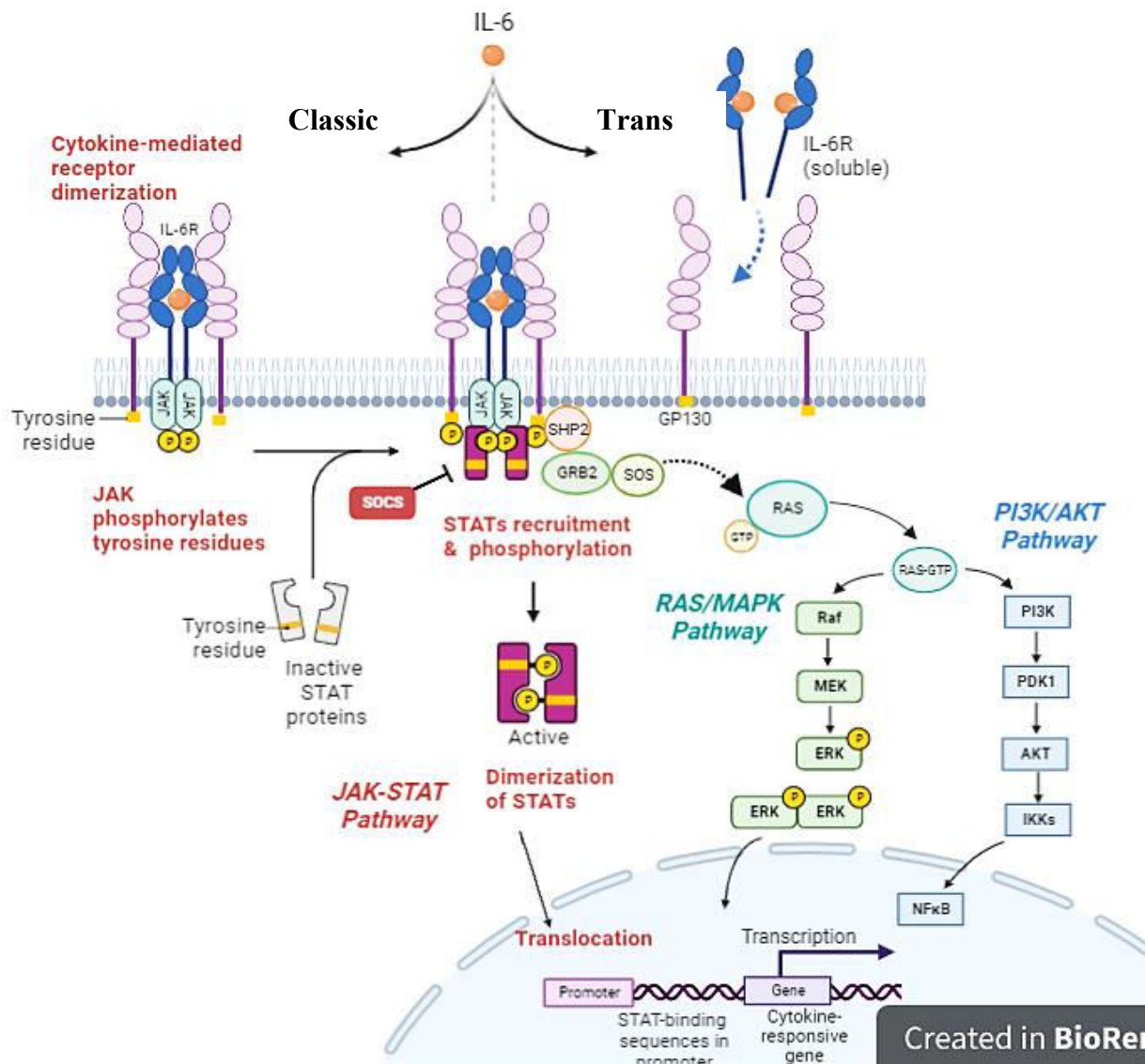


Figure 5. 2. IL-6 signalling pathways. IL-6 activates various cell types carrying the membrane bound mIL-6R α (classical IL-6 signalling) as well as via the soluble sIL-6R α (IL-6 trans-signalling). Binding of IL-6 to its receptor initiates cellular events including activation of Janus Kinase kinases and Ras-mediated signalling pathway. Phosphorylated JAK activates transcription factors such as STAT3 (Signal Transducers and Activators of Transcription-3) and SHP2 [SH2 (Src Homology-2 Domain-containing Tyrosine Phosphatase)]. Phosphorylation of these transcription factors then forms a dimer which translocates into the nucleus to activate transcription of gene response elements. The termination of the IL-6-type cytokine signalling is through the action of tyrosine phosphatases, proteasome, and JAK kinase inhibitors SOCS (Suppressor of Cytokine Signalling), PIAS (Protein Inhibitors of Activated STATs), and internalisation of the cytokine receptors via GP130. In addition to JAK/STAT and Ras/MAP kinase pathways, IL-6 also activates PI3K (Phosphoinositide-3 Kinase). The PI3K/Akt/NF-KappaB cascade activated by IL-6, functions cooperatively to achieve the maximal anti-apoptotic effect of IL-6 against TGF- β . (Figure created by author via BioRender.com).

RAS/MAPK

The master regulator of the classical mitogen-activated protein kinase (MAPK) cascade is the rat sarcoma (RAS) protein, which is encoded by three genes, *n-RAS*, *h-RAS* and *k-RAS*. RAS is a small GTPase that toggles between its GTP- bound active and the GDP-bound inactive state. Activation of the pathway begins when a signal binds to a protein tyrosine kinase receptor. The epidermal growth factor (EGF) receptor and the platelet-derived growth factor receptor are the best-known receptors in the pathway (Molina & Adjei, 2006; Guo *et al.*, 2020). However, receptors including cytokine receptors, integrins, serpentine receptors, other tyrosine kinase receptors and G-protein-coupled receptors (GPCRs) are able to activate k-RAS. Tyrosine kinase and cytokine receptors utilise the same mechanism to interact with the RAS cascade (Dillon *et al.*, 2021). After cytokine binding, subsequent receptor dimerisation allows transphosphorylation by the JAK2 proteins. The phosphorylated tyrosine residues on the receptor and JAKs serve as binding sites for transcription factor SHP2 (Src homology-2 domain-containing tyrosine phosphatase-2) and SH2 (Shc's src homology 2 domain) and adaptors that link the other cellular pathways such as PI3K/Akt (Fig. 5.2). At high cytokine concentrations, RAS/MAPK pathway activates through the SH2 and GRB2 (growth factor receptor bound protein-2). GRB2 can also associate with SHP2. This protein acts as a scaffolding protein, serving as a link to tyrosine kinase receptors via its two SH2 domains and GRB2 at its C terminus tail.

When an extracellular signal binds to the receptor, SHC (SH2 domain-containing transforming protein C1) serves as a phosphorylated anchor for the connector protein GRB2 to bind to the phosphotyrosine residues of the activated receptor and interact with the guanine nucleotide exchange factor (GEF) of Son of Sevenless (SOS) to form the receptor-GRB2-SOS complex. Binding of SOS to the Tyr phosphorylation site on the receptor leads to translocation of cytoplasmic SOS to the membrane, resulting in a high concentration of SOS near RAS. SOS and RAS-GDP promote the replacement of GDP with GTP in RAS, thereby activating to initiate the RAS pathway (Thatcher, 2010; Guo *et al.*, 2020). Activated RAS then activates the protein kinase activity of a RAF kinase. The phosphorylated RAF kinase activates a MEK1/2 (MAPK/ERK kinase). Then MEK phosphorylates and activates extracellular signal-regulated kinase 1/2 (ERK). Dimerised ERK then translocates into the nucleus to regulate target gene transcription factors such as Elk1 and NF-IL-6 (C/EBP-Beta) that can act through their own cognate response elements in the genome. These factors and other transcription factors like

Activating Protein-1 and SRF (serum response factor) that respond to many different signalling pathways come together to regulate a variety of complex promoters and enhancers that respond to IL-6. RAS signalling can be deactivated by GTPase-activating proteins (GAPs) that catalyse the hydrolysis of GTP (Plangger *et al.*, 2021) or members of the SOCS family can reduce receptor signalling via feedback regulation (Molina & Adjei, 2006).

FLLL-32

A novel JAK2/STAT3 inhibitor FLLL-32 is a synthetic analogue of curcumin. FLLL-32 reduces STAT3 phosphorylation by IL-6 at Tyr705 and induces proteasome mediated degradation of STAT3. The JAK2 and STAT3 SH2 domain is essential for STAT3 phosphorylation; interestingly, FLLL-32 can also decrease STAT3 DNA-binding activity by interacting with its SH2 domain (Fossey *et al.*, 2011; Manore *et al.*, 2022; Su *et al.*, 2021).

BAY-293

BAY-293 is a potent blocker of the interaction between k-RAS and SOS1 by binding to the GEF pocket on SOS1. BAY-293 is a high affinity inhibitor with moderate antiproliferative activity *in vitro*. Even though BAY-293 is not optimised for clinical use, it is described as a valuable chemical probe for a range of investigations targeting signalling pathways, metabolism and DNA damage.

Therefore, the key aim of this chapter was to investigate the potential of candidate cytokines to induce cytotoxicity and/or genotoxicity, particularly via micronucleus formation. Additionally, this exploration involves the utilisation of IL-6 signalling pathway inhibitors to elucidate the involvement of the IL-6 pathway in the induction of micronuclei.

5.2 Methods

5.2.1 Cytotoxicity assessment

Prior to determination of genotoxicity, a cell cytotoxicity/viability assay was performed every 24 hours for 2 days after TK6 cells were treated with recombinant cytokines. The trypan blue exclusion assay was used to assess the viability of both pre- and post-24 hours of treatment. Recombinant doses were determined according to table 2.2.

5.2.2 Micronucleus assay

Cytokines were analysed for their capacity to directly induce genotoxicity, measured using the MN assay as described in section 2.2.4 Treatment dosages were determined based on literature for baseline and storm cytokine measurements; indicated in table 2.2 and appendix II. Briefly, TNF- α and IL-6 baseline treatment dosage - 50, 250, 500, 1000 and 2000 pg/ml and for cytokine storm levels - 2000, 3000, and 4000 pg/ml. GM-CSF, G-CSF and TGF- β 1 baseline dosage are - 50, 250, 500, 750 and 1000 pg/ml and for cytokine storm levels - 1000, 2000, 3000 and 4000 pg/ml. Due to the natural variability of cytokine gene secretion, there are no clear threshold divides between healthy and storm levels in different individuals. Thus, there is an overlap between top end of the baseline level and bottom end of the storm levels (indicated by a double ended arrow in section 2.1.3 table 2.2).

The MN assay was performed as described in section 2.2.4 when cytotoxicity was found to meet OECD guidelines. Alongside the cytokines, TK6 were treated with MMC and PBS as a positive control and negative control respectively. For each treatment condition, three independent biological replicates of the MN assay were conducted. A minimum of two slides were prepared for each replicate to represent a single sample. Where deemed appropriate, the average of measurements from both slides was utilised to ensure comprehensive data representation and analysis.

5.2.3 IL-6 pathway inhibition *in vitro* MN assay

5.2.3.1 Optimisation of inhibitor dose

To analyse the effect of FLLL-32 and BAY-293 on the TK6 cells, the viability was evaluated by total live cell count after treating the TK6 cells with range of doses of each inhibitor.

Recommended concentrations were taken from Selleckchem.com (FLLL-32 at 5 μ M and BAY-293 at 0.021 μ M) and the literature. There were five different concentrations tested for each inhibitor. For FLLL-32; Lin *et al.* (2010), Su *et al.* (2021), Liu *et al.* (2010), Bill *et al.* (2010) and Fossey *et al.* (2011). For BAY-293; Plangger *et al.* (2021), Plangger *et al.* (2022) and Swiatnicki *et al.* (2022).

TK6 cells were seeded in two 12-well plates at 3×10^5 cells/ml in 1 ml. One plate was treated with FLLL-32: 0.5, 1.5, 2.5, 3.5 and 5 μ M and the other 12-well plate was treated with BAY-293: 1, 2.5, 5, 7.5 and 10 μ M. Both plates had TK6 untreated as negative control samples. Following 24 hours incubation, the live cell count was taken per ml for each sample in both plates.

5.2.3.2 Cytotoxicity and genotoxicity following chemical inhibition

The IL-6 signalling pathways in TK6 were inhibited by using two chemical inhibitors individually and in combination. FLLL-32 is a potential JAK2/STAT3 inhibitor which was used at 5 μ M in every treatment in this study. BAY-293 inhibits the k-RAS–SOS1 interaction and was used at 2 μ M in this study. IL-6 pathway inhibition by FLLL-32 and BAY-293 was done according to section 2.2.5.1 and 2.2.5.2 respectively. In brief, TK6 cells were seeded at half their seeding density in a 12-well plate and incubated for 24 hours overnight. Cells were treated with inhibitors in the respective wells (FLLL-32 and BAY293) and incubated for 2 hours, and subsequently 4000 pg/ml of IL-6 recombinant was added. Following 24-hour incubation, cells were counted and re-seeded at 3×10^5 cells/ml into fresh media for overnight incubation. Cytotoxicity was calculated to ensure treatments were above 50% to proceed with the MN assay. To explore any changes in genotoxicity after blocking the IL-6 pathway, the MN assay was followed as described in section 2.2.4.2. Each treatment involved the two chemical inhibitors, \pm IL-6, and was conducted in three independent biological replicates following the established protocol. For each replicate, 2-3 wells were dedicated to the same treatment condition to mitigate the impact of outliers.

The data analysis utilized GraphPad Prism software version 8.2.1, employing one-way or two-way ANOVA for group comparisons, followed by Tukey's multiple comparison test. Additionally, unpaired Student t-tests were conducted to assess direct significance between treated and untreated (control) samples. The results are presented as mean \pm SD for three

independent biological replicates, with significance levels denoted as follows: (*) for $p \leq 0.05$, (**) for $p \leq 0.01$, (***) for $p \leq 0.001$, and (****) for $p \leq 0.0001$.

5.3 Results

5.3.1 Cytotoxicity

Part of the data presented below has been already published by Asurappulige *et al.* (2023).

Figure 5.3 exhibits the cell percentage viability assessed every 24 hours following seeding, spanning a timeline from the seeding day to the day of performing the MN assay, covering the entirety of TK6 viability changes.

TK6 cells treated with TNF- α (Fig. 5.3A) showed initial viability at 91%, maintaining viability above 80% after 24 hours. However, at 48 hours post-seeding or 24 hours post-treatment, a notable non-significant drop was observed in TNF- α storm dosages. Levels of 3000 and 4000 pg/ml dropped below 65% after 24 hours, while other concentrations remained above 70%. At 72 hours, 250 and 1000 pg/ml exhibited a drop compared to 48 hours, with the lowest viability recorded at 50.4% at 72 hours with 2000 pg/ml. In figure 5.3B, high cell viability (81% - 91%) was observed following TGF- β 1 treatment day for all wells. Post-treatment (48 hours), doses from 1000 to 4000 pg/ml exhibited a drop in cell viability, with the highest cytotoxicity recorded at 48 hours with 2000 pg/ml (65% viability), while 50 pg/ml showed the lowest cell death at 78% viability. IL-6 treatment (Fig. 5.3C), with 50 pg/ml exhibited a drop to 70% at 48 hours, whereas for 500 and 1000 pg/ml, the most substantial viability drop occurred at 72 hours, reaching 52% and 54% respectively, while higher doses (2000, 3000, 4000 pg/ml) showed 60% - 65% viability after the treatment period. GM-CSF treatment (Fig. 5.3D) demonstrated viability around 80% on the treatment day (24 hours). After treatment, lower doses (50 and 250 pg/ml) exhibited lower viability (68% and 65%), while higher doses (1000, 2000, and 3000 pg/ml) show reasonably higher viability (75%, 75%, 78%). Notably, TK6 cells treated with 4000 pg/ml of GM-CSF exhibit the lowest cytotoxicity and highest viability at 48 hours and 72 hours (82% and 74.8%) compared to all lower dosage levels, emphasising GM-CSF's role in cell proliferation. The lowest viability or higher cytotoxicity is seen at 250 pg/ml at 48 hours and 500 pg/ml at 72 hours. G-CSF treated TK6 viability (Fig. 5.3E) at 24 hours post-treatment was the highest (75% - 85%) among the five cytokine treatments performed. At 72 hours, the highest viability (75%) or lowest cell death is observed with the highest level of G-CSF at 4000 pg/ml. Viability of 250 and 500 pg/ml drops to 58% and 53%, respectively, but remains within the limit. According to the above data, all cytokines reduced cellular viability with increasing dose and increasing timeframe, but all remained above 50% suggesting the doses would be

Understanding the chemotherapy- induced bystander effect; an evaluation of the role of cytokine storm in an in vitro model of the human bone marrow

acceptable for the MN assay. Similarly, even though there was some cell death, MMC treated TK6 also remained above the 50% as predicted.

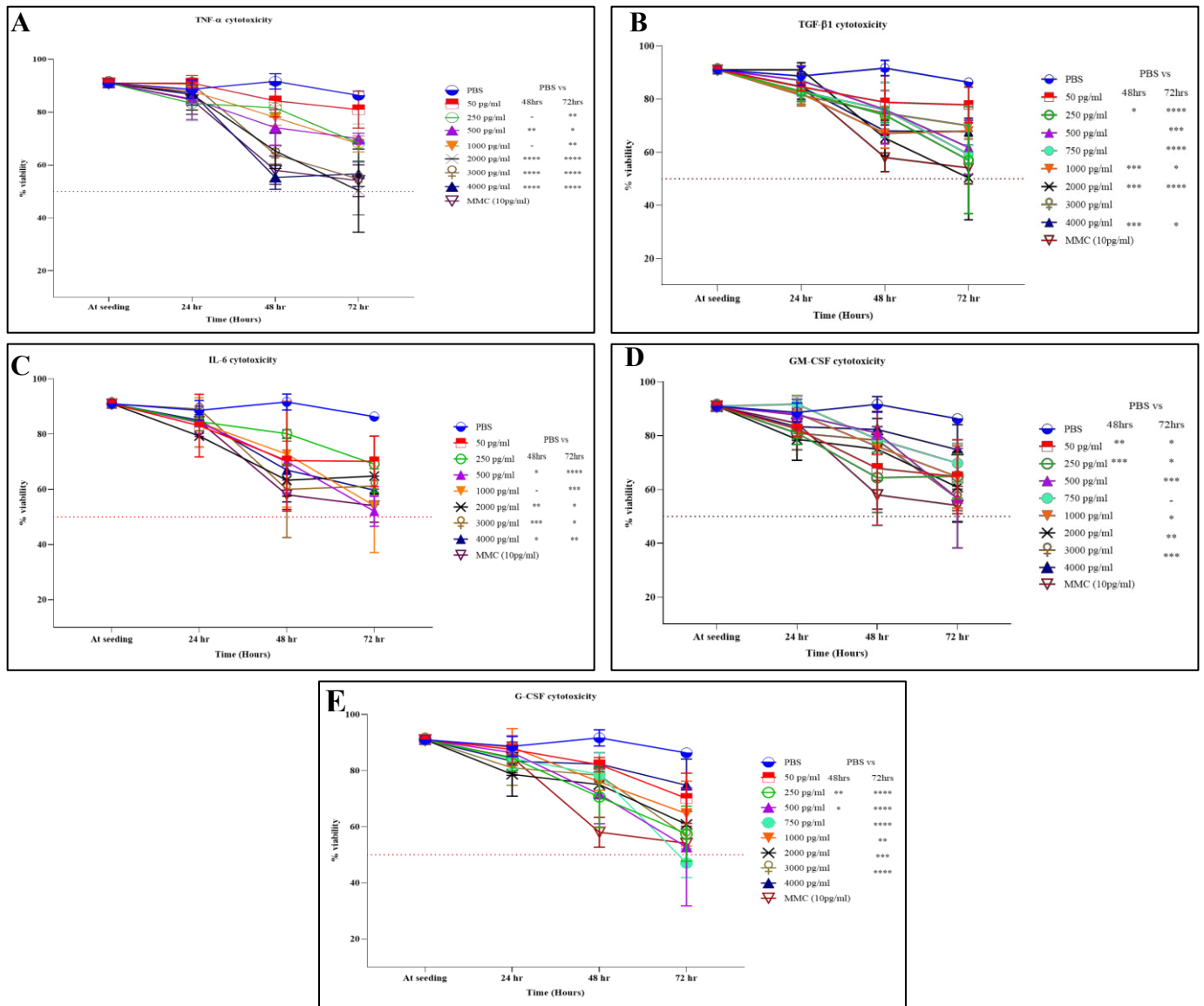


Figure 5. 3. TK6 cell viability following recombinant cytokines treatments. TK6 cell viability was evaluated by the trypan blue exclusion assay and analysed automatically with the LUNA cell counter over 2 days after seeding. Data presented is for mean \pm SD for all the concentrations analysed and significant differences are shown as * $p \leq 0.05$, ** $p \leq 0.01$, *** $p \leq 0.001$ and **** $p \leq 0.0001$ as determined by two-way ANOVA, Tukey's multiple comparisons test.

5.3.2 Genotoxicity evaluation

In order to detect the genotoxic capacity of these cytokines, induction of MN were assessed. MMC was used as a positive control and PBS was used as the negative control of this assay, and MN scoring for the PBS and MMC was consistent with historical laboratory data (Vernon *et al.*, 2022).

5.3.2.1 TNF- α recombinant treatments

Figure 5.4A shows TK6 treatment with TNF- α at healthy concentrations (baseline levels of TNF- α in healthy individuals). TNF- α showed a dose dependent decrease in RPD but remained above the 50% threshold set by the OECD guidelines for scoring MN. RPD at 1000 and 2000 pg/ml were significantly lower than the PBS control RPD ($p < 0.01$ and $P < 0.001$ respectively). The RPD of MMC was 47% (\pm SD) and also statistically different to negative control ($p < 0.0001$). Induction of MN at 1000 and 2000 pg/ml demonstrated a more than 2-fold increase compared to the PBS when all other historic data was consistent but this was not statistically significantly different. MN for MMC was elevated significantly compared to the PBS MN level ($p < 0.01$).

Figure 5.4B demonstrates the TNF- α treatments of TK6 from 2000 pg/ml to 4000 pg/ml representing cytokine storm levels. Cell viability clearly shows there is cytotoxicity at the high doses of TNF- α when compared to the PBS control. The lowest and highest cell cytotoxicity was 65% and 54% at 3000 pg/ml and 2000 pg/ml respectively. Although they were above 50% RPD, all IL-6 treated samples' RPDs were different to the PBS control at differing significance levels. However, the two highest doses at storm level of TNF- α produced 3-fold increases in MN at 3000 pg/ml and 2-fold increase at 4000 pg/ml compared with the PBS control, although these were not statistically significantly different; the MMC positive control was significantly different to the PBS negative control ($p < 0.05$).

In figure 5.4C, TNF- α was combined with the other candidate cytokines at selected healthy and storm doses; doses selected for TNF- α were those shown to produce high MN levels when TNF- α was used alone. The RPD for these combinations were above the 50% threshold, showing there is no cell death in any of the treatments. RPD for 1000 pg/ml alone was low (66%) whereas 3000 was higher than 100 (114%), but in general no cytotoxicity was perceived,

as all combinations were in the range of 90-110% (98.9% for TNF- α + TGF- β at 3000 pg/ml; 116% for TNF- α 3000 + G-CSF 1000 pg/ml).

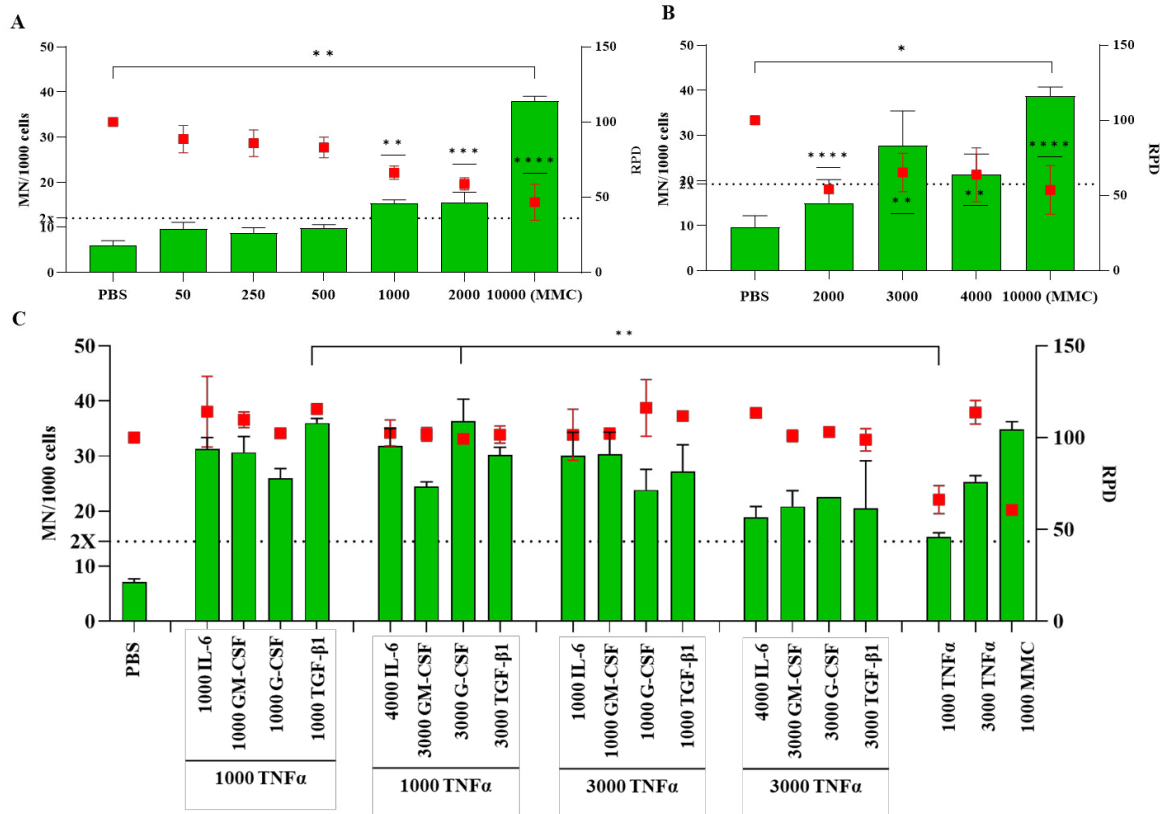


Figure 5. 4. The induction of micronuclei in TK6 cells due to direct treatment with recombinant TNF- α . (A) Healthy level treatments, (B) Storm level treatments, (C) Combination treatments. TK6 cells were cultured and treated with TNF- α alone as described in section 2.2.4 for 24 hours. After 24 hours recovery period, cells were harvested and evaluated for relative population doubling (RPD) and number of MN present. Mitomycin C (10 ng/ml; 30 nmol/L) was used as a positive control and PBS was the negative control for all experimental repeats. Data shows the mean \pm SD (n=3) and significant differences shown as ** $p \leq 0.01$, *** $p \leq 0.001$ and **** $p \leq 0.0001$ as determined by two-way ANOVA, Tukey's multiple comparisons test. Significant differences between MN and RPD are denoted on the graph using two distinct symbols.

In contrast to the individual TNF- α exposure, combination treatments of TNF- α with another cytokine increased the MN formation significantly for two combinations. In general, the lower dose of TNF- α (1000 pg/ml) showed higher overall MN formation in combination with high or low levels of other candidates, whereas higher doses of both TNF- α and the other candidate cytokines showed a general reduction of MN formation when compared with low or high TNF- α alone. The combination of 1000 pg/ml TNF- α with 1000 pg/ml TGF- β 1 and 3000 pg/ml G-

CSF were statistically significant compared to the single treatment of 1000 pg/ml TNF- α ($p < 0.01$). Of particular note is that storm levels of each of the candidate cytokines in combination with storm levels of TNF- α (3000 pg/ml), tended to reduce MN counts in comparison with storm TNF- α alone. However, these combinations remained more than 2-fold above the PBS control, but this was not statistically significant.

5.3.2.2 TGF- β 1 recombinant treatments

Figure 5.5A shows the TGF- β 1 treatments of TK6 at healthy doses. All the RPD values were significantly higher than the PBS viability level, except the sample treated with 1000 pg/ml. These data exhibit an increased cell proliferation over the treatment period with PBS RPD value (100%) lower than treatment RPD values (ranged between 146%-177%). However, MMC was also over 50% for RPD which was non-significantly lower than the PBS control. MN inductions were noticeably increased compared to PBS at more than 2-fold for every treatment level, but these were not significantly different.

In Figure 5.5B, TGF- β 1 treatment of TK6 cells at storm levels is depicted. Error bars of RPD in treatment samples overlap, and RPD for 2000, 3000, and 4000 pg/ml remain around 90%, while 1000 pg/ml shows 102% RPD which is slightly higher than the PBS control. There is no significant cell growth or death observed over time. MMC exhibits the lowest RPD, approximately 43% which is significantly different to the PBS control. At levels of 2000 pg/ml to 4000 pg/ml, there is a 3-fold MN induction, whereas 1000 pg/ml shows a 2-fold MN induction compared to the PBS control, but these were not significantly different.

Both 1000 and 3000 pg/ml of TGF- β 1 alone produced a greater than 2-fold induction of MN in treated TK6 cells in figure 5.5C, and the addition of healthy and storm doses of all other candidate cytokines increased MN further, however only the addition of healthy (1000 pg/ml) and storm (3000 pg/ml) doses of GM-CSF caused a statistically significant increase in MN. All other combinations caused non-significant increases in MN. Interestingly the MN counts for combinations of 1000 pg/ml TGF- β 1 with both doses of GM-CSF exceeded that of the known genotoxicant positive control MMC.

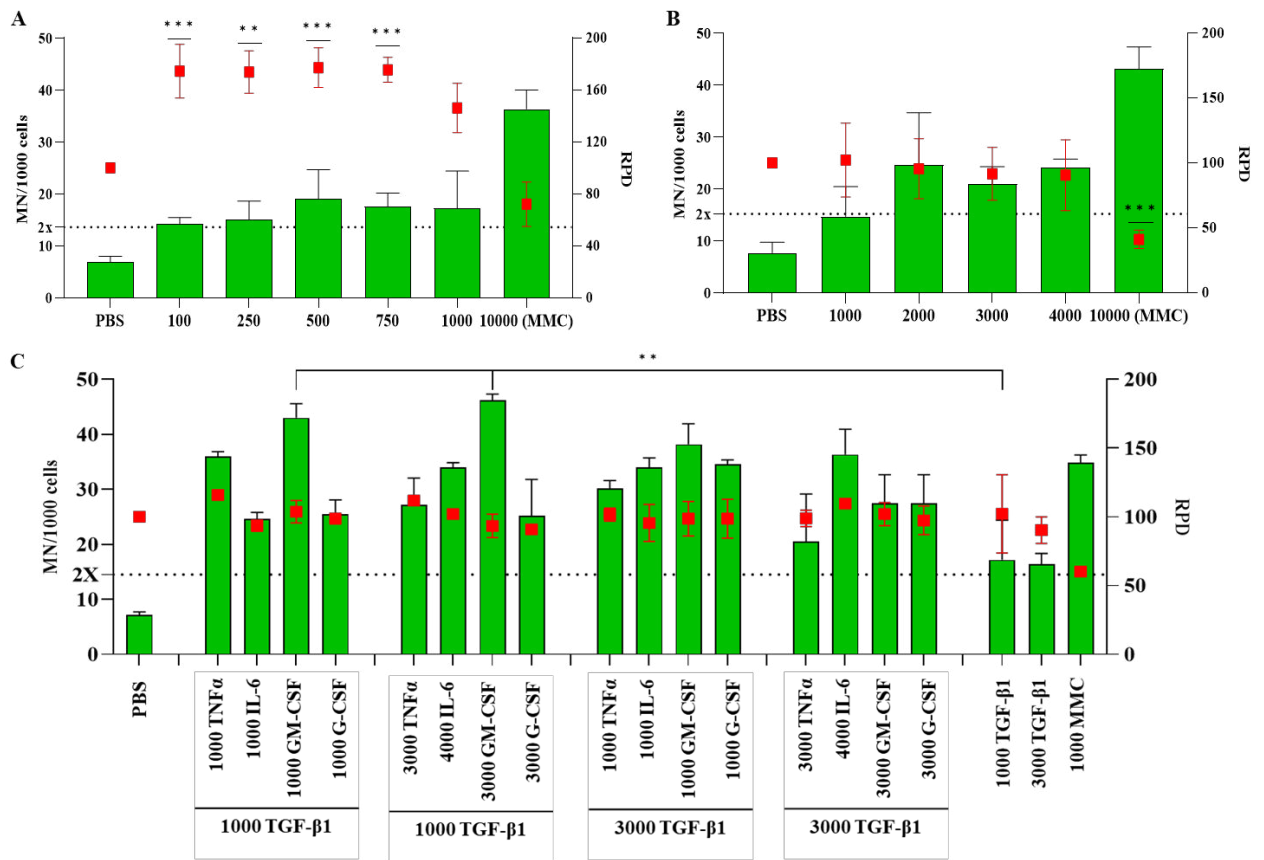


Figure 5. 5. The induction of micronuclei in TK6 cells due to direct treatment with recombinant TGF-β1. (A) Healthy level treatments, (B) Storm level treatments, (C) Combination treatments. TK6 cells were cultured and treated with TGF-β1 separately at different concentrations as described in section 2.2.4 for 24 hours. After 24 hours recovery period, cells were harvested and evaluated for relative population doubling (RPD) and chromosomal damage by scoring the number of MN present. Mitomycin C (10 ng/ml; 30 nmol/L) was the positive control and PBS was the negative control, which were used for all experimental repeats. Data shows the mean ± SD (n=3), and significant differences are shown as **p ≤ 0.01 and ***p ≤ 0.001 as determined by two-way ANOVA, Tukey's comparisons test. Significant differences for MN[□] and RPD[▭] are denoted using two distinct symbols.

5.3.2.3 IL-6 recombinant treatments

The data presented in figure 5.5A, shows the healthy concentrations of IL-6 treatment with TK6 cells. The RPD for all IL-6 treatments were slightly higher than the PBS control, but were not significantly different, with only the 50 pg/ml sample showing a lower RPD of 96%. However, the RPD of MMC was significantly reduced (58%; $p \leq 0.0001$) compared to the PBS control, but all samples were within the required limit to allow for accurate scoring of MN. MN induction showed a slight dose dependent increase at healthy doses. However, none of the treatments reached either statistical significance or MN 2-fold above the PBS control.

The treatments of IL-6 at storm levels illustrated in figure 5.6B demonstrate that cell viability reduced at storm levels to around 85% for 3000 pg/ml and 4000 pg/ml, whereas there was a significant reduction in 2000 pg/ml viability to around 65%. MMC also represented a much lower RPD value than the PBS control. MN formation at the first two doses was close to a 2-fold increase, but 4000 pg/ml achieved a 3-fold MN increase in comparison to the PBS control, whereas MMC was significantly increased compared to the PBS control.

Cell viabilities were not notably changed in the IL-6 combinations (Fig. 5.5C) compared to the vehicle control PBS (100%). Ranges were between 92% at high IL-6 and low GM-CSF combination and 114% at low IL-6 and low TNF- α combinations. Only the storm level of IL-6 alone exceeded the 2-fold increase of MN above the PBS control, but all the combinations of healthy and storm IL-6 with all the other candidate cytokines exceeded the 2-fold MN threshold above the vehicle control. The highest MN formation was exhibited in the combination of IL-6 at 4000 pg/ml with 1000 pg/ml G-CSF ($p < 0.05$). Additionally, the combination of IL-6 1000 pg/ml and 3000 pg/ml TGF- β 1 showed a significant increase above 1000 pg/ml IL-6 alone ($p < 0.05$).

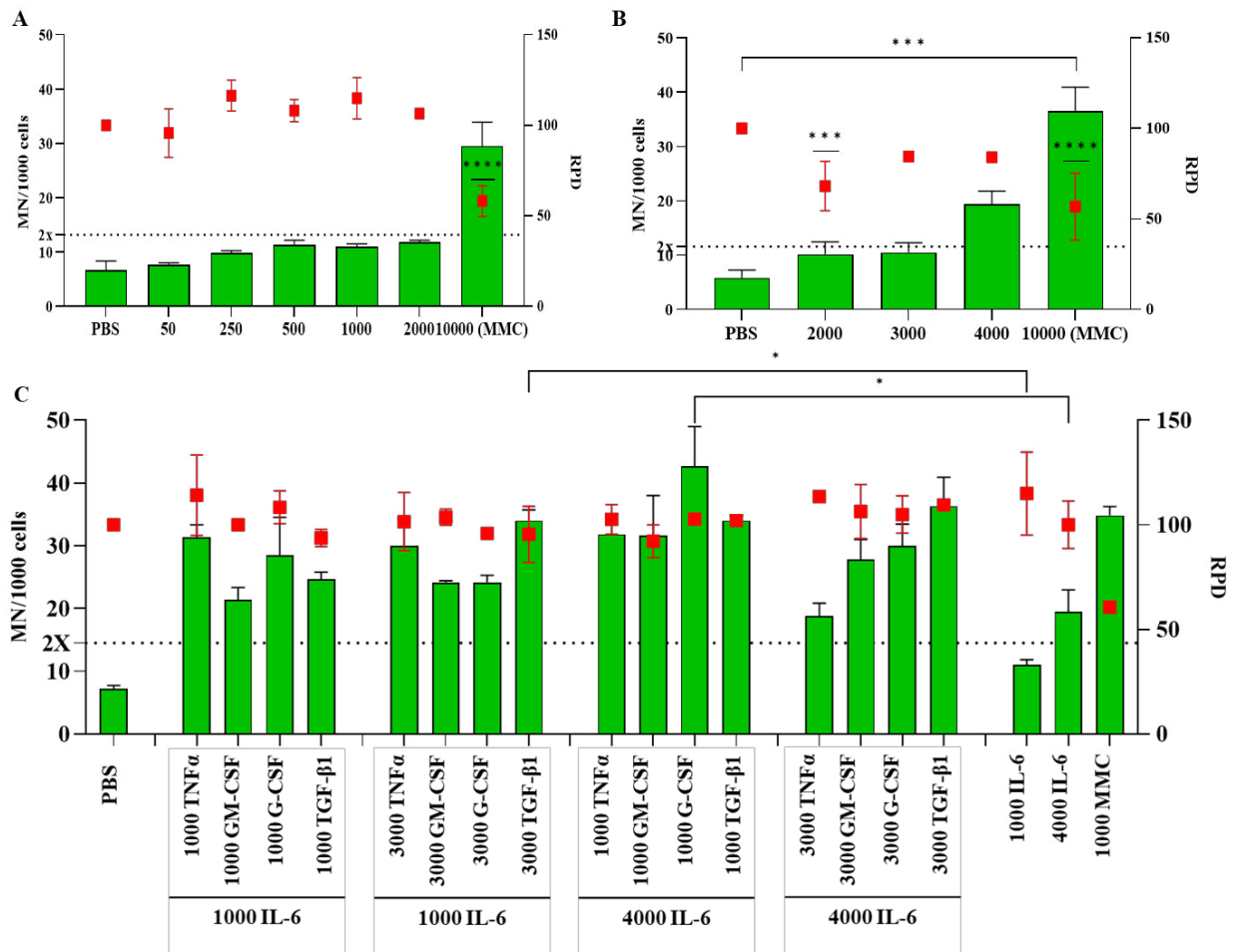


Figure 5.6. The induction of micronuclei in TK6 cells due to direct treatment of recombinant IL-6. (A) Healthy level treatments, (B) Storm level treatments, (C) Combination treatments. TK6 cells were cultured and treated with IL-6 at different concentrations following the standard micronucleus protocol. After a 24-hour recovery period, cells were harvested and evaluated for relative population doubling (RPD) and chromosomal damage by scoring the number of MN present. Mitomycin C (10 ng/ml; 30 nmol/L) served as the positive control, and PBS was used as the negative control in all experimental repeats. The data are presented as mean \pm SD (n=3), and significant differences are indicated as * $p \leq 0.05$, *** $p \leq 0.001$, and **** $p \leq 0.0001$, as determined by two-way ANOVA and Tukey's multiple comparisons test. Significant differences between MN and RPD are denoted with two distinct symbols.

5.3.2.4 GM-CSF recombinant treatments

TK6 treated with healthy doses of GM-CSF (Fig. 5.7A) showed increased RPD values above the PBS control. With the exception of the 250 pg/ml treatment, all the other RPDs were significantly higher than the PBS RPD. Whilst all doses at healthy levels showed slightly raised MN counts above the PBS control, none reached the 2-fold threshold increase and none were significantly different to the PBS control, except the MMC positive control.

Figure 5.7B demonstrates the GM-CSF treatments at storm levels and unlike the healthy dose treatments, the RPD dropped below the PBS control to about 77%. However, they were not significantly different due to wider error bars. All storm doses showed raised MN above the 1000 pg/ml (upper limit of healthy dose), but intriguingly only the intermediate doses of 2000 and 3000 pg/ml exceeded the 2-fold threshold, whereas the highest dose of 4000 pg/ml was almost the same as the 1000 pg/ml dose.

The combination treatments of GM-CSF with the other candidate cytokines were intriguing due to the number of significant differences in MN present (Fig. 5.7C). Except IL-6, all the other three cytokines at 1000 pg/ml with 1000 pg/ml of GM-CSF were significantly increased ($p < 0.01$) in comparison with GM-CSF alone at 1000 pg/ml. However, all cytokines at storm levels, except TGF- β 1, induced a statistically significant increase in MN when in combination with 1000 pg/ml GM-CSF. Only TGF- β 1 at 1000 pg/ml (healthy level) gave a statistically significant increase in MN formation when combined with storm levels of GM-CSF (3000 pg/ml; $p < 0.0001$).

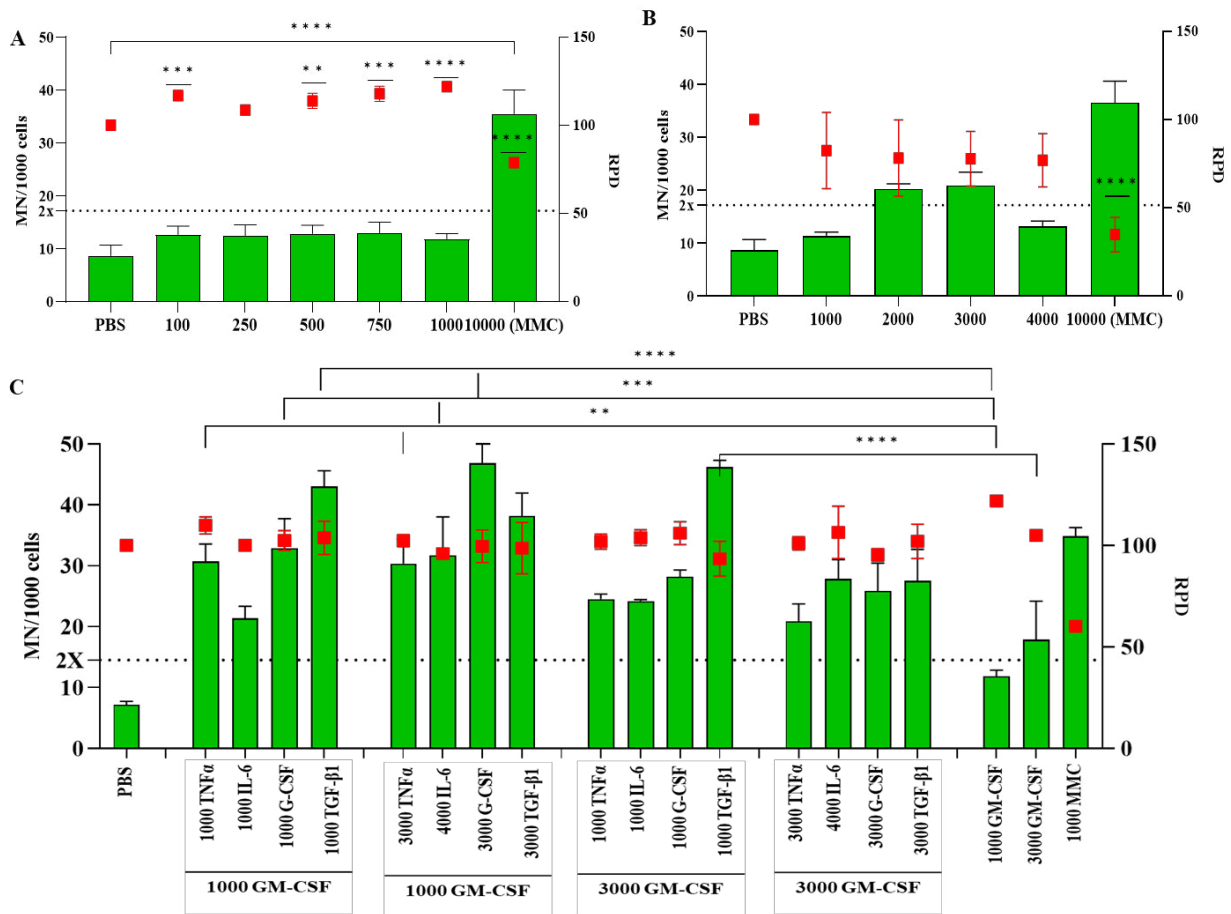


Figure 5. 7. The induction of micronuclei in TK6 cells due to direct treatment with recombinant GM-CSF at different concentrations (pg/ml). (A) Healthy level treatments, (B) Storm level treatments, (C) Combination treatments. TK6 cells were seeded at their seeding density, and after 24 hours, cells were treated with GM-CSF in isolation and combination in separate culture plates. Following a 24-hour recovery period, cells were harvested and evaluated for relative population doubling (RPD) before scoring micronuclei, as discussed in section 2.2.4. Mitomycin C (10 ng/ml; 30 nmol/L) served as the positive control, and PBS was the negative control. The data are presented as mean \pm SD (n=3), and significant differences are indicated as $**p \leq 0.01$, $***p \leq 0.001$, and $****p \leq 0.0001$, as determined by two-way ANOVA and Tukey's multiple comparisons test. On the graph, MN and RPD significant differences are denoted using two distinct symbols.

5.3.2.5 G-CSF recombinant treatments

The RPD values for the healthy G-CSF doses were similar to the PBS control in figure 5.8A. MN counts (~10 MN per 1000 mononucleated cells) were very close to the MN formation by the PBS control (9 MN per 1000 mononucleated cells), with only the 750 pg/ml dose having a small non-significant increase of 13 MN per 1000 mononucleated cells. MMC was significantly higher in MN and lower in RPD compared to PBS.

In figure 5.8B, storm concentrations of G-CSF, show RPD values similar to the PBS control and MMC was considerably lower. Doses of 3000 pg/ml and 4000 pg/ml showed approximately 2-fold increases in MN, whereas the 2000 pg/ml dose gave a 3-fold increase of MN compared to the PBS control. This outcome is intriguing as at storm levels (>2000 pg/ml), decreasing MN correlates with increasing dose.

When G-CSF was used in combination with the other candidate cytokines (Fig. 5.8C), even though all combinations exceeded the 2-fold higher MN than the PBS threshold, no other G-CSF combinations showed statistically significant differences when compared to their single G-CSF treatments. However, only 1000 pg/ml G-CSF with 4000 pg/ml IL-6 and 3000 pg/ml G-CSF with 1000 pg/ml GM-CSF were significantly different to the PBS control ($p < 0.05$). Even though most of the data for G-CSF are not statistically meaningful, there is a detectable increase in MN formation when the candidate cytokines are combined with G-CSF at both lower or higher concentrations.

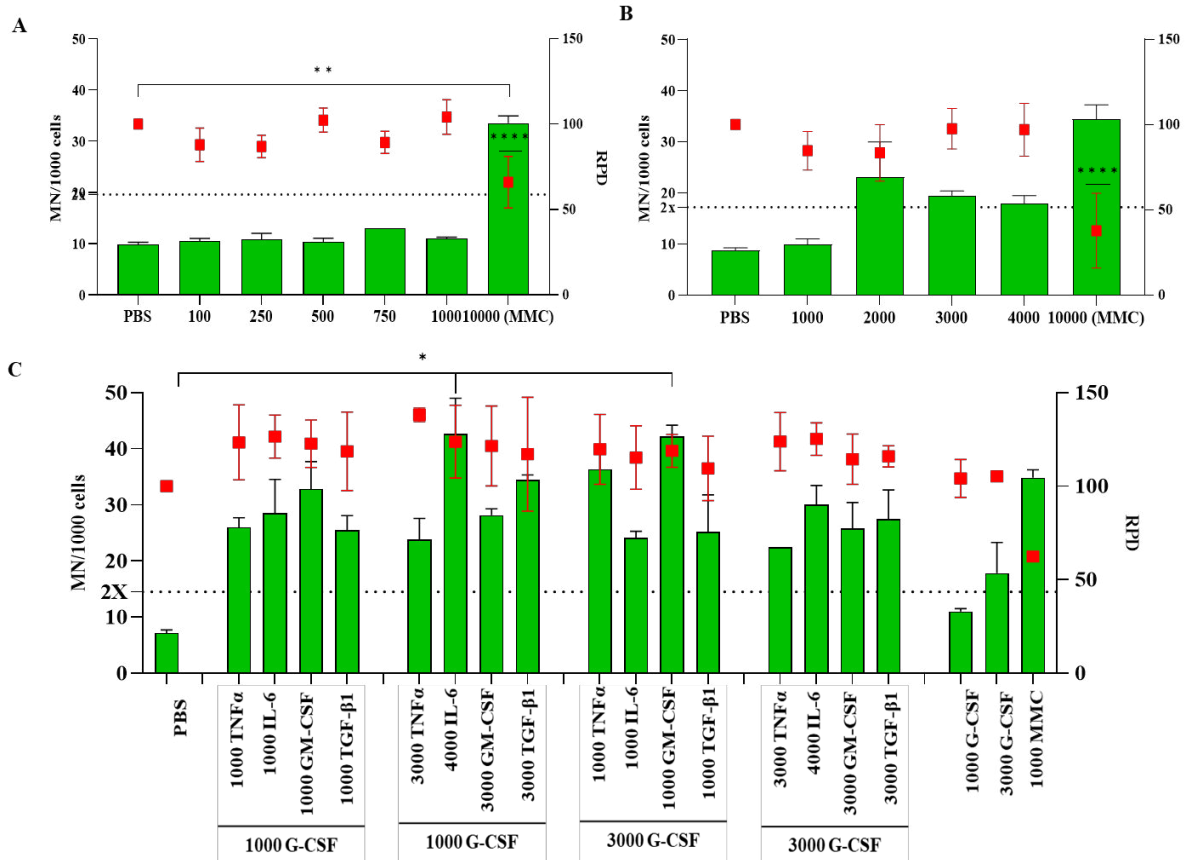


Figure 5. 8. The induction of micronuclei in TK6 cells due to direct treatment with recombinant G-CSF. (A) Healthy level treatments, (B) Storm level treatments, (C) Combination treatments. TK6 cells were treated with G-CSF at various concentrations at both healthy and storm levels, including combinations as described in table 2.2. The cells were incubated overnight for 24 hours, harvested, and assessed for relative population doubling (RPD) and chromosomal damage by scoring the number of micronuclei present. Mitomycin C (10 ng/ml; 30 nmol/L) served as the positive control, and PBS served as the negative control in all experimental repeats. The data are presented as mean \pm SD (n=3), with significant differences indicated as * $p \leq 0.05$, ** $p \leq 0.01$ and **** $p \leq 0.0001$, as determined by two-way ANOVA and Tukey's multiple comparisons test. Significant differences of MN and RPD are denoted with two distinct symbols.

5.3.3 Inhibition of IL-6 signalling pathways

IL-6 signalling pathways were blocked by FLLL-32 and BAY-293 with and without recombinant IL-6 cytokine treatment. The IL-6 recombinant dose utilised was 4000 pg/ml, as this dose generally produced higher MN counts in both single and combination treatments in this study (Fig 5.6).

5.3.3.1 Assessment of optimal inhibitor dosing

Recommended concentrations were taken from Selleckchem.com and literatures and the inhibition assay was performed as described in section 5.2.3.1. TK6 cells were assessed for toxicity via live cell count after treatment with a range of doses of the two inhibitors. Figure 5.9 shows the TK6 live cell count at different concentrations of FLLL-32 (Fig. 5.9A) and BAY-293 (Fig. 5.9 B).

In figure 5.9A, there was a slight dose dependent decrease in live cell count above 1.5 μM of FLLL-32, but these data were non-significant compared to the negative control. The recommended dose of 5 μM FLLL-32 resulted in a non-significant decrease in live cell count of $4.2 \times 10^5/\text{ml}$ compared to the untreated mean value ($5.6 \times 10^5/\text{ml}$). Considering the above viability data and supportive literatures (section 5.2.3.1), FLLL-32 at 5 μM was selected as the working concentration for the purpose of this research.

In figure 5.9B, BAY-293 significantly reduced TK6 live cell count in a dose dependent manner at doses of 5 μM and above. The untreated sample gave a mean value at $6 \times 10^5/\text{ml}$ which is consistent with the data for the control during FLLL-32 testing. Doses of 5 μM and above resulted in statistically significant reductions in cell counts, confirming cytotoxicity to TK6 cells at these doses. Cell counts for the 1 μM and 2.5 μM treated samples had total live cell mean at $5.2 \times 10^5/\text{ml}$ and $5.1 \times 10^5/\text{ml}$, which is closer to the untreated sample. Although the recommended dose from Selleckchem.com was 0.021 μM , this study opted for a concentration of 2 μM for BAY-293. This decision was informed by the successful inhibition results reported in the literature on BAY-293 (section 5.4), validating the use of the higher concentration with the best viability.

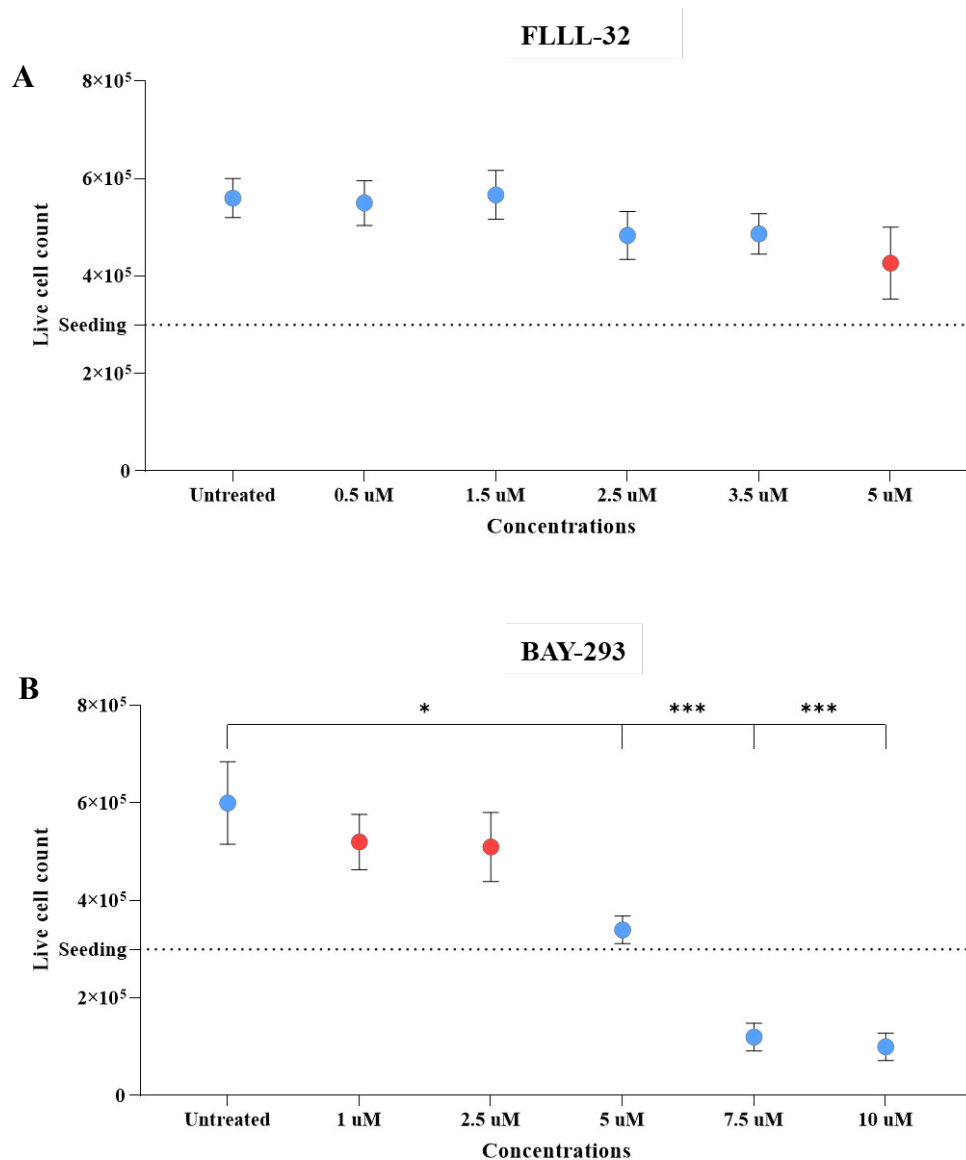


Figure 5. 9. TK6 cell counts following IL-6 pathway inhibitor treatment; FLLL-32 and BAY-293. TK6 cells were cultured and treated with (A) FLLL-32 and (B) BAY-293 inhibitors at a range of doses. Following 24 hours incubation in 5% CO₂, the live cell counts were analysed to determine toxicity caused by the inhibitor alone. Red dots in each graphs indicates the selected working concentration for each inhibitor; FLLL-32 at 5 µM and BAY-293 at 2 µM (between 1 - 2.5 µM). Data shows the mean ± SD (n=3) and significant differences shown as *p ≤ 0.05, and ***p ≤ 0.001 as analysed using student T-test.

5.3.3.2 Cytotoxicity assessment

After treating the TK6 cells with IL-6 pathway inhibitors and IL-6 recombinant cytokine, TK6 RPD count was determined before scoring MN to make sure there was not excessive cell death caused by the inhibitors alone or in combination with IL-6. Figure 5.10 shows the RPD (red square) after the recovery period of inhibitor treatments.

The IL-6 alone treated TK6 sample exhibited the highest RPD at 110%, while the lowest RPD value was observed in TK6 cells treated with a combination of both inhibitors, showing a significant reduction to 49.7% ($p \leq 0.0001$). Notably, the RPD values for samples treated with each inhibitor separately were also significantly lower than the negative control (PBS) but remained above the 50% threshold ($p \leq 0.05$; FLLL-32 and $p \leq 0.01$; BAY-293). In comparison to samples treated with the inhibitor/s individually, RPD levels were non-significantly higher in samples treated with a combination of IL-6 and inhibitor/s. Despite the RPD levels falling below the 50% limit for samples treated with combination inhibitors, the analysis for MN detection can still be conducted considering the \pm SD. Consequently, all the abovementioned samples were analysed for MN to assess whether there are any differences in MN frequency compared to IL-6 alone, and with reference to the IL-6 treated MN results in section 5.3.2.3.

5.3.3.3 Micronucleus assay

After taking enough TK6 cells per slide (2×10^4), the MN assay was performed as described in section 2.2.4.2. Figure 5.10 (green bars) demonstrates MN formation in TK6 cells following treatment with chemical inhibitors, both individually and in combination, with and without IL-6 recombinant cytokine. The MN analysis, depicted in the figure with various arrowheads, highlights substantial differences at different levels of p-values among various treatments and combinations.

All IL-6 treated samples exhibited higher MN formation compared to the PBS control, with the IL-6 alone sample aligning with the data presented earlier for IL-6 storm treatments (Fig. 5.6). The PBS negative control demonstrated the lowest MN formation, with a mean of 9.6 MN/1000 cells, validating historical MN data presented in section 5.3.2.3. In contrast, TK6 cells treated with a combination of inhibitors and IL-6 recombinant showed the highest MN formation, with a mean of 28.

The MN induction in samples treated with IL-6 ($p \leq 0.05$), IL-6 with inhibitors (FLLL-32; $p \leq 0.001$ and BAY-293; $p \leq 0.0001$), and a combination of inhibitors ($p \leq 0.05$) was significantly higher than the MN formation in PBS-treated samples, with different p-values.

Furthermore, samples treated with IL-6 in combination with BAY-293 ($p \leq 0.05$) exhibited significantly higher MN compared with the corresponding sample without inhibitor. Additionally, the combination of inhibitors with IL-6 showed the highest MN value, significantly higher at $p \leq 0.001$ than samples treated with the inhibitor alone without IL-6.

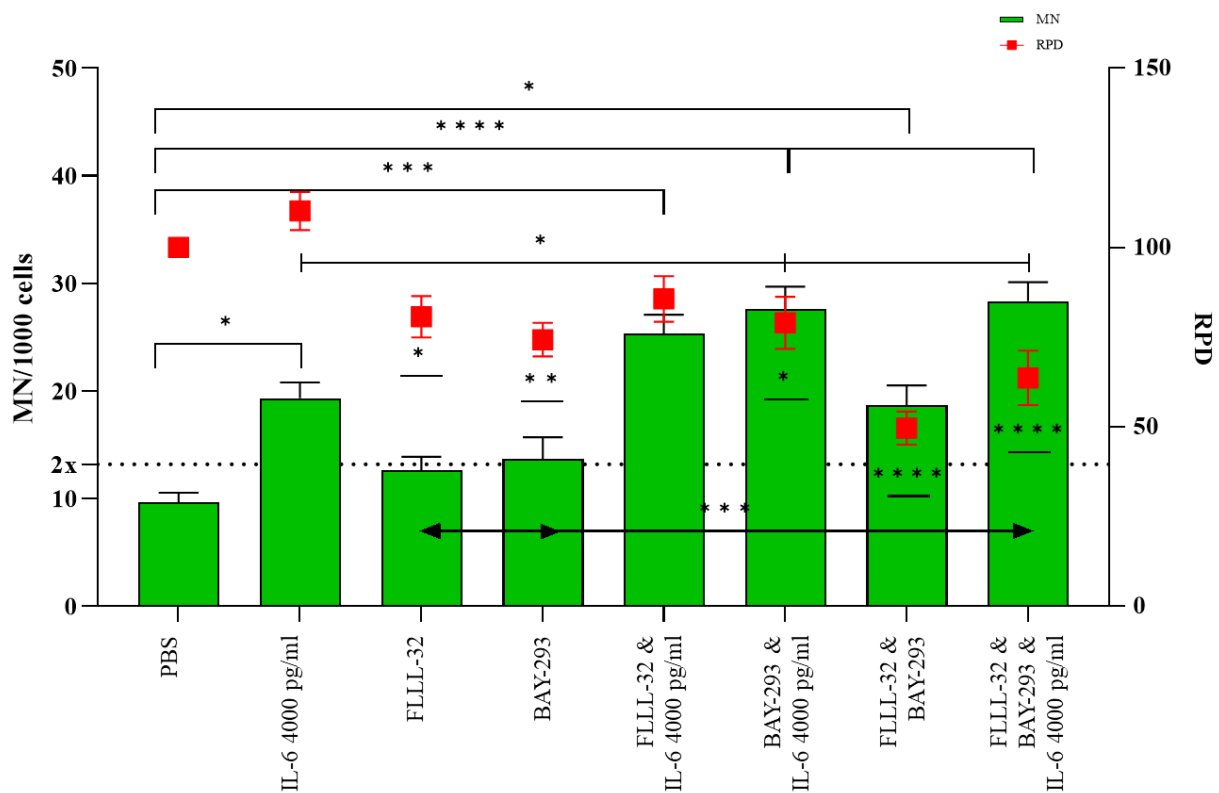


Figure 5. 10. Micronuclei in TK6 treated IL-6 signalling pathway inhibitors. TK6 cells were cultured at 1.5×10^5 /ml in 12-well plate a day before the treatment with FLLL-32 and BAY-293 inhibitors at their respective doses. Following 2 hours incubation, 4000 pg/ml of IL-6 was added to the relevant wells. Cells were incubated for 24 hours, and live cell counts were analysed using an automated cell counter. After determining the cell RPD, the MN assay was performed with each sample. Data shows the mean \pm SD ($n=3$) and significant difference shown as * $p \leq 0.05$, ** $p \leq 0.01$, *** $p \leq 0.001$ and **** $p \leq 0.0001$ as determined by one-way ANOVA, Tukey's multiple comparisons test.

5.4 Discussion

It is well established that BM-MSCs produce various cytokines which can maintain the HSC's survival, quiescence and self-renewal and provide the crosstalk between BM stroma and haematopoietic progenitors for better engraftment (Asada *et al.*, 2017; Kemp *et al.*, 2010; Kemp *et al.*, 2011; Yin & Li, 2006). In evidence of the cancer therapy potential mechanisms, the overproduction of cytokines involves communicating through the extracellular medium or gap junctions (Song *et al.*, 2016). Following numerous drug treatments, cytokines are involved in the transformation of malignant HSC precursor leukaemia stem cells related to changes in the BM environmental conditions (Catacchio *et al.*, 2013). Some studies showed that irradiated BM stromal cells released cytokines and induced GM-CSF/G-CSF dependent cell transformation, increasing the radiation-induced AML incidence *in vitro* and controlled *in vivo* studies (McCann & Wright, 2003).

However, some studies give evidence for genotoxicity by cytokines even though the mechanism is still yet to be discovered. Generally, cytokine genotoxicity has been established to originate through the immune system, the inflammatory processes, and the role of neighbouring cells, such as macrophages, as a potent source of ROS production. Clearly, within *in vivo* or *in vitro* studies utilising complex mixtures of immune cells as would be expected for cytokine research, the indirect activity of released ROS cannot be ignored and likely plays an important role in genotoxic endpoints. Even though there is very limited published information, these literatures support the fact that cytokines can induce direct genotoxicity within *in vitro* studies (Song *et al.*, 2016; Barcellos-Hoff *et al.*, 2005; McCann & Wright, 2003; Lazutka, 1996; Morgan, 2003).

Therefore, this research attempted to answer the question by directly exposing an *in vitro* TK6 model to the candidate cytokines selected from cytokine array (section 4.3.1) in the absence of an immune cell environment, to explore a possible direct genotoxic activity of these candidates. It is of note that TK6 is a B lymphoblastoid cell line, which might also express cytokines, however such secretion has not been fully elucidated by the literature to date. Limited data shows that secretion of IL-29, LIF, IFN- γ and TNFSF4 can be produced by TK6 cells (Glover *et al.*, 2015). However, for the first time, as a part of this research, TK6 expression of TNF- α , TGF- β 1, IL-6, GM-CSF and G-CSF were quantified using the ELISA assay in section 4.3.2. The study employed the *in vitro* MN assay to assess the direct genotoxic effects of

cytokines, which is a well-established technique for the detection of both clastogenic and aneugenic chromosomal mutations that are passed on to daughter cells during the process of cell division (Sommer *et al.*, 2020).

Figures 5.4 to 5.8 exhibit the cytotoxicity and genotoxicity data from each cytokine with MMC as the positive control and PBS as the negative control. MMC demonstrated consistently lower cell viability compared to the negative control in all assays involving healthy level and storm level cytokine treatments, with the exception of the TGF- β 1 healthy level treated graph (Fig. 5.5A). This decrease in cell viability aligns with the cytotoxic function of MMC described in the literature (section 1.6.3.2).

Among the cytokines tested, TNF- α displayed dose-dependent cell death under healthy level treatments (Fig. 5.4A), with a more pronounced effect observed during storm level treatments (Fig. 5.4B), resulting in significantly lower RPD values. This observation underscores the cytotoxicity and apoptotic functions of TNF- α at higher dosages, as discussed in section 5.1. In contrast to TNF- α , other cytokines exhibited relatively similar RPD levels across their treatment doses at healthy levels. Notably, TGF- β 1 and IL-6, under healthy treatments, demonstrated cell proliferation with increasing dosage, supporting the notion that cytokines play a role in cell survival and proliferation (Yin & Li, 2006). Contrary to the findings of Iyer and Lehnert (2000), which indicated a pro-mitogenic effect at low concentrations of TGF- β 1 and inhibitory effects at high concentrations, this research observed relatively high viability in TK6 samples treated with TGF- β 1 storm levels. GM-CSF healthy levels showed significant cell proliferation relative to PBS, but surprisingly storm level treatments showed some cell death, contrary to the expected role of this cytokine in promoting cell proliferation. However, during both healthy and storm level individual treatments, the viability of TK6 cells remained above the 50% threshold, as might be expected for natural biological molecules. Nonetheless, the overall cell viability during cytokine combination treatment was comparable to the PBS control, with some exceptional combinations in IL-6, GM-CSF, and G-CSF demonstrating higher cell viability than the PBS sample. This occurrence could be attributed to the synergistic induction of cell proliferation by the combination of other cytokines, as described in the cytokine function table 4.1 in section 4.3.1.5. As anticipated, MMC consistently exhibited the lowest RPD value in all the combination treatments across the five cytokines.

Maintaining robust viability in all the healthy level treatments, storm level and combinations of two cytokines at their highest storm levels is a crucial observation. Notably, some combinations even exhibited superior cell viability, greater than the PBS control. This highlights a critical consideration regarding the genotoxicity of these cytokines, both in isolation and in combination, as DNA damage is only evident in living cells. Consequently, there is a potential risk of sustained proliferation with damaged DNA, which could contribute to the inheritance of genotoxic lesions in daughter cells. Therefore, a comprehensive analysis of their MN data is imperative to assess the extent of genotoxic effects.

Lazutka (1996) conducted an extensive study on the genotoxic effects of cytokines, demonstrating that IFN- α / β / γ , TNF- α , and IL-2 can induce chromosome aberrations, MN and SCE in human peripheral blood lymphocyte cultures. Notably, with the exception of IL-2, a dose-dependent relationship was observed between the cytokine dosage and the frequency of SCE. A study by Sica & Bronte, (2007) showed that TNF- α , IL-6 and IL-12 support tumour growth with the help of the immunosuppressive cytokines TGF- β , IL-10, and ARG1 released by macrophages. Furthermore, there is currently controversy over the use of G-CSF in mobilising HSC from donors for subsequent transplantation, with some asserting that G-CSF has the capacity to induce haematological malignancy in the donor (Avalos *et al.*, 2011); however, the cytokine genotoxicity topic is still widely debated and difficult to understand. Even though the generation of free radicals or interactions with enzymes such as DNA topoisomerase-II are suspected to be involved, the precise mechanisms underlying these genotoxic actions remain largely elusive. Despite utilising human peripheral blood lymphocyte cultures in many studies, the observed genotoxic effects could originate from various cellular components, necessitating further investigation.

Although the MN assay is well-suited for identifying both aneugenic and clastogenic changes in DNA, this study did not extend to such analyses due to time constraints. Consequently, there is a paucity of data regarding whether any cytokines exhibit a preference for inducing aneugenic or clastogenic effects. Future studies employing FISH analysis could shed light on this aspect, as well as elucidate the specific mutation types induced by cytokines. This avenue of research gains significance as studies on DCL have documented frequent cytogenetic abnormalities, including the entire or partial loss of chromosomes 5 and/or 7 (Suárez-González *et al.*, 2018; Flynn & Kaufman, 2007), underscoring the potential importance of comprehending the role of cytokines in DCL pathogenesis.

In line with historical laboratory data reported by Vernon *et al.* (2022), MN scoring for the PBS and MMC controls employed in this study remained consistent. MMC was consistent throughout as a positive control and showed the highest MN level in all experiments, except in a few cases of cytokine combinations. With the exception of MMC, there was no statistically significant rise in MN counts compared to PBS in any of the single cytokine treatments for both healthy and storm level treated TK6 cells.

Utilising recorded concentrations from healthy individuals, these data supported the expected safety of IL-6, G-CSF, and GM-CSF, whereas TNF- α and TGF- β 1 had the capacity to non-significantly increase MN levels more than twice the untreated control at healthy levels. These findings align with the TNF- α genotoxicity study in mice conducted by Westbrook *et al.* (2012). The proposition of TNF- α interacting with DNA topoisomerase, as suggested by Lazutka (1996), may provide an explanation for the genetic effects induced by TNF- α . Notably, TGF- β 1 emerges as a significant player in regulating cellular apoptosis and proliferation. Therefore, if TGF- β 1 exhibits potential genotoxicity even at the lowest level (1000 pg/ml), there is a considerable risk of sustained proliferation of genotoxic (mutated) cells within the system following exposure to chemotherapy.

Importantly GM-CSF and G-CSF are myeloid development cytokines, and recombinant G-CSF alone or in combination with GM-CSF are used as stimulating factors to mobilise the donor HSC from the BM to the peripheral blood during HSCT (section 1.3) (Antin & Raley, 2013; Zhang *et al.*, 2019). However, significant considerations have been associated with G-CSF genotoxicity in the literature.

At the highest storm levels (2000–4000 pg/ml) both GM-CSF and G-CSF tend to increase the MN expression more than 3-fold above the PBS control. Therefore, this is an exciting point to follow up with more research to find out how these cytokines might affect the donor if both G-CSF and GM-CSF can cause MN at higher dosage/storm levels. However, the study of Filgrastim (recombinant G-CSF) by Petros *et al.* (1997) noted that some patients with high serum G-CSF have severe toxicities even though the dose they used is 400 times higher than storm dose used in this research. So, this G-CSF MN data supports the controversy over the use of high-dose G-CSF in donors. This might infer that the mobilisation in the donor might be more important than storm in the patient in the aetiology of post-transplant complications or might exacerbate the storm outcomes following HSCT. It is interesting that one study found

preferential proliferation of cultured cells with monosomy 7 after G-CSF therapy, with remission in some cases following G-CSF withdrawal (Sloand *et al.*, 2006). Of the reported DCLs, a highly frequent cytogenetic abnormality is chromosome 7 abnormalities (monosomy 7 and deletion of 7q). The appearance of transient monosomy 7 early after engraftment emphasises the relevance of early clonal dominance in the regenerating marrow that is responsive to many extrinsic and environmental cues, including growth factors, immunomodulation and a heavily pre-treated marrow microenvironment (Ma & Liu, 2016; Wiseman, 2011).

Interestingly, out of the analysed candidates, IL-6 (4000 pg/ml) and TGF- β 1 (2000 pg/ml) at their storm level concentrations showed increased MN formation more than 3-fold the MN for PBS. Even though IL-6 is a key player in many inflammatory associated complications and in tumour development, there has previously not been direct evidence to suggest that it is directly genotoxic. Ewan *et al.* (2002) showed the decreased p53 phosphorylation in irradiated mammary glands in TGF- β 1 depleted cells, suggesting that TGF- β 1 should be considered as a key regulator of genomic integrity. Indeed, the literature highlights post-transplant complications and has correlated transplant rejection with TGF- β 1 polymorphism (Bidwell *et al.*, 1999; Girnita *et al.*, 2008) indicating the need for further study of TGF- β 1 secretion related to genetic profiles for individuals. However, of note is that this research model was run without an immune system environment, so there must be less of a genotoxic effect during the *in vivo* setting, otherwise every patient who is has a cytokine storm due to different conditions will get genotoxicity and end up with cancer.

Individual treatments showed which cytokines might be more important in genotoxicity and at what concentrations. Patients have a heterogeneity of cytokine expression after cancer therapy, which is well-established as a 'cytokine storm' or 'cytokine release syndrome' (Dickinson & Charron, 2005; Morgan *et al.*, 2010; Melenhorst *et al.*, 2012). By knowing that cytokines can work as autocrine, paracrine or in synergy *in vivo*, there may be inhibition or potentiation of each other with respect to functional activity and/or genotoxicity. Therefore, it is very important to take into consideration combinations of cytokines (at least two together) at storm doses to determine potentiation of each other.

It is noted that *in vivo*, patients exposed to drugs produce a cytokine response which can vary depending on the genetic polymorphisms within their respective genes; with some cytokines

expressed at higher levels, and others at lower levels of the normal healthy range depending on what polymorphisms are carried by the individual. Similarly, these individuals tend to reflect higher and lower levels of secretion in response to a stimulus (e.g. drugs and in response to infection), with individuals showing a more pro- or anti-inflammatory profile depending on the combination of genetic polymorphisms. When determining concentrations for combination treatment based on above doses, consideration was applied to higher healthy level (the dose overlapping with the storm) and 'storm' levels which produced at least 2-fold increase in MN counts compared to PBS. The selection of these doses also prioritised good viability to mitigate the potential risks of cytotoxicity during combination treatment. For instance, IL-6 combination doses considered were 2000 pg/ml and 4000 pg/ml, but 2000 pg/ml exhibited the lowest RPD in storm level treatments (Fig. 5.6B). Consequently, for cytokine combination dosages, TNF- α , GM-CSF, G-CSF, and TGF- β 1 were utilised at 1000 pg/ml and 3000 pg/ml, while IL-6 was administered at selected doses of 1000 pg/ml and 4000 pg/ml, as indicated in table 2.2.

From figure 5.4C to 5.8C demonstrates an increased MN in TK6 following exposure to paired cytokines at high baseline and high storm dosage levels. Despite some instances of reduced cell viability at higher concentration levels, all cytokine combinations maintained viability above the 50% threshold including MMC. Remarkably, with the exception of a minor decrease in viability observed at the 1000 pg/ml treatment, the RPD values for all TNF- α combinations closely resembled those of PBS. This starkly contrasts with the cell viability observed in healthy and storm level treatments when TNF- α was administered in isolation where there was a noticeable dose-dependent cytotoxicity (Fig. 5.4A) and cell death (Fig. 5.4B). In the case of IL-6 and TGF- β 1 combinations, cell viability remained comparable to PBS treatment, contrary to their performance at healthy level treatments (Fig. 5.5A and 5.6A), where higher RPD values were evident, supporting the idea that IL-6 and TGF- β 1 can enhance cell proliferation and viability when administered individually. Conversely, GM-CSF and G-CSF combinations exhibited cell viability similar to PBS, aligning with RPD values for single exposure at both healthy and storm level treatments. The observed differences in cell viability between single and combination treatments suggest a synergistic activity among cytokines in combination, potentially regulating cell proliferation and differentiation, as discussed in Ruiz-Argüelles *et al.* (2007) and Pixley & Stanley (2010).

As the majority of the RPD values increased in combination treatments, MN were also induced during combination treatment compared to the individual treatments of each cytokine at both healthy and storm doses. However, a notable exception was identified with TNF- α at 3000 pg/ml, where the inclusion of the other four cytokines at their high doses led to a decrease in the MN count below that observed with TNF- α in isolation (Fig. 5.4C). Each combination induced MN counts that were above twice the value of PBS. It is noteworthy that four out of the five cytokines significantly elevated the MN count above that of at least one isolation treatment, with some combinations displaying greater genotoxicity (supported by better RPD) than the genotoxic positive control MMC in certain instances.

Interpreting the combination data becomes intricate given the numerous combination groups and various comparisons, including statistical differences, as well as the capacity for cytokines to be additive or potentiate MN induction. To aid in comprehending the discussion based on 'MN addition or potentiation,' refer to the table presented in appendix III, which was done for assessing the capacity of the cytokines to be additive or to potentiate the induction of MN when they are used in combination compared to in isolation.

Even though, all combinations demonstrated their involvement in inducing MN, even at lower doses of the combined cytokines (Fig. 5.4C to 5.8C), in most instances, combinations at their highest doses appeared to reduce MN production compared to other combinations. As indicated by the 'MN addition or potentiate' analysis in appendix III, MN formation in most combinations was lower than the addition of the MN for each cytokine when used in isolation. Furthermore, the majority of potentiation combinations occurred when a low storm level was combined with the low storm level of another cytokine. Intriguingly, no potentiation occurred when any cytokines were combined at high doses for both (Appendix III table). This implies an inhibition feedback loop or potential protective mechanism(s) during the consequences of a cytokine storm, providing insight into why individuals who survive from cytokine storms may encounter an increased risk of tumorigenesis. Nonetheless, the variability in outcomes among individuals could be linked to inter-individual variations.

Comparing with the respective cytokine administered in isolation, TNF- α , IL-6, GM-CSF, and TGF- β 1 exhibited statistically increased MN counts in certain combinations. On a broader scale, most of these combinations did not demonstrate an additive or potentiating effect on MN counts in combination compared to their individual MN counts. Two combinations involving

GM-CSF at 1000 pg/ml with 3000 pg/ml TNF- α and 4000 pg/ml IL-6, showed an additive effect with IL-6 and protective effect with TNF- α on MN counts in combination. Among the cytokines, GM-CSF, G-CSF, and TGF- β 1 showed the most synergistic events in inducing MN, each having six synergistic/potential events out of the 16 paired events. TNF- α and IL-6 both exhibited four synergistic events each (statistically different outcomes in the Fig 5.4C).

Additionally, two out of the 16 events were additive for IL-6 at 4000 pg/ml (with 1000 pg/ml GM-CSF and 3000 pg/ml TGF- β 1), while TNF- α , G-CSF, and TGF- β 1 each had one additive event. Interestingly, out of these synergistic and additive combinations, all the remaining paired events resulted in non-additive (reduced) MN counts compared to the individual MN counts. Consequently, there appears to be a delicate balance between strongly genotoxic events (exceeding those induced by MMC), with an overarching trend indicating a collective 'reduction' (non-additive) in MN counts when cytokines were used in combination.

Adding complexity to the above observations, recent studies by Decout *et al.* (2021), have shed light on the role of the cGAS-STING pathway, where disruption of the MN membrane during interphase results in the release of DNA fragments and the release of IFNs, potentially contributing to overall genotoxicity, as discussed by Fenech *et al.* (2020). If IFNs are shown to further potentiate the observations seen in this study, it could introduce an additional layer of complexity. While there is limited literature on cytokine secretion from TK6 cells, Glover *et al.* (2015) detected IFN- γ release from TK6 cells 24 hours after exposure to UVC light and 12-O-tetradecanoylphorbol-13-acetate (TPA). IFNs have been associated with genotoxicity, as noted by Lazutka *et al.* (1996), which might have contributed to the observed genotoxicity in the current study.

Although the presented data suggests that, overall, cytokine combinations exhibit less synergism and more additivity, it is possible that more intricate combinations could further complicate the picture. It's important to note that the model used operates in the absence of an immune system, so *in vivo*, detoxification processes may counteract some of the MN events observed; otherwise, one might expect all cytokine storm patients to develop further malignancies like DCL, which is not observed according to Suárez-González *et al.* (2018). On the contrary, an alternative perspective suggests that if it can be demonstrated that each of these cytokines individually exhibits genotoxic effects and also promotes genotoxicity through

immune cells, the combined effect *in vivo* may involve synergism, potentially leading to increased complexities and a higher likelihood of inducing malignancies.

Due to the intricacies of intracellular communication and the crosstalk among cytokines, understanding how and why these cytokines induce genotoxicity becomes challenging. However, the fact that these cytokines can either potentiate or inhibit MN induction in combination suggests the existence of signalling processes that can be activated when either one or both cytokines are present. It is proposed that elevated levels of some cytokines are also associated with maintaining cancers through different signalling pathways; JAK/STAT-3 and the RAS/Erk/C/EBP (Neurath & Finotto, 2011; Bill *et al.*, 2010) which trigger the transcription factors NF- κ B, JAK3, STAT1, JNK in cancer cells (Sica & Bronte, 2007) and contribute to the cells' proliferation and survival (Langowski *et al.*, 2006). IL-6–JAK/STAT3 signalling is a major intrinsic pathway for cancer inflammation due to its capability of inducing many genes that are crucial for inflammation (Yu *et al.*, 2009). Therefore, it is believed that gaining insights into cell communication and signalling pathways could provide additional evidence of cascade that occurs after exposure to these cytokines. Numerous studies provide support for the idea that knockdown, or antibody neutralization of these cytokines can modulate signalling pathways, subsequently exerting negative effects on tumour surveillance, altering mutation frequency, and reducing tumour growth (Langowski *et al.*, 2006; Masjedi *et al.*, 2020). Thus, blocking these cytokine activities, either by antibodies or specific inhibitors, may open novel therapeutic opportunities and this has yet to be demonstrated.

Based on the cytokine array data (section 4.3.1), IL-6 emerged as the highest cytokine secreted by HS-5 in untreated cultures, and this trend persisted following exposure to both chemotherapies. The subsequent array validation ELISA assay (section 4.3.2) further confirmed that the expression of IL-6 by HS-5 was notably higher, with a significant increase observed after treatment with CHL and MTX compared to other cytokines. Consequently, confirming knockdown with IL-6 appears more feasible than with the other cytokines.

Moreover, the expression of IL-6 by untreated TK6 cells was significantly lower ($p \leq 0.01$, section 4.3.2.3) compared to HS-5 untreated cells. This observation lends support to the notion that if IL-6 plays a role in the bystander effect in TK6 cells co-cultured with HS-5, the primary source of IL-6 is likely HS-5, not TK6. MN results in this chapter also support IL-6 as a key candidate with more than a 2-fold increase in MN production at storm levels and in

combination demonstrated a significantly increased MN formation compared to IL-6 single treatments ($p \leq 0.05$). Considering all these reflections, IL-6 has been chosen to advance for further analysis of genotoxicity in signalling pathway inhibition and knockdown in bystander models (chapter 6).

IL-6 can activate several pathways including JAK/STAT, RAS/MAPK, PI3K/AKT and MEK-ERK5, which are involved in controlling cell activation, proliferation, differentiation, and cell death/ apoptosis. As explained in section 5.1, the main focus was on JAK/STAT and RAS pathways to explore the involvement of IL-6 signalling in MN formation during IL-6 treatments. The IL-6/JAK/STAT3 signalling pathway represents an intrinsic pathway that orchestrates the expression of genes involved in proinflammation, apoptosis resistance, metastasis (Ferraz *et al.*, 2017; Manore *et al.*, 2022) and major role in cancer inflammation (Yu *et al.*, 2009). *In vivo* studies have indicated that IL-6/STAT3 siRNA knockdown inhibits cancer cell progression, angiogenesis, and migration, with *in vitro* observations showing reduced expression of IL-6 levels, STAT3, and mRNAs in breast cancer and melanoma cell lines (Masjedi *et al.*, 2020). On the other hand, the RAS/MAPK pathway can stimulate angiogenesis and tumorigenesis. Abnormal expression of RAS pathway proteins has been identified in various human cancers (Thatcher, 2010; Guo *et al.*, 2020).

There are several strategies for STAT3 inhibition, including blocking STAT3 phosphorylation, dimerisation and DNA binding. Inhibitors interacting with the STAT3 protein SH-2 domain, block the dimerisation and mobilisation to the cell nucleus and, consequently, block the DNA binding ability as a transcription factor (Ferraz *et al.*, 2017). In this study, FLLL-32 was employed to inhibit the JAK/STAT pathway, which is a curcumin analogue acting in part through direct inhibition of STAT3 phosphorylation and DNA binding through interaction with its SH2 domain critical for dimerisation (Fossey *et al.*, 2011). While there is limited research on IL-6 signalling-induced RAS/MAPK pathway inhibition, novel SOS1-directed inhibitors offer a broader anticancer coverage by impeding k-RAS through hindering SOS1-k-RAS interactions (Plangger *et al.*, 2022; Swiatnicki *et al.*, 2022). In this study, BAY-293 was utilised as an active inhibitor for RAS pathway signalling, disrupting the interaction between the RAS GTPase and its nucleotide exchange factor SOS1 (Plangger *et al.*, 2021). BAY-293 has demonstrated efficacy in targeting both wild-type and mutant k-RAS-SOS1 interactions (Bruggemann *et al.*, 2023).

These inhibitors are mostly used to kill the tumour or cancer cells *in vitro* and *in vivo* by blocking the essential signalling pathways for cell survival. Thus, it is very important to use optimum concentrations of the inhibitor which can block the respective signalling pathways but keep the cell alive. Consequently, by looking at the various literature and manufacturer recommendations, a dose optimisation viability assay was performed with the TK6 cell line. Most of the cell lines utilised in the literature are compatible with TK6 and may be used to test genotoxicity because they are p53 competent (Balcer-Kubiczek *et al.*, 1995). Thus, in the present study, FLLL-32 was tested from 0.5 to 5 μM and BAY-293 was tested from 1 to 10 μM in the TK6 cell line, in order to provide a greater range of safety in the risk assessment.

Although a slight difference in live cell numbers was evident between FLLL-32 treated and untreated TK6 cells (Fig. 5.9A), these variations were not statistically significant across all samples. Notably, cells treated with lower concentrations (0.5 μM and 1.5 μM) did not exhibit substantially different live cell counts compared to the untreated sample. This observation aligns with the findings of Su *et al.* (2021), who reported high cell viability at lower levels of FLLL-32. Conversely, studies on oral cancer cells indicated that treatment with overdose (>8 μM) of FLLL-32 significantly suppressed cell growth, viabilities, and induced G2/M phase arrest (Su *et al.*, 2021).

In hepatocellular cancer cell studies, Liu *et al.* (2010) demonstrated that 10 μM FLLL-32 promoted apoptosis alongside the downregulation of IL-6-induced STAT3 phosphorylation. Additionally, osteosarcoma cell line treatments with FLLL-32 at 7.5 μM resulted in significant decreases in proliferation and increased apoptotic markers (Fossey *et al.*, 2011). However, Bill *et al.* (2010) found that FLLL-32 at 8–10 μM did not cause cell death in PBMCs or NK cells but effectively inhibited IL-6-induced STAT3 phosphorylation. Furthermore, Lin *et al.* (2010) reported that the IC₅₀ of FLLL-32 was greater than 100 μM .

Given the variation in concentrations across different studies and cell cultures, it is reasonable to select a lower concentration of FLLL-32 that is still effective in inhibiting the IL-6 signalling pathway. Considering the supportive information about lower cell deaths but higher JAK/STAT pathway inhibitions in the literature and following the manufacturer's recommendations, 5 μM was chosen as the working concentration of FLLL-32 for this study. Additionally, evidence from Lin *et al.* (2010) supports the notion that 5 μM of FLLL-32 can significantly inhibit JAK2 kinase activity and decrease pSTAT.

Figure 5.9B depicts the cell viability of TK6 after treatment with varying concentrations of BAY-293, selected from multiple studies (Plangger *et al.*, 2021; Plangger *et al.*, 2022; Swiatnicki *et al.*, 2022). Untreated samples maintained their regular doubling rate with optimal live cell counts. Doses ≥ 5 μM of BAY-293 resulted in significant cell death, reflecting the antiproliferative effect of the inhibitor (Plangger *et al.*, 2021). Thus, doses ≥ 5 μM were excluded to ensure sufficient live cells for MN assays. Concentrations between 1–2.5 μM showed similar mean live cell counts to the untreated, and doses around 2–3 μM align with IC50 levels reported by Plangger *et al.* (2022) for SOS1 and MEK inhibition in RAS pathways. Additionally, IC50 values ranging from 1.7 to 3.7 μM were reported for the cytotoxic activity of BAY-293 in lung cancer cell lines (Plangger *et al.*, 2021). Considering the results in figure 5.9B and information in the literature, a working concentration of 2 μM for BAY-293 was chosen for this research.

After confirming the doses for both inhibitors, TK6 was subjected to an inhibition assay with and without IL-6 recombinant (section 5.2.3.2). TK6 cells were incubated with inhibitors for 2 hours before adding the IL-6 cytokine, according to the literature evidence for FLLL-32 (Lin *et al.*, 2010) and BAY-293 (Swiatnicki *et al.*, 2022). In some studies, it was suggested that exposure to FLLL-32 at 2 - 4 μM for only 4 hours was sufficient to reduce pSTAT3 and induce cell death (Bill *et al.*, 2010). However, findings of this research unequivocally suggest that using these concentrations (FLLL-32; 5 μM and BAY-293; 2 μM) under optimal conditions will yield reasonable viability, and it is presumed to result in a significant blockage of the IL-6 pathway. There are methods that could have been done to confirm inhibition of the pathways including Western blotting (Bill *et al.*, 2010; Lin *et al.*, 2010; Fossey *et al.*, 2011) and RT-PCR (Lin *et al.*, 2010; Bruggemann *et al.*, 2023), but time did not allow for it as the study progressed.

In figure 5.10, the data presents the cytotoxicity and genotoxicity of samples treated with inhibitors in isolation and combination, in the presence or absence of IL-6. The data indicates that all viabilities were above the 50% limit of detection, confirming the relevance of the chosen optimal concentration for each inhibitor in section 5.3.3.1. Across all samples, those treated with IL-6 consistently exhibited better RPD compared to their complementary sample without IL-6. The highest viability was observed in TK6 cells treated with IL-6 cytokine alone, followed by combinations of IL-6 with FLLL-32 and BAY-293. This observation is supported by existing literature highlighting IL-6's potential to induce cell growth and proliferation (Reeh *et al.*, 2019) even though the inhibitors were present. Given the nature of FLLL-32 and BAY-

293 as inhibitors designed to kill the tumour or cancer cells in most of the research studies (Su *et al.*, 2021; Bill *et al.*, 2010; Plangger *et al.*, 2022), it is reasonable to anticipate significantly lower RPD in samples treated with FLLL-32 and BAY-293 in isolation, as well as a substantially lower RPD in samples treated with a combination of inhibitors. The statistically lower ($p \leq 0.0001$) viability in the combination of inhibitors with IL-6 suggests that the role of inhibitors, by blocking cell proliferation pathways, may outweigh the cell proliferation role of IL-6 on TK6 cells.

Briefly, the JAK/STAT pathway plays a pivotal role in signalling through cytokine receptors, orchestrating anti-apoptotic, growth, proliferative, and differentiation signals (Vainchenker & Constantinescu, 2013). Similarly, the RAS/MAPK pathway transduces signals from the extracellular milieu to the cell nucleus, activating specific genes for cell growth, division, and differentiation (Molina & Adjei, 2006). Inhibiting these pathways is expected to inhibit cell growth, proliferation, and differentiation. Therefore, determining the target concentration that achieves optimal cell viability while blocking the IL-6 signalling pathway is crucial. Interestingly, Ferraz *et al.* (2017) in an *in vitro* study, demonstrated a reduction in the mitotic index after treatment with LLL-3 (a STAT3 inhibitor with similar effects to FLLL-32), supporting current findings and suggests a potential cytostatic effect and cell cycle arrest.

As all samples exhibited acceptable cell viability, they were subsequently evaluated for MN formation, as depicted in figure 5.10. The sample treated with PBS displayed the lowest MN, aligning with the vehicle control MN data in Asurappulige *et al.* (2023). TK6 treated with IL-6 alone produced over a >2-fold increase in MN, significantly differing ($p \leq 0.05$) from the PBS control.

When inhibitors were applied individually, there was a slight increase in MN counts compared to the negative control, but these differences were not statistically significant. Intriguingly, combining the inhibitors in treatment resulted in an increased MN induction compared to individual inhibitor treatments, reaching significance compared to the PBS sample ($p \leq 0.05$). Additionally, samples treated with inhibitor/s with IL-6 induced higher MN production than corresponding samples without IL-6. These combination samples were significantly higher than PBS, specifically FLLL-32 + IL-6 ($p \leq 0.001$), BAY-293 + IL-6 ($p \leq 0.0001$), and FLLL-32 + BAY-293 + IL-6 ($p \leq 0.0001$). Remarkably, the sample treated with combinations of inhibitors and IL-6 showed the highest MN formation among the listed conditions (28.3/1000

cells). While there was not much difference between IL-6 with combination inhibitors versus IL-6 with BAY-293, there was a slightly lower MN induction in the sample treated with IL-6 with FLLL-32. However, when considering the mean values separately in each category (IL-6 or FLLL-32 or BAY-293), the combination treatment did not exhibit an additive effect compared to the means of each inhibitor/s or IL-6 individually in any significant data discussed above.

Although there is no reported genotoxicity evidence in the literature for FLLL-32 or BAY-293, Ferraz *et al.* (2017) findings with the STAT-3 inhibitor LLL-3 demonstrated no mutagenic activity in tested *Salmonella* strains and no genotoxicity (MN) in a mouse cell line. Since, significantly high MN induction was observed only when inhibitor/s were combined with IL-6, not when inhibitor/s were used alone, and considering the genotoxicity-inducing ability of IL-6 in the MN assay in this study (section 5.3.2.3), the above findings suggest that IL-6 can induce MN compared to the untreated condition and exacerbate it when paired with inhibitors individually or in combinations.

Inhibiting IL-6 pathways, whether through STAT3 or RAS, does not conclusively block the subsequent signal from reaching the cell's nucleus and causing MN formation. As explained in section 5.1, cellular signalling pathways are extremely complex networks with multifaceted regulatory mechanisms. The understanding of the regulatory processes of cell signalling molecules and intracellular signalling pathways remains unclear.

Since this study did not investigate the role of all IL-6 signalling pathways and considering that the addition of a JAK/STAT or RAS pathway inhibitors potentiates MN formation, this may suggest that treating samples with IL-6 forces signalling down an alternative signalling pathway, that promotes MN generation - e.g. IP3 or NF-kB are the important pathways for genotoxicity in cancer formation (Sica & Bronte, 2007; Langowski *et al.*, 2006). Therefore, a comprehensive analysis of all IL-6 signalling pathways' roles in cellular processes is necessary to elucidate the exact role of IL-6 signalling in genotoxicity and MN formation. Until the confirmation of these pathways' involvement in MN induction, these data should be approached with caution.

5.5 Conclusion

In conclusion, the comprehensive investigation into the genotoxic effects of candidate cytokines, particularly TNF- α , IL-6, GM-CSF, G-CSF, and TGF- β 1, has revealed intriguing

findings with potential implications for HSCT and cancer therapy. The study employed an *in vitro* model using TK6 cells, focusing on direct exposure to cytokines and their combinations; the MN assay served as a valuable tool to assess genotoxicity.

The individual treatments with cytokines demonstrated varying degrees of weak genotoxicity, with TNF- α and TGF- β 1 consistently showing an ability to induce MN formation even at healthy concentrations. GM-CSF and G-CSF, critical for myeloid lineage development, exhibited genotoxic effects at storm levels. Importantly, the combination of these cytokines, as an attempt at partially mirroring the cytokine storm observed in cancer therapy, increased the MN produced, but this was not always additive or synergistic.

Notably, the study delved into the potential of cytokines to induce genotoxicity concentrations that may be observed in HSCT. The findings suggest a need for further exploration into the impact of cytokines on donor HSC, especially GM-CSF and G-CSF, which are commonly used during HSCT for HSC mobilisation.

Furthermore, the investigation extended to the role of IL-6 in genotoxicity with IL-6 pathway inhibitors. The study employed the inhibitors, FLLL-32 and BAY-293, targeting the JAK/STAT and RAS pathways, respectively, to explore the connection between IL-6 signalling and MN formation. Intriguingly, these inhibitors in combination with IL-6 led to a significant increase in MN formation, suggesting that these pathways are not involved in the production of MN and might infer other IL-6 pathways were potentiated to cause this genotoxicity.

The results underscore the importance of considering the broader cytokine milieu in cancer therapy, acknowledging the potential synergistic genotoxic effects of cytokine combinations. The study provides valuable insights into the intricate dynamics of cytokine-induced genotoxicity and its relevance to the field of haematopoiesis, HSCT, and cancer therapy. As the role of cytokines in genotoxicity is further elucidated, it opens avenues for targeted interventions and therapeutic strategies to mitigate genotoxic risks associated with cytokine treatments in clinical settings.

CHAPTER 6

KNOCKDOWN AND INHIBITION IN BYSTANDER MODELS

6.1 Introduction

As discussed in previous chapters 1, 4 and 5, the phenomenon of cytokine storm and subsequent chronic inflammatory responses following cancer therapy and HSCT represents a significant and challenging issue within the domain of cancer therapeutics and research. Cytokine storm is an excessive immune system response characterised by the release of a large amount of pro-inflammatory cytokines into the bloodstream which can lead to systemic inflammation and various side effects, including fever, fatigue, and in severe cases, organ damage. Furthermore, cytokine storms are associated with sepsis and septic shock, influenza, acute respiratory distress, blood transfusion and toxic response to medication (Yiu *et al.*, 2012). This phenomenon can also occur as a side effect of various medical treatments, including cancer therapy.

Cancer Therapy, such as certain immunotherapies, targeted therapies, and even traditional chemotherapy or radiation, can trigger an immune response that results in a cytokine storm. During HSCT, a patient's immune system is essentially reset by replacing their BM with healthy donor stem cells. However, this process can induce significant inflammation and immune reactions. Cytokine storm is one of the potential complications of HSCT, especially during the early post-transplant period. IL-6 seems to hold a key role in cytokine storm pathophysiology since highly elevated IL-6 levels are seen in every patient with cytokine release syndrome (Shimabukuro-Vornhagen *et al.*, 2018).

IL-6 is a pleiotropic, immunomodulatory cytokine produced by a variety of cell types, including fibroblasts, endothelial cells, monocytes and both benign and malignant lymphocytes of B and T cell origin (Yildizhan & Kaynar, 2018). IL-6 is a member of a family of cytokines which also includes leukaemia inhibitory factor (LIF), oncostatin M (OSM), ciliary neurotrophic factor (CNTF), and IL-11 (Robak *et al.*, 1998). It also plays a key role in the immune system, inflammation, and homeostasis. IL-6 is involved in many systems, such as neutrophil migration, acute phase response, angiogenesis, B-cell differentiation, antibody generation and lipid metabolism, that either directly concern the immune system or not (Yildizhan & Kaynar, 2018). In haematopoiesis, IL-6 acts synergistically with a number of

cytokines, including SCF, IL-3, KL, CSF-1, and TPO, to stimulate primitive multipotent haematopoietic cell proliferation, myelopoiesis, and megakaryocyte production, as well as lymphopoiesis. IL-6-deficient mice have reduced primitive multipotent progenitors and are severely defective in their responses to tissue damage or infection (Pixley & Stanley, 2019). Studies have also shown that T cells lacking IL-6 led to pancytopenia and BM failure, and deletions in the *IL-6* gene have been shown to induce a variable degree of immune mediated BM failure. It needs to be also mentioned, that BM failure syndromes as well as immune mediated aplastic anaemia predispose to leukaemia (Wang *et al.*, 2022).

IL-6 is indeed a critical multifaceted cytokine with a complex array of functions in the cytokine storm following chemotherapy (Robak *et al.*, 1998). Tissues damaged by conditioning therapy release various chemicals and cytokines into the system including IL-6. This initial release of IL-6 plays a critical role in immune cell activation and differentiation of T and B cells, which can trigger a cascade of inflammatory responses and increase IL-6 expression (Markey & Hill, 2017). This can affect cell membrane destruction in endothelial cells lining the blood vessels to result in vascular leakage, apoptosis that triggers the pro-inflammatory cascade and further exacerbates inflammation. Elevated IL-6 levels can lead to the hyperactivation of immune cells and more cytokines, contributing to severe inflammation and cytokine storm (Yildizhan & Kaynar, 2018). As a result of higher IL-6 and other pro-inflammatory cytokines, a positive feedback loop is created that sustains the cytokine storm and results in systemic damage. More than 70% of patients experience severe cytokine release syndrome, associated with high IL-6 levels, in the circulation and cerebrospinal fluid during T cell therapy for relapsed B lymphoblastic leukaemia (Kang *et al.*, 2020). As showed by Masjedi *et al.*, (2020), IL-6 and its signalling pathways play a crucial role in the development and progression of various cancers by promoting cell proliferation, reducing apoptosis, enhancing metabolism, increasing antiapoptotic factors, and stimulating angiogenesis and metastasis. Additionally, it can confer drug resistance and safeguard cancer cells from DNA damage. There is increasing evidence that severe inflammation contributes to the development of haematological neoplasia. It is thus conceivable that inflammation promotes haematopoietic failure, consecutive to malignant transformation (DNA damage induced by ROS) (Wang *et al.*, 2022). Given its pivotal role in coordinating immune responses and regulating diverse physiological processes, IL-6 has emerged as an appealing target for therapeutic intervention. Consequently, directing efforts

toward IL-6 and its associated pathways presents a promising and innovative approach for the effective treatment of cancer.

Management of cytokine storms and inflammation following cancer therapy and HSCT typically involves administering specific medications and cytokine inhibitors to dampen the immune response. It is important to note that the specific risk and management of cytokine storms can vary depending on the type of cancer therapy or transplant procedure, as well as individual patient factors (polymorphisms). Understanding its role and closely monitoring IL-6 levels can be crucial in managing patients undergoing cytokine storm-related complications (related to HSCT) and in the context of inflammatory diseases.

Given its role in inflammatory processes and cytokine storms, IL-6 signalling has been explored as a therapeutic approach to mitigate HSCT complications and management of toxicities of cancer immunotherapy. The clinical use of corticosteroids and IL-6 blockade have already improved the management of patients with cytokine storm. IL-6 signalling occurs through two different mechanisms. When IL-6 levels are low, IL-6 primarily binds to the mIL6R, resulting in classical signalling, however when IL-6 levels are high, trans-signalling occurs; both ultimately resulting in activation of the JAK/STAT pathway (section 5.1). Since gp130 is broadly expressed across many effector cells, high IL-6 levels result in a more robust immune activation. Subsequent studies confirmed that administration of mAbs against IL-6 (siltuximab) and its receptor (tocilizumab) led to rapid resolution of cytokine storm, because tocilizumab blocks both classic and trans-IL-6 signalling through directly binding to mIL-6R α or the sIL-6R α , respectively (Riegler *et al.*, 2019). However, many cells such as embryonic stem cells, early haematopoietic progenitor cells, neural cells, and endothelial cells do not carry mIL6R, but they do become sensitive when sIL6R is present. The absence of IL-6 in the donor T cell pool or systemic blockade of IL-6 results in decreased GvHD in the models used by Markey & Hill, (2017). They also detailed on Tocilizumab progressed through clinical trials for GvHD, and treatment of cytokine storms associated with severe COVID-19 and autoimmune diseases. However, tocilizumab does not cross the blood brain barrier and therefore fails to inhibit IL-6 signalling in the central nervous system (Markey & Hill, 2017; Shimabukuro-Vornhagen *et al.*, 2018; Yildizhan & Kaynar, 2018). While the primary focus of IL-6 research has traditionally revolved around its direct effects on immune cells and its involvement in various diseases, recent investigations have unveiled a compelling and intricate aspect of IL-6 biology: its role in bystander models. Understanding IL-6 bystander effects has

provided new insights into the complex interplay of cytokines within the body and opened up innovative avenues for therapeutic strategies.

The role of IL-6 in chemotherapy-induced bystander effect (CIBE)

The bystander effect in the context of chemotherapy refers to the phenomenon where cells adjacent to the targeted cancer cells also experience damage and stress responses even though they were not directly exposed to the chemotherapy agents. IL-6 produced by one cell type has a profound influence on neighbouring cells or tissues, even if those cells are not the immediate target of IL-6 signalling. This phenomenon is characterised by the paracrine or endocrine transmission of IL-6-mediated signals, which can exert substantial effects on cellular behaviour and tissue homeostasis.

IL-6 can play a role in this bystander effect in several ways. Induction of stress responses: IL-6 produced by cancer cells and damaged cells in response to conditioning could communicate the cellular stress to neighbouring cells. Immune activation: IL-6 produced by stressed cells can influence nearby immune cells, potentially contributing to immune activation and inflammation in the tumour microenvironment. Tissue remodelling: IL-6 can stimulate changes in the extracellular matrix and cell adhesion molecules that may affect the response of bystander cells to chemotherapy.

Understanding the role of IL-6 signalling in CIBE may ultimately lead to novel treatment strategies, offering new hope to patients and advancing understanding of cytokine-driven pathophysiology. It highlights the complexity of the tumour microenvironment and the need to consider not only the direct effects of chemotherapy on cancer cells but also its impact on neighbouring cells and the immune system. Targeting IL-6 or its signalling pathways may have therapeutic potential in modulating these BE and improving the overall efficacy of chemotherapy. According to Plangger *et al.* (2022), inhibiting SOS1 in the IL-6 signalling pathway may improve chemosensitivity to MEK inhibition and other SOS1 inhibitors. Furthermore, they contend that combinations are necessary to maximise the effectiveness because a single SOS1 inhibitor may not be sufficient to achieve clinical responses in tumour patients. Introduction of sh/siRNA to IL-6 signalling via STAT3 in cancer-derived cell lines leads to a marginal effect on *in vitro* but significant effect on *in vivo* tumour growth, probably due to a reduction in the tumour-secreted pro-inflammatory and angiogenic factors (Sansone & Bromberg, 2012). This demonstrates that IL-6 and its released factors are important

regulators of *in vivo* tumour formation and progression, and they may be the most effective targets to control aberrant cellular communication during cancer progression. Thus, this chapter explores the intriguing area of IL-6 inhibition and knockdown in bystander models (HS-5 and TK6). The data investigates the emerging molecular approaches aimed at inhibiting or knocking down IL-6 in bystander (co-culture) models, including the use of siRNA (RNA interference), and chemical inhibitor (resatorvid).

Co-culture in cancer research is an *in vitro* experimental system which has attracted research interest in recent times, involving the culture of two or more different cell types (often cancer cells with normal cells) together with some level of cell communication to study their interactions and behaviours. These systems were applied to the study of cellular interactions between populations and to mimic the complex interactions between cancer cells and the surrounding microenvironment, including stromal cells, immune cells, and extracellular matrix components (Zeyneloğlu *et al.*, 2011). Successful co-cultures have been employed in leukaemia research. This can help elucidate how these interactions influence cancer progression, angiogenesis, metastasis and therapy resistance, ultimately contributing to the development of more effective cancer therapies and personalised treatment strategies. These successes are believed to be attributed to several possible mechanisms, such as the expression of growth factors and cytokines including IL-1, -6, -11, and LIF (Fathi *et al.*, 2019). In RIBE, several research studies have used co-culture models (Wang *et al.*, 2018; Song *et al.*, 2016; Danzer *et al.*, 1994), but very few have been used in CIBE. Thus, a transwell co-culture system was used in this study to represent the BM bystander microenvironment and to provide the optimum standard culture conditions, that would elucidate the potential role of IL-6 in CIBE. More so, HS-5 and TK6 are human origin cell lines, but nothing is known as to their cytokine expression ability as a co-culture system. Thus, this study would provide an insight into their characteristics in co-culture with or without chemotherapy. Finally, the assessment of the genotoxic effects of TK6 cell lines in the co-culture model (\pm chemotherapy, \pm IL-6) would help inform about some cellular interactions within the BM microenvironment, as well as shed light into the pathology of CIBE and its possible mediators (IL-6).

RNAi and IL-6 knockdown by siRNA

Deletion or inactivation of genes is known as knockout or knockdown respectively. Gene knockout is the total removal or permanent deactivation of a gene through genetic

engineering. Studies where genes are deactivated, or the expression of a specific gene is reduced are referred to as gene knockdown. The goal of gene knockdown is to decrease the production of the corresponding protein, ultimately leading to reduced gene function. This can be achieved through various methods, for example an oligonucleotide may be used to bind to the gene's coding region or to its mRNA, leading to a temporary change in expression.

RNA interference gained international attention in 1998 when Fire, Mello and colleagues conducted groundbreaking research in the nematode worm and discovered that double-stranded RNA (dsRNA) could silence or inhibit the expression of specific genes in this organism. This phenomenon, initially termed "co-suppression" was later known as RNA interference (RNAi) (Takeshita *et al.*, 2005). RNAi is indeed a powerful mechanism for silencing or knockdown of a target gene at the post-transcriptional level by degrading mRNA molecules. It has become a fundamental tool in molecular biology research and has potential applications in gene therapy and the treatment of various genetic disorders. It allows scientists to study gene function, screen for potential drug targets, and develop therapies aimed at specific genes. RNAi is activated by dsRNA species delivered to the cytoplasm of cells to inhibit the expression of specific genes (Guo *et al.*, 2010). RNAi is a natural cellular process that regulates gene expression and can be found in many eukaryotic organisms, including humans. The silencing mechanisms can either lead to the degradation of a target mRNA, as induced by small interfering RNAs (siRNAs) or short hairpin RNAs (shRNAs) or the suppression of translation of specific mRNAs, as induced by microRNA (miRNA) (Whitehead *et al.*, 2009).

In 2001, Thomas Tuschl and his team published their study of using synthetic siRNAs to achieve sequence-specific gene knockdown in a mammalian cell line. The siRNA oligonucleotides are around 20-25 nucleotide ds-RNA molecules and are designed to be complementary to the target mRNA sequence. The siRNA duplex consists of a sense and an antisense strand, with a two-nucleotide overhang (typically dTdT) at the 3' end of each strand. The origin of siRNAs are mainly two types including

A) endogenous siRNAs: These siRNAs are naturally produced within the cell. They can be derived from various sources, such as transposons, repetitive sequences, or even from the processing of long ds-RNA precursors by an enzyme called dicer.

B) exogenous siRNAs. In practice, siRNA can be introduced into the cell from outside and are called exogenous siRNAs. It is possible to exploit this exogenous siRNA in three ways,

including: (1) the introduction of a plasmid or viral vectors to express siRNA; (2) the introduction of dsRNA into the cytoplasm to allow dicer processing; (3) the introduction of synthetic siRNA directly allow RNA-induced silencing complex (RISC) loading, thus circumventing dicer mechanics (Whitehead *et al.*, 2009; Guo *et al.*, 2010).

These latter siRNAs are introduced into the cell from externally. However, either endogenously or exogenously generated siRNA could start the same RNAi mechanism. These exogenous siRNA can be designed to be complementary to target genes of interest and deliver them into cells using various methods, such as transfection or electroporation.

The following section discusses the key stages in siRNA transfection and gene knockdown with respect to the IL-6 gene (Fig. 6.1). The target cells (HS-5) were cultured in RPMI-CCM and allowed to adhere and grow until they reach an appropriate confluence. siRNA-transfection reagent complex is used to deliver the siRNA into the target cells and pass through the cell membrane. This transfection complex may be taken up by cells through endocytosis and siRNA molecules are released into the cytoplasm. Once siRNA is present in the cytoplasm, it is incorporated into a protein complex RISC which is a multiprotein complex that consists of proteins such as argonaute and dicer. Activated argonaute within RISC, unwinds the siRNA duplex into its single-stranded form and then antisense strand (the guide strand) of the siRNA, which is complementary to the IL-6 mRNA, is loaded into the RISC (Whitehead *et al.*, 2009).

Once the guide siRNA strand is incorporated into RISC, the sense strand (passenger strand) is typically degraded. The guide strand within RISC guides the complex to the IL-6 mRNA and binds with the complementary mRNA by base-pairing. Once bound, the RISC complex triggers the activation of endonuclease activity within the argonaute protein and induces the cleavage and degradation of the IL-6 mRNA. Then the cleaved mRNA is rapidly degraded by cellular exonucleases. The activated RISC complex can then move on to destroy further complementary mRNA. With the mRNA degraded, there are no longer functional templates for IL-6 protein synthesis, and this effectively results in knockdown of the IL-6 gene's expression. Consequently, the production of IL-6 protein is significantly reduced and can have downstream effects on cellular processes regulated by IL-6. According to Whitehead *et al.* (2009), this extra potency ensures a therapeutic effect for 3–7 days in rapidly dividing cells, and for several weeks in non-dividing cells. To validate and confirm the knockdown, researchers often perform assays such as quantitative real-time PCR (qPCR) or western blotting to measure the mRNA

and protein levels of IL-6, respectively. IL-6 gene expression was assessed by qRT-PCR and RNA sequencing following IL-6 knockdown in CART-19 cells by shRNA (Kang *et al.*, 2020). Eventually, the duration of IL-6 gene knockdown can vary depending on factors such as the stability of the siRNA and the rate of mRNA turnover. It is typically temporary and may require repeated administration to maintain the desired level of knockdown and to achieve a persistent effect.

The field of RNAi therapeutics has made significant progress since the first demonstration of gene knockdown in mammalian cells. siRNA-based formulations offer significant potential as therapeutic agents to induce the potent, persistent and specific silencing of a broad range of genetic targets (Whitehead *et al.*, 2009). Indeed, evidence shows that synthetic siRNAs are capable of knocking down targets in various diseases *in vivo*, including hypercholesterolaemia, liver cirrhosis, hepatitis B virus, human papillomavirus, ovarian cancer and bone cancer (Takeshita *et al.*, 2005).

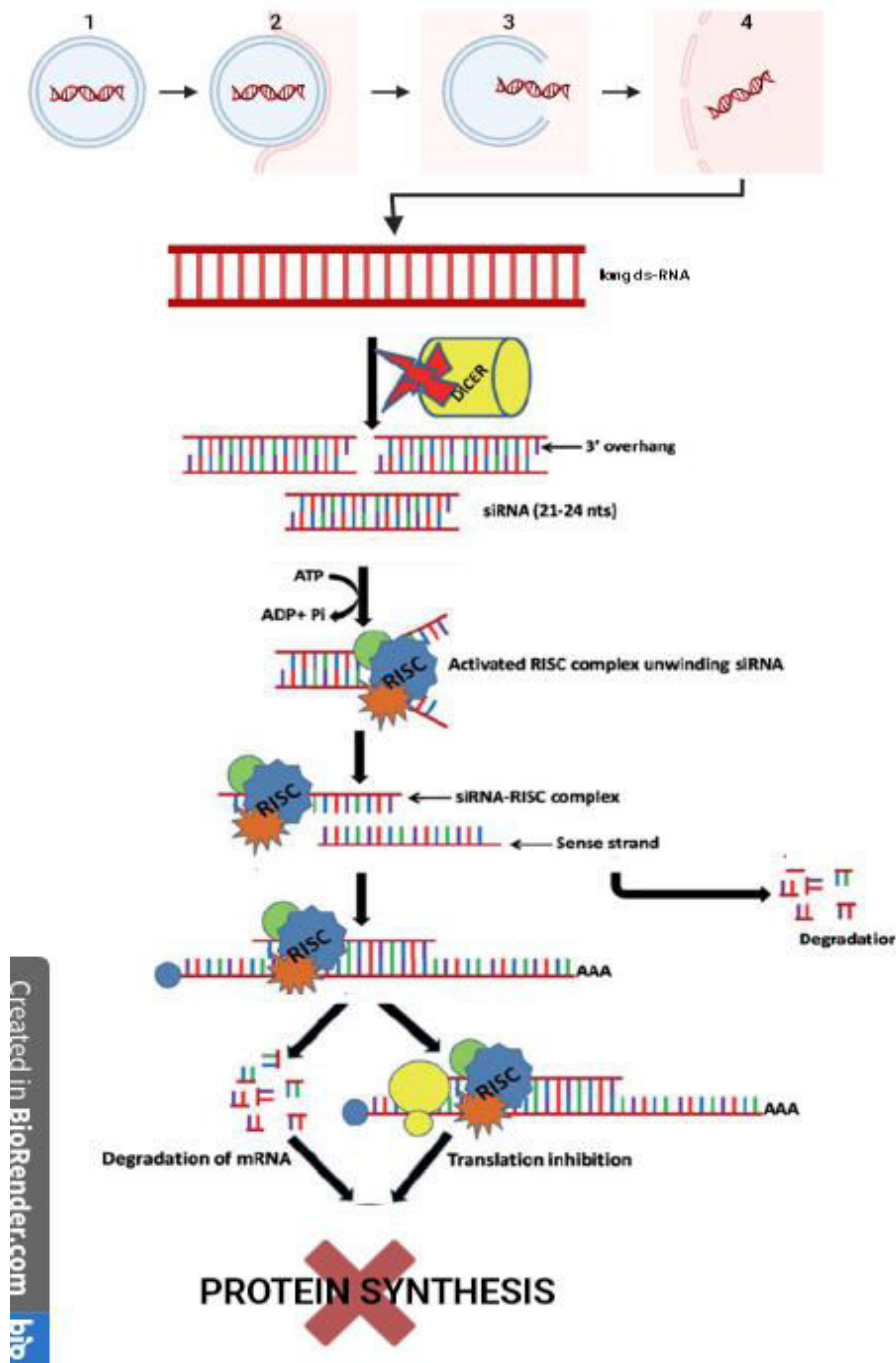


Figure 6. 1. The mechanism of RNA interference. Long double-stranded RNA (dsRNA) is introduced into the cytoplasm, where it is cleaved into small interfering RNA (siRNA) by the enzyme dicer. Alternatively, siRNA can be introduced directly into the cell. The siRNA is then incorporated into the RNA-induced silencing complex (RISC), resulting in the cleavage of the sense strand of RNA by argonaute 2 (AGO2). The activated RISC–siRNA complex seeks out, binds to and degrades complementary mRNA, which leads to the silencing of the target gene. The activated RISC–siRNA complex can then be recycled for the destruction of identical mRNA targets. (Figure created by the author via BioRender.com)

Resatorvid and IL-6 inhibition

Resatorvid, (TAK-242), is a small molecule compound which was originally developed to halt the progression of severe sepsis and acts as an inhibitor of Toll-like receptor 4 (TLR4) signalling. Amino acid Cys747 in intracellular domain of TLR4 has been identified as the binding site of resatorvid. However, the mechanism in which resatorvid inhibits TLR4 signalling remains unknown (Matsunaga *et al.*, 2011).

In 1998, Poltorak and colleagues identified TLR4 as the signalling receptor for lipopolysaccharide (LPS) or endotoxin from the gram-negative bacteria. TLR4 acts as a pattern recognition receptor that is involved in detecting various pathogen-associated molecular patterns (PAMPs). TLR4 is also known to respond to certain endogenous molecules released during tissue damage and inflammation, called damage-associated molecular patterns (DAMPs). These DAMPs released during tissue damage or inflammation can include molecules like high-mobility group box 1 (HMGB1) and heat shock proteins, which are released in response to cellular stress or necrotic cells (Suzuki *et al.*, 2012). TLR4 is the first identified member of the TLR family that can recognize PAMPs and DAMPs (Li *et al.*, 2017). As discussed by Zeuner *et al.* (2015), TLR4 signalling is extremely sensitive to the nature (bacterial species, DAMPs), purity and concentration of the ligand. TLR4 is a key receptor involved in the innate immune system and activation of proinflammatory cellular signalling pathways in response to infections and endogenous molecules. Accumulating evidence has implicated the activation or suppression of TLR4 in the development and progression of various inflammatory diseases. Additionally, TLR4 also seems to play a prominent role in cancer development and progression as well as being involved in tumour growth, progression, invasion and metastasis. In addition to many immune cells, TLR4 is expressed in endothelial cells, cardiac myocytes, and central nervous system cells including oligodendrocytes, microglia, astrocytes and neurons. Furthermore, TLR4 is known to be expressed in stem and progenitor cells in various tissues such as MSCs, HSCs and endothelial progenitor cells (Zeuner *et al.*, 2015). This broad spectrum of expression suggests that TLR4 function is not limited to immune response and is an excellent therapeutic target for the treatment of many different inflammatory diseases.

TLRs are type I integral membrane receptor which are composed of an extracellular domain, a transmembrane and intracellular domain (Li *et al.*, 2017). The N-terminal, extracellular end

consists of a leucine-rich binding domain for potential ligands. The C-terminal cytoplasmic end is referred to as Toll/IL-1 receptor (TIR) homology domain (Zeuner *et al.*, 2015). As described in figure 6.2, TLR4 signalling is mediated through the cytoplasmic domain TIR. The binding of ligands results in the activation of two distinct pathways. The first pathway is where activated TLR4 signals through the so-called ‘MyD88-dependent pathway’. LPS binding to the receptor leads to rapid recruitment of TIRAP, MyD88, IRAK4, IRAK1 and TRAF6. Subsequently, TAK1 activates the IKK (α & β) complex resulting in nuclear translocation of active NF- κ B dimers (p50 and p65). In addition to the activation of the NF- κ B pathway, TAK1 also can target ERK1/2, JNK and p38 culminating in activation of AP-1. The combined activity of NF- κ B and AP-1 then leads to increased expression and secretion of pro-inflammatory cytokines. For the second pathway, ligand binding to TLR4 activates the ‘MyD88-independent pathway’, which culminates in activation of IRF3 and synthesis of IFN- β . Here, ligand bound TLR4 is internalized with the help of CD14 into early endosomes leading to recruitment of TRAM and TRIF and activation of TRAF3. This activates TBK1 and IKK ϵ resulting in IRF3 phosphorylation, dimerization and nuclear translocation (Zeuner *et al.*, 2015; Suzuki *et al.*, 2012).

TLR4 is the only member of the TLR family able to induce either the pro-inflammatory cytokines including TNF- α (MyD88-dependent and NF- κ B-driven) or the anti-viral IFN- β (MyD88-independent and IRF3-driven). Importantly, the activation of NF- κ B also occurs through MyD88-independent pathway via activated TRAF6 even though this mode of NF- κ B is rather slow and weak. Thus, NF- κ B activation occurs in both TIR routes and appears to be central for TLR4 signalling. The balance of the pro-inflammatory NF- κ B signalling vs anti-inflammatory IRF3 signalling pathways seems to be dependent on the nature of the ligand (PAMPs and different DAMPs). However, the DAMPs activate TLR4-mediated signalling is a matter on ongoing scientific debate. Thus, more studies are needed to validate the DAMP-mediated TLR4 downstream signalling events (Zeuner *et al.*, 2015).

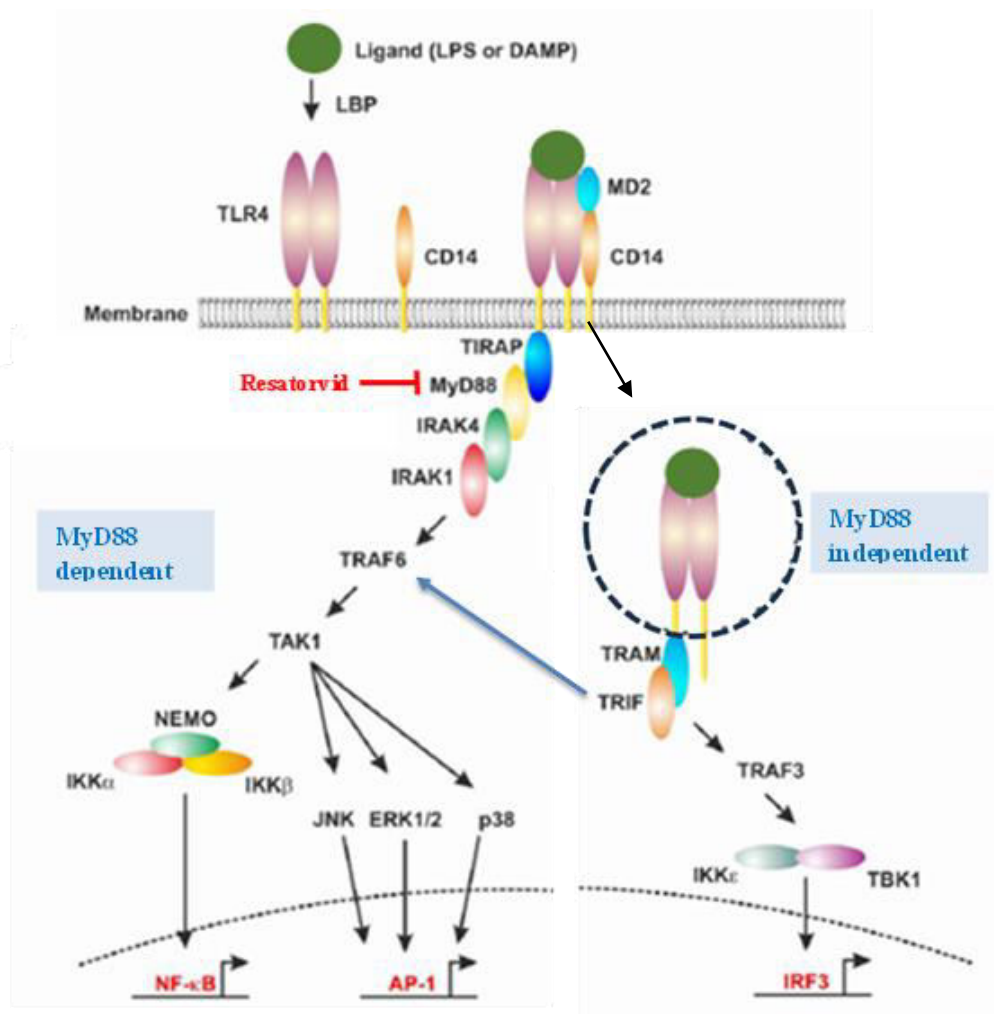


Figure 6. 2. TLR4 signalling pathway and resatorvid inhibition. The binding of the ligand to TLR4 is mediated by LP and DAMP at the plasma membrane and activation of MyD88-dependent and MyD88-independent signalling pathways. Importantly, the TLR4 co-receptor CD14 is believed to be crucial for activation of the MyD88-independent signalling. *MyD88-dependent signalling*; ligation of TLR4 leads rapid recruitment of TIRAP, MyD88, IRAK4, IRAK1 and TRAF6. TRAF6 transduces the signal to TAK1, which activates the IKK complex (NEMO, IKK α and IKK β). Active NF- κ B heterodimers (p50 and p65) translocate into the nucleus and regulate the transcription of pro-inflammatory genes such as TNF- α and IL-6. Further, TAK1 can activate ERK1/2, JNK and p38 leading to activation of AP-1. *MyD88-independent signalling*; ligand binding, assisted by LP, DAMP and CD14 leads to internalization of the ligand-bound receptor in endosomes. Subsequently, TRAM and TRIF get recruited followed by activation of TRAF3 and finally IKK ϵ /TBK1 complex. This leads to IRF3 phosphorylation, dimerization, and translocation into the nucleus. After binding to the DNA, IRF3-dimers regulate transcription of the respective target genes, including IFN- β and RANTES. (Figure created by the author via BioRender.com).

TLR4 expression in stem cells and tumours

HSCs are known to respond to mediators of inflammation including LPS. Moreover, they can also directly sense pathogens via TLRs. Expression of TLR4 has been detected in multipotent mouse HSCs. Ligation of TLRs activates HSCs and thus affects their downstream progeny.

In MSCs, the binding of LPS to TLR4 results in a potent NF- κ B activation and subsequent activation of its pro-inflammatory target genes including TNF- α and IL-6. Moreover, TLR4 mediates activation of MAPK pathways (JNK and p38) suggesting a fully functional MyD88-dependent TLR-signalling cascade. Although there is no direct evidence, TLR4 in MSCs seems to be also able to signal via the MyD88-independent pathway and activate IRF3 targets RANTES and IFN- β as well. Interesting *in vivo* data suggests that BM-MSCs can sense circulating TLR ligands, such as LPS, and induce monocyte mobilization from the BM by MCP-1 secretion (Zeuner *et al.*, 2015).

It was verified that TLR4 is also expressed in many types of tumours, such as hepatocarcinoma, glioblastoma, lung cancer, breast tumour and is involved in their progression, among which, DAMPs rather than PAMPs play a main role in activating TLR4 in the tumour microenvironment. TLR4 in tumour development is supported by the following studies. Lin *et al.* firstly demonstrated that TLR4 expressed on neutrophils or macrophages may be involved in pathological angiogenesis induced by HMGB1 (Li *et al.*, 2017). In response to LPS, macrophages undergo pro-inflammatory differentiation, and release large amounts of cytokines such as TNF- α , IL-1 β , and IL-6, as well as ROS (Yu *et al.*, 2020). Macrophages treated with resatorvid (1 μ M) and co-cultured with pulmonary artery endothelial cells reduced the inflammatory cytokines (IL-1 β , IL-18, IL-6 and TNF- α) in the supernatant (Xie *et al.*, 2022).

TLR4 and MyD88 have been demonstrated to be over-expressed in breast cancer. Down-regulation of TLR4 signal pathways in BM-MSCs gave rise to the reduction of IL-1 β and TNF- α in bone tissue, and thus contributed to efficient control of spinal cord inflammation. A recent study asserted that the levels of TLR4 mRNA expression in BM-MSCs isolated from AML patients as well as MSC from lung cancer patients, were much higher than healthy volunteers. Meanwhile, IL-6 and IL-8 levels were significantly upregulated by LPS in TLR4+ MSCs in comparison to unsorted MSCs. However, the level of MCP-1, was much higher in the supernatant of TLR4+MSCs, suggesting that TLR4 may play a vital role in induction of MCP-1, which has been defined as a promoter in breast cancer cell migration (Li *et al.*, 2017).

The impact of TLR4 signalling during chemotherapy and radiotherapy can vary depending on factors such as the type of cancer, the specific treatment regimen, and the patient's immune status (polymorphism). TLR4 activation on tumour cells definitely benefits the tumour; stimulation of this pathway in immune cells may have reversal consequences. TLR4 expressed on dendritic cells plays a role in anti-tumour immune response, but TLR4 expressed by myeloid-derived suppressor cells and macrophages plays the opposite role. Furthermore, activation of TLR4 on T cells has anticancer and pro-tumour consequences in the tumour microenvironment (Li *et al.*, 2017), thus the activation of TLR4 in this context can have both beneficial and detrimental effects.

As a benefit, TLR4 activation can stimulate MSC to produce anti-inflammatory cytokines and can clear dead or damaged cells to promote tissue repair following cancer therapies. But mostly, during cancer therapies, patients often experience tissue damage and inflammation as a result of the treatment. This damage can lead to the release of DAMPs, which can frequently activate TLR4 and initiate an immune response. Excessive or dysregulated TLR4 signalling can lead to uncontrolled inflammation and contribute to harmful conditions such as cytokine storm. When TLR4 on MSCs detects these inflammatory signals, it can trigger a signalling cascade that leads to the production of pro-inflammatory cytokines and chemokines, which are important for initiating and regulating the immune response. Prolonged activation of TLR4 can lead to immunosuppression, which can actually promote tumour growth and resistance to treatment.

Resatorvid contains an α , β unsaturated carbonyl group that reacts with biological nucleophiles, such as the sulphhydryl group on cysteine residues. With this chemical feature, it is presumed that resatorvid reacts with TLR4 to form a complex containing a covalently attached cyclohexene ring at position 747. Because resatorvid binds to the equivalent cysteine residue in TLR4, the binding of resatorvid may cause a conformational change in the TIR domain, subsequently inhibiting the recruitment of adaptor proteins MyD88 and TRIF with TLR4 (Matsunaga *et al.*, 2011).

Resatorvid has been found to protect against the effects induced by LPS, an exogenous TLR4 ligand, in a systemic inflammation model. Resatorvid binding directly to TLR4 via Cys747 in the TIR domain disrupts the interaction of TLR4 with adaptor molecules mainly MyD88 and TRIF. This leads to suppression of NF- κ B activation and down-stream pro-inflammatory

cytokine production (Fig. 6.2) (Suzuki *et al.*, 2012). Accumulating evidence from several studies underscores the efficacy of resatorvid treatment in mitigating the production of multiple pro-inflammatory cytokines.

In particular, a study by Zhang *et al.* (2021) observed a notable reduction in TNF- α , IL-1 β , and ROS levels within a 1mg/kg resatorvid treated group. These findings were further substantiated in a study by Wei *et al.* (2020), where ELISA and western blot analyses revealed a significant decrease in TNF- α , IL-1 β , and MCP-1 expression when cells were subjected to resatorvid treatment as compared to untreated cells. Moreover, a study by Wan *et al.* (2020) illuminated the intricate mechanism of action, demonstrating that resatorvid at a concentration of 3 μ M/L effectively silenced the TLR4/NF- κ B signalling pathway. This inhibition resulted in the reduced production of CXCL1, CXCL2, and CXCL8 chemokines. Additionally, in the *in vivo* mouse model, involving the injection of 10 mg/kg resatorvid, led to the inhibition of neutrophil infiltration, further emphasizing the multifaceted anti-inflammatory potential of resatorvid. However, the signalling pathway immediately down-stream of TLR4 in leukaemia or cytokine storm condition has remained unclear despite many studies approaching an answer.

The above data suggests that resatorvid has potential as a therapeutic agent to inhibit TLR4 overactivation and control the pro-inflammatory effect in vital disease types. As a prospective application, resatorvid inhibition can be used in the treatment of inflammatory diseases such as sepsis, rheumatoid arthritis, and conditions where cancer therapies induced excessive TLR4-mediated inflammation. MMP-9/2 activation and release of inflammatory cytokines TNF- α , IL-1, IL-6 can be reduced by the treatment of resatorvid (10 μ M & 1 μ M) in chemotherapy-induced cognitive impairment and chemotherapy-induced peripheral neuropathy respectively (Song *et al.*, 2022; Gu *et al.*, 2020). Researchers are actively studying TLR4 and its role in cancer therapy to better understand its effects and potential therapeutic strategies to modulate TLR4 signalling for improved treatment outcomes. This may involve the development of TLR4 agonists or antagonists to fine-tune the immune response during cancer treatment. Clinical trials are ongoing to explore these possibilities. However, the role of TLR4 activation in the tumour microenvironment is a complex, double-edged sword, with the potential for both beneficial and detrimental effects. Therefore, to gain a comprehensive understanding of how resatorvid disrupts signalling complexes and intracellular signal transduction at a molecular level, it is imperative to conduct a crystal structure analysis of the resatorvid complex.

Considering the pivotal role of IL-6 in inflammation, cytokine storm, and cancer, this chapter aimed to validate the involvement of IL-6 in the bystander effect. The targeted modulation of IL-6 through knockdown or chemical inhibition emerges as a promising approach, providing valuable insights into the potential contribution of IL-6 to the induction of bystander effects on micronuclei formation in co-culture models.

6.2 Methods

6.2.1 IL-6 siRNA oligo

IL-6 knockdown siRNA kit was purchased from Thermo Fisher, UK which comes with Silencer™ Select Negative Control No. 1 siRNA (Cat 4390843), Opti-MEM™ I Reduced Serum Medium (31985062), Lipofectamine™ RNAiMAX Transfection Reagent (13778030) and IL-6 siRNA (4390824). The general k/d protocol was performed as discussed in section 2.2.6.2 once the optimum concentration and timeline for HS-5 cell line was finalised.

6.2.1.1 IL-6 siRNA concentration and longevity optimisation

Prior to employing knockdown (k/d) reagents, it was crucial to optimise the working concentrations and ensure duration (longevity) of siRNA oligos. In this context, the analysis of IL-6 expression spanned a period of 5 days (120 hours), evaluating various concentrations (3 pmol, 6 pmol, 12 pmol) of siRNA treatment. Simultaneously, Opti-MEM media and Lipofectamine were employed as mock k/d to assess the impact of the reagents on knockdown efficiency. Silencer Select N/C (non-complementary IL-6 siRNA oligo) was administered at the same concentration regimen as the IL-6 siRNA. As a control, HS-5 without any reagents was also included in the investigation.

On the initial day, HS-5 cells were seeded at a density of 3.5×10^4 cells per well in a 24-well plate, 24-hour prior to the k/d. Seven wells were provided with 500 μ l RPMI-CCM, while two wells received 500 μ l Opti-MEM media. After a 24-hour incubation period, six RPMI-CCM wells were treated with varying concentrations (3 pmol, 6 pmol, 12 pmol) of siRNA, along with 3 pmol, 6 pmol, 12 pmol of siRNA N/C, reaching a final volume of 600 μ l. Two Opti-MEM wells were treated with 100 μ l Lipofectamine and 100 μ l Opti-MEM separately, followed by an overnight incubation.

The following day, microscopic observations and image capture were conducted to assess viability and morphology in all wells. Subsequently, the culture media in each well were replaced with fresh 600 μ l RPMI-CCM, and collected supernatants were stored at -80 °C for ELISA assay. This process, including k/d reagent treatment, was repeated over the course of 4 additional days, culminating in the collection of a 120-hour incubated sample. On the final day, cells were trypsinised, and viability assessments were conducted.

6.2.1.2 IL-6 siRNA longevity assay with drug

After optimising the siRNA concentration, the same procedure was applied to drug treatments involving CHL and MTX. HS-5 cells were seeded at the same density in a 24-well plate a day before k/d treatments. The twelve sample wells were designated for control HS-5, CHL treatment, MTX treatment, and treatment with 6 pmol IL-6 siRNA, 6 pmol siRNA N/C, Opti-MEM media, and without k/d reagents. The respective wells were treated with siRNA, N/C, and Opti-MEM reagents and left for overnight incubation.

On the following day, control HS-5 wells were treated with PBS, while the respective other wells were treated with 4 μ M of CHL and 1.12 μ M of MTX. The plate was left for a 1-hour incubation, followed by washing the cells with fresh PBS and replacing with new media. After 24 hours of incubation, supernatant was collected for ELISA assay, and new media was added to each well. This process was repeated until the 5th day (120 hours), and lastly, cell viability measurements were taken.

6.2.1.3 IL-6 knockdown HS-5 co-cultured with TK6

After optimising the best concentration and ensuring duration for IL-6 k/d reagents, the research proceeded to assess the bystander genotoxicity of IL-6 by co-culturing HS-5 cells (\pm k/d) with TK6, which would represent the connection between the recipient BM microenvironment using HS-5 and the donor HSC compartment represented by TK6 as a bystander model.

HS-5 cells were seeded at a density of 7×10^4 cells per well in a 12-well plate. Once the cells settled overnight, k/d reagents were added, corresponding to 6 pmol of IL-6 siRNA and siRNA N/C into their respective wells. The plates were left for overnight incubation. On the following day, the corresponding wells were treated with 4 μ M of CHL and 1.12 μ M of MTX, while the control well received the same volume of PBS. After a 1-hour incubation, cells were washed with PBS and replenished with culture medium. Cells were then incubated for an additional 48 hours (72 hours after k/d) at 37 °C in a CO₂ incubator. At 48 hours, the supernatant was changed, and bystander TK6 culture inserts were added to each well at a density of 3×10^5 cells/ml with 1 ml of medium. The bystander co-culture model assay was performed according to the description in section 2.2.6.1. This specific time period aligned with the highest bystander genotoxicity as detected by a senior research colleague, and also coincided with the

lowest IL-6 expression by the HS-5 cells following IL-6 siRNA k/d with and without chemotherapies (section 6.3.1.2). On the following day, the supernatant was centrifuged, and media were stored at -80 °C for ELISA. TK6 cell viabilities were assessed, and samples for MN assay were prepared as explained in section 2.2.4.2. The remaining TK6 cells were re-seeded into new wells with fresh RPMI-CCM to calculate their RPD.

For each siRNA treatment analysis, whether administered alone or in conjunction with drugs at various time points, three independent biological replicates were conducted. Throughout the cell treatment procedures, a minimum of 2-3 wells were allocated to represent each individual sample. This approach was consistently applied across the three biological replicates for both negative control and mock samples.

6.2.2 Resatorvid

Resatorvid, is a chemical inhibitor of IL-6 and TNF- α purchased from Selleckchem.com (Catalog S7455). The optimisation of resatorvid was conducted in accordance with the described sections below. Once the concentration and timeline were finalised, the general protocol for resatorvid as outlined in section 2.2.6.3 was followed.

6.2.2.1 Resatorvid dose response assay

Following the rationale outlined in the relevant literature (Matsunaga *et al.*, 2011; Zhou *et al.*, 2022; Hu *et al.*, 2022; Mateu *et al.*, 2015; Gu *et al.*, 2020; Wan *et al.*, 2020; Liu *et al.*, 2021; Wen *et al.*, 2021; Song *et al.*, 2022; Xie *et al.*, 2022; Cui *et al.*, 2021), this study aimed to analyse the impact of different dosages of resatorvid on the HS-5 cell line. Given the lack of studies on the MSC cell line with resatorvid, it was essential to optimise this approach, considering both cell viability and the duration of IL-6 expression following inhibitor treatment.

HS-5 cells were seeded in a 6-well plate at a seeding density of 1.4×10^5 cells/well. After allowing the cells to adhere overnight, they were treated with varying resatorvid concentrations, specifically 1, 3, 5, 7, 9, and 11 μ M. The samples were then incubated at 37 °C in a CO₂ incubator overnight. Following a 24-hour incubation, supernatant was collected and stored at -80°C. HS-5 cells in all samples were trypsinised separately, counted using a Luna

counter, and subsequently re-seeded in new media. This process was repeated at 24-hour intervals until day 5 (120 hours) following the addition of the inhibitor.

Utilising the cell count data obtained, an analysis of HS-5 viability at different concentrations of resatorvid was conducted. To assess the IL-6 expression by HS-5 following the inhibitor treatments, an IL-6 ELISA was performed using the aforementioned supernatant.

6.2.2.2 Resatorvid inhibition and longevity with drugs

To assess the potential of resatorvid to inhibit IL-6 secretion following chemotherapy exposure, the optimal resatorvid dosage determined through viability assays was utilised and resatorvid's inhibitory efficacy over time was determined.

HS-5 cells were initially seeded at a density of 7×10^4 cells/well in a 12-well plate and allowed to adhere overnight. On the following day, the cells were treated with 3 μM resatorvid and incubated at 37 °C in a CO₂ incubator for 2 hours. Following this, the cells were exposed to 4 μM of CHL and 1.12 μM of MTX in their respective wells. After a 1-hour incubation, the cells were washed with PBS and replenished with new RPMI-CCM before undergoing a 24-hour incubation. The supernatant was collected on the subsequent day and stored at -80 °C for ELISA, and new media was added to each well. This process continued for 5 days (120 hours) following chemotherapy treatments, and on the last day, cell counts were obtained.

6.2.2.3 Resatorvid inhibition of HS-5 co-cultured with TK6

HS-5 cells were initially seeded at a density of 7×10^4 cells/well in a 12-well plate and incubated overnight. On the following day, the cells were treated with 3 μM resatorvid and incubated at 37 °C in a CO₂ incubator for 2 hours. Subsequently, the cells were exposed to 4 μM of CHL and 1.12 μM of MTX in their respective wells. After a 1-hour incubation, the cells were washed with PBS and replenished with new RPMI-CCM before continuing incubation. The cells were then incubated for an additional 48 hours at 37 °C in a CO₂ incubator.

At the end of 48-hour mark, the supernatant was replaced with new media, and bystander TK6 culture inserts were added to each well at a density of 3×10^5 cells/ml with 1 ml. The bystander co-culture model assay was performed according to the description in section 2.2.6.1. Following a 24-hour incubation, the supernatant was centrifuged, and the media were stored at -80 °C for ELISA. TK6 cell viabilities were measured, and samples for the MN assay was

performed (section 2.2.4.2). The remaining TK6 cells were re-seeded into new wells with fresh RPMI-CCM to calculate their RPD.

The assay involving resatorvid chemical inhibition was conducted to include three biological replicates. To minimise the impact of outliers, a minimum of three wells were utilised on an open plate to represent each individual sample. This methodological consistency was maintained across all experimental iterations, ensuring robust data collection and analysis.

In this chapter, mean, standard deviation, and standard error of the mean were calculated using GraphPad Prism software version 8.2.1. Group comparisons were conducted through one-way or two-way ANOVA, followed by Dunnett's, Tukey's, or Šídák's multiple comparison tests as recommended by the software. All analyses represent results from three biological replicates unless explicitly stated otherwise. Statistical significance in the presented graphs is denoted as (*) for $p \leq 0.05$, (**) for $p \leq 0.01$, (***) for $p \leq 0.001$, and (****) for $p \leq 0.0001$.

6.3 Results

6.3.1 siRNA Oligo optimisation

6.3.1.1 Knockdown concentration and longevity optimisation

Before implementing the IL-6 knockdown kit, a pre-optimisation phase was undertaken to evaluate the compatibility of reagents with HS-5 adherent cell lines, particularly the challenges posed by the HS-5 cell line, which necessitates frequent trypsinisation and re-seeding every 24 hours for cell viability assessment. To address this, an alternative approach was adopted, involving microscopic examination of HS-5 cells to observe changes in morphological characteristics and spreading dynamics as indicators of their physical state. Subsequently, HS-5 cell images were captured at 24-hour intervals for a duration of 120 hours using an inverted light microscope set to a magnification of 10x (Fig. 6.3A).

The images suggest that, on each individual day, a similar number of cells cover a comparable amount of space overall. However, cells treated with IL-6 siRNA appeared to develop more rapidly than the other samples, with their cell count appearing larger compared to the untreated and N/C-treated wells. Importantly, the morphological characteristics of IL-6 siRNA-treated cells did not differ significantly from untreated cells. No significant alterations were observed in cells treated with three different doses either. The density and appearance of cells from the 3- and 6-pmol treatments were comparable, while cells treated with 12 pmol grew somewhat more than usual. The optimal time period for IL-6 siRNA added samples was found to be between 72 and 96 hours, displaying neither excessively low nor excessively high cell density for all analysed concentrations.

In figure 6.3B, the data focuses on the IL-6 expression by HS-5 cells following exposure to different concentrations of siRNA, N/C, and k/d reagents. Concentrations between 3, 6, and 12 pmol were selected for analysis based on the manufacturer's protocol and literature recommendations for BM-MSC lines. Control samples without any treatments exhibited results consistent with IL-6 ELISA results (section 4.3.2.3). Cells treated with k/d reagents, including Opti-MEM or Lipofectamine, did not show significant changes in IL-6 expression compared to untreated HS-5 cells. Furthermore, the combination treatment of Opti-MEM+Lipofectamine exhibited unchanged IL-6 levels over 5 days. siRNA N/C treatments at 3 pmol showed similar

results to the control sample, with 6 pmol-treated HS-5 cells being comparatively lower, and 12 pmol yielding the lowest result among the three N/C concentrations.

HS-5 cells treated with IL-6 siRNA showed the lowest IL-6 expression across all categories. Cells treated with 3 pmol did not exhibit any decrease over the time period but experienced an unexpected non-significant increase on day two, while siRNA 6 pmol-treated cells were decreased over time with day 3 (72 hours) showing the lowest levels. By day five (120 hours), the IL-6 level started to elevate slightly. The last siRNA dose, 12 pmol, did not change over time but slightly increased on the last day. Overall, the findings suggest that IL-6 knockdown is achievable from 72 to 96 hours using 6 pmol of siRNA (highlighted in red), and expression may restart at around 96 hours following knockdown.

Figure 6. 3. Morphology (A) and IL-6 expression (B) from HS-5 transfected with IL-6 siRNA over five days

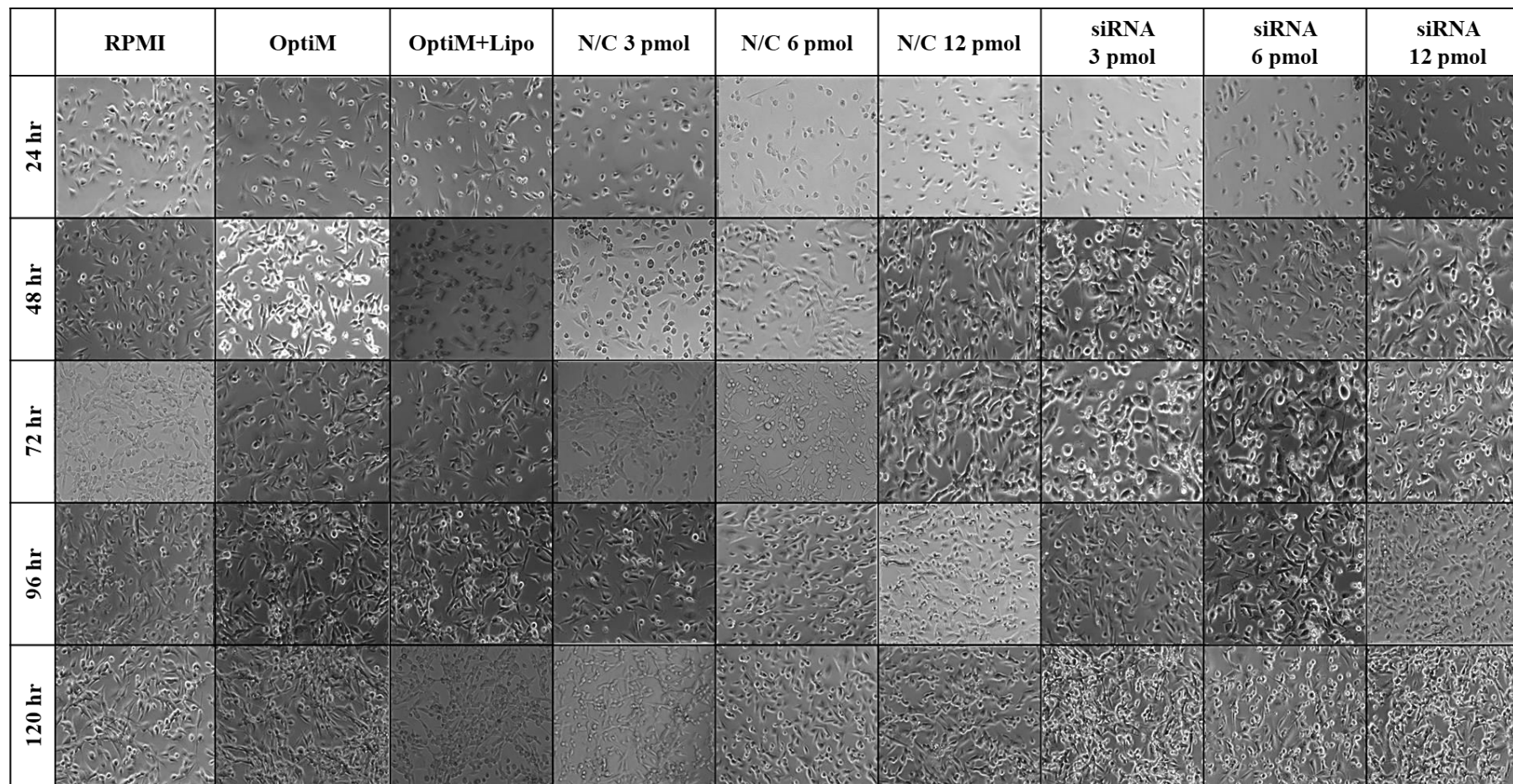


Figure 6.3A. Morphology of HS-5 exposed to IL-6 siRNA and knockdown reagents over five days. Cells were seeded at 3.4×10^4 per well in a 24 well plate and treated with three different siRNA concentrations (3, 6, 12 pmol), the IL-6 siRNA N/C and knockdown reagents (OptiM and Lipo). HS-5 images were taken with an inverted light microscope every 24 hours over 120 hours at 10x magnification. OptiM; Opti-MEM® I Reduced Serum Medium, Lipo; Lipofectamine™ RNAiMAX complexes, N/C; Silencer™ Select Negative Control No. 1 siRNA.

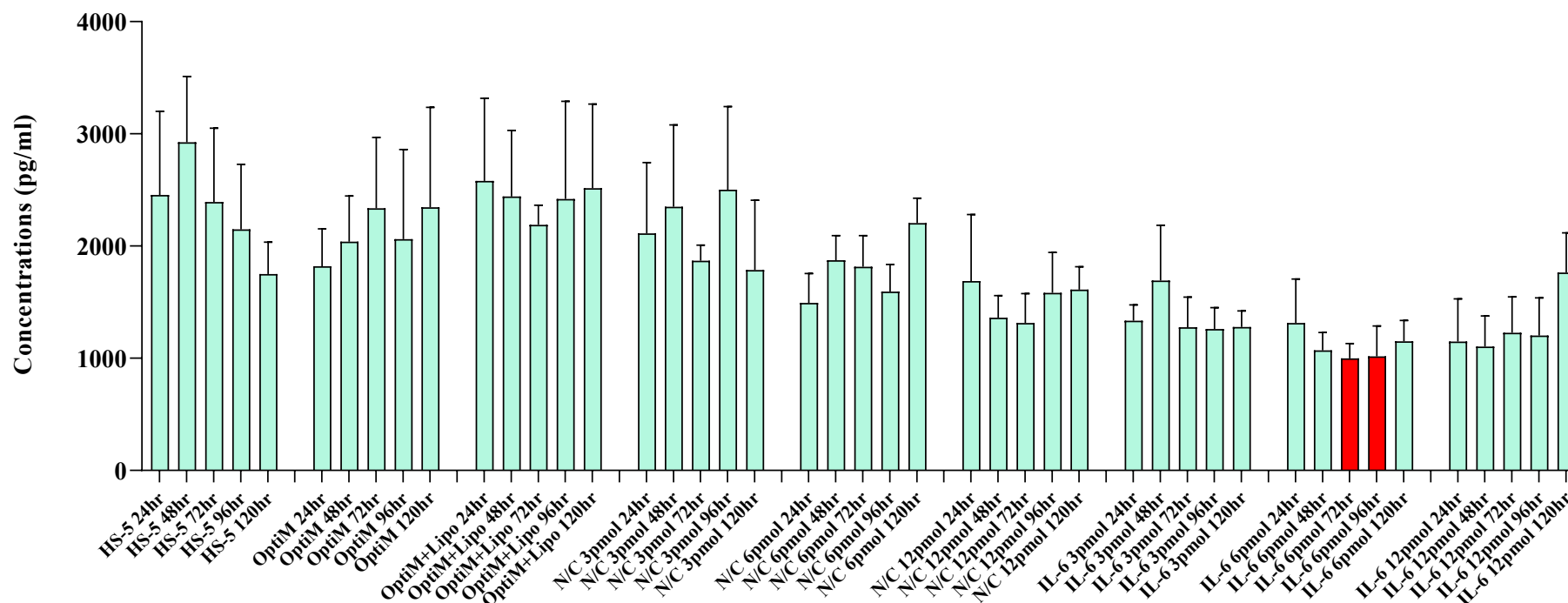


Figure 6.3B. IL-6 expression from HS-5 cells transfected with IL-6 siRNA over five days. This assay was planned to analyse the effect of siRNA oligo and knockdown reagents on IL-6 expression by HS-5. Cells were treated with three different siRNA concentrations (3, 6, 12 pmol) alongside the IL-6 siRNA N/C. Separate HS-5 samples were treated with knockdown reagents (OptiM and Lipo) to explain their effect on HS-5 cells. Culture media was collected every 24 hours over five days and analysed using the IL-6 ELISA. The bars highlighted in red represent the 72- and 96-hour time points, which correspond to the lowest levels of IL-6 expression. These time points will be considered when conducting the co-culture assay. Data shows the mean \pm SD (n=3). OptiM; Opti-MEM® I Reduced Serum Medium, Lipo; Lipofectamine™ RNAiMAX complexes, N/C; Silencer™ Select Negative Control No. 1 siRNA.

6.3.1.2 Knockdown longevity assay with drug treatments

Once the optimal concentration for siRNA treatment (6 pmol) was determined, the effectiveness of these siRNAs in the presence of two chemotherapies was assessed. As depicted in figure 6.4, samples were treated separately with 4 μM CHL and 1.12 μM MTX for control HS-5, N/C mock siRNA, and IL-6 siRNA.

HS-5 cells (without k/d) treated with CHL and MTX resulted in the highest IL-6 expression on day 3 (72 hours). Notably, CHL-treated cells exhibited significant expression ($p \leq 0.05$) relative to PBS, and this was greater than MTX expression and all the analysed categories in this graph. These data align with the time period used within the cytokine array (section 4.2.1) for measuring CHL response, but for MTX, it was day 2 in the array (48 hours). Most interestingly, k/d treated CHL exposure samples expressed significantly lower ($p \leq 0.01$) IL-6 compared to its corresponding pair without k/d at 72 hours.

The mock k/d did not show much difference compared to the control HS-5 samples. However, the expression levels on respective days differed when compared to the control samples. The expression levels of all N/C categories; untreated, CHL-treated, and MTX-treated were lower than those of HS-5 control samples. The lowest overall IL-6 expression was observed in untreated HS-5 with IL-6 siRNA at 48 hours (1256 pg/ml). However, to maintain consistency with the results of the previous investigations, samples at 72 hours were considered as the optimal k/d periods for HS-5 with and without both chemotherapies (results are highlighted in red in the Fig. 6.4).

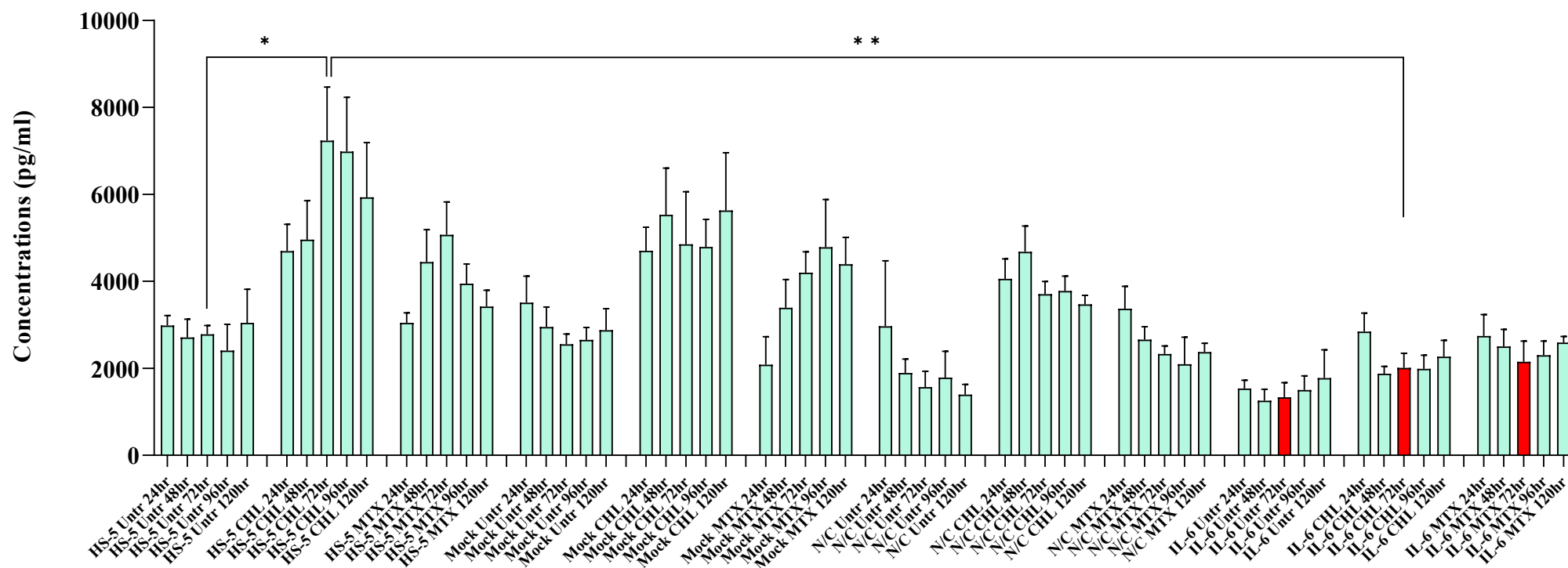


Figure 6. 4. IL-6 expression from HS-5 cells transfected with IL-6 siRNA with and without chemotherapies. Once the optimum siRNA was confirmed, drug treatment was done to IL-6 knocked down HS-5 and the expression levels analysed. The experiment was planned with control HS-5 (+/- drugs), Mock knockdown (+/- drugs), N/C (+/- drugs) and siRNA (+/- drugs). Culture media was collected every 24 hours over five days from every culture well and analysed using IL-6 ELISA. The bars highlighted in red at the 72 hours mark, observed across all IL-6 k/d samples both with and without drugs, signify the optimal time point for conducting the co-culture assay. This time point not only demonstrates the lowest IL-6 expression but also aligns with the time points utilised in the cytokine array analysis. Data shows the mean \pm SD (n=3) and significant difference is shown as * $p \leq 0.05$ and ** $p \leq 0.01$, as determined by one-way ANOVA, Tukey's multiple comparisons test.

6.3.1.3 TK6 co-cultured with IL-6 knockdown HS-5

Once the timeline with drugs were finalised, IL-6 knocked down HS-5 were co-cultured (section 2.2.1.7) with TK6 in the bystander model, both with and without chemotherapies. Supernatant from each well was assessed for IL-6 levels using ELISA (Fig. 6.5), and co-cultured TK6 cells were analysed in the MN assay (Fig. 6.6).

The data in figure 6.5 depicts the IL-6 expression from IL-6 knocked down HS-5 (green bars on the graph) and their co-culture with TK6 in the bystander model (purple bars on the graph). Notably, there was a reduction in IL-6 expression in the bystander models compared to the HS-5 single compartment across all analysed criteria.

The highest IL-6 expression was observed in the single compartment HS-5 treated with CHL but without knockdown (7237 pg/ml). This level was significantly ($p \leq 0.001$) higher than the negative control of the assay (HS-5 without drug and knockdown) and its k/d-treated bystander sample ($p \leq 0.0001$), representing the lowest IL-6 expression in the obtained data. Remarkably, this highest IL-6 expressing sample (single compartment HS-5 treated with CHL but without k/d) was significantly ($p \leq 0.0001$) higher than its corresponding sample (single compartment HS-5 treated with CHL but with k/d), validating the efficacy of the k/d kit in properly reducing IL-6 expression in HS-5 cells under the same culture conditions.

When comparing the two models, without IL-6 k/d, both drug-treated HS-5 cells expressed significant IL-6 in their single compartment models compared to their bystander models. This difference was more pronounced in CHL-treated cells ($p \leq 0.0001$) compared to MTX-treated cells ($p \leq 0.05$). Although not directly comparable as a 'pair', IL-6 was lower in the k/d-treated MTX bystander model compared to its single compartment model without k/d ($p \leq 0.01$).

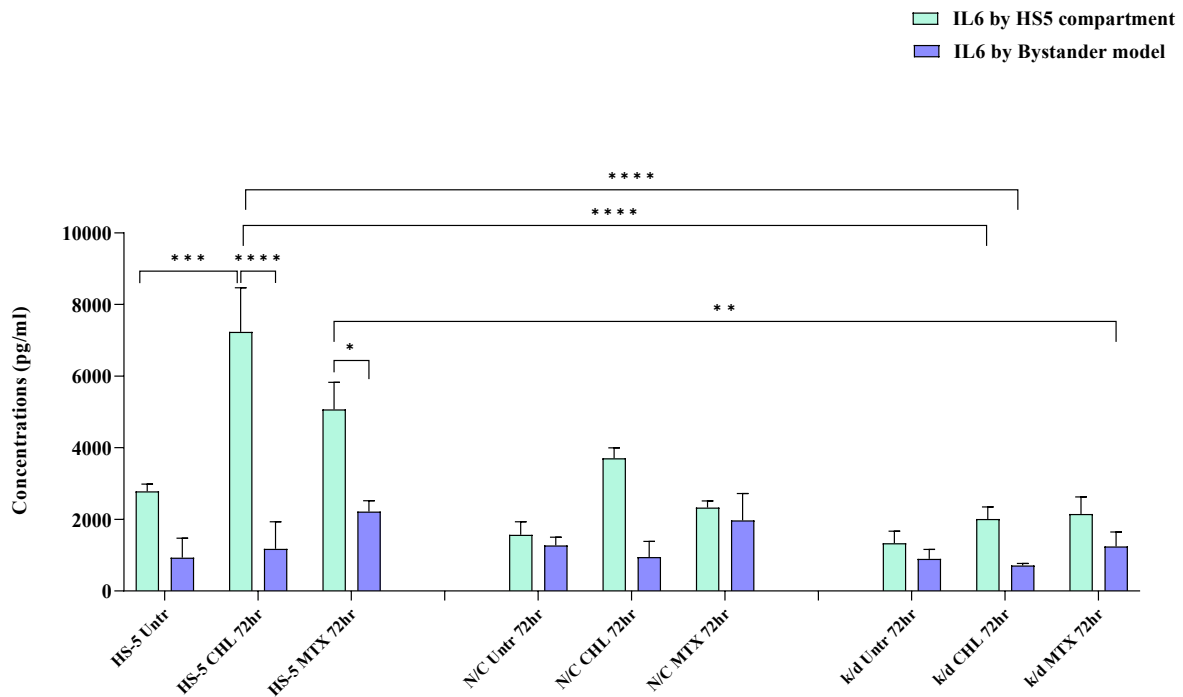


Figure 6. 5. IL-6 expression from IL-6 knockdown HS-5 alone vs co-culture with TK6. HS-5 cells were seeded, knockdown performed and chemotherapy treatments administered as described in section 6.2.1.3. The TK6 bystander cell basket was inserted into the well of the IL-6 knocked down HS-5 cells at 48 hours following drug treatments and the supernatants were collected 72 hours after drug exposure. The experiment was performed with control HS-5 (+/- drugs), N/C (+/- drugs) and siRNA (+/- drugs) and IL-6 expression was analysed by ELISA. Data shows the mean \pm SD (n=3) and significant difference is shown as * $p \leq 0.05$, ** $p \leq 0.01$, *** $p \leq 0.001$ and **** $p \leq 0.0001$ using two-way ANOVA, Tukey's multiple comparisons test.

6.3.1.4 MN analysis in TK6 co-cultured with IL-6 knockdown HS-5

Although there was a non-significant drop in viability for the treatment samples compared to the negative control (HS-5 without drugs and knockdown), all the cell RPD values were above 50% for all detected samples in figure 6.6. Therefore, the MN assay was conducted following OECD guidelines.

MN levels in k/d treated samples displayed non-significantly lower values compared to their respective N/C samples. Only CHL-treated HS-5 with k/d samples exhibited a significant reduction ($p \leq 0.01$, two-way ANOVA) in MN counts compared to those without k/d treatment. Despite a modest effect, siRNA N/C samples demonstrated an impact on decreasing MN counts in both chemotherapeutic agent-treated HS-5 cells compared to those without treatments. The fold reduction of MN in N/C samples (1.2-fold) and k/d treated samples (1.5-fold without drugs, 1.9-fold with drugs) relative to untreated samples suggests a greater reduction in MN levels upon k/d treatment, particularly in the presence of chemotherapeutic agents.

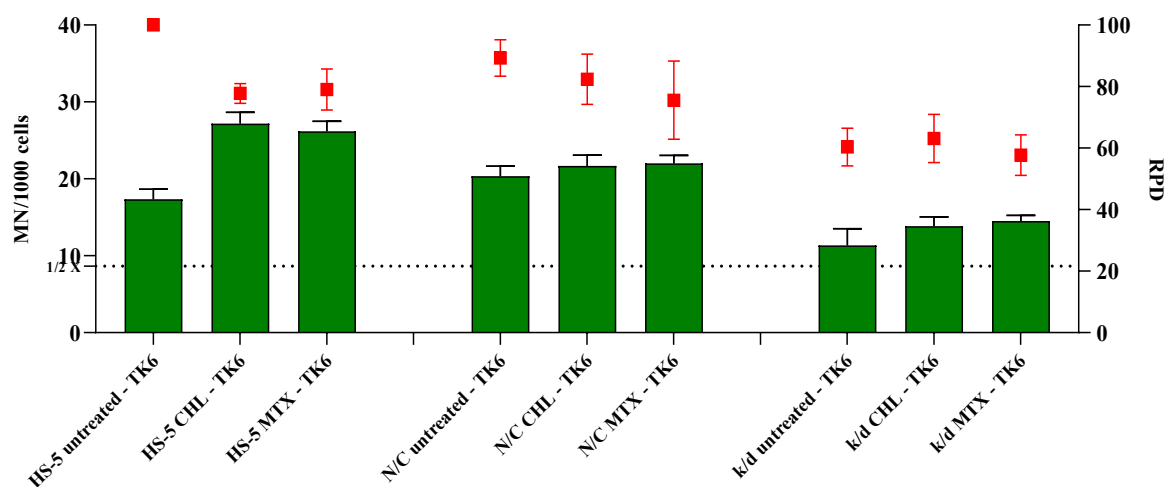


Figure 6. 6. The induction of micronuclei in TK6 cells co-cultured with IL-6 knockdown HS-5. HS-5 cells were seeded, and knockdown and chemo treatments were performed according to the protocol. TK6 bystander cell basket was insert into the IL-6 knockdown HS-5 cells and incubated overnight. Following day TK6 cells evaluated for MN and relative population doubling (RPD) were calculated subsequent day. The experiment was planned with control HS-5 (+/- drugs), N/C (+/- drugs) and siRNA (+/- drugs). The 1/2X dotted line represents 50% of the MN count of untreated HS-5. Data show mean \pm SD (n=3).

6.3.2 Resatorvid

Resatorvid concentrations were tested according to the literature evidence from *in vivo* and *in vitro* studies. Therefore, a range of concentrations were analysed and an IL-6 inhibition longevity assay for HS-5 was performed with resatorvid as following.

6.3.2.1 Resatorvid cell viability and IL-6 inhibition longevity assay

HS-5 untreated cells were growing at their normal doubling time. After 24 hours of incubation, concentrations of 9 and 11 μM began to lose cell counts. However, after 24 hours the live cell counts in these samples remained constant (5.7×10^4) until day 5. Furthermore, over the course of 5 days, both the 9 μM and 11 μM treated samples had p values ($p \leq 0.01$) considerably lower than the untreated control. HS-5 treated with 7 μM also exhibited some subtle indication of cell death. Unexpectedly, 1 μM treated samples also demonstrated unexpected cell death and proliferated in tandem with the 7 μM sample. According to figure 6.7A, however, samples treated with 3 μM and 5 μM had the highest live cell counts and produced results that were very close to the untreated HS-5 cell count. Thus, it was decided to analyse the IL-6 concentrations in the supernatant obtained from these samples in order to discover the optimal concentration between 3 μM and 5 μM .

Figure 6.7B shows the IL-6 concentrations detected using the in-house ELISA assay in the resatorvid treated HS-5. Control HS-5 cells demonstrated ELISA data with similar IL-6 expression levels over 5 days. The 3 μM and 5 μM samples showed the best live cell counts and had comparable levels of IL-6 expression over 5 days. In the 3 μM treated samples, IL-6 secretion started to reduce on day 2 (48 hours), whereas for the 5 μM samples reduction started on day 3 (72 hours), but both concentrations started to increase on day 5. Except for day 4 (96 hours) the IL-6 expression for both 3 μM and 5 μM exposure samples across 120 hours were greater than control HS-5 IL-6 levels. The levels of IL-6 expression at 72 hours by HS-5 treated with 3 μM and 5 μM resatorvid samples are not notably different from one another (highlighted in red).

Since 3 μM started to reduce IL-6 levels from 48 hours and stayed at a lower level compared to IL-6 levels by 5 μM treated cells, the resatorvid optimum concentration was selected as 3 μM in subsequent tests.

Figure 6. 7. Live cell count (A) and IL-6 expression (B) by HS-5 exposed to IL-6 inhibitor resatorvid.

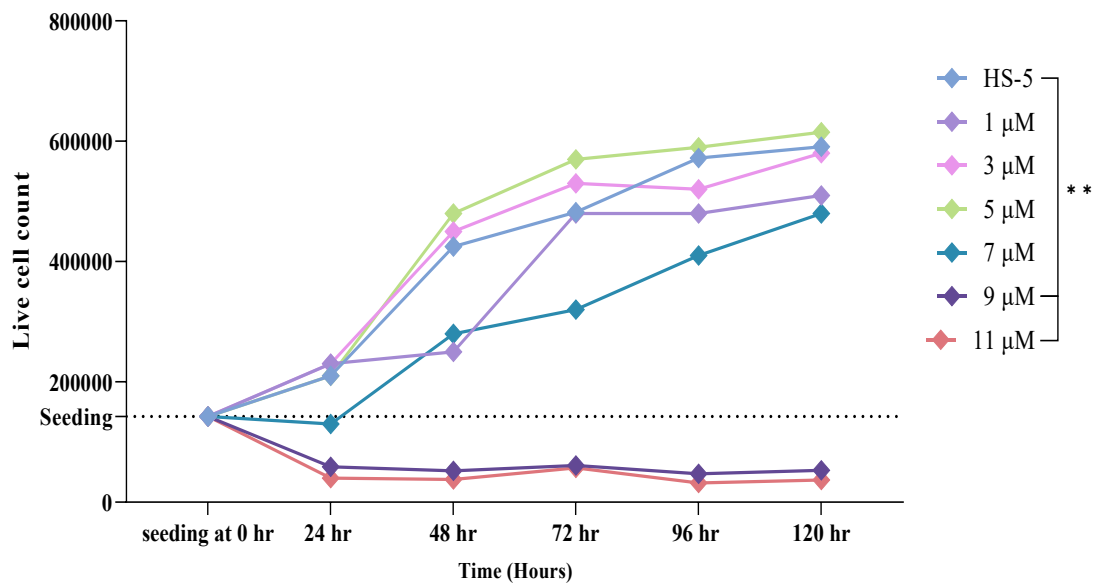


Figure 6.7A. Live cell counts of the HS-5 cell line following treatment with resatorvid at a range of doses. HS-5 cells were seeded and treated with resatorvid doses. Over 120 hours, cell counts were evaluated every 24 hours by the trypan blue exclusion assay and analysed automatically with the LUNA cell counter. Data shows the mean \pm SD (n=3) and significant difference is shown as $**p \leq 0.01$ as determined by two-way ANOVA, Tukey's multiple comparisons test.

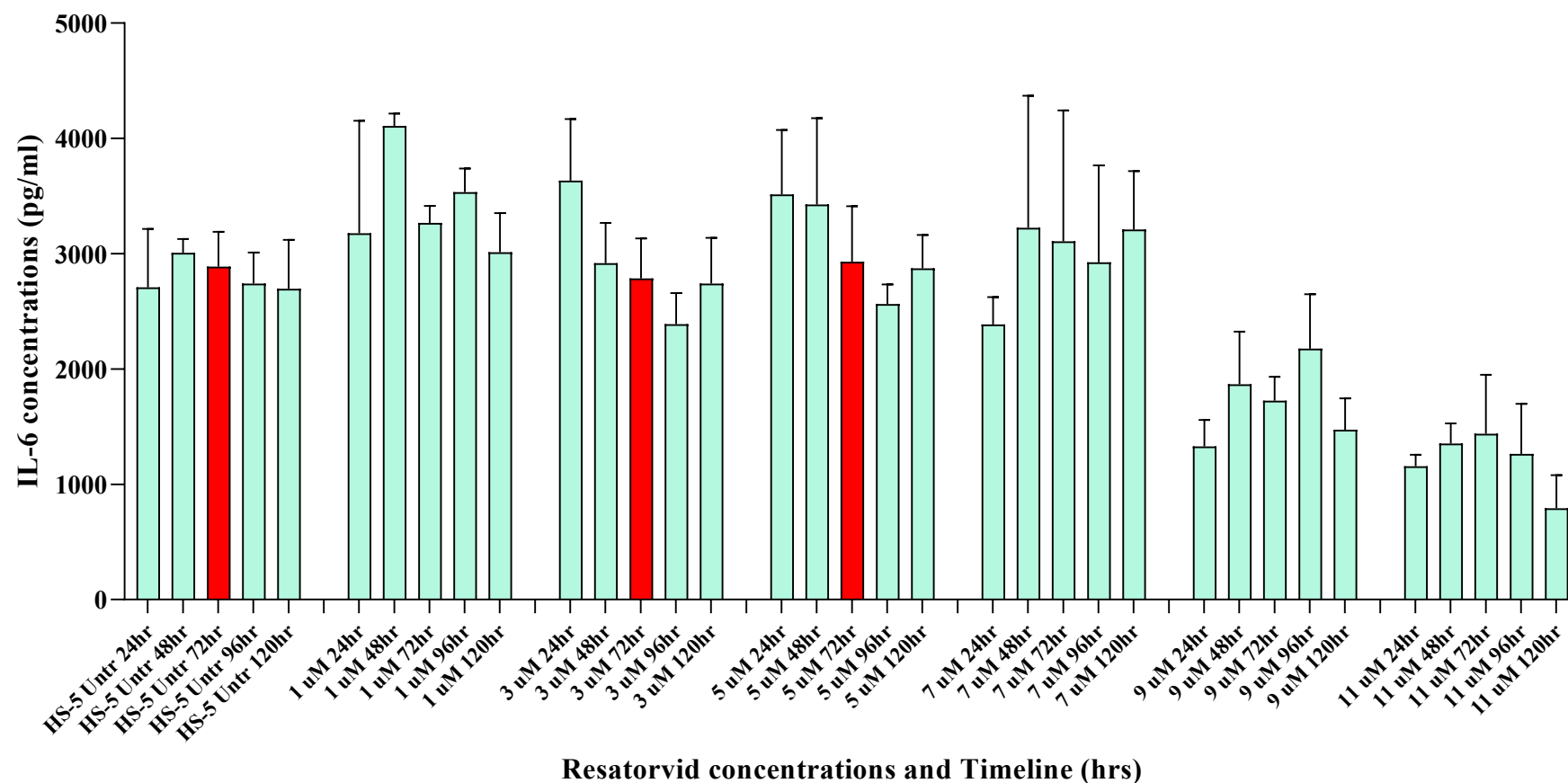


Figure 6.7B. IL-6 expression from HS-5 cells exposed to resatorvid at different concentrations. HS-5 cells were treated with six different resatorvid concentrations (1, 3, 5, 7, 9, and 11 µM) alongside the untreated HS-5 control sample. Culture media was collected every 24 hours over five days and analysed using IL-6 ELISA. Only concentrations of 3uM and 5uM exhibit a reduction in IL-6 expression over time and lowest IL-6 expression in the presence of inhibitor was at 72hrs compared to the without resatorvid samples (highlighted in red). Thus, these will be considered for the co-culture assay. Data shows the mean ± SD (n=3).

6.3.2.2 Resatorvid longevity assay with chemotherapies

Once the resatorvid concentration (3 μM) was finalised, the effectiveness of the inhibitor in the presence of chemotherapies was assessed. As discussed in section 6.2.2.2, HS-5 were treated with resatorvid and then separately with 4 μM CHL and 1.12 μM MTX. As shown in figure 6.8, cells treated with drugs generally expressed higher IL-6 than untreated HS-5 \pm resatorvid.

As previously, CHL treated HS-5 showed the greatest IL-6 expression for both with and without resatorvid samples. Without chemotherapies, IL-6 levels in untreated HS-5 were lower than in resatorvid treated HS-5 at 72 hours. Nonetheless when HS-5 were treated with either drug, levels at 72 hours were lower in resatorvid treated cells (highlighted in red) compared to their counterparts without resatorvid. However, in order to be consistent with previous experiments, resatorvid treatment at 3 μM and 72 hours were used as the optimal parameters for subsequent resatorvid and bystander assays.

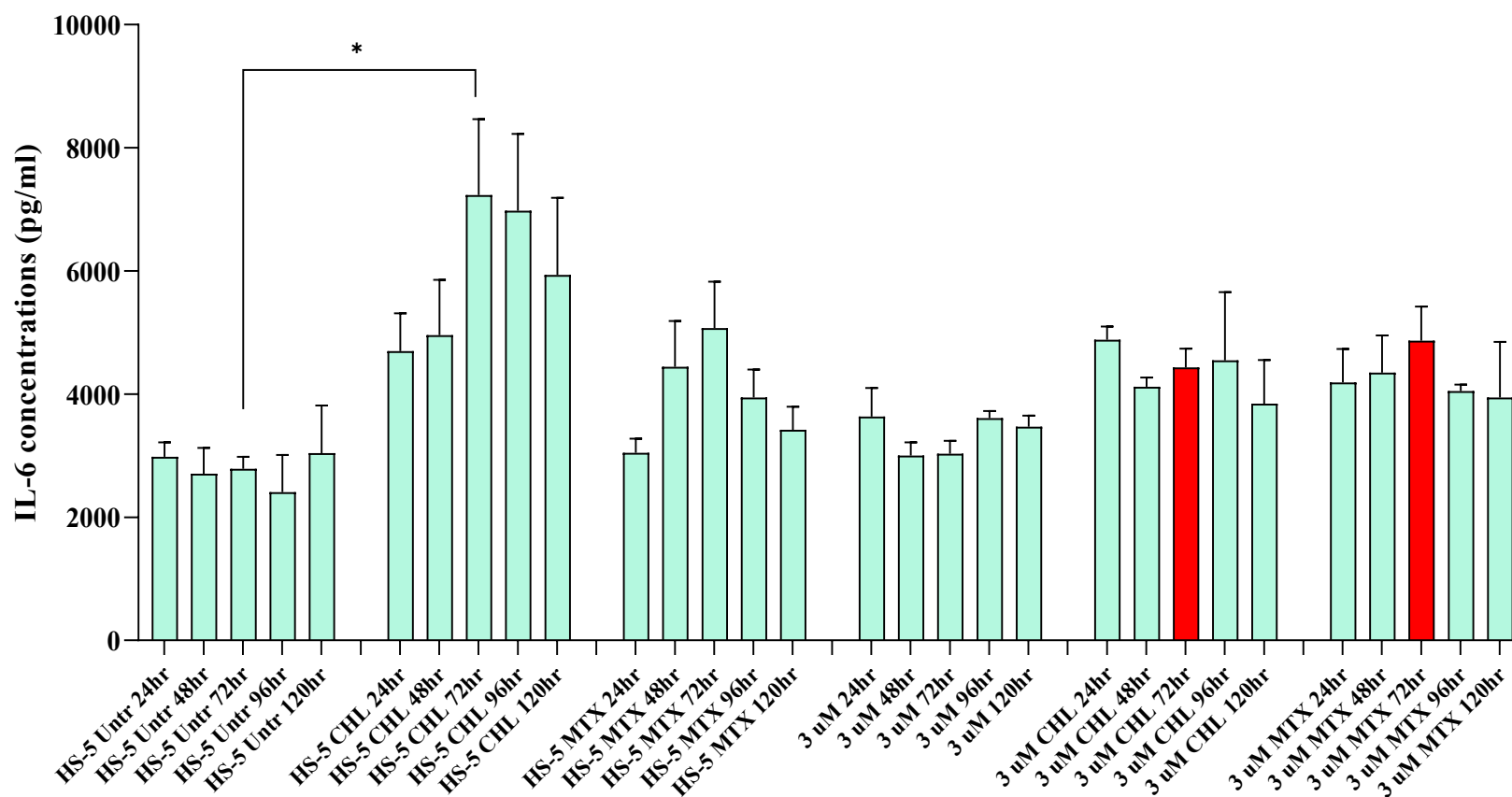


Figure 6. 8. IL-6 expression from HS-5 cells exposed to resatorvid with and without chemotherapies. HS-5 cells were treated with resatorvid (3 μ M) with and without CHL and MTX. Culture media was collected every 24 hours over five days and analysed using IL-6 ELISA. At 72 hours, the resatorvid-treated samples were compared with their no-resatorvid counterparts to assess the reduction in IL-6 expression following exposure to the drugs (highlighted in red). This time point was specifically selected for the co-culture assay to ensure alignment with the siRNA k/d timeline, thus enabling effective comparison of the results. Data shows the mean \pm SD (n=3) and significant difference is shown as * $p \leq 0.05$ as determined by two-way ANOVA, Tukey's multiple comparisons test.

6.3.2.3 Resatorvid treated HS-5 co-cultured with TK6 in the bystander assay

Figure 6.9 shows the IL-6 expression from HS-5 cells treated with resatorvid inhibitor in single compartment and in co-culture with TK6. Overall IL-6 expression in HS-5 treated with resatorvid were lower than without resatorvid in single HS-5 models, but this was the opposite in co-culture models, where resatorvid bystander models had greater amounts of IL-6 than resatorvid negative bystander samples. CHL-treated HS-5 with resatorvid in single compartments had highly significant reductions ($p \leq 0.01$) in IL-6 secretion in comparison to CHL-treated HS-5 without resatorvid. In contrast, in bystander models these same treatments showed an increase in IL-6 with resatorvid in comparison to without resatorvid ($p \leq 0.05$). Without resatorvid treatments, HS-5 treated with drugs expressed significantly higher IL-6 levels in their single compartment than bystander model. Generally, bystander samples in the presence of resatorvid are higher than without which is in contrast to what would expect for samples in the presence of the inhibitor.

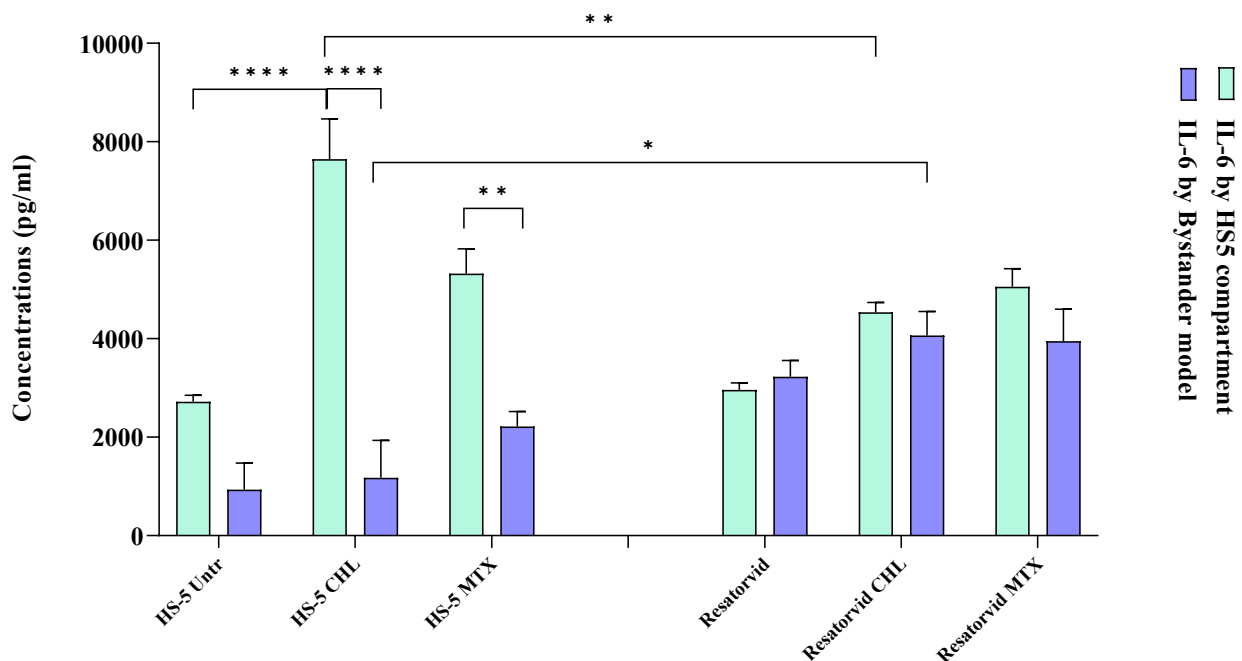


Figure 6. 9. IL-6 expression in resatorvid treated HS-5 alone vs HS-5 co-cultured with TK6 in a bystander assay. HS-5 cells were seeded, then resatorvid and chemotherapy treatments were performed. The TK6 bystander cell basket was inserted into the well and the supernatants were collected on the subsequent day. Data shows the mean \pm SD (n=3) and significant difference is shown as * $p \leq 0.05$, ** $p \leq 0.01$ and **** $p \leq 0.0001$ as determined by two-way ANOVA, Šídák's multiple comparisons test

6.3.2.4 MN analysis in bystander TK6 co-cultured with IL-6 resatorvid inhibited HS-5

Bystander TK6 cells were subjected to the MN test in accordance with OECD recommendations, both with and without resatorvid treatments. Although there is a modest decrease in MN induction for samples that have been treated with resatorvid and drugs, these samples were not substantially different across any groups (Fig. 6.10). In comparison to HS-5 without resatorvid, the reduction of MN by CHL and MTX treatment with resatorvid was 15% and 34%, respectively. However, the MN in the HS-5 sample without both drug and resatorvid treatments were lower (17) than the untreated HS-5 sample with resatorvid (20).

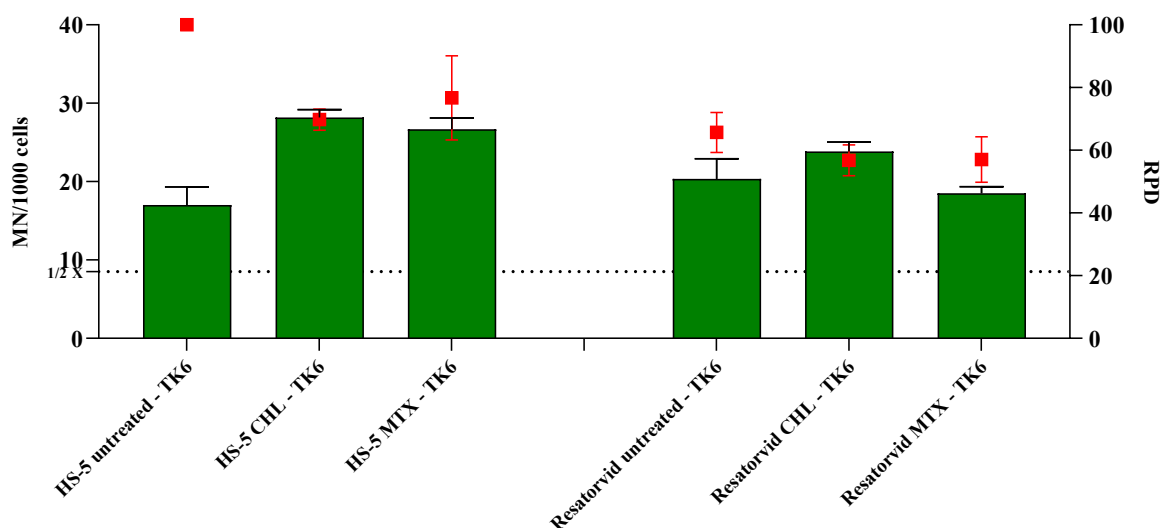


Figure 6. 10. The induction of micronuclei in TK6 cells co-cultured with resatorvid treated HS-5. HS-5 cells were seeded, then resatorvid and chemotherapy treatments were performed according to the protocol. The TK6 bystander cell basket was inserted into the well containing IL-6 inhibited HS-5 cells and incubated overnight. The following day, the TK6 cells were harvested and evaluated for relative population doubling (RPD) and MN score. The 1/2X dotted line represents 50% of the MN count of untreated HS-5. Data shows the mean \pm SD (n=3).

6.4 Discussion

The significance of pro-inflammatory cytokines in the context of cytokine storms and cancer development cannot be overstated. These cytokines serve as crucial mediators of immune responses and inflammatory processes that, when dysregulated, can contribute to the initiation and progression of various diseases, including cancer. Pro-inflammatory cytokines such as IL-1 β and TNF- α cause an increase in more inflammatory cytokines such as IL-6 following radiation therapy. In response to an increase in the number of inflammatory signals, HSCs are forced to exit their homeostatic quiescent state and proliferate to generate more cells. In this scenario, the chances to acquire and accumulate cellular mutations increases, as more DNA divisions occur. Indeed, long-term exposure to IFN- α or TNF- α mimicking chronic inflammatory stimuli resulted in an increased mitochondrial ROS-induced DNA damage in HSCs, which is another mechanism that may happen during secondary malignancy (Yildizhan & Kaynar, 2018; Wang *et al.*, 2022).

IL-6 and TNF- α are key proinflammatory cytokines which play central roles in cytokine storms, manifesting many inflammatory diseases, mediating different pathways and inducing the expression of other cytokines (Pandi *et al.*, 2017). IL-6 and its signalling pathways JAK/STAT3 play a crucial role in the development and progression of various cancers by promoting cell proliferation, reducing apoptosis, enhancing metabolism, increasing antiapoptotic factors, stimulating angiogenesis and metastasis which could lead to drug resistance and safeguard cancer cells from DNA damage (Masjedi *et al.*, 2020). Given the pivotal role of these cytokines in various pathologies, there is a growing focus on the development of strategies to effectively suppress or downregulate the genes responsible for these cytokines. Researchers have explored various therapeutic agents to achieve this goal. Notably, some studies have employed TNF- α blocking agents like adalimumab, etanercept, infliximab, certolizumab and golimumab to inhibit TNF- α in many inflammatory diseases including rheumatoid arthritis, ankylosing spondylitis, psoriasis and Crohn's disease (Kleiner *et al.*, 2013; Pandi *et al.*, 2017). Conversely, some studies have explored the use of hormone therapy, mAb tocilizumab and siltuximab to treat many diseases associated with high IL-6 levels (Riegler *et al.*, 2019; Shimabukuro-Vornhagen *et al.*, 2018). Nevertheless, many of these treatment strategies are associated with cost implications and additional side effects. Most importantly, is that mAbs cannot cross the blood-brain barrier, and hormone therapy can impair T cell function (Kang *et al.*, 2020).

Given the importance of aberrant IL-6 signalling in cancers, IL-6 blockade using IL-6 ligand-binding antibodies and IL-6R blocking antibodies have been tested preclinically, demonstrating tumour growth inhibition either alone or in combination with cytotoxic chemotherapies. The study of JAK inhibitors (IL-6 signalling) led to inhibition of both *in vitro* and *in vivo* growth of relapsed B-cell leukaemia (Sansone & Bromberg, 2012). Since then, a number of natural products (curcumin, resveratrol, flavopiridol and piceatannol) have been tested preclinically and demonstrated to inhibit pathways involved in inflammation and IL-6 STAT3 phosphorylation through a decrease in cytokine production or as a direct inhibitor of the JAKs (Sansone & Bromberg, 2012). These diverse approaches are aimed at attenuating the inflammatory responses driven by IL-6, thereby offering potential avenues for the management of conditions marked by cytokine storms and inflammatory diseases. Hence, targeting IL-6 and its pathways holds promise as a novel and effective approach for cancer therapy.

This chapter places a specific emphasis on IL-6 among the various cytokines. IL-6 has emerged as a pivotal factor that plays a central role in initiating cytokine storms and fuelling inflammatory responses in the aftermath of conditioning therapy for cancer patients. Given that IL-6 direct treatment can induce high MN and higher genotoxicity in combination with other candidates, the research aims were to investigate the potential impact of IL-6 expression by HS-5 cells on neighbouring bystander cells in co-culture models. To achieve this, this chapter adopts a specific focus on inhibiting IL-6 expression in the cell nucleus and knockdown of IL-6 gene using an RNA interference technique. This strategic intervention serves a dual purpose. First, it is designed to reduce the inflammatory effects within the affected cells. Second, it aims to mitigate the harm that excessive inflammation can cause to nearby (bystander) cells. In doing so, it is hoped to provide a promising avenue for better management and control of the severity of conditions associated with cytokine storms and inflammatory diseases, particularly within the context of cancer therapy.

This research used Silencer™ Select IL-6 siRNA (Thermo Fisher, UK) to knockdown IL-6 mRNA in HS-5 bystander models. siRNA-mediated gene knockdown involves the introduction of IL-6 siRNA molecules into target cells, their incorporation into the RISC complex, and the subsequent cleavage and degradation of IL-6 mRNA, leading to reduced IL-6 protein production and its associated effects on cellular processes. This technology has significant therapeutic potential in treating diseases where IL-6 is overexpressed, such as certain inflammatory conditions.

There are two types of transfections, forward and reverse. In forward transfections, cells are plated in the wells (adherent cells) and the transfection mix is generally prepared and added the next day whereas in reverse transfections, the complexes are prepared inside the wells, after which cells and medium are added. Lipofectamine was used to provide high transfection efficiencies and maximise knockdown at low concentrations with minimal cytotoxicity. To obtain the highest transfection efficiency and low non-specific effects, all the knockdown reagents were optimised. As the first optimisation phase, different concentrations of IL-6 siRNA were assessed on HS-5 cell growth and IL-6 expression over a 120 hour period, offering valuable insights into the suitability of the reagents and the optimal concentration for effective IL-6 knockdown. The concentrations of 3, 6 and 12 pmol of siRNA were selected for analysis based on the manufacturer's protocols, particularly in the context of BM-MSCs.

Figure 6.3A demonstrated that the physical state and morphology of HS-5 cells remained largely consistent over the 120-hour period, regardless of the treatment group. This finding is important as it suggests that the reagents employed, including Opti-MEM media, Lipofectamine, and Silencer Select Negative Control, did not induce significant cell deaths or adverse effects on the cells' appearance. At all three concentrations (3 pmol, 6 pmol, and 12 pmol), it was apparent that the cells treated with IL-6 siRNA exhibited faster growth and a higher cell count when compared to the untreated and negative control-treated groups. However, it is worth noting that the morphological characteristics of the cells treated with IL-6 siRNA did not significantly differ from those of the untreated cells. This suggests that the siRNA treatment was effective in promoting cell growth without causing noticeable alterations in cell morphology. When comparing the different siRNA concentrations, the 6 pmol concentration demonstrated a more consistent cell density and appearance when compared to the higher 12 pmol concentration, which showed somewhat promoted growth. Thus, it can be concluded that the 6 pmol concentration strikes a balance between effective IL-6 knockdown and maintaining favourable cell number in the HS-5 cell line.

Furthermore, figure 6.3B focuses on the expression of IL-6 by HS-5 cells after exposure to various concentrations of siRNA, negative control (N/C), and other knockdown reagents. A combination treatment of Opti-MEM and Lipofectamine showed consistent IL-6 levels over the course of five days which is quite similar to untreated HS-5. These control samples exhibited results consistent with ELISA findings discussed in Chapter 4. IL-6 expression from untreated HS-5 were between 2000-3000 pg/ml. Even though the levels were different between

each time points, overall the IL-6 levels by Opti-MEM and Lipofectamine treated cells were not far away from the untreated samples, suggesting that these knockdown reagents did not cause any changes in IL-6 expression from HS-5.

In the case of siRNA N/C treatments, 3 pmol siRNA yielded results similar to the control group, whereas 6 pmol treated samples had lower IL-6 levels but the lowest results were observed in the 12 pmol group. Further analysis of IL-6 siRNA revealed interesting dynamics over time. The 3 pmol treated cells did not exhibit a decrease over the incubation period but showed a sudden increase on day two. The 12 pmol dose did not show significant changes over time but exhibited an increase on the last day. In contrast a study on shRNA consistently maintained 4-fold lower IL-6 levels and 70% reduced IL-6 mRNA over 6 days (144 hours) (Kang *et al.*, 2020). Among all the categories, the most significant reduction in IL-6 expression was seen in HS-5 cells treated with siRNA at 6 pmol concentration. When determining the optimal concentrations for siRNA, caution is warranted due to recent reports indicating that synthetic siRNAs can saturate specific elements within the cellular RNAi pathway, resulting in a limited capacity to assemble the RISC complex on exogenous siRNAs. Thus, it is important to use doses of siRNA as low as possible to prevent saturation of some factors in the RNAi pathway (Guo *et al.*, 2010). Based on above information and findings of this research, the 6 pmol concentration of IL-6 siRNA treatment is the most promising choice for achieving effective IL-6 knockdown without significant alterations to cell morphology (Fig 6.3A). Administering this concentration within the optimal 72 to 96 hour time frame (Fig. 6.3B) represents the most suitable condition for conducting subsequent experiments with the IL-6 knockdown kit on HS-5 adherent cell lines.

Figure 6.4 explored the effectiveness of siRNA treatment at a concentration of 6 pmol in the presence of two chemotherapies: 4 μ M CHL and 1.12 μ M MTX. This was done to investigate whether the optimal time frame for siRNA treatment of HS-5 cells, which was found to be between 72 to 96 hours in figure 6.3B, would change in the presence of chemotherapy treatment. HS-5 cells treated with CHL and MTX exhibited the highest IL-6 expression on day 3 (72 hours). CHL-treated cells had the overall highest IL-6 expression at 7235 pg/ml, which was greater than MTX-treated cells (5072 pg/ml). This time frame aligns with when the cytokine array was performed for the respective drugs, suggesting a strong correlation between drug treatment, IL-6 expression and maximal bystander effect (indicated by the work of a previous research team member). Technically N/C siRNAs are non-targeting siRNA designed

not to target any gene but are used for determining the non-specific effects of siRNA delivery. Neither the mRNA nor protein level of the experimental gene should be affected by the N/C siRNA (Kang *et al.*, 2020). However, N/C siRNA treated categories (untreated, CHL, MTX) in figure 6.4 showed slightly lower IL-6 levels compared to their control counterparts. Another N/C strategy is the mock knockdown that did not exhibit a significant difference from control HS-5 samples, even though the expression levels on the respective days show differences between the two categories. The lowest IL-6 expression was observed in untreated HS-5 with siRNA at 48 hours (1256 pg/ml). Nonetheless, for consistency with other investigations, the 72 hour time point was considered the best period for knockdown for HS-5 cells, both with and without chemotherapy treatment, resulting in 1332 pg/ml of IL-6 in knockdown IL-6 treated HS-5 (highlighted in red). The findings indicate that there was not a significant alteration in this regard compared to the findings in figure 6.3B. Even after drug treatment, the optimal time frame for siRNA treatment remained at 72 to 96 hours. As a result, for the duration of this research, the 72-hour time frame following drug treatment (96 hours after knockdown) was adopted as the best knockdown period for IL-6.

Studies have revealed that the expression levels of IL-6 can be modulated based on the presence of bystander cells in co-culture scenarios. This was supported by Kang *et al.* (2020) showing significantly high IL-6 mRNA and IL-6 expression by CART-19 cells when they co-cultured with B lymphoma in comparison to single cell models. Also, IL-6 secreted by the co-culture models triggered a significant level of IL-6 and other cytokines from monocytes in a media transfer assay. This cascade of events is proposed as the primary mechanism underpinning the development of cytokine release syndrome/cytokine storm.

Upon finalising the optimal parameters in this study, the research advanced to a pivotal phase, where the co-culture experiments involved IL-6 knocked down HS-5 cells with TK6 cells in a bystander model. This step was undertaken with and without the presence of chemotherapies. In figure 6.5, the supernatant from each well was evaluated for IL-6 levels through ELISA. The IL-6 concentration in the supernatant is a key metric because it signifies the impact of chemotherapies on the cytokine milieu in IL-6 knockdown HS-5 co-culture, and also determines the influence of IL-6 in CIBE to produce a genotoxic impact on TK6 bystander cells.

Figure 6.5 observed significant differences in IL-6 expression levels when comparing drug-treated HS-5 cells (without siRNA) to their respective bystander models. Specifically, the differences were highly significant ($p \leq 0.0001$) for CHL (7235 pg/ml vs 1176 pg/ml) and moderately significant ($p \leq 0.05$) for MTX (5072 pg/ml vs 2214 pg/ml). Consequently, the reduction percentages in IL-6 expression for drug-treated (without siRNA) samples were 83% and 56% for CHL and MTX, respectively. Furthermore, the IL-6 expression in CHL-treated samples without siRNA was significantly higher ($p \leq 0.0001$) compared to both the single (2008 pg/ml) and bystander (711 pg/ml) HS-5 samples treated with CHL and siRNA. IL-6 expression by siRNA-treated HS-5 cells (with or without drugs) in the bystander models were considerably lower than those observed in the single HS-5 cell compartment, which infers take up of the IL-6 by the TK6 cells. The reduction percentages in samples with siRNA were 32% without drugs, 64% for CHL, and 42% for MTX.

An interesting *in vivo* study by Kang *et al.* (2020) found significantly lower serum IL-6 levels when IL-6 was knocked down in CART-19 cells in B lymphoma mice. Furthermore, they confirmed that IL-6 knockdown did not affect IFN- γ or IL-2 expression by CART-19 cells. Although the reductions in the current study did not reach statistically significant levels, this observation suggests that either siRNA treatment may have a suppressive effect on IL-6 expression in the context of bystander models compared to single HS-5 compartments or that the bystander cells are taking up the IL-6. The findings provide valuable insights into the potential regulatory roles of siRNA and drug treatments on IL-6 expression within single and bystander models. It is essential to consider that bystander cells (TK6) can also exert an influence on IL-6 levels in the co-culture system by either secreting IL-6 or modulating expression by HS-5 cells. This assertion is verified by Kang *et al.* (2020) in media transfer from IL-6 knocked down CART-19 cells which dramatically reduced IL-6 release from monocytes in *in vitro* study. Furthermore, it is imperative to acknowledge that the outcomes of these findings may be influenced by the specific siRNA delivery methods and the low stability of siRNA (Takeshita *et al.*, 2005). Researchers have devised various strategies to address these limitations. The *in vitro* results from Masjedi *et al.* (2020) showed that specific siRNA-loaded nanoparticles significantly reduced the IL-6 and STAT3 expression up to 90% in three cell lines (breast, colorectal and melanoma). Subsequent *in vivo* investigation indicated that IL-6/STAT3 siRNAs significantly inhibited the cancer cell proliferation and migration, and also

reduced the tumoral bulk and inhibited angiogenetic function via downregulation of tumour-promoting factors such as VEGF, FGF and TGF- β .

Within the current study, bystander co-cultured TK6 cells were subsequently assessed for RPD values and MN assays in accordance with OECD guidelines (Fig. 6.6). It is evident that all knockdown samples consistently exhibited lower MN levels when compared to the MN levels in non-knockdown HS-5 and N/C HS-5 cells. Also, siRNA N/C samples demonstrated some effect in decreasing MN counts when compared to HS-5 cells without any knockdown treatments. Interestingly, the MN assay revealed that CHL-treated samples in the knockdown co-culture context exhibited a significant reduction ($p \leq 0.01$) in MN levels compared to its non-knockdown counterpart. Notably, MN in bystander TK6 cells exhibited a 35% reduction for knockdown untreated co-culture conditions compared with non-knockdown untreated HS-5 cells. In contrast, this reduction increased to 50% in chemotherapy co-culture models involving knockdown samples. This suggests that IL-6 knockdown in bystander samples can exert a partial, albeit non-significant, reduction in MN induction in bystander cells. Most interestingly, IL-6 knockdown reduced MN induction, bringing it in line with baseline MN levels observed in TK6 cells treated with recombinant IL-6 cytokines (Chapter 5, Fig. 5.6).

It is essential to acknowledge that cell interactions can occur through both chemical signalling and physical cell-to-cell contact. Experiments by Cheleuitte *et al.* (1998) provided evidence suggesting that the increased formation of osteoclast cells in co-cultures of HSC and marrow stromal cells may be primarily mediated through direct cell-to-cell contacts. This conclusion was supported by the fact that attempts to physically separate these cell types using a Millipore membrane or by introducing neutralising antibodies against IL-6 and IL-1 β did not promote osteoclast development. Hence, it is crucial to consider the role of HS-5 cells in signalling, particularly their involvement in inducing IL-6 production when exposed to various cells or chemical compounds. To explore this further, chemical inhibition was used to block and reduce the IL-6 signalling, which ultimately leads to alterations in IL-6 gene expression within the HS-5 nucleus.

Resatorvid is a chemical inhibitor of IL-6 in TLR4-mediated inflammatory conditions. The findings of Matsunaga *et al.* (2011) suggest that resatorvid selectively inhibits the TLR4 receptor among 10 human TLRs, due to distinctive binding regions of TLR4 without effect on TLR4 dimerization. This disrupts the interaction of TLR4 with MyD88 molecules, ultimately

leading to the suppression of NF- κ B activation and the subsequent reduction in the production of pro-inflammatory cytokines such as IL-6 and TNF- α . This mechanism helps attenuate the inflammatory response of MSCs in various contexts, potentially making it useful in the treatment of inflammatory conditions involving MSCs (Zeuner *et al.*, 2015). By inhibiting pro-inflammatory cytokine expression, resatorvid can help modulate the immune response and mitigate inflammatory processes, making it a potential therapeutic option for conditions characterised by excessive IL-6 production, such as certain autoimmune diseases and cytokine release syndrome (Matsunaga *et al.*, 2011; Suzuki *et al.*, 2012). Due to the limited available information regarding the use of resatorvid on the HS-5 cell line or co-culture models, it becomes necessary to fine-tune the optimal concentration and duration of resatorvid treatment for specific cell lines. This process of optimisation will enable the determination of the most effective dosage and duration for inhibiting the desired cellular responses.

HS-5 cells were subjected to various concentrations of resatorvid based on findings from relevant literature (section 6.2.2.1) and were then monitored for cell viability and live cell count over a span of 5 days (120 hours), as depicted in figure 6.7A. Among the various concentrations examined, the higher doses of 7, 9 and 11 μ M displayed lower live cell counts over time when compared to the untreated control. However, the concentrations of 1, 3 and 5 μ M exhibited live cell counts similar to those of the untreated HS-5 samples. However, it is essential to not only consider cell viability but also the levels of IL-6 in these samples before making any decisions. because the optimal resatorvid concentration should strike a balance between maintaining robust cell viability and achieving maximum IL-6 inhibition, leading to lower IL-6 levels by HS-5. To address this, IL-6 concentrations were analysed in the supernatant obtained from these samples and are shown in figure 6.7B.

Among the different treatment categories, it was observed that HS-5 treated with 9 μ M and 11 μ M of resatorvid exhibited the lowest IL-6 levels. However, due to the inadequate number of live cells, as depicted in figure 6.7A, these lower IL-6 levels were not taken into account. Nonetheless, following studies have demonstrated the efficacy of high-dose treatment (10 μ M) in effectively inhibiting IL-6 mRNA expression and IL-6 secretion across various cell lines. For instance, when articular disc cells were exposed to resatorvid (10 μ M), a substantial reduction in the activation of NF- κ B and AKT pathways with the downregulation of IL-6 expression was observed (Hu *et al.*, 2022). Moreover, BV-2 microglial cell lines treated with

resatorvid (10 μM) resulted in significantly reduced pro-inflammatory cytokines, including TNF- α , IL-1 β , and IL-6 (Cui *et al.*, 2021).

On the other hand, Liu *et al.* (2021) demonstrated that 1 μM resatorvid could inhibit the TNF- α , IL-6 and IL-8 release in BV2 cell line. Qu *et al.* (2021) exhibited significantly decreased expression of IL-1 β , IL-2, and TNF- α in resatorvid treated BV2 cells. However, in the current study when the analysis of IL-6 expression was performed in cells treated with 3 μM and 5 μM of resatorvid, it was observed that both concentrations produced fairly similar IL-6 expression patterns (Fig. 6.7B). However, these patterns tended to exceed the IL-6 levels exhibited by HS-5 cells without resatorvid inhibition, with the exception of data recorded on day 4 (96 hours). In line with the previous experiments, resatorvid inhibition focused on the time period from 72 to 96 hours, to maintain consistency. Notably, at 72 and 96 hours, the IL-6 expression levels in untreated HS-5 (2888 to 2740 pg/ml), 3 μM treated HS-5 (2784-2388 pg/ml), and 5 μM treated HS-5 (2930-2563 pg/ml) samples showed relatively minor differences. Among these concentrations, it is worth highlighting that only the 3 μM treatment displayed consistently lower IL-6 levels at both 72 and 96 hours, where in contrast the 5 μM treatment exhibited higher IL-6 levels at 72 hours when compared to the untreated control. Based on the comprehensive analysis of the data from both figures, the decision was taken to advance with 3 μM as the optimal concentration for resatorvid in forthcoming experiments. This choice is informed by the combined considerations of maintaining cell viability, effectively inhibiting IL-6 expression, and ensuring consistency with prior findings.

The experiment was repeated to ensure whether the observed outcomes would exhibit alterations when HS-5 cells are also exposed to specific drugs. This aimed to explore how these drugs might influence the IL-6 expression dynamics under resatorvid inhibition and whether any shifts in expression patterns would manifest over the course of 5 days. Thus, as part of this inquiry, the experiment was replicated using 3 μM resatorvid while introducing treatments with CHL and MTX, as detailed in figure 6.8. In Matsunaga *et al.* (2011) experiments, resatorvid exhibited a time and concentration-dependent inhibition of inflammatory mediators. Their ELISA showed a sufficient inhibitory effect on IL-6 and TNF- α secretion by resatorvid (1 μM) pretreatment for only 5 minutes, but lower concentrations with longer incubation time (60 minutes) increased the efficacy. Another study by Zhou *et al.* (2022) measured lower levels of TNF- α , IL-1 β following resatorvid (1 μM) for 30 minutes and Wen *et al.* (2021) measured significantly reduced IL-6, TNF- α and NO with 1 μM resatorvid pre-treatment for 2 hours. In

contrast, a study by Mateu *et al.* (2015) treated their cells with 5 μ M of resatorvid for only 45 minutes before other treatments. Considering all this evidence, it was decided to incubate HS-5 cells with inhibitor for 2 hours before adding the drugs.

Consistently, CHL-treated HS-5 cells exhibited the highest IL-6 expression, both with and without resatorvid. Without the presence of chemotherapies, the IL-6 levels in HS-5 cells (2785 pg/ml) at 72 hours were lower than the IL-6 expression observed in resatorvid-inhibited HS-5 cells (3029 pg/ml) (Fig 6.8). However, when both resatorvid and non-resatorvid-treated samples were subjected to drug treatments, a noteworthy trend emerged: IL-6 levels were lower in resatorvid-treated cells (highlighted in red; CHL; 4434 pg/ml, MTX; 4869 pg/ml) compared to HS-5 cells without resatorvid (CHL; 7235 pg/ml, MTX; 5072 pg/ml). This suggests that resatorvid has the potential to inhibit IL-6 expression signals when cells are exposed to external factors, such as drugs or ligands, as compared to HS-5 cells without any treatments. Gu *et al.* (2020) showed a high MMP-9/2 expression by SH-SY5Y cell line treated with oxaliplatin (platinum compound) in chemotherapy-induced peripheral neuropathy, where this was reduced by treatment with 1 μ M resatorvid. Given the observed reduction in IL-6 expression in the drug-treated samples, it is plausible that there will be alterations in IL-6 expression in resatorvid-treated HS-5 cells in co-culture with TK6 (Fig. 6.9). Furthermore, due to the changes in IL-6 levels in the co-culture medium, the induction of MN in bystander TK6 cells may also experience variations (Fig. 6.10).

The ELISA data concerning IL-6 expression in HS-5 single culture revealed that, when the cells were exposed to drugs, the IL-6 expression in resatorvid-treated HS-5 cells was lower (CHL: 4535, MTX: 5053 pg/ml) than in non-resatorvid-treated cells (CHL: 7644, MTX: 5323 pg/ml). This aligns with the findings presented in figure 6.8. However, in the bystander models, this pattern displayed an opposite trend. Here, all inhibitor-treated cells exhibited higher IL-6 levels than those without inhibitor treatments. This indicates that in bystander models, either resatorvid may not be as effective or alternatively an underlying, unobservable factor may be causing an increase in IL-6 expression. There are significant differences between the IL-6 levels in HS-5 samples treated with drugs (CHL: 7644, MTX: 5323 pg/ml) but without resatorvid, in comparison to their corresponding bystander models (CHL: 1176, MTX: 2214 pg/ml). However, only the CHL-treated samples showed a significant reduction in IL-6 levels following resatorvid treatment in the single HS-5 model. In the single cell model, HS-5 treated with CHL but without inhibitors exhibited significantly higher IL-6 levels than the same

samples with inhibitors (4535 pg/ml). There was not much information regarding use of resatorvid in bystander models in the literature. The inflammatory cytokines including IL-1 β , IL-6 and TNF- α in the supernatant of macrophages co-cultured with pulmonary artery endothelial cells were shown to be decreased by the treatment with resatorvid (1 μ M) (Xie *et al.*, 2021). Conversely, in the current bystander model, the CHL pair (with/without resatorvid) again showed significant differences, but in the opposite direction. In this case, the inhibitor-treated HS-5 cells with CHL exhibited higher IL-6 levels (4066 pg/ml) than those without inhibitors.

Evidently, resatorvid demonstrates an inhibitory effect on IL-6 production in HS-5 cells when studied in isolation. However, in the context of bystander cultures alongside TK6 cells, a distinct mechanism seems to come into play, resulting in elevated IL-6 levels. This phenomenon could potentially be linked to the presence of TLR4 expression by HSC cells. It is plausible that resatorvid may impact TLR4 expression in HSC, thereby modulating their signalling pathways. This, in turn, could influence the expression of pro-inflammatory cytokines from both cell types and lead to alterations in IL-6 levels. Because as Zeuner *et al.* (2015) mentioned, TLR4 is expressed in most adult stem cell types and affects their fundamental functions; thus there is a high interest in a deeper understanding of the underlying molecular cascades. Therefore, careful evaluation of the role of TLR4 in stem cell populations should be considered. The most intriguing challenge is how the respective stem cell populations shift the inflammatory balance between NF- κ B (pro-inflammatory) and IRF3 (anti-inflammatory), following TLR4 ligation. As discussed by Matsunaga *et al.* (2011), TIRAP and TRAM are anticipated to bind to the same site on the TLR4 dimer interface. It remains uncertain whether a single activated TLR4 dimer can simultaneously recruit both proteins and is it possible that one interaction may influence the other. Therefore, the regulation of the delicate balance between cellular processes such as proliferation, differentiation, migration, and apoptosis are intricately modulated by the activation of either MyD88-dependent or MyD88-independent pathways.

This underscores the importance of assessing MN induction in these respective samples, as illustrated in figure 6.10. The assessment of MN in TK6 co-cultured with HS-5 results suggest there was a modest decrease in MN induction in samples treated with inhibitors plus drugs, the differences observed across various groups were not substantial. When comparing samples treated with resatorvid to those without resatorvid, it appears that resatorvid had a limited

impact on reducing MN induction. For instance, in comparison to the HS-5 without resatorvid, the reduction in MN induction was 15% with CHL treatment and 34% with MTX treatment when resatorvid was included. It is noteworthy that the samples without both drug and resatorvid treatments had a lower MN induction (17) compared to the samples treated with resatorvid (20). Considering the limited availability of literature regarding resatorvid and its potential impact on DNA damage, it is noteworthy that an *in vivo* study conducted by Suzuki *et al.* (2012) demonstrated that resatorvid (0.01 µg) significantly downregulated NOX4 expression by inhibiting TLR4. NADPH oxidases (NOX) are a major enzymatic source of ROS. TLR4 interacts with NOX4 leading to overproduction of ROS, induces oxidative stress and this damages DNA, proteins and lipids, leading to tissue degeneration. However, findings of this research highlight the complexity of the interactions between resatorvid and drugs in the context of MN induction. While some reductions in MN induction were observed with resatorvid in combination with drugs, the presence of resatorvid alone may have led to a slight increase in MN induction compared to the untreated control group.

6.5 Conclusion

This study has provided valuable insights into the intricate dynamics of cytokine regulation within the context of HS-5 cells and their interactions with various factors, including chemotherapies and siRNA/inhibitors. Investigation of this work focused on IL-6, a cytokine that holds significant importance due to its central role in triggering cytokine storms and driving inflammatory responses, particularly in the context of cancer therapy. The IL-6 experiments presented in this chapter uncover the potential impact of IL-6 expression by HS-5 cells on neighbouring bystander cells, particularly TK6, within co-culture models. This was employed as a dual-pronged approach that encompassed the inhibition of IL-6 signalling within the cell nucleus and the knockdown of the IL-6 mRNA using siRNA techniques. This strategic intervention was designed to not only mitigate the inflammatory effects within the affected cells but also to curtail the potential harmful excessive inflammation could be inflicted on nearby bystander cells. However, further research and analysis may be necessary to elucidate the underlying mechanisms responsible for these observations and to determine the clinical significance of these findings.

IL-6 siRNA concentrations of 6 pmol was deemed ideal for achieving efficient IL-6 reduction while keeping cell viability intact. This optimal knockdown period of 72 to 96 hours was found

to be consistent, even in the presence of chemotherapy treatment. The co-culture experiments involving IL-6 knockdown HS-5 cells and TK6 bystander cells provided a crucial turning point in the research. These experiments yielded significant differences in IL-6 expression between drug-treated HS-5 cells (without and without siRNA) and their corresponding bystander models. These findings suggested that siRNA treatment may exert a suppressive effect on IL-6 expression in bystander models compared to single HS-5 compartments. The assessment of MN induction in TK6 bystander cells in co-culture further expanded this understanding. The results indicated that IL-6 knockdown in bystander samples could partially reduce MN induction in these cells, with the reduction percentage increasing in the presence of chemotherapy. These findings offered promising avenues for addressing genotoxicity and CIBE in the context of IL-6 signalling. So, it is compelling that IL-6 is a significant factor in this research. Delving deeper into the underlying mechanisms driving these observations and to then address critical challenges in siRNA technology, can gain valuable insights into the role of IL-6 in CIBE.

There are key challenges which serve as the most significant barriers between siRNA technology and its therapeutic application; non-toxic delivery, free from potential IFN- γ responses and reduced off-target effects (Whitehead *et al.*, 2009; Takeshita *et al.*, 2005). Naked siRNA delivery also faces challenges with large molecular weight, hydrophilic properties, negative charge and they are also prone to *in vivo* degradation by enzymes present in plasma and via renal elimination (Pandi *et al.*, 2017). Furthermore, the off-target effects due to the presence of common base pair sequences in siRNA and ability to stimulate the innate immune response are the main challenges *in vivo*. As siRNA can possess the same molecular signatures as viral RNA, which are prone to activate TLR-3, -7, -8 and produce proinflammatory cytokines upon stimulation (Guo *et al.*, 2012), future research endeavours should prioritise the development of materials for siRNA delivery that are not only safe but also effective, ensuring the broadest possible clinical applications of RNAi technology. By addressing these challenges, the understanding of IL-6's role in CIBE can be advanced and potentially unlock its therapeutic potential.

Additionally, the incorporation of resatorvid into the experiments provided insights into its potential to modulate IL-6 expression and cytokine regulation. Resatorvid exhibited the ability to inhibit IL-6 production in HS-5 cells when studied in isolation. However, a distinct mechanism seemed to come into play in the context of bystander cultures with TK6 cells,

resulting in elevated IL-6 levels. This phenomenon may be linked to TLR4 expression by HSC cells and the intricate molecular cascades related to TLR4 activation. Overall, these findings underscore the multifaceted nature of cytokine regulation and the importance of considering both chemical signalling and physical cell-to-cell interactions. While resatorvid demonstrated the potential to modulate cytokine expression and response to drugs, further research is needed to understand the interactions between resatorvid and chemotherapies, which is crucial for assessing its safety and efficacy in relevant therapeutic contexts. The complexities of IL-6 regulation and its impacts on genotoxicity and bystander effects offer exciting opportunities for future investigations in the realm of inflammatory diseases and cancer therapy.

CHAPTER 7

FINAL DISCUSSION

7.1 Summary of findings

Leukaemia is a malignancy of the BM, resulting in reduced production of normal blood cells, accumulation of abnormal white blood cells due to uncontrolled proliferation, lack of differentiation, and apoptosis in the BM due to haematopoietic dysregulation and immune suppression. HSCT is considered a curative, but last resort, therapy for leukaemia although it is life-threatening due to multiple complications that come with myeloablative therapy (Barcellos-Hoff *et al.*, 2005). As described earlier in this research, cytokine storm exists, and consistently happens following myeloablative therapy. The BM microenvironment, exposed to ionising radiation, undergoes chronic inflammation, leading to the persistent production of numerous cytokines including: elevated levels of G-CSF and GM-CSF, which promote progenitor cells recruitment; TNF- α and IL-6 which contribute to both local and systemic inflammation, while TGF- β promotes the development of myofibroblasts that break down tissue barriers, facilitating malignant invasion.

The presented research hypothesises that DCL might result from a bystander effect through intercellular communication between the BM mesenchymal stromal cells and incoming donated stem cells, with a pivotal role played by cytokines. Cytokines are the major inflammatory mediators produced by recipient cells in response to pretransplant conditioning and play a key role in inflammation derived HSCT post-malignancy (Markey & Hill, 2017). Currently, the reasons for DCL occurrence, the involved pathways, and the variability in susceptibility among individuals remain unknown. AML is the most common DCL in adults, but also manifests as myelodysplasia, whereas paediatric DCL manifests as mostly AML and/or ALL (Flynn and Kaufman, 2007). Cytokines and their corresponding receptors are key regulators determining the lineage development of stem cells (Fig. 1.9). Thus, it is reasonable to suggest that the levels/types of cytokines involved in myeloid development would support the development of DCL as an AML in children, with other cytokines also involved in adults. Two potential scenarios could explain the involvement of these cytokines in the *in vivo* BE: 1) HSC mutated due to an hitherto unknown or random genotoxicant differentiate into the myeloid lineage following contact with these cytokines, and/or 2) cytokines are directly implicated in

the BE and cause/contribute to genotoxicity in HSC (supported by the presented data). This thesis sought to answer the question, 'Do cytokines play a role in chemotherapy-induced bystander effect'. Thus, this work has explored the possibility that cytokines released from chemotherapy-exposed BM cells can induce genotoxicity in bystander cells, potentially contributing to the aetiology of DCL *in vivo*. This research employed various parameters to address this question. To closely mimic the BM microenvironment *in vitro*, the human BM- MSC line HS-5 was used and the lymphoblast cell line TK6 served as a model for bystander cells (or incoming donated stem cells in a DCL context).

For the first time, a wide profile of cytokine secretion was performed from HS-5 cells as a model of healthy versus chemotherapy-treated BM- MSC cells, reiterating an increase in cytokine secretion in response to chemotherapy (chapter 4). Given that the most highly secreted cytokines from the BM cell line, both at baseline and following chemotherapy, promote myeloid differentiation, it may be reasonable to suggest that cytokines could influence the occurrence of DCL as predominantly AML. Then key candidates were selected (TNF- α , IL-6, GM-CSF, G-CSF, and TGF- β 1) out of 80 cytokines analysed and using in-house developed ELISA (chapter 3) their expression from HS-5 and TK6 cells was measured at different treatment conditions and at different time points.

Moreover, the direct treatment of TK6 cells with these cytokines at both healthy and cytokine storm doses induced genotoxicity when administered individually. Notably, the combination of these cytokines could either be additive or potentiate the genotoxic effects of known genotoxic compounds in the micronucleus assay (chapter 5). Finally, the knockdown of the IL-6 cytokine signal from HS-5 cells to nearby TK6 bystander cells resulted in a significant reduction in genotoxicity in TK6 to near normal levels. This implies that within a heterogeneous mix of HS-5-secreted cytokine storm, IL-6 plays a pivotal role in generating genotoxicity in bystander cells *in vitro* (chapter 6). In summary, these findings provide evidence that cytokines are potential candidates for *in vitro* CIBE within BM models, and that they have the capacity to promote genotoxicity, particularly when used in combination, with IL-6 as a crucial cytokine in the BM microenvironment, as underscored by knockdown experiments.

This study demonstrated the presence of a diverse pool of cytokines released from the BM, as evidenced by the array results capable of detecting 80 cytokines (Fig. 4.1). The expression levels of these cytokines were notably altered (majority upregulated), following treatment with

two chemotherapies (Fig. 4.2 and Fig. 4.3). The choice of chemotherapy agents for this study was initially guided by reports implicating alkylating agents and topoisomerase inhibitors in TRL (Kondo *et al.*, 2010; Evison *et al.*, 2016). From the 80 cytokines analysed, TNF- α , IL-6, GM-CSF, G-CSF, and TGF- β 1 were identified as strong candidates. Although statistical significance was not achieved in measured differences, subtle changes in cytokine expression may still have biological relevance. Additionally, it's important to note that array measurements are relative, making the attainment of significant p-values more challenging compared to ELISA assays that measure in pg/ml.

To meet the objectives of this study, in-house ELISAs were developed and optimised, enabling the measurement of selected cytokines under various conditions throughout the research. The ELISA for IL-6 and GM-CSF was successfully established, while additional optimisation was necessary for G-CSF and TGF- β 1. ELISA results revealed a high expression of the selected cytokines by the BM-MSK line (HS-5), with a lesser contribution from the lymphoblast cell line (TK6). Notably, this study demonstrated, for the first time, that HS-5 expresses significantly high levels of IL-6 even after just one hour of exposure to both chemotherapies. IL-6 levels peak significantly three to four days post-exposure and do not return to normal until five days later (Fig. 4.7 and Fig. 6.4).

ELISA findings were consistent with the results obtained from the array, revealing elevated secretions both at baseline and following drug treatments. Furthermore, the ELISA results demonstrated peak expression of all cytokines between day 3 to 4, providing strong validation for the array performed on those specific days following exposure to two chemotherapies. However, it is worth noting that TNF- α expression in the ELISA data did not entirely align with the TNF- α findings from the array.

This study, for the first time, demonstrated the ability of all tested cytokine candidates (TNF- α , IL-6, GM-CSF, G-CSF, TGF- β 1) to induce MN formation directly in TK6 cells, while maintaining overall good cell viability (>50%) for each treatment (Fig 5.4 to Fig. 5.8). This finding was observed at both healthy and cytokine storm levels; levels typically seen in the literature following HSCT or conditioning therapy. The study established that the analysed cytokines could prompt direct genotoxicity, showing MN formation at their healthy levels and induce it at their storm level treatments. It is crucial to note that *in vivo*, patients experience exposure to a heterogeneous mix of cytokine responses, and this can vary depending on the

genetic polymorphisms carried by each individual. Recognising the active interaction between cytokines, the study paired the five candidate cytokines at higher levels of both healthy and storm concentrations. Genotoxicity was increased in every paired combination compared to the control sample. Importantly, some combinations exhibited statistically significant increases in MN compared to cytokines in isolation, and certain combinations exceeded the positive (known genotoxicant) control.

Among the tested cytokines, IL-6 emerged as particularly significant, given its highest baseline expression among 80 cytokines. This suggests that IL-6 may play a crucial role in the physiology of these cells even in the absence of any treatment or stimulation. Moreover, IL-6 expression increased following both chemotherapy treatments, indicating that cancer treatments might induce IL-6 production, potentially influencing immune response and inflammation *in vivo*. Notably, IL-6 was the only cytokine exhibiting a significant difference between untreated HS-5 and chemotherapy-treated cells in the ELISA results, confirming that IL-6 production is specifically influenced by CHL and MTX treatments. Furthermore, IL-6 demonstrated significant differences in genotoxicity of single IL-6 treatments to combination treatments at cytokine storm levels. These findings suggest that IL-6 is a key player out of range of cytokines, consequently, it was subjected to further investigation. Thus, IL-6 signalling pathways were blocked using two chemical inhibitors for JAK/STAT (FLLL-32) and RAS/MAPK (BAY293) to assess the reduction of genotoxicity in TK6.

The literature highlights the significance of IL-6/JAK/STAT3 signalling pathways due to their role in driving cancer cell proliferation, invasiveness and suppressing apoptosis, and STAT3 enhances IL-6 signalling to promote a vicious inflammatory loop contributing to cancer progression (Manore *et al.*, 2022). Consequently, the development of STAT3 inhibitors has emerged as a promising avenue in cancer treatment, as STAT3 inhibition can counteract tumour resistance (Ferraz *et al.*, 2017). Surprisingly, despite the potential anti-cancer effects of STAT3 inhibitors, the samples treated with these inhibitors and IL-6 showed a significant increase in MN induction compared to the controls (Fig. 5.10). This suggests that IL-6 treatment may force the response down an alternative signalling pathway that promotes MN generation. While the exact mechanism of IL-6 induced genotoxicity remains unclear, it raises the possibility that IL-6 downstream signalling could activate gene expression promoting genomic instability by reducing DNA repair, detecting damage, and increasing proliferation. However, further robust investigations are needed to substantiate this hypothesis.

Given the very low expression of IL-6 in TK6 cells compared to HS-5 expression, this study proposes that genotoxicity in bystander cells was induced by IL-6 originating exclusively from HS-5 cells in co-culture models. Therefore, knocking down the IL-6 secretion from the HS-5 in the bystander model would demonstrate changes in genotoxicity frequency and possible importance of IL-6. The knockdown data provided evidence that IL-6 is directly responsible for creating genotoxicity in the bystander model (Fig. 6.6) even though the precise mechanism remains unknown. Co-culture samples with IL-6 knockdown through siRNA treatments exhibited reduced genotoxicity levels, approaching those of the control sample.

This is even more relevant in the concept that intracellular communications play a vital role in cancer initiation and outcome, but this concept is further complicated by the idea that genotoxicity may not only occur through direct exposure to cytokines but also through indirect signalling of chemotherapy from the microenvironment. Moreover, in complex *in vivo* multicellular environments, the contribution of immune cells, the production of ROS, and interindividual differences in overall cytokine secretion cannot be ignored. This prompts inquiries about the mechanisms involved in inducing bystander effects by these chemotherapies *in vivo*, where genotoxicity may result from direct cytokine exposure, indirect chemotherapy exposure, and ROS generated by neighbouring immune cells.

For all assays, the HS-5 were only treated for an hour and then cultured for 2-4 days to detect genotoxicity in bystander cells. Because the drugs have a very short half-life (CHL 1.5 hours and MTX 8-200 hours) except if bound to (a) protein(s), the possibility that the drug eluted from the HS-5 and trafficked to the TK6 is unlikely to be possible. Indeed, human mesenchymal stem cells, from which HS-5 are derived, are not known to express the p-glycoprotein/multidrug resistance gene, which ordinarily might serve as a general mechanism to expel most drugs from the cells (Bosco *et al.*, 2015). Even if the drugs persisted at very low concentration, simple elution of the drug and travel to the bystander cells is unlikely to be the major mechanism of bystander when considering the timing of peak bystander signals (2-4 days following drug exposure). This was supported by a colleague from the research team whose data showed that peak bystander genotoxicity was on 3-4 days following drug treatments, and the measurement of drugs using LC-MS failed within minutes of sample spiking due to drug instability at body temperature. This supports why cytokines represent good candidates for bystander, because it is known that they respond (cytokine storm) a couple of days after stimulus (cancer therapy) and the data presented here supports the storm levels

correlating with the genotoxicity observed. Further in support of the cytokine storm being central to the bystander signal in inducing carcinogenesis in the donated cells, other scenarios that do not have chemotherapies but induce cytokine storm due to other stimuli (e.g. COVID-19, sepsis) show an increased risk of developing cancer later (Costa *et al.*, 2022; Liu *et al.*, 2019). These epidemiology studies support the idea that cytokines may be a commonality between all of these conditions, and the chemotherapies may not be as involved as suspected.

7.2 Limitations of the study

As an initial determination of the scope of cytokines' roles in CIBE, this study lays the foundation for significant future work and improvement. This study was limited to the use of only one BM cell line, as HS-5 is the only commercially available cell line, and TK6, a well-described genotoxicity model, was employed as a surrogate for HSC. It is important to acknowledge that these limitations may yield different outcomes in actual HSCs and samples from individuals secreting varying cytokine levels compared to HS-5. Additionally, due to the COVID-19 pandemic, obtaining primary HSC samples was not feasible, preventing the validation of the first argument regarding cytokines' role in bystander effects—that cells mutate through other genotoxicants, and cytokines drive these mutated stem cells to become myeloid. Therefore, further research is warranted, involving other cell lines and primary BM/HSC samples, to enable a comparative assessment of bystander effects.

While the genotoxicity assay (micronuclei) employed in this study is efficient and sensitive in detecting observed damages, no technique is without flaws. To enhance objectivity and reduce subjectivity, it would be highly relevant to adopt an automated or high-throughput assay to replace the visual and manual counting methods used for MN in this study. Also, it is important to highlight that this study primarily focused on the induction of MN as a genotoxic endpoint, as these were the predominant events observed within the *in vitro* model of CIBE. The exploration of cytokines' potential to induce other genotoxic endpoints and the implications for an individual's overall quality of life remains an area for future investigation.

As previously discussed, within intricate multicellular environments, one must consider the significant contribution of immune cells, the generation of ROS, and the inherent inter-individual variations in overall cytokine secretion *in vivo*, thus, caution should be exercised in interpreting the findings presented here. Therefore, relying solely on a 2D culture model with

just two cell lines may not be sufficient to yield robust and comprehensive experimental outcomes.

However, some problems must be resolved before conclusively answering the question regarding genotoxicity of cytokines in general. First, cytokines need to have an appropriate test system with competent cells having specific receptors to react. Second, the functioning of cytokines requires an appropriate balance between positive and negative regulators. For example, both TGF- β 1 and TNF- α can induce apoptosis, and this effect can be suppressed by IL-6, G-CSF, GM-CSF or IL-3. Third, the action of cytokines on cells is often very complex and involves the induction of expression of different transcriptional factors and other cytokines. Thus, there needs to be some experimental evidence that the observed effects were caused by the cytokine under investigation and not by other factors (Lazutka, 1996).

7.3 Future considerations

DCL presents a unique opportunity to prospectively study the events experienced by HSCs leading to their malignant transformation, because leukaemia in the general population is usually sporadic and unpredictable, whereas HSCT patients are routinely subjected to relevant and repeated investigations; these are informative prospectively but also provide useful samples for retrospective analysis. It is clear, though, that DCL as an entity exists and should be considered in any cases of acute leukaemia developing in the posttransplant period, particularly if features differ from those of the original disease. With growing awareness and increasingly sophisticated diagnostic tools, it should become feasible to report larger series, to identify risk factors and optimal treatment strategies. A greater understanding of the biology and impact of DCL will raise other issues regarding donor recruitment, selection, and notification, particularly in the context of the increasing age of potential donors and the rising popularity of CBT. Future cases should also provide valuable human models for investigating mechanisms of leukemogenesis *in vivo* (Wiseman, 2011).

As explained by Sala-Torra & Loeb (2011), study of DCL not only provides information about leukaemogenesis but also has important prognostic and therapeutic implications because the majority of DCL patients are difficult to treat and have therapeutic resistance. Because DCL is a relatively rare but serious event and is currently unable to be predicted in individuals, clinicians are limited in long-term follow-up of patients. However, the knowledge of high-risk drugs and/or genetic predisposition in individuals might guide future therapies. In line with the

knowledge that earlier reviewed DCL cases are majorly AML in nature, but not every recipient stem cell transplant gets a DCL and not every individual that gets DCL is going to die or survive; it goes to say that at present every condition is unique regardless of donor origin.

IL-6 is a significant factor in this research, both in terms of its baseline expression and its response to various treatments. These findings have implications for understanding how IL-6 may contribute to the effects observed in this study, including genotoxicity and expression responses to chemotherapy and could provide valuable insights into the role of IL-6 in CIBE. This also supports the further investigation into the mechanisms underlying how dysregulated IL-6 bystander signalling contributes to the progression of diseases such as cancer, autoimmune disorders, and chronic inflammatory conditions, and most importantly how IL-6 bystander signalling contributes to the development of HSCT complications such as DCL.

Because control of both the soluble (cytokines) and cellular effectors (inflammatory cells) in HSCT-derived post-complications (DCL and TRL) is critical to gaining control over these secondary malignancies, improving a convenient therapeutic strategy would therefore broaden the applicability of HSCT. Targeting of multiple cytokines, via the knockdowns or downstream signalling pathway inhibition would represent a more effective therapeutic strategy and treat secondary malignancy in the future. IL-6 is likely responsible for many inflammatory disease signals via common intracellular signalling pathways (JAK-STAT); thus an *in vivo* study targeting JAK2 via ruxolitinib in myelofibrosis treatment has shown significant inhibition of IL-6, IL-1, TNF- α and IFN- γ and proven extremely effective in GvHD (Markey & Hill, 2017). In addition to the inhibition of tumour cell proliferation and survival, STAT3 inhibitors would be predicted to convert inflammation in the tumour microenvironment from tumour-promoting to tumour-suppressing (Yu *et al.*, 2009). Instead of cell lines, it is worth using animal models to inhibit all IL-6 pathways in isolation and combination for better downstream signalling inhibition and MN reduction.

Knowledge regarding the role of cytokines in post-transplant malignancy has been established using preclinical models (knockout mice), and studies of the genetic polymorphisms in cytokine genes which can be correlated with posttransplant outcome (Markey & Hill, 2017; Melenhorst *et al.*, 2012). Cytokines and their receptors are highly genetically polymorphic, leading to changes in protein levels dependent on the individual's genotype (Girnita *et al.*, 2008). As polymorphisms in cytokine genes are associated with levels of cytokine production,

analysis of SNP data by Morgan *et al.* (2010) indicated that the IL-6 (-174G/C) genotype was associated with 2-fold IL-6 production in sepsis shock with increased mortality in severe sepsis patients. Markey & Hill (2017) also demonstrated studies on TNF and TNFR polymorphisms in HSCT and suggested they were directly affecting the recipient's high TNF production and post-HSCT complications. Polymorphism detection in primary samples can therefore be highly important to see whether it can predict the patients who have a higher risk for high genotoxicity following CIBE and are more prone to DCL. Analysis of the polymorphism of key cytokines (IL-6), and their receptors which align with expression levels to predict which patients were most likely to secrete high cytokine levels and develop DCL, will give the hope of steering future cytokine-directed therapy. So therapeutically, administration of neutralising antibodies or inhibitors to reduce the IL-6 response to prevent the genotoxicity, could be offered in advance. At the same time, it is relevant to consider the co-expressers alongside the IL-6 signalling, because combination MN data indicated high IL-6 with low TNF- α showed higher MN induction than high combinations of both of them (Fig. 5.6). This helps explain and supports the fact that unchanged MN during resatorvid treatment (IL-6 and TNF- α inhibitor) in the bystander models (Fig. 6.10), may be due to the reduction of TNF- α in the models. However, in this case, even though this suggests that high TNF- α can be given to the patients to reduce the IL-6-inducing genotoxicity risk, instead of having an IL-6 neutralising antibody, it remains that TNF- α on its own is quite a difficult treatment to give patients due to its potency found in different studies. High TNF- α can cause high toxicity in patients.

The bystander model used in this study has served as a basis for the initial outcome of this study and evaluated mostly soluble factors. A better model to mimic the *in vivo* BM microenvironment would be the use of a three-dimensional (3D) cell culture. It may be also vital to develop a model that will accommodate other cells in the same culture of the BM that may play a role (macrophages express significant cytokines levels) and may promote direct cellular contact which may change the bystander effect. It should be noted that within these data, the research has only focussed on the induction of MN as a genotoxic endpoint, as these were the main events. It remains to be seen if cytokines can induce other genotoxic endpoints and the contribution this might make to an individual's quality of life.

Finally, it is possible that each candidate may exhibit varying mechanisms in bystander relative to another and thus, there is much further work to be performed. The key to interpreting this mechanism is to understand if either the recipient or the donor is more important in the

generation of DCL/bystander, which may point towards primary sample analysis with and without disease and chemotherapy. The use of primary cultures isolated directly from cancer patients possesses the correct genetic characteristic features of cancer cells *in vivo* and would represent the full scope of potential bystander signalling following combination chemotherapy protocols *in vivo*. A study of CIBE in patient samples would be highly beneficial in answering the question of whether the donor or recipient is more important in DCL induction. Therefore, these data could be much more solid if the study had primary BM and HSC samples from healthy and leukaemia groups to compare the *in vivo* outcome. It should be remembered that cytokine changes are likely to vary considerably according to the regimen and the type of transplant (Melenhorst *et al.*, 2012). Thus, excessive further study can be made on peri- and post-transplant cytokine dynamics in patients undergoing myeloablative conditioning and T-cell-depleted or T-cell-manipulated HSCT to explore the contribution of the conditioning regimen, donor engraftment, infections, and GvHD to cytokine fluctuations (homeostatic, inflammatory and anti-inflammatory cytokines, and chemokines).

7.4 Final conclusion

The pathogenesis of DCL has previously been suggested to involve multifactorial processes, with different intrinsic and extrinsic influences. Disruption to BM stromal functionality through chemotherapy as previously evidenced is long term and could alter the cytokine expression and build cytokine storm status, inferring that cytokines potentially play a role in CIBE, but it is unlikely to be the sole mechanism involved. Although DCL has been previously reported with very low incidence, following improvements in cytogenetic analysis to confirm donor origin of ‘relapses’, the number of cases that have been reported has increased since the year 2000. This suggests more awareness and better diagnosis so the implications of the current study could be highly important in clinical research in the future.

Given that the most highly secreted cytokines from the BM cells, both at baseline and following chemotherapy, promote myeloid differentiation, it may be reasonable to suggest that cytokines could influence the occurrence of DCL as predominantly AML. The data presented within this thesis does support the idea that CIBE could be induced by both CHL and MTX investigated here, and both of these drugs can increase higher levels of cytokines which may align with the cytokine storm levels in *in vivo* studies following conditioning therapy in HSCT.

Furthermore, this study has shown that direct exposure to selected cytokines in isolation at storm doses, as well as combinations of high 'healthy' doses, can induce MN in TK6 cells at levels close to, or exceeding, known genotoxic compounds. The major effects of this study are the potential clinical insights related to DCL. This study has shown evidence in support of CIBE that is potentially long-lived and an important outcome to consider in HSCT. By showing reduced MN induction in TK6 cells co-cultured with IL-6 knocked down HS-5, this study was able to prove that IL-6 is a high-impact candidate in MN induction in a bystander model which may align with the consequences for donated HSC within a DCL setting. IL-6 knockdown data demonstrates equivalent micronuclei counts between control and drug following knockdown, inferring a prominent role of IL-6 in BM which may be involved in the induction of a CIBE in the form of micronuclei *in vivo*. It would be pertinent to note individuals with genetic variants leading to high IL-6 expression levels and to determine if they are more at risk for genotoxicity; IL-6 may offer a possible target for therapy to reduce long-term clinical complications.

While these data may infer a role in the promotion of leukaemogenesis following HSCT, the occurrence of DCL is currently not considered to be as frequent as the presence of cytokine storm, suggesting that inter-individual levels of secretion coupled with other detoxification processes need to be fully explored to predict risk. If we speculate this is the initial genotoxic event starting from IL-6 following cytokine storm in HSCT, but still have not addressed the fact why only some people get DCL but not all, why some people get it very quickly after the transplant and why others get it years after, and most importantly why some people die from it and why some people are treatable. Many more factors play a role in the prognosis and the outcome for the patients. But maybe this goes some way towards at least explaining why donor HSC get genotoxicity in the first place.

REFERENCES

- Agematsu, K. and Nakahori, Y. (1991) Recipient origin of bone marrow-derived fibroblastic stromal cells during all periods following bone marrow transplantation in humans. *British Journal of Haematology*. 79 (3), pp. 359-365.
- Alhaji, M., Zubair, M. and Farhana, A. (2023) Enzyme Linked Immunosorbent Assay Publishing; 2023 Jan-. Available from: <https://www.ncbi.nlm.nih.gov/books/NBK555922/>
- American Cancer Society (2019) How Chemotherapy Drugs Work, Available at; <https://www.cancer.org/treatment/treatments-and-side-effects/treatment-types/chemotherapy/how-chemotherapy-drugs-work.html>
- Antin, J. H. and Raley, D. Y. (2013) *Manual of stem cell and bone marrow transplantation*. Cambridge University Press.c
- Arican, O., Aral, M., Sasmaz, S. and Ciragil, P. (2005) Serum levels of TNF- α , IFN- γ , IL-6, IL-8, IL-12, IL-17, and IL-18 in patients with active psoriasis and correlation with disease severity. *Mediators of inflammation*. 5 (2005), pp. 273-279.
- Asada, N., Takeishi, S. and Frenette, P. S. (2017) Complexity of bone marrow hematopoietic stem cell niche. *International journal of hematology*. 106 (1), pp. 45-54.
- Asur, R. S., Thomas, R. A. and Tucker, J. D. (2009) Chemical induction of the bystander effect in normal human lymphoblastoid cells. *Mutation Research/Genetic Toxicology and Environmental Mutagenesis*. 676 (1-2), pp. 11-16.
- Asurappulige, H.S.H., Thomas, A.D. and Morse, H.R. (2023) Genotoxicity of cytokines at chemotherapy-induced 'storm' concentrations in a model of the human bone marrow. *Mutagenesis*. 38 (4), pp. 201-215. doi: 10.1093/mutage/gead018. PMID: 37326959; PMCID: PMC10448863.
- Athanosou, N.A., Quinn, J., Brenner, M.K., Prentice, H.G., Graham, A., Taylor, S., Flannery, D. and McGee, J.O. (1990) Origin of marrow stromal cells and haematopoietic chimerism following bone marrow transplantation determined by in situ hybridization. *British Journal of Cancer*. 61 (3), pp. 385-389.
- Avalos BR, Lazaryan A, Copelan EA. Can G-CSF cause leukemia, in hematopoietic stem cell donors? *Biol Blood Marrow Transplant*, 2011;17:1739–46.
- Avots, A., Harder, F., Schmittwolf, C., Petrovic, S. and Müller, A.M. (2002) Plasticity of haematopoietic stem cells and cellular memory. *Immunological Reviews*. 187, pp. 9-21.

- Baehring, J.M. and Marks, P.W. (2012) Treatment-related myelodysplasia in patients with primary brain tumors. *Neuro-oncology*. 14(5), pp. 529-540.
- Balcer-Kubiczek, E. K., Yin, J., Lin, K., Harrison, G. H., Abraham, J. M. and Meltzer, S. J. (1995) p53 mutational status and survival of human breast cancer MCF-7 cell variants after exposure to X rays or fission neutrons. *Radiation research*. 142 (3), pp. 256-262.
- Baldus, C.D., Mrózek, K., Marcucci, G. and Bloomfield, C.D. (2007) Clinical outcome of de novo acute myeloid leukaemia patients with normal cytogenetics is affected by molecular genetic alterations: a concise review. *Br. J. Haematol*. 137 (5), pp. 387–400.
- Banfi, A., Bianchi, G., Galotto, M., Cancedda, R. and Quarto, R. (2001) Bone marrow stromal damage after chemo/radiotherapy: occurrence, consequences and possibilities of treatment. *Leukemia & lymphoma*. 42 (5), pp. 863-870.
- Barcellos-Hoff, M.H., Park, C. and Wright, E.G. (2005) Radiation and the microenvironment–tumorigenesis and therapy. *Nature Reviews Cancer*. 5 (11), pp. 867.
- Barker, C. A., Kim, S. K., Budhu, S., Matsoukas, K., Daniyan, A. F. and D’Angelo, S. P. (2018) Cytokine release syndrome after radiation therapy: case report and review of the literature. *Journal for immunotherapy of cancer*. 6, pp. 1-7.
- BAY-293, Selleckchem.com (2023), <https://www.selleckchem.com/products/bay-293.html>
- Berz, D., McCormack, E. M., Winer, E. S., Colvin, G. A. and Quesenberry, P.J. (2007) Cryopreservation of Hematopoietic Stem Cells. *Hematol*. 82 (6), pp. 463–472.
- Bhattacharya, P., Thirupathi, M., Elshabrawy, H. A., Alharshawi, K., Kumar, P. and Prabhakar, B. S. (2015) GM-CSF: An immune modulatory cytokine that can suppress autoimmunity. *Cytokine*. 75 (2), pp. 261-271.
- Bidwell, J., Keen, K., Gallagher, G., Kimberly, R., Huizinga, T., McDermott, MF., Oksenberg, J., McNicholl, J., Pociot, F., Hardt, C. and D’Alfonso, S. (1999) Cytokine gene polymorphism in human disease: on-line databases. *Genes and Immunity*. 1, pp. 3–19.
- Bieghs, L., Brohus, M., Kristensen, I.B., Abildgaard, N., Bøgsted, M., Johnsen, H.E., Conover, C.A., Bruyne, E.D., Vanderkerken, K., Overgaard, M.T. and Nyegaard, M. (2016) Abnormal IGF-Binding Protein Profile in the Bone Marrow of Multiple Myeloma Patients. *PLOS ONE*. 11 (4), pp. 1-10.

- Bill, M. A., Fuchs, J. R., Li, C., Yui, J., Bakan, C., Benson Jr, D. M., Schwartz, E. B., Abdelhamid, D., Lin, J., Hoyt, D. G., Fossey, S. L., Young, G. S., Carson, W. E., Li, P-K and Lesinski, G. B. (2010) The small molecule curcumin analog FLLL32 induces apoptosis in melanoma cells via STAT3 inhibition and retains the cellular response to cytokines with anti-tumor activity. *Molecular cancer*. 9, pp. 1-12.
- Binaschi, M., Zunino, F. and Capranico, G. (1995) Mechanism of action of DNA topoisomerase inhibitors. *Stem Cells*. 13 (4), pp. 369-79.
- Blau, O., Hofmann, W. K., Baldus, C. D., Thiel, G., Serbent, V., Schümann, E., Thiel, E. and Blau, I. W. (2007) Chromosomal aberrations in bone marrow mesenchymal stroma cells from patients with myelodysplastic syndrome and acute myeloblastic leukemia. *Experimental hematology*. 35 (2), pp. 221-229.
- Bosco, D. B., Kenworthy, R., Zorio, D. A. and Sang, Q. X. A. (2015) Human mesenchymal stem cells are resistant to Paclitaxel by adopting a non-proliferative fibroblastic state. *PloS one*. 10 (6), pp. e01285.
- Brenner, D. J. and Hall, E. J. (2007) Computed tomography—an increasing source of radiation exposure. *New England Journal of Medicine*. 357 (22), pp. 2277-2284.
- Bruggemann, L., Falls, Z., Mangione, W., Schwartz, S. A., Battaglia, S., Aalinkeel, R., Mahajan, S. D. and Samudrala, R. (2023) Multiscale analysis and validation of effective drug combinations targeting driver kras mutations in non-small cell lung cancer. *International Journal of Molecular Sciences*. 24 (2), pp. 997.
- Brüsehafer, K., Manshian, B.B., Doherty, A.T., Zoulikha Zair, M., Johnson, G.E., Doak, S.H. and Jenkins, G.J.S. (2015) The clastogenicity of 4NQO is cell-type dependent and linked to cytotoxicity, length of exposure and p53 proficiency. *Mutagenesis*. 31, pp. 171–180.
- Bydlowski, S.P., Levy, D., Ruiz, J.M.L. and Pereira, J. (2013) Haematopoietic Stem Cell Niche: Role in Normal and Malignant Hematopoiesis. *Intech Open Science*. <http://dx.doi.org/10.5772/55508>.
- Camacho, V., McClearn, V., Patel, S. and Welner, R. S. (2017) Regulation of normal and leukemic stem cells through cytokine signaling and the microenvironment. *International journal of hematology*. 105, pp. 566-577.
- Cancer Research UK, https://www.cancerresearchuk.org/health-professional/cancer-statistics/incidence/age?_gl=1*ilp0t6*_gcl_au*ODgxMDI1MzQxLjE3MDI0Nzc5NzE.*

[ga*OTA4NTYwMjc3LjE3MDI0NzY4ODg.* ga 58736Z2GNN*MTcwMjQ3Njg4Ny4xLjEuMTcwMjQ4MTkwNy4wLjAuMA..& ga=2.237460294.755621299.1702476888-908560277.1702476888#heading-Two](https://pubmed.ncbi.nlm.nih.gov/36888888/), Accessed Dec, 2023.

- Cancer Research, UK (2017) Cancer Statistics for the UK, Available at; <https://www.cancerresearchuk.org/health-professional/cancer-statistics-for-the-uk#heading-Two>
- Cancer treatment centre of America, (2020), Diagnostic imaging tests, Available at; <https://www.cancercenter.com/diagnosing-cancer/diagnostic-imaging>
- Cancer treatment centre of America, (2020), Leukemia stages, Available at; <https://www.cancercenter.com/cancer-types/leukemia/stages>
- Candelaria, M. and Dueñas-Gonzalez, A. (2015) Therapy-related myelodysplastic syndrome. *Expert opinion on drug safety*. 14 (5), pp. 655-665.
- Catacchio, I., Berardi, B., Reale, A., Luisi, A. and Racanelli, V (2013) Properties, Molecular Mechanisms, Negative Aspects, and Clinical Applications of Haematopoietic and Mesenchymal Stem Cells Trans-differentiation. *Stem Cells International*. 1, pp. 11.
- Celikler, S., Bilaloglu, R. and Aydemir, N. (2006) Genotoxic effects induced by fotemustine and vinorelbine in human lymphocytes. *Naturforsch*. 61 (11-12), pp. 903 - 910.
- Cellosaurus (2023) TK6 (CVCL_0561) https://www.cellosaurus.org/CVCL_0561
- Cetin, Z., Tezcan, G., Karauzum, S.B., Kupesiz, A., Manguoglu, A.E., Yesilipek, A., Luleci, G and Hazar, V. (2006) Donor Cell-derived Acute Myeloblastic Leukaemia After Allogeneic Peripheral Blood Haematopoietic Stem Cell Transplantation for Juvenile Myelomonocytic Leukaemia. *Journal of Podiatry Hematologic Oncology*. 28, pp. 763-767.
- Champlin, R. (2013) Recued intensity allogeneic haematopoietic transplantation is an established standard of care for treatment of older patients with acute myeloid leukaemia. *Best Practice and Research Clinical Haematology*. 26 (3), pp. 297-300.
- Cheleuitte, D., Mizuno, S. and Glowacki, J. (1998) *In vitro* secretion of cytokines by human bone marrow: effects of age and estrogen status. *The Journal of Clinical Endocrinology & Metabolism*. 83 (6), pp. 2043-2051.

- Chen, L., Deng, H., Cui, H., Fang, J., Zuo, Z., Deng, J., Li, Y., Wang, X. and Zhao, L. (2018) Inflammatory responses and inflammation-associated diseases in organs. *Oncotarget*. 9 (6), pp. 7204.
- Chen, P., Wu, B., Ji, L., Zhan, Y., Li, F., Cheng, L., Cao, J., Chen, H., Ke, Y., Min, Z., Sun, L., Hua, F., Chen, H. and Cheng, Y. (2021) Cytokine consistency between bone marrow and peripheral blood in patients with Philadelphia-negative myeloproliferative neoplasms. *Frontiers in Medicine*. 8, pp. 598182.
- Chen, S., Liu, G., Chen, J., Hu, A., Zhang, L., Sun, W., Tang, W., Liu, C., Zhang, H., Ke, C., Wu, J. and Chen, X. (2019) Ponatinib protects mice from lethal influenza infection by suppressing cytokine storm. *Frontiers in Immunology*. 10, pp.1393.
- Chhipa, R. R. and Bhat, M. K. (2007) Bystander killing of breast cancer MCF-7 cells by MDA-MB-231 cells exposed to 5-fluorouracil is mediated via Fas. *Journal of cellular biochemistry*. 101 (1), pp. 68-79.
- Chinnadurai, M., Chidambaram, S., Ganesan, V., Baraneedharan, U., Sundaram, L., Paul, S. F. and Venkatachalam, P. (2011) Bleomycin, neocarzinostatin and ionising radiation-induced bystander effects in normal diploid human lung fibroblasts, bone marrow mesenchymal stem cells, lung adenocarcinoma cells and peripheral blood lymphocytes. *International journal of radiation biology*. 87 (7), pp. 673-682.
- Chua, M. W., Lin, M. Z., Martin, J. L. and Baxter, R. C. (2015) Involvement of the insulin-like growth factor binding proteins in the cancer cell response to DNA damage. *Journal of Cell Communication and Signalling*. 9, pp. 167-176.
- Cilloni, D., Carlo-Stella, C., Falzetti, F., Sammarelli, G., Regazzi, E., Colla, S., Rizzoli, V., Aversa, F., Martelli, M.F. and Tabillo, A. (2000) Limited engraftment capacity of bone marrow derived mesenchymal cells following T-cell depleted haematopoietic stem cell transplantation. *Blood*. 96 (10), pp. 3637-3643.
- Clark, I. A. and Vissel, B. (2017) The meteorology of cytokine storms, and the clinical usefulness of this knowledge. *Seminars in immunopathology*. 39, pp. 505-516. Springer Berlin Heidelberg.
- Clauson, C., Scharer, O.D. and Niedernhofer, L. (2013) Advances in Understanding the Complex Mechanisms of DNA Interstrand Cross-Link Repair. *Cold Spring Harb Perspect Biol*. 5.

- Coates, P.J., Rundle, J.K., Lorimore, S.A. and Wright E.G. (2008) Indirect macrophage responses to ionizing radiation: implications for genotype-dependent bystander signaling. *Cancer research*. 68 (2), pp. 450-456.
- Costa, B. A., da Luz, K. V., Campos, S. E. V., Lopes, G. S., Leitão, J. P. D. V., & Duarte, F. B. (2022). Can SARS-CoV-2 induce hematologic malignancies in predisposed individuals? A case series and review of the literature. *Hematology, Transfusion and Cell Therapy*, 44, 26-31
- Cottler-Fox, M.H., Lapidot, T., Petit, I., Kollet, O., DiPersio, J.F., Link, D. and Devine, S. (2003) Stem Cell Mobilization. *Hematology*. 419(1), pp. 419-37.
- Crespi, C.L. and Thilly, W.G. (1984) Assay for gene mutation in a human lymphoblast line, AHH-1, competent for xenobiotic metabolism. *Mutat Res*. 128 (2), pp. 221-30.
- Cui, Y., Yang, M., Wang, Y., Ren, J., Lin, P., Cui, C., Song, J., He, Q., Hu, H., Wang, K. and Sun, Y. (2021) Melatonin prevents diabetes-associated cognitive dysfunction from microglia-mediated neuroinflammation by activating autophagy via TLR4/Akt/mTOR pathway. *The FASEB Journal*. 35 (4), pp. e21485.
- Danzer, S. G., Kirchner, H. and Rink, L. (1994) Cytokine interactions in human mixed lymphocyte culture. *Transplantation*. 57 (11), pp. 1638-1642.
- Davis, A. S., Viera, A. J. and Mead, M. D. (2014) Leukemia: An overview for primary care. *American family physician*. 89 (9), pp. 731-738.
- Decout, A., Katz, J.D., Venkatraman, S., et al. (2021) The cGAS-STING pathway as a therapeutic target in inflammatory diseases. *Nat Rev Immunol*. 21, pp. 548–69.
- Demidem, A., Morvan, D. and Madelmont, J. C. (2006) Bystander effects are induced by CENU treatment and associated with altered protein secretory activity of treated tumor cells A relay for chemotherapy?. *International journal of cancer*. 119 (5), pp. 992-1004.
- Desjardins, P. and Conklin, D. (2010) Nano-Drop microvolume quantitation of nucleic acids. *Journal of visualized experiments: JoVE*. 2010;45.
- Dhami, S. P. S., Kappala, S. S., Thompson, A. and Szegezdi, E. (2016) Three-dimensional ex vivo co-culture models of the leukaemic bone marrow niche for functional drug testing. *Drug discovery today*. 21 (9), pp. 1464-1471.
- Di, X., Bright, A. T., Bellott, R., Gaskins, E., Robert, J., Holt, S., Gewirtz, D. A. and Elmore, L. (2008) A chemotherapy-associated senescence bystander effect in breast cancer cells. *Cancer biology & therapy*. 7 (6), pp. 864-872.

- DiCarlo, J., Agarwal-Hashmi, R., Shah, A., Kim, P., Craveiro, L., Killen, R., Rosenberg-Hasson, Y. and Maecker, H. (2014) Cytokine and Chemokine Patterns Across 100 Days after Haematopoietic Stem Cell Transplantation in Children. *Biol Blood Marrow Transplant.* 20 (3), pp. 361–369.
- Dickey, J.S., Baird, B.J., Redon, C.E., Solokov, M.V., Sedelnikova, O.A. and Boner, W.M. (2009) Intercellular communication of cellular stress monitored by γ -H2AX induction. *Carcinogenesis.* 30 (10), pp. 1686 – 1695.
- Dickinson, A.M. and Charron, D. (2005) Non-HLA immunogenetics in hematopoietic stem cell transplantation. *Current Opinion in Immunology.* 17, pp. 517–525.
- Dickson, M.A., Papadopoulos, E.B., Hedvat, C.V., Jhanwar, S.C. and Brentjens, R.J. (2014) Acute myeloid leukemia arising from a donor derived premalignant hematopoietic clone: a possible mechanism for the origin of leukemia in donor cells. *Leuk Res Rep.* 3, pp. 38-41.
- Dillon, M., Lopez, A., Lin, E., Sales, D., Perets, R. and Jain, P. (2021) Progress on Ras/MAPK signaling research and targeting in blood and solid cancers. *Cancers.* 13 (20), pp. 5059.
- Dolgachev, V. A., Ullenbruch, M. R., Lukacs, N. W. and Phan, S. H. (2009) Role of Stem Cell Factor and Bone Marrow-Derived Fibroblasts in Airway Remodeling. *The American Journal of Pathology.* 174 (2).
- Döring, M., Stanchi, K.M.C., Mezger, M., Erbacher, A., Feucht, J., Pfeiffer, M., Lang, P., Handgretinger, R. and Müller, I. (2015) Cytokine serum levels during post-transplant adverse events in 61 pediatric patients after haematopoietic stem cell transplantation. *Döring et al. BMC Cancer.* 15, pp. 607.
- Drabløs, F., Feyzi, E., Aas, P. A., Vaagbø, C. B., Kavli, B., Bratlie, M. S., Peña-Diaz, J., Otterlei, M., Slupphaug, G. and Krokan, H. E. (2004) Alkylation damage in DNA and RNA—repair mechanisms and medical significance. *DNA repair.* 3 (11), pp. 1389-1407.
- Driessen, R.L., Johnston, H.M. and Nilsson, S.K. (2003) Membrane-bound stem cell factor is a key regulator in the initial lodgment of stem cells within the endosteal marrow region. *Experimental Hematolog.* 31, pp. 1284–1291.
- Duhrsen, U. and Metcalf, D. (1990) Effects of irradiation of recipient mice on the behavior and leukemogenic potential of factor-dependent hematopoietic cell lines. *Blood.* 75 (1), pp. 190-197.

- Edwardson, D. W., Boudreau, J., Mapletoft, J., Lanner, C., Kovala, A. T. and Parissenti, A. M. (2017) Inflammatory cytokine production in tumor cells upon chemotherapy drug exposure or upon selection for drug resistance. *PloS one*. 12 (9), e0183662.
- Ergen, A.V., Boles, N.C. and Goodell, M.A. (2012) Rantes/Ccl5 influences hematopoietic stem cell subtypes and causes myeloid skewing. *BLOOD*. 119 (11).
- Evison, B.J., Sleebs, B.E., Watson, K.G., Phillips, D.R. and Cutts, S.M. (2016) Mitoxantrone, More than Just Another, Topoisomerase II Poison. *Medicinal Research Reviews*. 36 (2), pp. 248–299.
- Ewan, K.B., Henshall-Powell, R.L., Ravani, S.A., Pajares, M.J., Arteaga, C., Wartens, R., Akhurst, R. J. and Barcellos-Hoff, M. H. (2002) Transforming growth factor- β 1 mediates cellular response to DNA damage in situ. *Cancer research*. 62 (20), pp. 5627-5631.
- Fasouli, E. S. and Katsantoni, E. (2021) JAK-STAT in early hematopoiesis and leukemia. *Frontiers in Cell and Developmental Biology*. 9, pp. 669363.
- Fathi, E., Farahzadi, R., Valipour, B. and Sanaat, Z. (2019) Cytokines secreted from bone marrow derived mesenchymal stem cells promote apoptosis and change cell cycle distribution of K562 cell line as clinical agent in cell transplantation. *PloS one*. 14 (4), pp. e0215678.
- Fausel, C. (2007) Targeted chronic myeloid leukemia therapy: seeking a cure. *J Manag Care Pharm*. 13 (8 Suppl A), pp. 8–12.
- Fellows, M.D. and Michael O'Donovan, M.R. (2007) Cytotoxicity in cultured mammalian cells is a function of the method used to estimate it. *Mutagenesis*. 22 (4), pp. 275–280.
- Fenech, M. (2008) The micronucleus assay determination of chromosomal level DNA damage. *Environmental genomics*. 410, pp. 185-216. Humana Press.
- Fenech, M., Knasmueller, S., Bolognesi, C., (2020) Micronuclei as biomarkers of DNA damage, aneuploidy, inducers of chromosomal hypermutation and as sources of pro-inflammatory DNA in humans. *Mutat Res*. 786, pp. 108342.
- Fernandez-Real, J. M., Vayreda, M., Richart, C., Gutierrez, C., Broch, M., Vendrell, J. and Ricart, W. (2001) Circulating interleukin 6 levels, blood pressure, and insulin sensitivity in apparently healthy men and women. *The Journal of Clinical Endocrinology & Metabolism*. 86 (3), pp. 1154-1159.

- Ferraz, E. R. A., Fernandes, A. S., Salviano, I., Felzenszwalb, I. and Mencialha, A. L. (2017) Investigation of the mutagenic and genotoxic activities of LLL-3, a STAT3 inhibitor. *Drug and Chemical Toxicology*. 40 (1), pp. 30-35.
- Fialkow, P.J., Bryant, J.I., Thomas, E.D. and Neiman, P.E. (1971) Leukaemic transformation of engrafted human marrow cells *in vivo*. *The Lancet*. 297 (7693), pp. 251-255.
- FLLL-32, Selleckchem.com (2023)<https://www.selleckchem.com/products/flll32.html>
- Flores-Figueroa, E., Gutiérrez-Espíndola, G., Montesinos, J.J., Arana-Trejo, R.M. and Mayani, H. (2002) *In vitro* characterization of haematopoietic microenvironment cells from patients with myelodysplastic syndrome. *Leukemia research*. 26 (7), pp. 677-686.
- Flynn, C.M. and Kaufman, D.S. (2007) Donor cell leukaemia: insight into cancer stem cells and the stem cell niche. *Blood*. 109 (7), pp. 2688-2692.
- Fomenko, L., Sirota, N., Ravin, V., et al. (1997) Interferon alpha reduces the level of radiation-induced micronuclei in mouse bone marrow cells. *Arch Immunol Ther Exp (Warsz)*. 45, pp. 475–8.
- Fossey, S. L., Bear, M. D., Lin, J., Li, C., Schwartz, E. B., Li, P-K., Fuchs, J. R., Fenger, J., Kisseberth, W. C. and London, C. A. (2011) The novel curcumin analog FLLL32 decreases STAT3 DNA binding activity and expression, and induces apoptosis in osteosarcoma cell lines. *BMC cancer*. 11 (1), pp. 1-15.
- Fowler, P., Smith, K., Young, J., Jeffrey, L., Kirkland, D., Pfuhler, S. and Carmichael, P. (2012) Reduction of misleading (“false”) positive results in mammalian cell genotoxicity assays. I. Choice of cell type. *Mutation Research/Genetic Toxicology and Environmental Mutagenesis*. 742 (1-2), pp. 11-25.
- Gaaib., J. and Al-Assie, A. (2011) Simple salting- out method for genomic DNA extraction from whole blood, *Tikrit Journal of Pure Science*. 16 (2).
- Gallet, P., Phulpin, B., Merlin, J. L., Leroux, A., Bravetti, P., Mecellem, H., Tran, N. Dolivet, G. (2011) Long-term alterations of cytokines and growth factors expression in irradiated tissues and relation with histological severity scoring. *PloS one*. 6 (12), pp. e29399.
- Galotto, M., Berisso, G., Delfino, L., Podesta, M., Ottaggio, L., Dallorso, S., Dufour, C., Ferrara, G. B., Abbondandolo, A., Dini, G., Bacigalupo, A., Cancedda, R. and Quarto, R.

- (1999) Stromal damage as consequence of high-dose chemo/radiotherapy in bone marrow transplant recipients. *Experimental hematology*. 27 (9), pp. 1460-1466.
- Ganta, S., Paxton, J.W., Baguley, B.C. and Garg, S. (2008) Pharmacokinetics and pharmacodynamics of chlorambucil delivered in parenteral emulsion. *Int J Pharm*. 360, pp. 115–21.
 - Ganta, S., Sharma, P., Paxton, J.W., Baguley, B. C. and Garg, S. (2010) Pharmacokinetics and pharmacodynamics of chlorambucil delivered in long-circulating nanoemulsion. *J Drug Target*. 18(2), pp. 125–133.
 - Garibyan, L. and Avashia, N. (2013) Research techniques made simple: polymerase chain reaction (PCR). *The Journal of investigative dermatology*. 133, pp. 1-6.
 - Gekara, N. O. (2017) DNA damage-induced immune response: Micronuclei provide key platform. *J Cell Biol*. 216 (10), pp. 2999-3001.
 - Georg, F. and Weber, G.F. (2015) DNA Damaging Drugs. *Molecular Therapies of Cancer*. pp 9-112.
 - Gerson, S.L., Caimi, P.F., William, B.M. and Creger, R.J. (2018) Pharmacology and molecular mechanisms of antineoplastic agents for hematologic malignancies. *Hematology*. pp. 849-912.
 - Gheita, T.A., Azakalany, G.A., Gaber, W. and Mohey, A. (2015) Clinical significance of serum TNF and G/A promoter polymorphism in rheumatoid arthritis. *Egyptian Society of Rheumatic Diseases*. 37, pp. 49-54.
 - Girnita, D.M., Burckart, G. and Zeevi, A. (2008) Effect of cytokine and pharmacogenomic genetic polymorphisms in transplantation. *Current Opinion in Immunology*. 20 (5), pp. 614–625.
 - Gleitz, H., Kramann, R. and Schneider, R. K. (2018) Understanding deregulated cellular and molecular dynamics in the hematopoietic stem cell niche to develop novel therapeutics in bone marrow fibrosis: The hematopoietic stem cell niche in bone marrow fibrosis. *Journal of Pathology*. 245, pp. 138-146.
 - Glover, K. P., Chen, Z., Markell, L. K. and Han, X. (2015) Synergistic gene expression signature observed in TK6 cells upon co-exposure to UVC-irradiation and protein kinase C-activating tumor promoters. *PLoS One*. 10 (10), pp. e0139850.
 - Goussetis, E., Varela, I., Peristeri, I., Kitra, V., Spanou, K., Moraloglou, O., Paisiou, A., Karatasaki, S., Soldatou, A., Constantinidou, N. and Graphakos, S. (2011) Cytokine gene

polymorphisms and graft-versus-host disease in children after matched sibling haematopoietic stem cell transplantation: a single-center experience. *Cellular & Molecular Immunology*. 8, pp. 276–280.

- Greenberger, J.S., Anderson, J., Berry, L.A., Epperly, M., Cronkite, E.P. and Boggs, S.S. (1996) Effects of irradiation of CBA/CA mice on haematopoietic stem cells and stromal cells in long-term bone marrow cultures. *Leukemia*. 10 (3), pp. 514-527.
- Greenhill, C. J., Rose-John, S., Lissilaa, R., Ferlin, W., Ernst, M., Hertzog, P. J., Mansell, A. and Jenkins, B. J. (2011) IL-6 trans-signaling modulates TLR4-dependent inflammatory responses via STAT3. *The Journal of Immunology*. 186 (2), pp. 1199-1208.
- Grigoropoulos, N.F., Petter, N., Van't Veer, M., Scott, M.A. and Follows, G.A. (2013) Leukaemia update. Part 1: diagnosis and management. *BMJ*. 346, pp. 1660.
- Gu, H., Wang, C., Li, J., Yang, Y., Sun, W., Jiang, C., Li, Y., Ni, M., Liu, W-T., Cheng, Z. and Hu, L. (2020) High mobility group box-1-toll-like receptor 4-phosphatidylinositol 3-kinase/protein kinase B-mediated generation of matrix metalloproteinase-9 in the dorsal root ganglion promotes chemotherapy-induced peripheral neuropathy. *International journal of cancer*. 146 (10), pp. 2810-2821.
- Guan, D., Qing, W., Ma, C., Zhang, Z., Wei, H. and Wu, G. (2018) Bone marrow stromal-cell line HS-5 affects apoptosis of acute myeloid leukemia cells HL-60 through GLI1 activation.
- Guillermo, J., Ruiz-Argüelles, A. and Garcés-Eisele, J. (2007) Donor cell leukemia: A critical review. *Leukemia & Lymphoma*. 48 (1), pp. 25-38.
- Guo, J., Fisher, K. A., Darcy, R., Cryan, J. F. and O'Driscoll, C. (2010) Therapeutic targeting in the silent era: advances in non-viral siRNA delivery. *Molecular Biosystems*. 6 (7), pp. 1143-1161.
- Guo, Y. J., Pan, W. W., Liu, S. B., Shen, Z. F., Xu, Y. and Hu, L. L. (2020) ERK/MAPK signalling pathway and tumorigenesis. *Experimental and therapeutic medicine*. 19 (3), pp. 1997-2007.
- Gurwitz, D. (2016) Human lymphoblastoid cell lines: a valuable tool for personalized medicine research. *Biochemical Society*. pp. 6-9.
- Hamerschlak, N. (2008) Leukemia: genetics and prognostic factors. *J Pediatr (Rio J)*. 84 (4 Suppl), pp. S52-57.

- Hayashi, M. (2016) The micronucleus test—most widely used *in vivo* genotoxicity test. *Genes and Environment*. 38 (1), pp. 18.
- He, X., Wang, H., Jin, T., Xu, Y., Mei, L. and Yang, J. (2016) TLR4 activation promotes bone marrow MSC proliferation and osteogenic differentiation via Wnt3a and Wnt5a signaling. *PloS one*. 11 (3), pp. e0149876.
- Henden, A.S. and Hill, G.R. (2015) Cytokines in Graft-versus-Host Disease. *The Journal of Immunology*. 194, pp. 4604-4612.
- Hertenstein, B., Hambach, L., Bacigalupo, A., Schmitz, N., McCann, S., Slavin, S., Gratwohl, A., Ferrant, A., Elmaagacli, A., Schwertfeger, R., Locasciulli, A., Zander, A., Bornhäuser, M., Niederwieser, D. and Ruutu, T. (2005) Development of leukaemia in donor cells after allogeneic stem cell transplantation- a survey of the European Group for Blood and Marrow Transplantation (EBMT). *Haematologica*. 90, pp. 969-975.
- Higgins, N. (2014) National Foundation Trust. 10, pp. 1-42.
- Hoffbrand, A.V., Moss, P.A.H. and Pettit, J.E. (2011) Essential Haematology. 7th ed. Oxford: Blackwell Publishing.
- Hong, W.K., Bast, R.C., Hait, W.N., Kufe, D.W., Pollock, R.E., Weichselbaum, R.R., Holland, J.F., and Frei, E. (2010) Holland-Frei Cancer Medicine 8th. ed. *American association for cancer Research*. Peoples medical publishing house-USA, Shelton, Connecticut.
- <https://www.sinobiological.com/resource/cytokines/cytokine-function>
- Hu, Z., Xiao, M., Cai, H., Li, W., Fang, W. and Long, X. (2022) Glycyrrhizin regulates rat TMJOA progression by inhibiting the HMGB1-RAGE/TLR4-NF-κB/AKT pathway. *Journal of cellular and molecular medicine*. 26 (3), pp. 925-936.
- Huang, Y. and Li, L. (2013) Transl DNA crosslinking damage and cancer - a tale of friend and foe. *Cancer Res*. 2 (3), pp. 144–154.
- International Agency for Research on Cancer; IARC (2014) Cancer Incidence and Mortality Worldwide. Available from: <http://globocan.iarc.fr>
- Isi, H., Erdal, M.E., Akdeniz, S., Oral, D., Ay, O.I., Tekes, S., Sula, B., Edgunlu, T.G., Balkan, M. and Budak, T. (2010) The Tumor Necrosis Factor-A (TNF-A) Gene -308 G/A Polymorphism and the Tumor Necrosis Factor-Related Apoptosis-Inducing Ligand (Trail) Gene Polymorphisms in Behcet'S Disease. *Biotechnical & Biotechnological Equipment*. 27, pp. 2014-2019.

- Iyer, R. and Lehnert, B. E. (2000) Factors underlying the cell growth-related bystander responses to α particles. *Cancer research*. 60 (5), pp. 1290-1298.
- Jin, M.W., Xu, S.M., An, Q. and Wang, P. (2016) A review of risk factors for childhood leukaemia. *European Review for Medical and Pharmacological Sciences*. 20, pp. 3760-3764.
- Johnson, G. E. (2012) Mammalian cell HPRT gene mutation assay: test methods. In *Genetic Toxicology*. pp. 55-67. Springer, New York, NY.
- Joseph, J. S., Malindisa, S. T. and Ntwasa, M. (2018) Two-dimensional (2D) and three-dimensional (3D) cell culturing in drug discovery. *Cell Culture*. 2, pp. 1-22.
- Kang, L., Tang, X., Zhang, J., Li, M., Xu, N., Qi, W., Tan, J., Lou, X., Yu, Z., Sun, J., Wang, Z., Dai, H., Chen, J., Lin, G., Wu, D. and Yu, L. (2020) Interleukin-6-knockdown of chimeric antigen receptor-modified T cells significantly reduces IL-6 release from monocytes. *Experimental hematology & oncology*. 9, pp.1-13.
- Kato, M., Yamashita, T., Suzuki, R., Matsumoto, K., Nishimori, H., Takahashi, S., Iwato, K., Nakaseko, C., Kondo, T., Imada, K., Kimura, F., Ichinohe, T., Hashii, Y., Kato, K., Atsuta, Y., Taniguchi, S. & Fukuda, T. (2016) Donor cell-derived haematological malignancy: a survey by the Japan Society for Hematopoietic Cell Transplantation. *Leukemia*. 30 (8), pp. 1742-1745.
- Kawakami, M., Tsutsumi, H., Kumakawa, T., Abe, H., Hirai, M., Kurosawa, S., Mori, M. and Fukushima, M. (1990) Levels of serum granulocyte colony-stimulating factor in patients with infections. *Blood*. 76 (10), pp. 1962-1964.
- Kemp, K., Morse, R., Sanders, K., Hows, J. and Donaldson, C. (2011) Alkylating chemotherapeutic agents cyclophosphamide and melphalan cause functional injury to human bone marrow-derived mesenchymal stem cells. *Annals of Haematology*. 90 (7), pp. 777-789.
- Kemp, K., Morse, R., Wexler, S., Cox, C., Mallam, E., Hows, J. & Donaldson, C. (2010) Chemotherapy-induced mesenchymal stem cell damage in patients with hematological malignancy. *Ann Hematol*. 89 (7), pp. 701-713.
- Kenneth, R.H. (2008) Topoisomerase II Inhibitors. *Update on cancer therapeutics*. 3 (3), pp. 26.

- Khalade, A., Jaakkola, M. S., Pukkala, E. and Jaakkola, J. J. (2010) Exposure to benzene at work and the risk of leukemia: a systematic review and meta-analysis. *Environmental Health*. 9 (1), pp. 31.
- Khan, A., and Ali, Z. (2014) Normal ranges for acute phase reactants (interleukin-6, tumour necrosis factor-alpha and C-reactive protein) in Umbilical Cord Blood of Healthy Term Neonates at the Mount Hope Women's Hospital, Trinidad. *The West Indian Medical Journal*. 63 (5), pp. 465.
- Khan, S.N., Lal, S.K., Kumar, P. and Khan, A.U. (2010) Effect of mitoxantrone on proliferation dynamics and cell-cycle progression. *Bioscience Reports*. 30 (6), pp. 375-381.
- Kikuchi, T., Nakahara, S. and Abe, T. (1996) Granulocyte colony-stimulating factor (G-CSF) production by astrocytoma cells and its effect on tumor growth. *Journal of neuro-oncology*. 27, pp. 31-38.
- Kim, H. O., Kim, H. S., Youn, J. C., Shin, E. C. and Park, S. (2011) Serum cytokine profiles in healthy young and elderly population assessed using multiplexed bead-based immunoassays. *Journal of translational medicine*. 9 (1), pp. 1-7.
- Kleiner, G., Marcuzzi, A., Zanin, V., Monasta, L. and Zauli, G. (2013) Cytokine levels in the serum of healthy subjects. *Mediators of inflammation*. 2013, 434010.
- Kondo, N., Takahashi, A., Ono, K. and Ohnishi, T. (2010) DNA damage induced by alkylating agents and repair pathways. *Journal of Nucleic Acids*. 21, 543531.
- Kumari, R., Sharma, A., Ajay, A. K. and Bhat, M. K. (2009) Mitomycin C induces bystander killing in homogeneous and heterogeneous hepatoma cellular models. *Molecular cancer*. 8 (1), pp. 87.
- Kuznetsova, I. S., Labutina, E. V. and Hunter, N. (2016) Radiation risks of leukemia, lymphoma and multiple myeloma incidence in the Mayak cohort: 1948–2004. *PLoS one*. 11 (9), e0162710.
- Lal, A. and Ames, B.N. (2011) Association of chromosome damage detected as micronuclei with haematological diseases and micronutrient status. *Mutagenesis*. 26 (2), pp. 57-62.
- Langowski, J. L., Zhang, X., Wu, L., Mattson, J. D., Chen, T., Smith, K., Basham, B., McClanahan, T., Kastelein, R. A. and Oft, M. (2006) IL-23 promotes tumour incidence and growth. *Nature*. 442 (7101), pp. 461-465.

- Larizza, L., Magnani, I. and Beghini, A. (2005) The Kasumi-1 cell line: at (8; 21)-kit mutant model for acute myeloid leukemia. *Leukemia & lymphoma*. 46 (2), pp. 247-255.
- Lau, A., Belanger, C.L. and Winn, L.M. (2009) In utero and acute exposure to benzene: investigation of DNA double-strand breaks and DNA recombination in mice. *Mutation Research*. 676 (1-2), pp. 74-82.
- Lazutka, J. R. and Rudaitienė, S. (1991) Effect of tumor necrosis factor on cell proliferation kinetics and sister chromatid exchange frequency in human lymphocytes. *Carcinogenesis*. 12 (7), pp. 1355-1357.
- Lazutka, J.R. (1996) Genetic toxicity of cytokines. *Mutation Research/Environmental Mutagenesis and Related Subjects*. 361 (2-3), pp. 95-105.
- Lee, J., Kim, Y., Lim, J., Kim, M. and Han, K. (2008) G-CSF and GM-CSF concentrations and receptor expression in peripheral blood leukemic cells from patients with chronic myelogenous leukemia. *Annals of Clinical & Laboratory Science*. 38 (4), pp. 331-337.
- Leone, G., Mele, L., Pulsoni, A., Equitani, F. and Pagano, L. (1999) The incidence of secondary leukemias. *Haematologica*. 84, pp. 937-945.
- Leuning, D. G., Beijer, N. R., du Fossé, N. A., Vermeulen, S., Lievers, E., van Kooten, C. and de Boer, J. (2018) The cytokine secretion profile of mesenchymal stromal cells is determined by surface structure of the microenvironment. *Scientific reports*. 8 (1), pp. 1-9.
- Li, J., Law, H.K., Lau, Y.L. and Chan, G.C. (2004) Differential damage and recovery of human mesenchymal stem cells after exposure to chemotherapeutic agents. *British Journal of Haematology*. 127 (3), pp. 326-334.
- Li, J., Yang, F., Wei, F. and Ren, X. (2017) The role of toll-like receptor 4 in tumor microenvironment. *Oncotarget*. 8 (39), pp: 66656-66667.
- Li, T., Forbes, M. E., Fuller, G. N., Li, J., Yang, X. and Zhang, W. (2020) IGFBP2: integrative hub of developmental and oncogenic signaling network. *Oncogene*. 39 (11), pp. 2243-2257.
- Lin, L., Hutzen, B., Zuo, M., Ball, S., Deangelis, S., Foust, E., Pandit, B., Ihnat, M. A., Shenoy, S. S., Kulp, S., Li, P-K., Li, C., Fuchs, J. and Lin, J. (2010) Novel STAT3 phosphorylation inhibitors exhibit potent growth-suppressive activity in pancreatic and breast cancer cells. *Cancer research*. 70 (6), pp. 2445-2454.

- Liu, J., Ma, W., Zang, C. H., Wang, G. D., Zhang, S. J., Wu, H. J., Zhu, K. W., Xiang, X. L., Li, C. Y., Liu, K. P., Guo, J. H. and Li, L. Y. (2021) Salidroside inhibits NLRP3 inflammasome activation and apoptosis in microglia induced by cerebral ischemia/reperfusion injury by inhibiting the TLR4/NF- κ B signaling pathway. *Annals of translational medicine*. 9 (22), pp. 1694.
- Liu, Y., Fuchs, J., Li, C. and Lin, J. (2010) IL-6, a risk factor for hepatocellular carcinoma: FLLL32 inhibits IL-6-induced STAT3 phosphorylation in human hepatocellular cancer cells. *Cell cycle*. 9 (17), pp. 3423-3427.
- Liu, Z., Mahale, P., & Engels, E. A. (2019). Sepsis and risk of cancer among elderly adults in the United States. *Clinical Infectious Diseases*, 68(5), 717-724.
- Liviak, D., Creus, A. and Marcos, R. (2010) Genotoxicity testing of three monohaloacetic acids in TK6 cells using the cytokinesis-block micronucleus assay. *Mutagenesis*. 25 (5), pp. 505-509.
- Lorimore, S. A. and Wright, E. G. (2003) Radiation-induced genomic instability and bystander effects: related inflammatory-type responses to radiation-induced stress and injury? A review. *International journal of radiation biology*. 79 (1), pp. 15-25.
- Lorimore, S.A., Coates, P.J., Scobie, G.E., Milne, G. and Wright, E.G. (2001) Inflammatory-type responses after exposure to ionizing radiation *in vivo*: a mechanism for radiation-induced bystander effects?. *Oncogene*. 20 (48), pp.7085.
- Ma, H. and Liu, T. (2016) Development of donor cell leukaemia following peripheral blood stem cell transplantation for severe aplastic anaemia: A case report. *Oncology letters*. 11 (6), pp. 3858-3862.
- Maele-Fabry, G., Gamet-Payrastre, L. and Lison, D. (2019) Household exposure to pesticides and risk of leukemia in children and adolescents: Updated systematic review and meta-analysis. *International journal of hygiene and environmental health*. 222 (1), pp. 49-67.
- Majzner, R.G., Mogri, H., Varadhan, R., Brown, P., Cooke, K.R., Bolaños-Meade, J., Swinnen, L., Kanakry, J., Luznik, L., Jones, R.J., Fuchs, E., Ambinder, R., Kasamon, Y. and Symons, H.J. (2017) Post-Transplantation Cyclophosphamide after Bone Marrow Transplantation Is Not Associated with an Increased Risk of Donor-Derived Malignancy. *Blood and Marrow Transplantation*. 23, pp. 612-617.

- Maltzman, J.D. and Millar, L.B. (2012) Chemotherapy Primer: Why? What? and How?, OncoLink
- Manore, S. G., Doheny, D. L., Wong, G. L. and Lo, H. W. (2022) IL-6/JAK/STAT3 signaling in breast cancer metastasis: Biology and treatment. *Frontiers in oncology*. 12, pp.866014.
- Markey, K. A. and Hill, G. R. (2017) Cytokines in Hematopoietic Stem Cell Transplantation. *Cytokine Effector Functions in Tissues*. pp. 219-236. Academic Press.
- Masjedi, A., Ahmadi, A., Atyabi, F., Farhadi, S., Irandoust, M., Khazaei-Poul, Y., Chaleshtari, M. G., Fathabad, M. E., Baghaei, M., Haghnavaz, N., Baradaran, B., Hojjat-Farsangi, M., Ghalamfarsa, G., Sabz, G., Hasanzadeh, S. and Jadidi-Niaragh, F. (2020) Silencing of IL-6 and STAT3 by siRNA loaded hyaluronate-N, N, N-trimethyl chitosan nanoparticles potently reduces cancer cell progression. *International journal of biological macromolecules*. 149, pp. 487-500.
- Mateu, A., Ramudo, L., Manso, M. A. and De Dios, I. (2015) Cross-talk between TLR4 and PPAR γ pathways in the arachidonic acid-induced inflammatory response in pancreatic acini. *The International Journal of Biochemistry & Cell Biology*. 69, pp. 132-141.
- Matsubara, K., Ochi, H., Kitagawa, H., Yamanaka, K., Kusanagi, Y. and Ito, M. (1999) Concentrations of serum granulocyte-colony-stimulating factor in normal pregnancy and preeclampsia. *Hypertension in pregnancy*. 18 (1), pp. 95-106.
- Matsunaga, N., Tsuchimori, N., Matsumoto, T. and Ii, M. (2011) TAK-242 (resatorvid), a small-molecule inhibitor of Toll-like receptor (TLR) 4 signaling, binds selectively to TLR4 and interferes with interactions between TLR4 and its adaptor molecules. *Molecular pharmacology*. 79 (1), pp. 34-41.
- McCann, S. and Wright, E. (2003) Donor leukaemia: perhaps a more common occurrence than we thought. *Bone Marrow Transplantation*. 32, pp. 455–457.
- Medinger, M., Lengerke, C. and Passweg, J. (2016) Novel therapeutic options in acute myeloid leukaemia. *Leukaemia research reports*. 6, pp. 39-49.
- Meer, W.V.D., Gelder, W.V., Keijzer, R.D. and Willems, H. (2007) The divergent morphological classification of variant lymphocytes in blood smears. *Journal of clinical pathology*. 60 (7), pp.m838–839.

- Melenhorst, J. J., Tian, X., Xu, D., Sandler, N. G., Scheinberg, P., Biancotto, A., Scheinberg, P., McCoy Jr, J. P., Hensel, N. F., McIver, Z., Douek, D. C. and Barrett, A. J. (2012) Cytopenia and leukocyte recovery shape cytokine fluctuations after myeloablative allogeneic hematopoietic stem cell transplantation. *Haematologica*. 97 (6), pp. 867.
- Mendelson, A. and Frenette, P.S. (2014) Haematopoietic stem cell niche maintenance during homeostasis and regeneration. *Nature Medicine*. 20 (8), pp. 833–846.
- Merle, P., Morvan, D., Caillaud, D. and Demidem, A. (2008) Chemotherapy-induced bystander effect in response to several chloroethylnitrosoureas: an origin independent of DNA damage?. *Anticancer research*. 28 (1A), pp. 21-27.
- Miller, S.A., Dykes, D.D. and Polesky, H.F. (1988) A simple salting out procedure for extracting DNA from human nucleated cells. *Nucleic Acids Research Volume*. 16 (3).
- Molina, J. R. and Adjei, A. A. (2006) The ras/raf/mapk pathway. *Journal of Thoracic Oncology*. 1 (1), pp. 7-9.
- Moqattash, S. and Lutton, J. D. (1998) Leukemia cells and the cytokine network. *Proceedings of the Society for Experimental Biology and Medicine*. 219 (1), pp. 8-27.
- Moqattash, S. and Lutton, J. D. (2004) Leukemia cells and the cytokine network: therapeutic prospects. *Experimental Biology and Medicine*. 229 (2), pp. 121-137.
- Morgan, R. A., Yang, J. C., Kitano, M., Dudley, M. E., Laurencot, C. M. and Rosenberg, S. A. (2010) Case report of a serious adverse event following the administration of T cells transduced with a chimeric antigen receptor recognizing ERBB2. *Molecular therapy*. 18 (4), pp. 843-851.
- Morgan, W.F. (2003) Is there a common mechanism underlying genomic instability, bystander effects and other nontargeted effects of exposure to ionizing radiation. *Oncogene*. 22, pp. 7094-7099.
- Morse, H.R., Olomolaiye, O.O., Wood, N.A.P., Keen, L.J. and Bidwell, J.L. (1999) Induced Heteroduplex Genotyping of TNF- α , IL-1 β , IL-6 And IL-10 Polymorphisms Associated With Transcriptional Regulation. *Cytokine*. 11 (10), pp. 789-795.
- Mousavi, S. F., Fatemi, S., Siadat, S. D., Zahraei, S. M., Nikanpour, E., Malekan, M. A., Khabiri, A. R. and Janani, A. R. (2016) Development and optimization of a homemade ELISA kit for detection of antibodies against Haemophilus influenzae type b. *Jundishapur Journal of Microbiology*. 9 (5), pp. e30629.

- Mullis, K.B. and Smith, M. (1993) The Polymerase Chain Reaction. *Nobel Lecture*. 1993. Available at: https://www.nobelprize.org/nobel_prizes/chemistry/laureates/1993/mullis-lecture.html
- Neta, R. and Oppenheim, J.J. (1991) Radioprotection with cytokines-learning from nature to cope with radiation damage. *Cancer cells*. 3 (10), pp. 391-397.
- Neurath, M. F. and Finotto, S. (2011) IL-6 signaling in autoimmunity, chronic inflammation and inflammation-associated cancer. *Cytokine & growth factor reviews*. 22 (2), pp. 83-89.
- Newell, D.R., Calvert, A.H., Harrap, K.R. and McElwain (1983) Studies on the pharmacokinetics of chlorambucil and prednimustine in man. *Br J Clin Pharmacol*. 15, pp.253–258.
- Nitiss, J. L. (2009) Targeting DNA topoisomerase II in cancer chemotherapy. *Nature Reviews Cancer*. 9 (5), pp. 338-350.
- Noll, D.M., Mason, T.M. and Miller, P.S. (2006) Formation and Repair of Interstrand Cross- Links in DNA. *Chemical Review*. 106 (2), pp. 277–301.
- Noori, N. M., Shahramian, I., Teimouri, A., Keyvani, B. and Mahjoubifard, M. (2017) Serum levels of tumor necrosis factor- α and interleukins in children with congenital heart disease. *The Journal of Tehran University Heart Center*. 12 (1), pp. 15.
- OECD Guidelines For The Testing Of Chemicals (2016) Proposal For Updating Test Guideline 487, *In Vitro* Mammalian Cell Micronucleus Test.
- Olomolaiye, O., Wood, N.A.P. and Bidwell, J.L. (2008) A novel *Nla*III polymorphism in the human IL-6 promoter. *European Journal of Immunogenetics*. 25, pp. 267-267.
- Pandi, P., Jain, A., Raju, S. and Khan, W. (2017) Therapeutic approaches for the delivery of TNF- α siRNA. *Therapeutic Delivery*. 8 (5), pp. 343-355.
- Park, C.W., Kim, K.S., Bae, S., Son, H.K., Myung, P.K., Hong, H.J. and Kim, H. (2009) Cytokine Secretion Profiling of Human Mesenchymal Stem Cells by Antibody Array. *International Journal of Stem Cells*. 2 (1), pp. 59-68.
- Parker, B. S., Buley, T., Evison, B. J., Cutts, S. M., Neumann, G. M., Iskander, M. N. and Phillips, D. R. (2004) A molecular understanding of mitoxantrone-DNA adduct formation effect of cytosine methylation and flanking sequences. *Journal of Biological Chemistry*. 279 (18), pp. 18814-18823.

- Passweg, J. R., Baldomero, H., Bader, P., Bonini, C., Cesaro, S., Dreger, P., Duarte, R. F., Dufour, C., Kuball, J., Farge-Bancel, D., Gennery, A., Kröger, N., Lanza, F., Nagler, F., Sureda, A. and Mohty, M. (2016) Hematopoietic stem cell transplantation in Europe 2014: more than 40 000 transplants annually. *Bone marrow transplantation*. 51(6), pp. 786-792.
- Pedersen-Bjergaard, J., Andersen, M.K., Christiansen, D.H. and Nerlov, C. (2002) Genetic pathways in therapy-related myelodysplasia and acute myeloid leukaemia. *Blood*. 99 (6), pp. 1909-1912.
- Peled, A., Lee, B.C., Sternberg, D., Toledo, J., Aracil, M. and Zipori, D. (1996) Interactions between leukaemia cells and bone marrow stromal cells: stroma-supported growth vs. serum dependence and the roles of TGF-beta and M-CSF. *Experimental hematology*. 24 (6), pp. 728-737.
- Petros, W.P., Rabinowitz, J., Stuart, A. and Peters, W.P. (1997) Clinical pharmacology of filgrastim following high-dose chemotherapy and autologous bone marrow transplantation. *Clin Cancer Res*. 3 (5), pp. 705-11. PMID: 9815739.
- Pettitt, A. R., Jackson, R., Carruthers, S., Dodd, J., Dodd, S., Oates, M., Johnson, G. G., Schuh, A., Matutes, E., Dearden, C. E., Catovsky, D., Radford, J. A., Bloor, A., Follows, G. A., Devereux, S., Kruger, A., Blundell, J., Agrawal, S., Allsup, D., Proctor, S., Hartin, E., Oscier, D., Hamblin, T. J., Rawstron, A. and Hillmen, P. (2012) Alemtuzumab in combination with methylprednisolone is a highly effective induction regimen for patients with chronic lymphocytic leukemia and deletion of TP53: final results of the national cancer research institute CLL206 trial. *Journal of Clinical Oncology*. 30 (14), pp. 1647-1655.
- Pipes, B.L., Tsang, T., Peng, S-X, Fiederlein, R., Graham, M. and Harris, D.T. (2006) Telomere length changes after umbilical cord blood transplant. *Transfusion*. 46, pp. 1038-1043.
- Pixley, F. J. and Stanley, E. R. (2010) Cytokines and cytokine receptors regulating cell survival, proliferation, and differentiation in hematopoiesis. *Handbook of cell signaling*. pp. 2733-2742. Academic Press.
- Plangger, A., Rath, B., Hochmair, M., Funovics, M. and Hamilton, G. (2021) Cytotoxicity of combinations of the pan-KRAS inhibitor BAY-293 against primary non-small lung cancer cells. *Translational Oncology*. 14 (12), pp. 101230.

- Plangger, A., Rath, B., Stickler, S., Hochmair, M., Lang, C., Weigl, L., Funovics, M. and Hamilton, G. (2022) Cytotoxicity of combinations of the pan-KRAS SOS1 inhibitor BAY-293 against pancreatic cancer cell lines. *Discover Oncology*. 13 (1), pp. 84.
- Podrzywalow-Bartnicka, P., Kominek, A., Wolczyk, M., Kolba, M.D., Swatler, J. and Piwocka, K. (2018) Characteristics of live parameters of the HS-5 human bone marrow stromal cell line cocultured with the leukemia cells in hypoxia, for the studies of leukemia stroma crosstalk. *Cytometry Part A*. 93 (9), pp. 929-940.
- Pokharel, M. (2012) Leukemia: A review article. *International Journal of Advanced Research in Pharmaceutical Bio Sciences*. 2 (3), pp. 397-407.
- Proietti, E., Greco, G., Garrone, B., Baccarini, S., Mauri, C., Venditti, M., Carlei, D. and Belardelli, F. (1998) Importance of cyclophosphamide-induced bystander effect on T cells for a successful tumor eradication in response to adoptive immunotherapy in mice. *The Journal of clinical investigation*. 101 (2), pp. 429-441.
- Qu, S., Liu, M., Cao, C., Wei, C., Meng, X. E., Lou, Q., Wang, B., Li, X., She, Y., Wang, Q., Song, Z., Han, Z., Zhu, Y., Huang, F. and Duan, J. A. (2021) Chinese medicine formula Kai-Xin-San ameliorates neuronal inflammation of CUMS-induced depression-like mice and reduces the expressions of inflammatory factors via inhibiting TLR4/IKK/NF- κ B pathways on BV2 cells. *Frontiers in Pharmacology*. 12, pp. 626949.
- Raaijmakers, M. H. G. P., Mukherjee, S., Guo, S., Zhang, S., Kobayashi, T., Schoonmaker, J. A., Ebert, B. L., Alshahrour, F., Hasserjian, R. P., Scadden, E. O., Aung, Z., Matza, M., Merckenschlager, M., Lin, C., Rommens, J. M. and Scadden, D. T. (2010) Bone progenitor dysfunction induces myelodysplasia and secondary leukaemia. *Nature*. 464 (7290), pp. 852-857.
- Ralhan, R. and Kaur, J. (2007) Alkylating agent and cancer therapy. *Expert Opinion on Therapeutic Patents*.
- Reeh, H., Rudolph, N., Billing, U., Christen, H., Streif, S., Bullinger, E., Schliemann-Bullinger, M., Findeisen, R., Schaper, F., Huber, H. J. and Dittrich, A. (2019) Response to IL-6 trans- and IL-6 classic signalling is determined by the ratio of the IL-6 receptor α to gp130 expression: fusing experimental insights and dynamic modelling. *Cell Communication and Signalling*. 17, pp. 1-21.
- Resatorvid (TAK-242), Selleckchem.com (2023), <https://www.selleckchem.com/products/resatorvid.html>

- Riegler, L. L., Jones, G. P. and Lee, D. W. (2019) Current approaches in the grading and management of cytokine release syndrome after chimeric antigen receptor T-cell therapy. *Therapeutics and clinical risk management*. 15, pp. 323-335.
- Robak, T., Gladalska, A., Stepień, H. and Robak, E. (1998) Serum levels of interleukin-6 type cytokines and soluble interleukin-6 receptor in patients with rheumatoid arthritis. *Mediators of inflammation*. 7, pp. 347-353.
- Robb, L. (2007) Cytokine receptors and hematopoietic differentiation. *Oncogene*. 26, pp. 6715–6723.
- Robb, L. (2007) Cytokine receptors and hematopoietic differentiation. *Oncogene*. 26 (47), pp. 6715-6723.
- Rocha, J. C., Busatto, F. F., Guecheva, T. N. and Saffi, J. (2016) Role of nucleotide excision repair proteins in response to DNA damage induced by topoisomerase II inhibitors. *Mutation Research/Reviews in Mutation Research*. 768, pp. 68-77.
- Roecklein, B.A. and Torok-Storb, B. (1995) Functionally distinct human marrow stromal cell lines immortalized by transduction with the human papilloma virus E6/E7 genes. *Blood*. 85 (4), pp. 997–1005.
- Roux, K.H. (1995) Optimization and troubleshooting in PCR. *Genome Research*. 4, pp. 185-94.
- Rozenberg, G. (2011) Microscope Haematology.
- Rugo, R. E., Almeida, K. H., Hendricks, C. A., Jonnalagadda, V. S. and Engelward, B. P. (2005) A single acute exposure to a chemotherapeutic agent induces hyper-recombination in distantly descendant cells and in their neighbors. *Oncogene*. 24 (32), pp. 5016-5025.
- Sala-Torra, O. and Loeb, K.R. (2011) Donor cell-derived leukaemia and myelodysplastic neoplasm: unique forms of leukaemia. *American Journal of Clinical Pathology*. 135 (4), pp. 501-504.
- Sansone, P. and Bromberg, J. (2012) Targeting the interleukin-6/Jak/stat pathway in human malignancies. *Journal of Clinical Oncology*. 30 (9), pp. 1005.
- Schmidmaier, R., Baumann, P. and Meinhardt, G. (2006) Cell-Cell Contact Medicated Signalling — No Fear of Contact. *Experimental Oncology*. 28 (1), pp. 12–15.
- Shi, H., Wang, Y., Li, R., Xing, W., Yang, F. C., Bai, J. and Zhou, Y. (2018) Alteration in the cytokine secretion of bone marrow stromal cells from patients with chronic

myelomonocytic leukemia contribute to impaired hematopoietic supportive activity. *Stem cells international*. 2018, 5921392.

- Shi, M.M., Bleavins, R. and Igllesia, F.A. (1999) Technologies for detecting genetic polymorphisms in pharmacogenomics. *Molecular Diagnosis*. 4 (4), pp. 343-351.
- Shi, Y., Liu, C. H., Roberts, A. I., Das, J., Xu, G., Ren, G., Zhang, Y., Zhang, L., Yuan, Z. R., Tan, H. S. W., Das, G. and Devadas, S. (2006) Granulocyte-macrophage colony-stimulating factor (GM-CSF) and T-cell responses: what we do and don't know. *Cell research*. 16 (2), pp. 126-133.
- Shimabukuro-Vornhagen, A., Gödel, P., Subklewe, M., Stemmler, H. J., Schlöber, H. A., Schlaak, M., & von Bergwelt-Baildon, M. S. (2018) Cytokine release syndrome. *Journal for immunotherapy of cancer*. 6 (1), pp.1-14.
- Shiomi, A. and Usui, T. (2015) Pivotal roles of GM-CSF in autoimmunity and inflammation. *Mediators of inflammation*. 2015, pp. 568543.
- Sica, A. and Bronte, V. (2007) Altered macrophage differentiation and immune dysfunction in tumor development. *The Journal of clinical investigation*. 117 (5), pp. 1155-1166.
- Silvennoinen, R., Malminiemi, K., Malminiemi, O., Seppala, E. and Vilpo, J. (2000) Pharmacokinetics of chlorambucil in patients with chronic lymphocytic leukaemia: comparison of different days, cycles and doses. *Pharmacol Toxicol*. 87, pp. 223–8.
- Singh, R.K., Ino, I., Varney, M.L., Heimann, D.G. and Talmadge, J.E. (1999) Immunoregulatory cytokines in bone marrow and peripheral blood stem cell products. *Bone Marrow Transplantation*. 23, pp. 53–62.
- Sloand, E.M., Yong, A.S., Ramkissoon, S., (2006) Granulocyte colony-stimulating factor preferentially stimulates proliferation of monosomy 7 cells bearing the isoform IV receptor. *Proc Natl Acad Sci U S A*. 103, pp. 14483-14488.
- Smyth, J.F., Macpherson, J.S., Warrington, P.S., Leonard, R.C.F. and Wolf, C.R. (1986) The clinical pharmacology of mitozantrone. *Cancer Chemotherapy and Pharmacology*. 17, pp. 149-152.
- Sommer, S., Buraczewska, I. and Kruszewski, M. (2020) Micronucleus assay: The state of art, and future directions. *International journal of molecular sciences*. 21 (4), pp. 1534.
- Son, D. S., Parl, A. K., Montgomery Rice, V. and Khabele, D. (2007) Keratinocyte chemoattractant (KC)/human growth-regulated oncogene (GRO) chemokines and pro-

inflammatory chemokine networks in mouse and human ovarian epithelial cancer cells. *Cancer biology & therapy*. 6 (8), pp. 1308-1318.

- Song, C., Gao, C. and Wang, Z. (2022) Grape-Seed-Derived Procyanidin Attenuates Chemotherapy-Induced Cognitive Impairment by Suppressing MMP-9 Activity and Related Blood–Brain-Barrier Damage. *Brain Sciences*. 12 (5), pp. 571.
- Song, M., Wang, Y., Shang, Z.F., Liu, X.D., Xie, D.F., Wang, Q., Guan, H. and Zhou, P.K. (2016) Bystander autophagy mediated by radiation-induced exosomal miR-7-5p in non-targeted human bronchial epithelial cells. *Scientific reports*. 6, 30165.
- Spinelli, O., Giussani, U., Borleri, G., Lazzari, M., Michelato, A., Dotti, G., Barbui, T. and Rambaldi, A. (2000) Need for an accurate molecular diagnosis to assess the donor origin of leukemia relapse after allogeneic stem cell transplantation. *Haematologica*. 85, pp. 1153 – 1157.
- Stellwagen, N.C. (2009) Electrophoresis of DNA in agarose gels, polyacrylamide gels and in free solution. *Electrophoresis*. 30.
- Stieglitz, E. and Loh, M.L. (2013) Therapeutic Advances in Hematology Review Genetic predispositions to childhood leukemia. *Ther Adv Hematol*. 4 (4), pp. 270 –290.
- Su, C. W., Chuang, C. Y., Chen, Y. T., Yang, W. E., Pan, Y. P., Lin, C. W. and Yang, S. F. (2021) FLLL32 triggers caspase-mediated apoptotic cell death in human oral cancer cells by regulating the p38 pathway. *International Journal of Molecular Sciences*. 22 (21), pp. 11860.
- Suárez-González, J., Martínez-Laperche, C., Kwon, M., Balsalobre, P., Carbonell, D., Chicano, M., Rodríguez-Macías, G., Serrano, D., Gayoso, J., Díez-Martín, J.L. and Buño, I. (2018) Donor Cell–Derived Hematologic Neoplasms after Hematopoietic Stem Cell Transplantation. *A Systematic Review, Blood and Marrow Transplantation*. 24, pp. 1505-1513.
- Suzuki, Y., Hattori, K., Hamanaka, J., Murase, T., Egashira, Y., Mishiro, K., Ishiguro, M., Tsuruma, K., Hirose, Y., Tanaka, H., Yoshimura, S., Shimazawa, M., Inagaki, N., Nagasawa, H., Iwama, T. and Hara, H. (2012) Pharmacological inhibition of TLR4-NOX4 signal protects against neuronal death in transient focal ischemia. *Scientific reports*. 2 (1), pp. 896.
- Sweeney, C. and Vyas, P. (2019) The Graft-versus-Leukemia Effect in AML. *Frontiers in Oncology*. 9, pp. 1217.

- Swerdlow, S. H., Campo, E., Pileri, S. A., Harris, N. L., Stein, H., Siebert, R., Advani, R., Ghielmini, M., Salles, G. A., Zelenetz, A. D. and Jaffe, E. S. (2016) The 2016 revision of the World Health Organization classification of lymphoid neoplasms. *Blood*. 127 (20), pp. 2375-2390.
- Swiatnicki, M., Engel, L., Shrestha, R., Alves, J., Goueli, S. A. and Zegzouti, H. (2022) Profiling oncogenic KRAS mutant drugs with a cell-based Lumit p-ERK immunoassay. *SLAS Discovery*. 27 (4), pp. 249-257.
- Swift, L. and Golsteyn, R. (2014) Genotoxic anti-cancer agents and their relationship to DNA damage, mitosis, and checkpoint adaptation in proliferating cancer cells. *International journal of molecular sciences*. 15 (3), pp. 3403-3431.
- Szumilas, P., Barcew, K., Bakiewicz-Masiuk, M., Wiszniewska, B., Ratajczak, M.Z. and Machalinski, B. (2005) Effect of stem cell mobilization with cyclophosphamide plus granulocyte colony-stimulating factor on morphology of haematopoietic organs in mice. *Cell Proliferation*. 38, pp. 47–61.
- Takagi, S., Saito, Y., Hijikata, A., Tanaka, S., Watanabe, T., Hasegawa, T., Mochizuki, S., Kunisawa, J., Kiyono, H., Koseki, H., Ohara, O., Saito, T., Taniguchi, S., Shultz, L.D. and Ishikawa, F. (2012) Membrane-bound human SCF/KL promotes *in vivo* human hematopoietic engraftment and myeloid differentiation. *Blood*. 119 (12).
- Takeshita, F., Minakuchi, Y., Nagahara, S., Honma, K., Sasaki, H., Hirai, K., Teratani, T., Namatame, N., Yamamoto, Y., Hanai, K., Kato, T., Sano, A. and Ochiya, T. (2005) Efficient delivery of small interfering RNA to bone-metastatic tumors by using atelocollagen *in vivo*. *Proceedings of the National Academy of Sciences*. 102 (34), pp. 12177-12182.
- Tanaka, T., Narazaki, M. and Kishimoto, T. (2014) IL-6 in inflammation, immunity, and disease. *Cold Spring Harbor perspectives in biology*. 6 (10), pp. a016295.
- Tanaka, T., Narazaki, M. and Kishimoto, T. (2016) Immunotherapeutic implications of IL-6 blockade for cytokine storm. *Immunotherapy*. 8 (8), pp. 959-970.
- Thatcher, J. D. (2010) The Ras-MAPK signal transduction pathway. *Science signaling*. 3 (119 tr1).
- Thomas, A. D., Jenkins, G. J. S., Kaina, B., Bodger, O. G., Tomaszowski, K. H., Lewis, P. D., Doak, S. H. and Johnson, G. E. (2013) Influence of DNA repair on nonlinear dose-responses for mutation. *toxicological sciences*. 132 (1), pp. 87-95.

- Tisoncik, J. R., Korth, M. J., Simmons, C. P., Farrar, J., Martin, T. R. and Katze, M. G. (2012) Into the eye of the cytokine storm. *Microbiology and molecular biology reviews*. 76 (1), pp. 16-32.
- Toubai, T., Tanaka, J., Paczesny, S., Shono, Y., Reddy, P. and Imamura, M. (2012) Role of Cytokines in the Pathophysiology of Acute Graft-Versus-Host Disease (GVHD)—Are Serum/Plasma Cytokines Potential Biomarkers for Diagnosis of Acute GVHD Following Allogeneic Hematopoietic Cell Transplantation (Allo-HCT)?. *Current stem cell research & therapy*. 7 (3), pp. 229-239.
- Tzur, A., Kafri, R., LeBleu, V.S., Lahav, G. and Kirschner, M.W. (2009) Cell Growth and Size Homeostasis in Proliferating Animal Cells. *Science*. 325 (5937), pp. 167–171.
- Vaillant A. A. J. and Quirie A. Interleukin. [Updated 2022 Aug 22]. In: StatPearls. Treasure Island (FL): StatPearls Publishing; 2023 Jan-. Available from: <https://www.ncbi.nlm.nih.gov/books/NBK499840/>
- Vainchenker, W. and Constantinescu, S. N. (2013) JAK/STAT signaling in hematological malignancies. *Oncogene*. 32 (21), pp. 2601-2613.
- Van Belle, S.J.P., de Planque, M.M., Smith, I.E., van Oosterom, A.T., Schoemaker, T.J., Deneve, W. and McVie, J.G. (1986) Pharmacokinetics of mitoxantrone in humans following single agent infusion or intra-arterial injection therapy or combined-agent infusion therapy. *Cancer Chemotherapy and Pharmacology*. 18, pp. 27–32.
- Vernon, A.R., Pemberton, R. and Morse, H.R. (2022) A novel *in vitro* 3D model of the human bone marrow to bridge the gap between *in vitro* and *in vivo* genotoxicity testing. *Mutagenesis*. 37, pp. 112–29.
- Vogel, E. W., Nivard, M. J. M., Ballering, L. A. B., Bartsch, H., Barbin, A., Nair, J., Comendador, M.A., Sierra, L.M., Agmrrrezabalaga, I., Tosal, L., Ehrenberg, L., Fuchs, R.P.P., Janel-Blntz, R., Maenhaut-Michel, G., Montesano, R., Hall, J., Kang, H., Miele, M., Thomale, J., Bender, K., Engelbergs, J. and Rajewsky, M.F. (1996) DNA damage, and repair in mutagenesis and carcinogenesis: implications of structure-activity relationships for cross-species extrapolation. *Mutation Research/Fundamental and Molecular Mechanisms of Mutagenesis*. 353 (1-2), pp. 177-218.
- Vollmer, T., Stewart, T. and Baxter, N. (2010) Mitoxantrone and cytotoxic drugs' mechanisms of action. *Neurology*. 74 (Supplement 1), pp. S41-S46.

- Wakefield, L. M., Letterio, J. J., Chen, T., Danielpour, D., Allison, R. S. H., Pai, L. H., Denicoff, A. M., Noone, M. H., Cowan, K. H., O'Shaughnessy, J. A. and Sporn, M. B. (1995) Transforming growth factor-beta1 circulates in normal human plasma and is unchanged in advanced metastatic breast cancer. *Clinical cancer research: an official journal of the American Association for Cancer Research*. 1 (1), pp. 129-136.
- Walshauer, M.A., Go, A., Sojitra, P., Venkataraman, G. and Stiff, P. (2014) Donor Cell Myeloid Sarcoma. *Case Reports in Haematology*. Volume 2014, Article ID 153989, 4 pages.
- Wan, R., Jiang, J., Hu, C., Chen, X., Chen, C., Zhao, B., Hu, X., Zheng, Z. and Li, Y. (2020) Neutrophil extracellular traps amplify neutrophil recruitment and inflammation in neutrophilic asthma by stimulating the airway epithelial cells to activate the TLR4/NF- κ B pathway and secrete chemokines. *Aging (Albany NY)*. 12 (17), pp. 16820.
- Wang, E., Hutchinson, C.B., Huang, Q., Mark Lu, C., Crow, J., Wang, F. F., Sebastian, S., Rehder, C., Lagoo, A., Horwitz, M., Rizzieri, D., Yu, J., Goodman, B., Datto, M. and Buckley, P. (2011) Donor Cell-Derived Leukemias/Myelodysplastic Neoplasms in Allogeneic Haematopoietic Stem Cell Transplant Recipients. A Clinicopathologic Study of 10 Cases and a Comprehensive Review of the Literature. *American Journal of Clinical Pathology*. 135, pp. 525-540.
- Wang, J., Erlacher, M. and Fernandez-Orth, J. (2022) The role of inflammation in hematopoiesis and bone marrow failure: What can we learn from mouse models?. *Frontiers in immunology*. 13, pp. 951937.
- Wang, R., Zhou, T., Liu, W. and Zuo, L. (2018) Molecular mechanism of bystander effects and related abscopal/ cohort effects in cancer therapy. *Oncotarget*. 9, pp. 18637-18647.
- Wei, J., Wang, Y., Qi, X., Fan, Z. and Wu, Y. (2020) Melatonin ameliorates hyperglycaemia-induced renal inflammation by inhibiting the activation of TLR4 and TGF- β 1/Smad3 signalling pathway. *American Journal of Translational Research*. 12 (5), pp. 1584.
- Welch, G.N. and Loscalzo, J. (1996) Nitric Oxide Synthase: Characterization and Functional Analysis. *Chemiluminescence*.
- Wen, Y., Bi, S., Hu, X., Yang, J., Li, C., Li, H., Yu, D. B., Zhu, J., Song, L. and Yu, R. (2021) Structural characterization and immunomodulatory mechanisms of two novel

glucans from *Morchella importuna* fruiting bodies. *International Journal of Biological Macromolecules*. 183, pp. 145-157.

- Westbrook AM, Wei B, Hacke K, et al. The role of tumour necrosis factor- α and tumour necrosis factor receptor signalling in inflammation-associated systemic genotoxicity. *Mutagenesis* 2012;27:77–86.
- Whitehead, K. A., Langer, R. and Anderson, D. G. (2009) Knocking down barriers: advances in siRNA delivery. *Nature reviews Drug discovery*. 8 (2), pp. 129-138.
- Winkler, U., Jensen, M., Manzke, O., Schulz, H., Diehl, V. and Engert, A. (1999) Cytokine-release syndrome in patients with B-cell chronic lymphocytic leukemia and high lymphocyte counts after treatment with an anti-CD20 monoclonal antibody (rituximab, IDEC-C2B8). *Blood, The Journal of the American Society of Hematology*. 94 (7), pp. 2217-2224.
- Wiseman, D.H. (2011) Donor cell leukaemia: a review. *Biology of Blood and Marrow Transplantation*. 17 (6), pp. 771-789.
- Wood, N.A.P., Keen, L.J., Tilley, L.A. and Bidwell, J.L. (2001) Determination of cytokine regulatory haplotypes by induced heteroduplex analysis of DNA. *Journal of Immunological Methods*. 249, pp. 191–198.
- Wu, S.L., Lee, M.L. and Romano, J.M. (2011) Detection of Dengue Viral RNA Using a Nucleic Acid Sequence-Based Amplification Assay. *Journal of Clinical Microbiology*. 39, pp. 2794-2798.
- Wynn, R.F., Cross, M.A., Hatton, C., Will, A. M., Lashford, L.S., Dexter, T. M. and Testa, N. G. (1998) Accelerated telomere shortening in young recipients of allogeneic bone-marrow transplants. *Lancet*. 351, pp. 178-181.
- Xie, S. S., Deng, Y., Guo, S. L., Li, J. Q., Zhou, Y. C., Liao, J., Wu, D. D. and Lan, W. F. (2022) Endothelial cell ferroptosis mediates monocrotaline-induced pulmonary hypertension in rats by modulating NLRP3 inflammasome activation. *Scientific Reports*. 12 (1), pp. 3056.
- Xu, S., Ding, N., Pei, H., Hu, W., Wei, W., Zhang, X., Zhou, G. & Wang, J. (2014) MiR-21 is involved in radiation-induced bystander effects. *RNA biology*. 11(9), pp. 1161-1170.
- Yamada, H., Vijayachandra, K., Penner, C. and Glick, A. (2001) Increased sensitivity of transforming growth factor (TGF) β 1 null cells to alkylating agents reveals a novel link

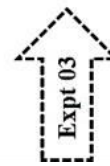
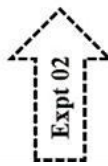
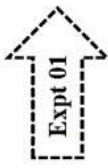
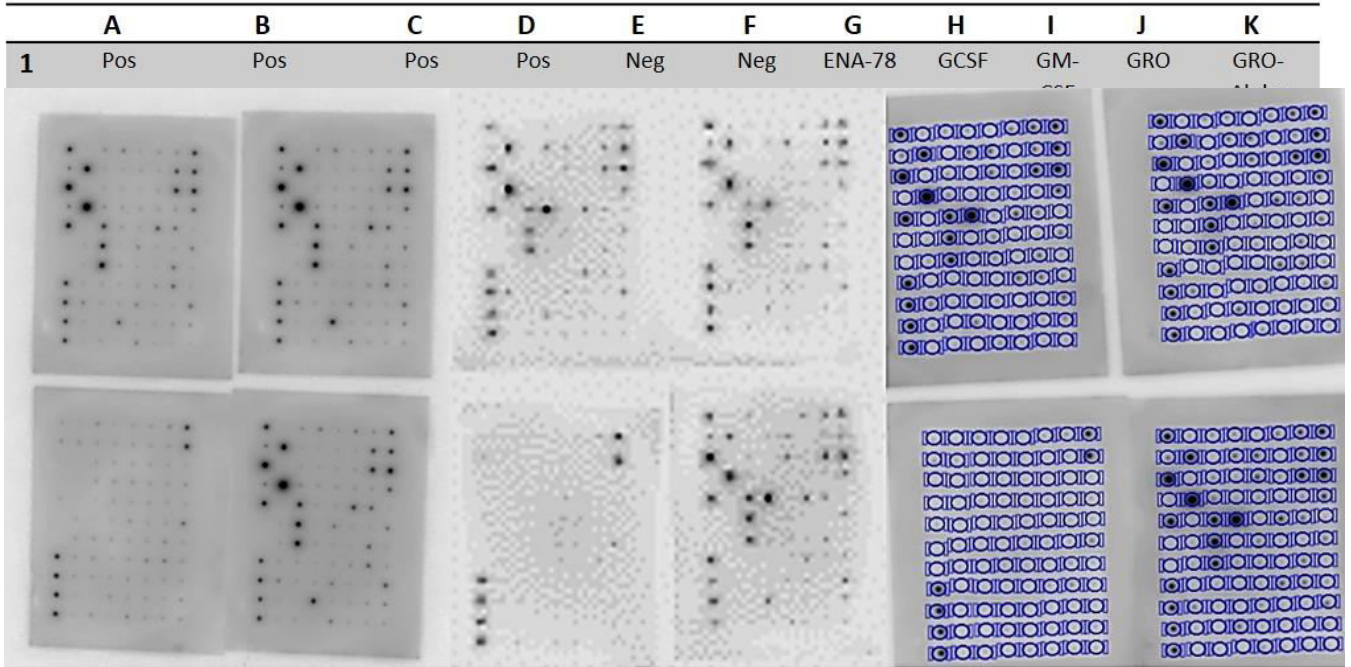
between TGF β signaling and O 6-methylguanine methyltransferase promoter hypermethylation. *Journal of Biological Chemistry*. 276 (22), pp. 19052-19058.

- Yan, B., Wang, H., Rabbani, Z. N., Zhao, Y., Li, W., Yuan, Y., Li, F., Dewhirst, M. W. and Li, C. Y. (2006) Tumor necrosis factor- α is a potent endogenous mutagen that promotes cellular transformation. *Cancer Research*. 66 (24), pp. 11565-11570.
- Yang, L., Aror, K., Beard, W.A., Wilson, S.H. and Schlick, T. (2004) Critical role of magnesium ions in DNA polymerase β 's closing and active site assembly. *Journal of the American Chemical Society*. 126, pp. 8441-8453.
- Yao, T. and Asayama, Y. (2017) Animal cell culture media: History, characteristics, and current issues. *Reprod Med Biol*. 16 (2), pp. 99–117.
- Yasui, M., Honma, M., Takeda, S., Sasanuma, H., Hirota, K. and Kamiya, H. (2019) TK6 Mutants Consortium, Division of genetics and mutagenesis, national institute of health science
- Yildizhan, E. and Kaynar, L. (2018) Cytokine release syndrome. *Journal of Oncological Sciences*. 4 (3), pp. 134-141.
- Yin, T. and Li, L. (2006) The stem cell niches in bone. *The Journal of clinical investigation*. 116 (5), pp. 1195-1201.
- Yiu, H. H., Graham, A. L. and Stengel, R. F. (2012) Dynamics of a cytokine storm. *PLOS ONE*. 7 (10), pp. e45027.
- Yu, H., Pardoll, D. and Jove, R. (2009) STATs in cancer inflammation and immunity: a leading role for STAT3. *Nature reviews cancer*. 9 (11), pp. 798-809.
- Yu, W., Wang, X., Zhao, J., Liu, R., Liu, J., Wang, Z., Peng, J., Wu, H., Zhang, X., Long, D., Kong, D., Li, W. and Hai, C. (2020) Stat2-Drp1 mediated mitochondrial mass increase is necessary for pro-inflammatory differentiation of macrophages. *Redox Biology*. 37, pp. 101761.
- Yves, P., Elisabetta, L., Ganta Liang, Z. and Christophe, M. (2010) DNA Topoisomerases and Their Poisoning by Anticancer and Antibacterial Drugs. *Chem.Biol*. 17 (5), pp. 421-433.
- Zeuner, M., Bieback, K. and Widera, D. (2015) Controversial role of Toll-like receptor 4 in adult stem cells. *Stem cell reviews and reports*. 11 (4), pp. 621-634.

- Zeyneloğlu, H., Kahraman, S. and Pirkevi, C. (2011) Co-culture techniques in assisted reproduction: history, advances and the future. *Journal of Reproductive and Stem Cell Biotechnology*. 2 (1), pp. 29-40.
- Zhang, J. M. and An, J. (2007) Cytokines, inflammation and pain. *International anesthesiology clinics*. 45 (2), pp. 27.
- Zhang, P., Zhang, C., Li, J., Han, J., Liu, X. and Yang, H. (2019) The physical microenvironment of hematopoietic stem cells and its emerging roles in engineering applications. *Stem Cell Research & Therapy*. 10 (1), pp. 1-13.
- Zhang, Y., Ma, L., Lu, E. and Huang, W. (2021) Atorvastatin upregulates microRNA-186 and inhibits the TLR4-mediated MAPKs/NF-κB pathway to relieve steroid-induced avascular necrosis of the femoral head. *Frontiers in Pharmacology*. 12, pp. 583975.
- Zhou, X., Liu, Y., Xiong, X., Chen, J., Tang, W., He, L., Zhang, Z., Yin, Y. and Li, F. (2022) Intestinal accumulation of microbiota-produced succinate caused by loss of microRNAs leads to diarrhea in weanling piglets. *Gut Microbes*. 14 (1), pp. 2091369.
- Zhukareva, V., Obrocka, M., Houle, J. D., Fischer, I. and Neuhuber, B. (2010) Secretion profile of human bone marrow stromal cells: donor variability and response to inflammatory stimuli. *Cytokine*. 50 (3), pp. 317-321.
- Zou, W., Feng, R. and Yang, Y. (2018) Changes in the serum levels of inflammatory cytokines in antidepressant drug-naïve patients with major depression. *PloS one*. 13 (6), pp. e0197267.

Appendices

Appendix I: Cytokine names according to the membrane spot







Cytokine Array membrane

Appendix II: Cytokine concentrations reference to literature

Cytokines	Serum levels (pg/mL)	Age / Range	Reference	
IL-6	~ 10 - 20	>18 years	Kleiner <i>et al.</i> , 2013	
	~ 3		Kim <i>et al.</i> , 2011	
	16.4		Khan <i>et al.</i> , (2014)	
	5.1	(20<78 yr)	Robak <i>et al.</i> , (1998)	
	5.8 - 6.4 W & M		Fernandez-Real <i>et al.</i> , (2001)	
	1.50	(35-45 years)	Zou <i>et al.</i> , 2018	
	26	<15 years	Noori <i>et al.</i> , 2017	
	4.2	(7–79 years)	Arican <i>et al.</i> , 2005	
	25		Winkler <i>et al.</i> , 1999	
	Mixed lymphocyte culture (PBMC)	81780		Danzer <i>et al.</i> , 1994
Storm	4000		Yiu <i>et al.</i> , (2012)	
(mAb anti-CD20)	280		Winkler <i>et al.</i> , 1999	
T-cell & mAb	34467		Morgan <i>et al.</i> , 2010	
HSCT	3524		Melenhorst <i>et al.</i> , 2012	
Congenital Heart Disease	55.3		Noori <i>et al.</i> , 2017	
Irradiated	103300		Danzer <i>et al.</i> , 1994	
TNF-α	20		Winkler <i>et al.</i> , 1999	
	~ 20-60	>18 years	Kleiner <i>et al.</i> , 2013	
	~ 5		Kim <i>et al.</i> , 2011	
	29.4		Khan <i>et al.</i> , (2014)	
	2.69	(35-45 years)	Zou <i>et al.</i> , 2018	
	23.3	<15 years	Noori <i>et al.</i> , 2017	
	11.2	(7–79 years)	Arican <i>et al.</i> , 2005	
	Mixed lymphocyte culture (PBMC)	1577		Danzer <i>et al.</i> , 1994
	Storm	4500		Yiu <i>et al.</i> , (2012)
	(mAb anti-CD20)	500 (mAb anti-CD20)		Winkler <i>et al.</i> , 1999
T-cell & mAb	380		Morgan <i>et al.</i> , 2010	
HSCT	186.6		Melenhorst <i>et al.</i> , 2012	
Congenital Heart Disease	56.6		Noori <i>et al.</i> , 2017	
Irradiated	1401		Danzer <i>et al.</i> , 1994	
GM-CSF	38.3 – 97.4	1 - >18 years	Kleiner <i>et al.</i> , 2013	
	2.5		Lee <i>et al.</i> , 2008	
	~ 20 - 40		Kim <i>et al.</i> , 2011	
	20-100		Bhattacharya <i>et al.</i> , 2015	
T-cell therapy	10191		Morgan <i>et al.</i> , 2010	
G-CSF	36.2 - 45.5	1 - >18 years	Kleiner <i>et al.</i> , 2013	
	19.38		Lee <i>et al.</i> , 2008	
	~ 15		Kim <i>et al.</i> , 2011	
	20 - 95	65 - 101	Kawakami <i>et al.</i> , 1990	
	20.3		Matsubara <i>et al.</i> , 1999	
	Acute infection	731.8 (range 30 – 3199)		Kawakami <i>et al.</i> , 1990
HSCT	38310		Melenhorst <i>et al.</i> , 2012	
TGF-β1	36.13	35-45 years	Zou <i>et al.</i> , 2018	
	4100	20-60 years	Wakefield <i>et al.</i> , 1995	
	33		Zou <i>et al.</i> , 2018	
	Breast cancer	20000 & 40000		Wakefield <i>et al.</i> , 1995

Appendix III: Micronuclei addition or potentiation.

This table was designed using the individual counts of micronuclei (MN) formed during the isolation and combination assay. The number of MN induced by respective cytokines or combinations is depicted within the respective box corresponding to each cytokine. If the number of MN in the isolation of two cytokines is lower than the number of MN when they are in combination, it indicates ‘**potentiation**’ of MN induction during the combination. Conversely, if the number of MN in isolation of two cytokines is higher than the number of MN when they are in combination, it suggests a ‘**decrease**’ in MN induction during the combination. In cases where the number of MN in isolation of two cytokines is additive to the number of MN when they are in combination, it signifies an ‘**additive**’ effect of MN induction during the combination.

Additive  Decrease  Potentiate or synergistic  Statistical difference 	<table border="1"> <tr><td>1000 TNFα</td><td>1000 IL-6</td><td>31</td></tr> <tr><td>1000 GM-CSF</td><td>1000 IL-6</td><td>31</td></tr> <tr><td>1000 G-CSF</td><td>1000 IL-6</td><td>26</td></tr> <tr><td>1000 TGF-β</td><td>1000 IL-6</td><td>36</td></tr> </table>	1000 TNF α	1000 IL-6	31	1000 GM-CSF	1000 IL-6	31	1000 G-CSF	1000 IL-6	26	1000 TGF- β	1000 IL-6	36	<table border="1"> <tr><td>1000 TNFα</td><td>1000 IL-6</td><td>31</td></tr> <tr><td>1000 GM-CSF</td><td>1000 IL-6</td><td>21</td></tr> <tr><td>1000 G-CSF</td><td>1000 IL-6</td><td>29</td></tr> <tr><td>1000 TGF-β</td><td>1000 IL-6</td><td>25</td></tr> </table>	1000 TNF α	1000 IL-6	31	1000 GM-CSF	1000 IL-6	21	1000 G-CSF	1000 IL-6	29	1000 TGF- β	1000 IL-6	25	<table border="1"> <tr><td>1000 TNFα</td><td>1000 IL-6</td><td>31</td></tr> <tr><td>1000 GM-CSF</td><td>1000 IL-6</td><td>21</td></tr> <tr><td>1000 G-CSF</td><td>1000 IL-6</td><td>33</td></tr> <tr><td>1000 TGF-β</td><td>1000 IL-6</td><td>43</td></tr> </table>	1000 TNF α	1000 IL-6	31	1000 GM-CSF	1000 IL-6	21	1000 G-CSF	1000 IL-6	33	1000 TGF- β	1000 IL-6	43	<table border="1"> <tr><td>1000 TNFα</td><td>1000 IL-6</td><td>26</td></tr> <tr><td>1000 GM-CSF</td><td>1000 IL-6</td><td>29</td></tr> <tr><td>1000 G-CSF</td><td>1000 IL-6</td><td>33</td></tr> <tr><td>1000 TGF-β</td><td>1000 IL-6</td><td>26</td></tr> </table>	1000 TNF α	1000 IL-6	26	1000 GM-CSF	1000 IL-6	29	1000 G-CSF	1000 IL-6	33	1000 TGF- β	1000 IL-6	26	<table border="1"> <tr><td>1000 TNFα</td><td>1000 IL-6</td><td>36</td></tr> <tr><td>1000 GM-CSF</td><td>1000 IL-6</td><td>25</td></tr> <tr><td>1000 G-CSF</td><td>1000 IL-6</td><td>43</td></tr> <tr><td>1000 TGF-β</td><td>1000 IL-6</td><td>26</td></tr> </table>	1000 TNF α	1000 IL-6	36	1000 GM-CSF	1000 IL-6	25	1000 G-CSF	1000 IL-6	43	1000 TGF- β	1000 IL-6	26												
	1000 TNF α	1000 IL-6	31																																																																										
	1000 GM-CSF	1000 IL-6	31																																																																										
	1000 G-CSF	1000 IL-6	26																																																																										
1000 TGF- β	1000 IL-6	36																																																																											
1000 TNF α	1000 IL-6	31																																																																											
1000 GM-CSF	1000 IL-6	21																																																																											
1000 G-CSF	1000 IL-6	29																																																																											
1000 TGF- β	1000 IL-6	25																																																																											
1000 TNF α	1000 IL-6	31																																																																											
1000 GM-CSF	1000 IL-6	21																																																																											
1000 G-CSF	1000 IL-6	33																																																																											
1000 TGF- β	1000 IL-6	43																																																																											
1000 TNF α	1000 IL-6	26																																																																											
1000 GM-CSF	1000 IL-6	29																																																																											
1000 G-CSF	1000 IL-6	33																																																																											
1000 TGF- β	1000 IL-6	26																																																																											
1000 TNF α	1000 IL-6	36																																																																											
1000 GM-CSF	1000 IL-6	25																																																																											
1000 G-CSF	1000 IL-6	43																																																																											
1000 TGF- β	1000 IL-6	26																																																																											
<table border="1"> <tr><td>1000 TNFα</td><td>3000 IL-6</td><td>32</td></tr> <tr><td>3000 GM-CSF</td><td>3000 IL-6</td><td>25</td></tr> <tr><td>3000 G-CSF</td><td>3000 IL-6</td><td>36</td></tr> <tr><td>3000 TGF-β</td><td>3000 IL-6</td><td>30</td></tr> </table>	1000 TNF α	3000 IL-6	32	3000 GM-CSF	3000 IL-6	25	3000 G-CSF	3000 IL-6	36	3000 TGF- β	3000 IL-6	30	<table border="1"> <tr><td>3000 TNFα</td><td>3000 IL-6</td><td>30</td></tr> <tr><td>3000 GM-CSF</td><td>3000 IL-6</td><td>24</td></tr> <tr><td>3000 G-CSF</td><td>3000 IL-6</td><td>24</td></tr> <tr><td>3000 TGF-β</td><td>3000 IL-6</td><td>34</td></tr> </table>	3000 TNF α	3000 IL-6	30	3000 GM-CSF	3000 IL-6	24	3000 G-CSF	3000 IL-6	24	3000 TGF- β	3000 IL-6	34	<table border="1"> <tr><td>3000 TNFα</td><td>3000 IL-6</td><td>30</td></tr> <tr><td>4000 GM-CSF</td><td>3000 IL-6</td><td>32</td></tr> <tr><td>3000 G-CSF</td><td>3000 IL-6</td><td>47</td></tr> <tr><td>3000 TGF-β</td><td>3000 IL-6</td><td>38</td></tr> </table>	3000 TNF α	3000 IL-6	30	4000 GM-CSF	3000 IL-6	32	3000 G-CSF	3000 IL-6	47	3000 TGF- β	3000 IL-6	38	<table border="1"> <tr><td>3000 TNFα</td><td>3000 IL-6</td><td>30</td></tr> <tr><td>3000 GM-CSF</td><td>3000 IL-6</td><td>24</td></tr> <tr><td>3000 G-CSF</td><td>3000 IL-6</td><td>47</td></tr> <tr><td>3000 TGF-β</td><td>3000 IL-6</td><td>38</td></tr> </table>	3000 TNF α	3000 IL-6	30	3000 GM-CSF	3000 IL-6	24	3000 G-CSF	3000 IL-6	47	3000 TGF- β	3000 IL-6	38	<table border="1"> <tr><td>3000 TNFα</td><td>3000 IL-6</td><td>24</td></tr> <tr><td>3000 GM-CSF</td><td>3000 IL-6</td><td>43</td></tr> <tr><td>3000 G-CSF</td><td>3000 IL-6</td><td>28</td></tr> <tr><td>3000 TGF-β</td><td>3000 IL-6</td><td>35</td></tr> </table>	3000 TNF α	3000 IL-6	24	3000 GM-CSF	3000 IL-6	43	3000 G-CSF	3000 IL-6	28	3000 TGF- β	3000 IL-6	35	<table border="1"> <tr><td>3000 TNFα</td><td>3000 IL-6</td><td>27</td></tr> <tr><td>3000 GM-CSF</td><td>3000 IL-6</td><td>34</td></tr> <tr><td>3000 G-CSF</td><td>3000 IL-6</td><td>46</td></tr> <tr><td>3000 TGF-β</td><td>3000 IL-6</td><td>25</td></tr> </table>	3000 TNF α	3000 IL-6	27	3000 GM-CSF	3000 IL-6	34	3000 G-CSF	3000 IL-6	46	3000 TGF- β	3000 IL-6	25
1000 TNF α	3000 IL-6	32																																																																											
3000 GM-CSF	3000 IL-6	25																																																																											
3000 G-CSF	3000 IL-6	36																																																																											
3000 TGF- β	3000 IL-6	30																																																																											
3000 TNF α	3000 IL-6	30																																																																											
3000 GM-CSF	3000 IL-6	24																																																																											
3000 G-CSF	3000 IL-6	24																																																																											
3000 TGF- β	3000 IL-6	34																																																																											
3000 TNF α	3000 IL-6	30																																																																											
4000 GM-CSF	3000 IL-6	32																																																																											
3000 G-CSF	3000 IL-6	47																																																																											
3000 TGF- β	3000 IL-6	38																																																																											
3000 TNF α	3000 IL-6	30																																																																											
3000 GM-CSF	3000 IL-6	24																																																																											
3000 G-CSF	3000 IL-6	47																																																																											
3000 TGF- β	3000 IL-6	38																																																																											
3000 TNF α	3000 IL-6	24																																																																											
3000 GM-CSF	3000 IL-6	43																																																																											
3000 G-CSF	3000 IL-6	28																																																																											
3000 TGF- β	3000 IL-6	35																																																																											
3000 TNF α	3000 IL-6	27																																																																											
3000 GM-CSF	3000 IL-6	34																																																																											
3000 G-CSF	3000 IL-6	46																																																																											
3000 TGF- β	3000 IL-6	25																																																																											
<table border="1"> <tr><td>3000 TNFα</td><td>4000 IL-6</td><td>30</td></tr> <tr><td>1000 GM-CSF</td><td>4000 IL-6</td><td>30</td></tr> <tr><td>1000 G-CSF</td><td>4000 IL-6</td><td>24</td></tr> <tr><td>1000 TGF-β</td><td>4000 IL-6</td><td>27</td></tr> </table>	3000 TNF α	4000 IL-6	30	1000 GM-CSF	4000 IL-6	30	1000 G-CSF	4000 IL-6	24	1000 TGF- β	4000 IL-6	27	<table border="1"> <tr><td>4000 TNFα</td><td>4000 IL-6</td><td>32</td></tr> <tr><td>1000 GM-CSF</td><td>4000 IL-6</td><td>32</td></tr> <tr><td>1000 G-CSF</td><td>4000 IL-6</td><td>43</td></tr> <tr><td>1000 TGF-β</td><td>4000 IL-6</td><td>34</td></tr> </table>	4000 TNF α	4000 IL-6	32	1000 GM-CSF	4000 IL-6	32	1000 G-CSF	4000 IL-6	43	1000 TGF- β	4000 IL-6	34	<table border="1"> <tr><td>3000 TNFα</td><td>4000 IL-6</td><td>25</td></tr> <tr><td>1000 GM-CSF</td><td>4000 IL-6</td><td>24</td></tr> <tr><td>1000 G-CSF</td><td>4000 IL-6</td><td>28</td></tr> <tr><td>1000 TGF-β</td><td>4000 IL-6</td><td>46</td></tr> </table>	3000 TNF α	4000 IL-6	25	1000 GM-CSF	4000 IL-6	24	1000 G-CSF	4000 IL-6	28	1000 TGF- β	4000 IL-6	46	<table border="1"> <tr><td>3000 TNFα</td><td>4000 IL-6</td><td>25</td></tr> <tr><td>1000 GM-CSF</td><td>4000 IL-6</td><td>24</td></tr> <tr><td>1000 G-CSF</td><td>4000 IL-6</td><td>28</td></tr> <tr><td>1000 TGF-β</td><td>4000 IL-6</td><td>46</td></tr> </table>	3000 TNF α	4000 IL-6	25	1000 GM-CSF	4000 IL-6	24	1000 G-CSF	4000 IL-6	28	1000 TGF- β	4000 IL-6	46	<table border="1"> <tr><td>3000 TNFα</td><td>4000 IL-6</td><td>36</td></tr> <tr><td>1000 GM-CSF</td><td>4000 IL-6</td><td>24</td></tr> <tr><td>1000 G-CSF</td><td>4000 IL-6</td><td>47</td></tr> <tr><td>1000 TGF-β</td><td>4000 IL-6</td><td>25</td></tr> </table>	3000 TNF α	4000 IL-6	36	1000 GM-CSF	4000 IL-6	24	1000 G-CSF	4000 IL-6	47	1000 TGF- β	4000 IL-6	25	<table border="1"> <tr><td>3000 TNFα</td><td>4000 IL-6</td><td>30</td></tr> <tr><td>1000 GM-CSF</td><td>4000 IL-6</td><td>34</td></tr> <tr><td>1000 G-CSF</td><td>4000 IL-6</td><td>38</td></tr> <tr><td>1000 TGF-β</td><td>4000 IL-6</td><td>35</td></tr> </table>	3000 TNF α	4000 IL-6	30	1000 GM-CSF	4000 IL-6	34	1000 G-CSF	4000 IL-6	38	1000 TGF- β	4000 IL-6	35
3000 TNF α	4000 IL-6	30																																																																											
1000 GM-CSF	4000 IL-6	30																																																																											
1000 G-CSF	4000 IL-6	24																																																																											
1000 TGF- β	4000 IL-6	27																																																																											
4000 TNF α	4000 IL-6	32																																																																											
1000 GM-CSF	4000 IL-6	32																																																																											
1000 G-CSF	4000 IL-6	43																																																																											
1000 TGF- β	4000 IL-6	34																																																																											
3000 TNF α	4000 IL-6	25																																																																											
1000 GM-CSF	4000 IL-6	24																																																																											
1000 G-CSF	4000 IL-6	28																																																																											
1000 TGF- β	4000 IL-6	46																																																																											
3000 TNF α	4000 IL-6	25																																																																											
1000 GM-CSF	4000 IL-6	24																																																																											
1000 G-CSF	4000 IL-6	28																																																																											
1000 TGF- β	4000 IL-6	46																																																																											
3000 TNF α	4000 IL-6	36																																																																											
1000 GM-CSF	4000 IL-6	24																																																																											
1000 G-CSF	4000 IL-6	47																																																																											
1000 TGF- β	4000 IL-6	25																																																																											
3000 TNF α	4000 IL-6	30																																																																											
1000 GM-CSF	4000 IL-6	34																																																																											
1000 G-CSF	4000 IL-6	38																																																																											
1000 TGF- β	4000 IL-6	35																																																																											
<table border="1"> <tr><td>3000 TNFα</td><td>3000 IL-6</td><td>19</td></tr> <tr><td>3000 GM-CSF</td><td>3000 IL-6</td><td>21</td></tr> <tr><td>3000 G-CSF</td><td>3000 IL-6</td><td>23</td></tr> <tr><td>3000 TGF-β</td><td>3000 IL-6</td><td>21</td></tr> </table>	3000 TNF α	3000 IL-6	19	3000 GM-CSF	3000 IL-6	21	3000 G-CSF	3000 IL-6	23	3000 TGF- β	3000 IL-6	21	<table border="1"> <tr><td>3000 TNFα</td><td>3000 IL-6</td><td>19</td></tr> <tr><td>3000 GM-CSF</td><td>3000 IL-6</td><td>28</td></tr> <tr><td>3000 G-CSF</td><td>3000 IL-6</td><td>30</td></tr> <tr><td>3000 TGF-β</td><td>3000 IL-6</td><td>36</td></tr> </table>	3000 TNF α	3000 IL-6	19	3000 GM-CSF	3000 IL-6	28	3000 G-CSF	3000 IL-6	30	3000 TGF- β	3000 IL-6	36	<table border="1"> <tr><td>3000 TNFα</td><td>3000 IL-6</td><td>21</td></tr> <tr><td>4000 GM-CSF</td><td>3000 IL-6</td><td>28</td></tr> <tr><td>3000 G-CSF</td><td>3000 IL-6</td><td>26</td></tr> <tr><td>3000 TGF-β</td><td>3000 IL-6</td><td>28</td></tr> </table>	3000 TNF α	3000 IL-6	21	4000 GM-CSF	3000 IL-6	28	3000 G-CSF	3000 IL-6	26	3000 TGF- β	3000 IL-6	28	<table border="1"> <tr><td>3000 TNFα</td><td>3000 IL-6</td><td>21</td></tr> <tr><td>3000 GM-CSF</td><td>3000 IL-6</td><td>28</td></tr> <tr><td>3000 G-CSF</td><td>3000 IL-6</td><td>26</td></tr> <tr><td>3000 TGF-β</td><td>3000 IL-6</td><td>28</td></tr> </table>	3000 TNF α	3000 IL-6	21	3000 GM-CSF	3000 IL-6	28	3000 G-CSF	3000 IL-6	26	3000 TGF- β	3000 IL-6	28	<table border="1"> <tr><td>3000 TNFα</td><td>3000 IL-6</td><td>23</td></tr> <tr><td>3000 GM-CSF</td><td>3000 IL-6</td><td>30</td></tr> <tr><td>3000 G-CSF</td><td>3000 IL-6</td><td>26</td></tr> <tr><td>3000 TGF-β</td><td>3000 IL-6</td><td>28</td></tr> </table>	3000 TNF α	3000 IL-6	23	3000 GM-CSF	3000 IL-6	30	3000 G-CSF	3000 IL-6	26	3000 TGF- β	3000 IL-6	28	<table border="1"> <tr><td>3000 TNFα</td><td>3000 IL-6</td><td>21</td></tr> <tr><td>4000 GM-CSF</td><td>3000 IL-6</td><td>36</td></tr> <tr><td>3000 G-CSF</td><td>3000 IL-6</td><td>28</td></tr> <tr><td>3000 TGF-β</td><td>3000 IL-6</td><td>28</td></tr> </table>	3000 TNF α	3000 IL-6	21	4000 GM-CSF	3000 IL-6	36	3000 G-CSF	3000 IL-6	28	3000 TGF- β	3000 IL-6	28
3000 TNF α	3000 IL-6	19																																																																											
3000 GM-CSF	3000 IL-6	21																																																																											
3000 G-CSF	3000 IL-6	23																																																																											
3000 TGF- β	3000 IL-6	21																																																																											
3000 TNF α	3000 IL-6	19																																																																											
3000 GM-CSF	3000 IL-6	28																																																																											
3000 G-CSF	3000 IL-6	30																																																																											
3000 TGF- β	3000 IL-6	36																																																																											
3000 TNF α	3000 IL-6	21																																																																											
4000 GM-CSF	3000 IL-6	28																																																																											
3000 G-CSF	3000 IL-6	26																																																																											
3000 TGF- β	3000 IL-6	28																																																																											
3000 TNF α	3000 IL-6	21																																																																											
3000 GM-CSF	3000 IL-6	28																																																																											
3000 G-CSF	3000 IL-6	26																																																																											
3000 TGF- β	3000 IL-6	28																																																																											
3000 TNF α	3000 IL-6	23																																																																											
3000 GM-CSF	3000 IL-6	30																																																																											
3000 G-CSF	3000 IL-6	26																																																																											
3000 TGF- β	3000 IL-6	28																																																																											
3000 TNF α	3000 IL-6	21																																																																											
4000 GM-CSF	3000 IL-6	36																																																																											
3000 G-CSF	3000 IL-6	28																																																																											
3000 TGF- β	3000 IL-6	28																																																																											
<table border="1"> <tr><td>1000 TNFα</td><td>3000 TNFα</td><td>15</td></tr> <tr><td>3000 TNFα</td><td>3000 TNFα</td><td>25</td></tr> </table>	1000 TNF α	3000 TNF α	15	3000 TNF α	3000 TNF α	25	<table border="1"> <tr><td>1000 IL-6</td><td>4000 IL-6</td><td>11</td></tr> <tr><td>4000 IL-6</td><td>4000 IL-6</td><td>20</td></tr> </table>	1000 IL-6	4000 IL-6	11	4000 IL-6	4000 IL-6	20	<table border="1"> <tr><td>1000 GM-CSF</td><td>3000 GM-CSF</td><td>12</td></tr> <tr><td>3000 GM-CSF</td><td>3000 GM-CSF</td><td>18</td></tr> </table>	1000 GM-CSF	3000 GM-CSF	12	3000 GM-CSF	3000 GM-CSF	18	<table border="1"> <tr><td>1000 G-CSF</td><td>3000 G-CSF</td><td>11</td></tr> <tr><td>3000 G-CSF</td><td>3000 G-CSF</td><td>18</td></tr> </table>	1000 G-CSF	3000 G-CSF	11	3000 G-CSF	3000 G-CSF	18	<table border="1"> <tr><td>1000 TGF-β</td><td>3000 TGF-β</td><td>17</td></tr> <tr><td>3000 TGF-β</td><td>3000 TGF-β</td><td>16</td></tr> </table>	1000 TGF- β	3000 TGF- β	17	3000 TGF- β	3000 TGF- β	16																																											
1000 TNF α	3000 TNF α	15																																																																											
3000 TNF α	3000 TNF α	25																																																																											
1000 IL-6	4000 IL-6	11																																																																											
4000 IL-6	4000 IL-6	20																																																																											
1000 GM-CSF	3000 GM-CSF	12																																																																											
3000 GM-CSF	3000 GM-CSF	18																																																																											
1000 G-CSF	3000 G-CSF	11																																																																											
3000 G-CSF	3000 G-CSF	18																																																																											
1000 TGF- β	3000 TGF- β	17																																																																											
3000 TGF- β	3000 TGF- β	16																																																																											

